TG

FIFTEENTH TRANSDUCER WORKSHOP

20-22 JUNE 1989

COCOA BEACH, FLORIDA

TELEMETRY GROUP

RANGE COMMANDERS COUNCIL

WHITE SANDS MISSILE RANGE
KWAJALEIN ATOLL
YUMA PROVING GROUND
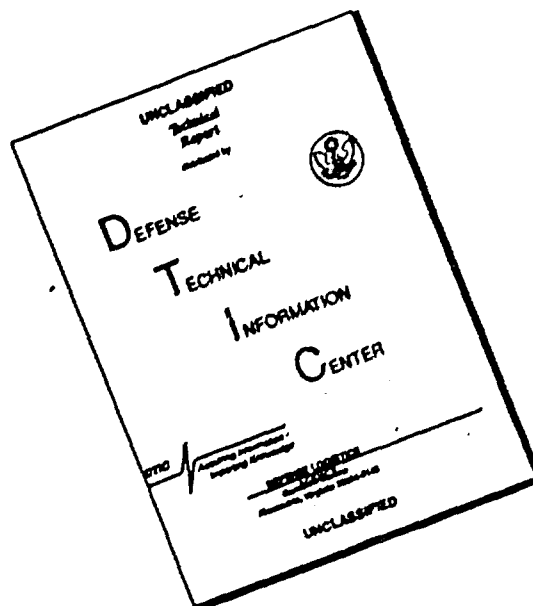## ELECTRONIC PROVING GROUND

PACIFIC MISSILE TEST CENTER
NAVAL WEAPONS CENTER
ATLANTIC FLEET WEAPONS TRAINING FACILITY
NAVAL AIR TEST CENTER

EASTERN SPACE AND MISSILE CENTER
MUNITIONS SYSTEMS DIVISION
WESTERN SPACE AND MISSILE CENTER
CONSOLIDATED SPACE TEST CENTER
AIR FORCE FLIGHT TEST CENTER
AIR FORCE TACTICAL FIGHTER WEAPONS CENTER

89 11 00 008

DISCLAIMER NOTICE

THIS DOCUMENT IS BEST QUALITY AVAILABLE. THE COPY FURNISHED TO DTIC CONTAINED A SIGNIFICANT NUMBER OF PAGES WHICH DO NOT REPRODUCE LEGIBLY.

REPORT DOCUMENTATION PAGE

1a REPORT SECURITY CLASSIFICATION UNCLASSIFIED	1b RESTRICTIVE MARKINGS
2a SECURITY CLASSIFICATION AUTHORITY	3 DISTRIBUTION/AVAILABILITY OF REPORT APPROVED FOR PUBLIC RELEASE: DISTRIBUTION UNLIMITED
2b DECLASSIFICATION/DOWNGRADING SCHEDULE	

4 PERFORMING ORGANIZATION REPORT NUMBER(S) UNNUMBERED	5 MONITORING ORGANIZATION REPORT NUMBER(S)

6a NAME OF PERFORMING ORGANIZATION Telemetry Group Range Commanders Council	6b OFFICE SYMBOL (If applicable) STEWS-SA-R	7a NAME OF MONITORING ORGANIZATION STEWS-SA-R Range Commanders Council
6c. ADDRESS (City, State, and ZIP Code) White Sands Missile Range, NM 88002		7b ADDRESS (City, State, and ZIP Code) White Sands Missile Range, NM 88002

8a. NAME OF FUNDING/SPONSORING ORGANIZATION	8b OFFICE SYMBOL (If applicable)	9 PROCUREMENT INSTRUMENT IDENTIFICATION NUMBER

8c. ADDRESS (City, State, and ZIP Code)	10 SOURCE OF FUNDING NUMBERS			
	PROGRAM ELEMENT NO	PROJECT NO	TASK NO	WORK UNIT ACCESSION NO

11 TITLE (Include Security Classification)

FIFTEENTH TRANSDUCER WORKSHOP   (UNCLASSIFIED)

12 PERSONAL AUTHOR(S)

13a TYPE OF REPORT Final	13b TIME COVERED FROM _____ TO _____	14 DATE OF REPORT (Year, Month, Day) June 1989	15 PAGE COUNT 277

16 SUPPLEMENTARY NOTATION

New Document

17	COSATI CODES		18 SUBJECT TERMS (Continue on reverse if necessary and identify by block number)
FIELD	GROUP	SUB-GROUP	Transducer, telemetry, calibration, vehicular instrumentation

19 ABSTRACT (Continue on reverse if necessary and identify by block number)

"DISCLAIMER" - This document has been published for information purposes only. The material contained herein does not necessarily represent the position or conclusions of the Range Commanders Council (RCC).

THE COMMITTEE APPRISES THE TELEMETRY GROUP OF SIGNIFICANT PROGRESS IN THE FIELD OF TRANSDUCERS USED IN TELEMETRY SYSTEMS: MAINTAINS ANY NECESSARY LIAISON BETWEEN THE TG AND THE NATIONAL BUREAU OF STANDARDS AND THEIR TRANSDUCER'S PROGRAM OR OTHER RELATED TELEMETRY TRANSDUCER EFFORTS; COORDINATES TG ACTIVITIES WITH OTHER PROFESSIONAL TECHNICAL GROUPS; COLLECTS AND PASSES ON INFORMATION ON TECHNIQUES OF MEASUREMENT, EVALUATION, RELIABILITY, CALIBRATION, REPORTING AND MANUFACTURING, RECOMMENDS UNIFORM PRACTICES FOR CALIBRATION, TESTING AND EVALUATION OF VEHICULAR INSTRUMENTATION COMPONENTS; AND CONTRIBUTES TO STANDARDS IN THE AREA OF VEHICULAR INSTRUMENTATION.

20 DISTRIBUTION/AVAILABILITY OF ABSTRACT ☐ UNCLASSIFIED/UNLIMITED ☐ SAME AS RPT ☐ DTIC USERS	21 ABSTRACT SECURITY CLASSIFICATION UNCLASSIFIED	
22a NAME OF RESPONSIBLE INDIVIDUAL SUSAN WOOD	22b TELEPHONE (Include Area Code) 505-678-1107	22c OFFICE SYMBOL STEWS-SA-R

DD FORM 1473, 84 MAR

83 APR edition may be used until exhausted
All other editions are obsolete
SECURITY CLASSIFICATION OF THIS PAGE

FIFTEENTH
TRANSDUCER
WORKSHOP

20-22 JUNE 1989

COCOA BEACH, FLORIDA

VEHICULAR INSTRUMENTATION/TRANSDUCER COMMITTEE
TELEMETRY GROUP
RANGE COMMANDERS COUNCIL

Published and Distributed by

Secretariat
Range Commanders Council
White Sands Missile Range,
New Mexico 88002

TABLE OF CONTENTS

SESSION 3:   TUTORIALS

SESSION 4:   DATA ACQUISITION

Accession For

NTIS GRA&I		X
DTIC TAB		☐
Unannounced		☐
Justification		

By___
Distribution/

Availability Codes

Dist	Avail and/or Special
A-1	

TELEMETRY GROUP COMMITTEES

Chairman, Phillip D. Sharp (WSMR)
Vice Chairman, J. W. Rymer (NATC)

Data Multiplex
RF Systems
Recorder/Reproducer
Vehicular Instrumentation/Transducer

MEMBERSHIP OF THE VEHICULAR INSTRUMENTATION/TRANSDUCER COMMITTEE

Leroy Bates (Chairman)
NSWSES - Code 4R13
Port Hueneme, CA 93043

Gary Bartlett
NWC - Code 3143
China Lake, CA 93555

Richard Hasbrouck
Lawrence Livermore National Lab.
P.O. Box 808, L154
Livermore, CA 94550

Steve Kuehn
Sandia National Lab.
P.O. Box 5800, Div. 2543
Albuquerque, NM 87185

William A. Xavier
EG&G Energy Measurements
P.O. Box 9051
Pleasanton, CA 94566

John Ach
AFWAL/FIBGA
Wright Patterson AFB, OH 45433

Dennis Henry
Lawrence Sires
NWC - Code 6213
China Lake, CA 93555

Physical Science Lab.
New Mexico State University
Las Cruces, NM 88003

Raymond Faulstich
NATC - Code RD43
Patuxent River, MD 20670

Richard Krizan
ESMC/RSL
Patrick AFB, FL 32925

Archie Amos
6521 RANGES/ENRE
Edwards AFB, CA 93523

Andrew Hooper
STEYP-MT-TE-T
Yuma Proving Ground
Yuma, AZ 85365

TRANSDUCER COMMITTEE OBJECTIVES

This committee apprises the Telemetry Group (TG) of significant progress in the field of transducers used in telemetry systems; maintains any necessary liaison between the TG and the National Bureau of Standards and their transducers' program or other related telemetry transducer efforts; coordinates TG activities with other professional technical groups; collects and passes on information on techniques of measurement, evaluation, reliability, calibration, reporting and manufacturing; recommends uniform practices for calibration, testing and evaluation of vehicular instrumentation components; and contributes to standards in the area of vehicular instrumentation.

TRANSDUCER WORKSHOP SUMMARY

Workshop Number	Date	Host	General Chairman	Number Attendees	RCC TG Transducer Chairman
1	March 1960	Albuquerque, NM			
2	25-26 July 1961	Holloman AFB Alamogordo, NM	W. H. Sanders Holloman AFB, NM	46	Paul Polishuk Wright-Patterson Dayton, OH
3	21-23 June 1962	NBS Washington, D.C.	Arnold Wexler NBS Washington, D.C.	106	Paul Polishuk Wright-Patterson Dayton, OH
4	13-19 June 1964	Wright-Patterson Dayton, OH	Jack Lynch NATC Patuxent River, MD	53	Jack Lynch NATC Patuxent River, MD
5	3-4 October 1967	NBS Gaithersburg, MD	Loyt L. Lathrop Sandia Labs Albuquerque, NM	106	Loyt L. Lathrop Sandia Labs Albuquerque, NM
6	22-24 October 1969	Langley Research Ctr. NASA Hampton, VA	Paul Lederer NBS Washington, D.C.	49	Loyt L. Lathrop Sandia Labs Albuquerque, NM
7	4-6 April 1972	Sandia Labs Albuquerque, NM	W. G. James AEFDL Wright-Patterson Dayton, OH	111	Pat Walter Sandia Labs First Mfg's Panel Boo-Boos
8	22-24 April 1975	Wright-Patterson Dayton, OH	Pierre F. Fuselier Lawrence Livermore Labs Livermore, CA	74	Pat Walter Sandia Labs Albuquerque, NM
9	26-28 April 1977	Eglin AFB Fort Walton Beach, FL	Kenny Cox NWC China Lake, CA	100	William Anderson NATC Patuxent River, MD
10	12-14 June 1979	North American Air Defense Command Colorado Springs, CO	Richard Hasbrouck Lawrence Livermore Labs Livermore, CA	106	William Anderson NATC Patuxent River, MD
11	2-4 June 1981	Air Force Plant Rep. Office, Det. 9 Seattle, WA	Leroy Bates NSWSES Port Hueneme, CA	96	William Anderson NATC Patuxent River, MD

Workshop Number	Date	Host	General Chairman	Number Attendees	RCC TG Transducer Chairman
12	7-9 June 1983	Patrick AFB Melbourne, FL	Kenny Cox NWC China Lake, CA	116	William Anderson NATC Patuxent River, MD
13	4-6 June 1985	Naval Postgraduate School Monterey, CA	Richard Krizan Patrick AFB, FL	112	Leroy Bates NSWSES Port Hueneme, CA
14	16-18 June 1987	Air Force Academy Colorado Springs, CO	Stephen F. Kuehn Sandia National Labs Albuquerque, NM	118	Leroy Bates NSWSES Port Hueneme, CA
15	20-22 June 1989	ESMC, Patrick AFB Cocoa Beach, FL	John T. Ach WRDC/FIBGA Wright-Patterson AFB, OH	90	Leroy Bates NSWSES Port Hueneme, CA
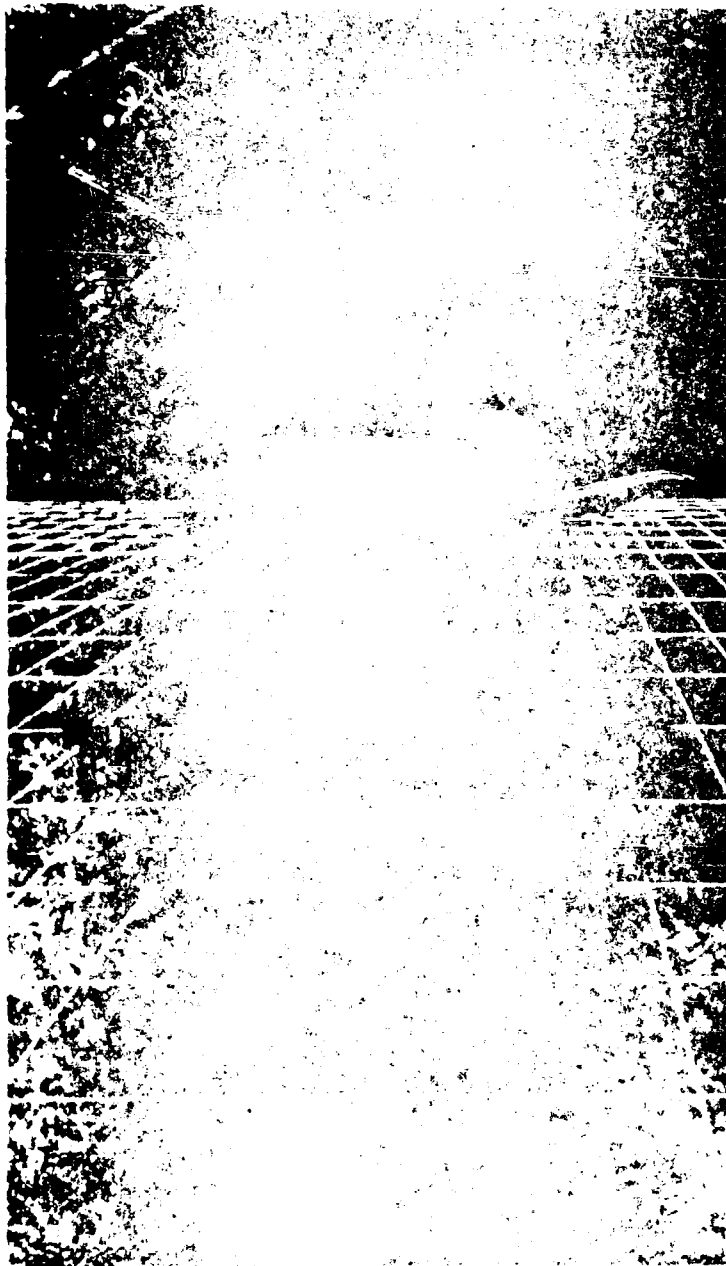
DEFINITION OF THE
TRANSDUCER WORKSHOP

History:

The Workshop is sponsored by the Vehicular Instrumentation/Transducer Committee, Telemetry Group of the Range Commanders Council. This committee develops and implements standards and procedures for transducer applications. The fourteen previous workshops, beginning in 1960, were held at two-year intervals at or near various U.S. Government installations around the country.

Attendees:

Attendees are working-level people who must solve real-life hardware problems and who are strongly oriented to the practical approach. Their field is making measurements of physical parameters using transducers. Test and project people who attend will benefit from exposure to the true complexity of transducer evaluation, selection, and application.

Subjects:

Practical problems involving transducers, signal conditioners, and read-out devices will be considered as separate components and in systems. Engineering tests, laboratory calibrations, transducer developments and evaluations represent potential applications of the ideas presented. Measurands include force, pressure, flow, acceleration, velocity, displacement, temperature and others.

Emphasis:

The workshop

- is a practical approach to the solution of measurement problems,
- strongly focuses on transducers and related instrumentation used in measurements engineering,
- has a high ratio of discussion to presentation of papers, and
- shares knowledge and experience through open discussion and problem solving.

Each session chairman encourages questions from the audience after each presentation.

Goals:

The workshop brings together those people who use transducers to identify problems and to suggest some solutions, identifies areas of common interest, and provides a communication channel within the community of transducer users. Some examples are

Vehicular
Transd...
Range C...
Telemet...

- improve the coordination of information regarding transducer standards, test techniques, evaluations, and application practices among the national test ranges, range users, range contractors, other transducer users, and transducer manufacturers;
- encourage the establishment of special sessions so that attendees with measurement problems in specific areas can form subgroups and remain to discuss these problems after the workshop concludes; and
- solicit suggestions and comments on past, present, and future Vehicular Instrumentation/Transducer Committee efforts.

General Chairman:
John T. Ach
Wright Research and Development Center, WRDC/FIBGA
Wright-Patterson AFB OH 45433-6523
(513) 255-5200
(AUTOVON) 785-5200

PROGRAM

MONDAY, JUNE 19, 1989

2000   Social Hour, at the Cocoa Beach Hilton, courtesy of the Vehicular Instrumentation/Transducer Committee
All attendees welcome!

TUESDAY, JUNE 20, 1989

0730   Registration
0800   JOHN ACH, General Chairman
15th Transducer Workshop
Welcome: Eastern Space and Missile Test Center Representative
Introductions: LEROY BATES
Chairman Vehicular Instrumentation/Transducer Committee RCC/TG
0845   Session 1: Calibration Techniques
Chairman: RICHARD TALMADGE
Wright Research and Development Center
Cochairman: P. HARVEY
U.S. Army Yuma Proving Ground
- "Two Wire Automatic Remote Sensing and Evaluation System"
E.A. DAHL and LEROY BATES
Naval Ship Weapon Systems Engineering Station
- "Evaluation of a Digital Dead Weight Tester",
J.R. MILLER
U.S. Army TMDE Support Group

- "Development of Prototype System for the Impulse Calibration of Microphones"
DAVID L. MULLENDORE
Dayton Scientific, Inc. and
RICHARD D. TALMADGE
Wright Research and Development Center
1015   Break
- "Concurrent Accelerometer Calibration Utilizing Rigid Body Assumptions"
MICHAEL J. LALLY
University of Cincinnati
- "Comparison of Wide Band Back-to-Back and Interferometric Vibration Transducer Calibration"
TORBEN R. LIGHT and ERNST SCHONTHAL
Bruel & Kjaer Instruments, Inc.
- "Large High Explosive Driven Flyer Plate Technique for the Calibration of Soil Stress and Motion Instrumentation"
JOSEPH D. RENICK and GORDON H. GOODFELLOW
Air Force Weapons Laboratory
- "Performance Evaluation of Piezoelectric Accelerometers Using a FFT Based Vibration Transducer Calibration System", minipaper
ERNST SCHONTHAL and TORBEN R. LIGHT
Bruel & Kjaer Instruments, Inc.
1200   LUNCH
1330   Session 2: Applications
Chairman: MARTHA P. WILLIS
Rockwell/Rocketdyne Division
Cochairman: PETER K. STEIN
Stein Engineering Services, Inc.
- "An Increased Accuracy, Dual Channel Telemetry Accelerometer"
ROBERT HARTZELL and ROBERT GATCHEL
Columbia Research Laboratories, Inc.
- "A Microwave Transducer for Measuring Piston and Projectile Velocities in a Two-Stage Light-Gas Gun"
LUCIEN NAPPERT
Defence Research Establishment Valcartier National Defence, Canada
- "Built-in Mechanical Filter in a Shock Accelerometer"
ANTHONY S. CHU
Endevco Corp.
- "A Pressure Transducer to Measure Blast-Induced Porewater Pressure in Water Saturated Soil", minipaper
DR. WAYNE A. CHARLIE
Colorado State University
1515   Break

- "Difficulties/Remedies in Pressure Measurements
  With Piezoresistive Sensors"
  STEVEN NICKLESS and R. MAGLIC
  Honeywell Solid State Electronics
- "The PVF2 Piezoelectric Polymer Shock Stress
  Sensor — Some Techniques for Application Under
  Field Test Conditions"
  R.P. REED and J.I. GREENWALL
  Sandia National Laboratories
- "Piezoelectric Polymer Shock Gauge Applications"
  L.M. LEE
  KTECH Corporation
- "Selected Time Histories and Power Spectral
  Densities of Environmental Data Taken on the Smart
  Radar at the Army Proving Grounds Yuma, Arizona
  During March 1988", minipaper
  WESLEY PAULSON
  Naval Ship Weapon Systems Engineering Station

WEDNESDAY, JUNE 21, 1989

0830   Session 3: Tutorials
        Chairman ROBERT M. WHITTIER
        Endevco
        Cochairman: LAWRENCE M. SIRES
        Naval Weapons Center
- "Grounding and Shielding for Instrumentation
  Systems"
  GORDON DEAN
  Pacific Instruments
- "Dynamic Measurements Are Seldom Routine"
  JIM LALLY
  PCB Piezotronics, Inc.
1030   Break
- "The Successful Engineering of Measurement
  Systems"
  DR. PATRICK WALTER
  Sandia National Laboratories
1200   Lunch
1300   Tour of Space Center
1830   No-Host Social Hour at Hotel
1930   Banquet at Hotel

THURSDAY, JUNE 22, 1989

0830   Session 4: Data Acquisition
        Chairman: WILLIAM M. SHAY
        Lawrence Livermore National Laboratory
        Cochairman: MELTON A. HATCH
        EG & G/EM

- "A Computer Programmable Transducer Micro Circuit
  RICHARD D. TALMADGE
  Wright Research and Development Center and
  KENNETH APPLEY
  Vibra-Metrics, Inc.
- "A Remote Sensor/Cable Identifier"
  WILLIAM H. ANDREWS JR. and STEVEN P. BAKER
  Oak Ridge National Laboratory
- "Voice Activated Hot Mic."
  SIDNEY R. JONES Jr.
  Naval Air Test Center
- "Improving the Response Time and Accuracy of
  Transient Thermal Measurements in Live Fire Testing
  (LFT)", minipaper
  JAMES G. FALLER
  U.S. Army Aberdeen Proving Ground
1015   Break
- "A Very Wide Dynamic Range Data Acquisition
  System"
  JACK R. CARREL
  EG&G, Inc.
- "Shock Response of Second Order Dynamical
  Systems"
  DR. G.A. ARTICOLO
  Schaevitz Engineering and Rutgers University
- "In Search of More Output — Two Strain Gage
  Bridge Circuits Revisited"
  ROGER NOYE and JOHN KALNOWSKI
  EG&G, Inc.
- "The Nyquist Sampling Criterion: You Don't Always
  Have To Obey It, But When You Do, It's Worse Than
  You Think!", minipaper
  PETER STEIN
  Stein Engineering Services, Inc.
1200   Lunch
1330   Wrap Up Session

GENERAL INFORMATION

This Fifteenth Transducer Workshop will be held 20 - 22
June 1989 at the Cocoa Beach Hilton in Cocoa Beach, Florida.
The hosting agency is the Eastern Space and Missile Center,
Patrick AFB FL.

Registration

The registration consists of a completed registration
form, a written "Murphyism" and a fee of $80.00 (payable in
advance or at the door).

A "Murphyism" can describe any measurement attempt that went astray with the objective of learning from our errors and keeping our feet on the ground. It should be something generic rather than common human oversight; something from which we can learn. The tone should be anonymous to not embarrass any person, organization, or company. While a "Murphyism" is not a mandatory requirement, submissions are strongly encouraged, and the best will be included in the program.

Advance registration is desirable. Please use the enclosed registration form, include a check or money order for $80.00 payable to the Fifteenth Transducer Workshop, and mail to the Workshop Registration Chairman by 26 May 1989. (Note: Purchase orders are not acceptable.)

Hotel Accommodations

The official hotel for the Workshop is the Cocoa Beach Hilton, 1550 North Atlantic Avenue, Cocoa Beach, Florida 32931. A fixed block of rooms has been reserved at the special rates indicated on the enclosed hotel registration card. Early hotel reservations are strongly encouraged. Hotel registrations must be received by 26 May 1989.

No formal program will be provided for spouses or guests; however, they will be most welcome at the Social Hour on Monday and the banquet on Wednesday ($20.00 additional per guest for the dinner). Note: Final count for the banquet must be known by 11:00 a.m., 20 June 1989.

Tour—Wednesday Afternoon

A tour of the Space Center is planned for Wednesday, 21 June 1989. Please indicate on the registration form if you will be accompanied by guests so that adequate transportation may be provided.

Format and Background

Workshops are just what the name implies! Everyone should come prepared to contribute something from his knowledge and experience. In a workshop, the attendees become the program in the sense that the extent and enthusiasm of their participation determines the success of the workshop.

Participants will have the opportunity to hear what their colleagues have been doing and how it went; to explore areas of common interest and common problems; to offer ideas and suggestions about what is needed in transducers, techniques, and applications. Several instrumentation experts have been invited to give presentations

Additional Information

May be obtained from the General Chairman or,

Committee Chairman and Workshop Treasurer
LEROY BATES
NSWSES CODE 4R8
Port Hueneme CA 93043-5007
(805) 984-0445, Ext 7568
(AUTOVON) 360-0445, Ext 7568

Facilities and Registration Chairman
RICHARD T. HASBROUCK
Lawrence Livermore National Laboratory
P.O. Box 808, L-154
Livermore, CA 94550
(415) 422-1256
FTS 532-1256

Paper Chairman
RAYMOND FAULSTICH
c/o Naval Air Test Center
Range Directorate, Bldg 1492
Patuxent River, MD 20670-5304
(301) 863-1567
(AUTOVON) 356-1567

LIST OF ATTENDEES

Ach, John
WRDC/FIBGA
Wright-Patterson AFB, OH 45385-6553
(513) 255-5200

Appley, Kenneth
Vibra-Metrics, Inc.
1014 Sherman Ave.
Hamden, CT 06514
(203) 288-6158

Banks, Daniel
Naval Weapons Center
Code 3292
China Lake, CA 93555

Bates, LeRoy
NSWSES
Code 4R13
Port Hueneme, CA 93043-5007
(805) 984-0445

Billia, Richard
Lawrence Livermore National Labs.
P.O. Box 808, M/S L-113
Livermore, CA 94550
(415) 423-3400

Budenstein, David
3246 Test Wing/TFES-1
Bldg. 100
Eglin AFB, FL 32542
(904) 882-2997

Amos, Archie
6521 RANS/RE
Edwards AFB, CA 93523-5000
(805) 277-2785

Baker, Steven
Oak Ridge National Laboratory
P.O. Box 2009
Oak Ridge, TN 37831-8066
(615) 574-5687

Bartlett, Gary
Naval Weapons Center
Code 3143
China Lake, CA 93555
(619) 939-5942

Bean, Vern
National Bureau of Standards
A55 MET
Gaithersburg, MD 20899
(301) 975-4830

Brady, Leo
Sandia National Laboratories
P.O. Box 238
Mercury, NV 89023
(702) 295-3928

Bullock, Charles
Aberdeen Proving Ground
Ballistic Research Lab.
ATTN: SLCRR-IB-B
Aberdeen, MD 21005-5066
(301) 278-4616

Cardwell, William
General Electric Company
1 Neumann Way, M/S E-44
Cincinnati, OH 45215
(513) 243-9363

Charlie, Wayne
Colorado State University
Dept. of Civil Engineering
AF Eng. Service Center
Fort Collins, CO 80523
(303) 491-5048

Cooley, William
Endevco Inc.
Suite 304A
1849 Old Bayshore Hwy
Burlingame, CA 94010
(415) 697-9887

Dahl, Ernest
NSWSES
Port Huenueme, CA 93043
(805) 982-3151

Doretti, William
Pratt & Whitney Aircraft Group
P.O. Box 109600, M/S 731-64
West Palm Beach, FL 33410-9600
(407) 796-3015

Carrell, Jack
EG&G Energy Measurements, Inc.
P.O. Box 1912, M/S S-05
Las Vegas, NV 89125
(702) 295-2928

Chu, Anthony
Endevco, Inc.
30700 Rancho Viejo Road
San Juan Capistrano, CA 92675
(714) 493-8181

Crounse, Dave
AFFTC
6510 Test Wing/TSID
Edwards AFB, CA 93523-5000
(805) 277-2976

Dean, Gordon
Pacific Instruments
215 Mason Circle
Concord, CA 94520
(415) 827-9010

Duda, Leonard
Sandia National Laboratories
P.O. Box 5800, Org. 7116
Albuquerque, NM 87185
(505) 844-1570

Faller, Dr. James
U.S. Army Combat Systems Test Act.
317 Wilson Road
Newark, DE 19711
(301) 278-4461

Faulstich, Raymond
Naval Air Test Center
Range Directorate AID (RDCC)
Patuxent River, MD 20670-5304
(301) 863-1567

Gates, John
Boeing Aerospace - KSC
2907 N. Indian River Road
Cocoa, FL 32922
(407) 867-3475

Gilcrease, Billy
Boeing Commercial Airplanes
P.O. Box 3707, M/S 47-06
Seattle, WA 98124
(206) 655-8582

Goodfellow, Gordon
Weapons Laboratory WL/NTEDS
Kirkland AFB, NM 87117
(505) 846-7204

Greenwoll, James
Sandia National Laboratories
P.O. Box 5800, Org. 7116
Albuquerque, NM 87185
(505) 844-8993

Harvey, Robert
U.S. Army Yuma Proving Ground
STEYO-MT-TE-T
Yuma, AZ 85365

Hatch, Melton
EG&G Energy Measurements, Inc.
P.O. Box 9051, M/S A-5
Pleasanton, CA 94566
(415) 847-1371

Gates, Robert
Boeing - KSC
BAO - FA56
Kennedy Space Center, FL 32899
(407) 867-3475

Gillingham, Fred
Pacific Missile Test Center
Point Mugu, CA 93042
(805) 989-8644

Granath, Ben
PCB Piezotronics, Inc.
3425 Walden Ave.
Depew, NY 14043
(716) 684-0001

Hartzell, Robert
Columbia Research Labs
Woodlyn, PA 19094
(215) 872-3900

Hasbrouck, Richard
Lawrence Livermore National Labs.
P.O. Box 808, M/S L-154
Livermore, CA 94550
(415) 422-1256

Zhu, Hongsheng
VAMC Rehab
Muwauk, WI

Henry, Dennis
Physical Science Laboratory
New Mexico State University
P.O. Box 30002
Las Cruces, NM 88003
(505) 522-9225

Hoge, Larry
Pacific Missile Test Center
Code 1063, Bldg. 362
Point Mugu, CA 93042
(805) 989-8644

Johnson, Thomas
Naval Ordnance Station
Code 3410N
Indian Head, MD 20540-5000
(301) 743-4153

Judd, John
Vibra-Metrics
1014 Sherman Ave.
Hamden, CT 06514
(203) 288-6158

Klingaman, Kenneth
U.S. Army ARDEC
Picatinny Arsenal, B-382
Dover, NJ 07840
(201) 724-4531

Krizan, Richard
ESMC/DVEC
Patrick AFB, FL 32937
(407) 494-5107

Kuehn, Stephen
Sandia National Laboratories
P.O. Box 5800, Org. 2543
Albuquerque, NM 87185-5800
(505) 846-7449

Hueckel, John
Pacific Instruments, Inc.
215 Mason Circle
Concord, CA 94520
(415) 827-9010

Jones, Sidney
Navy (RDCB)
P.O. Box 320
Patuxent River, MD 20670

Kalinowski, John
EG&G Energy Measurements, Inc.
P.O. Box 9051, M/S A-5
Pleasanton, CA 94566
(415) 847-1355

Kramer, Don
Pacific Missile Test Center
Code 1063, Bldg 362
Point Mugu, CA 93042
(805) 989-8644

Kubler, John
Kistler Instrument Corporation
75 John Glenn Drive
Amherst, NY 14120
(716) 691-5100

Lally, James
PCB Piezotronics, Inc.
3425 Walden Ave.
Depew, NY 14043
(716) 684-0001

Lally, Michael
PCB Piezotronics, Inc.
3425 Walden Ave.
Depew, NY 14043
(716) 648-0001

Leisher, William
Sandia National Laboratories
P.O. Box 5800, Org. 7241
Albuquerque, NM 87185-5800
(505) 844-2755

Mentzer, James
3246 Test Wing/TFES
Bldg 100
Eglin AFB, FL 32542
(904) 882-2995

Miller, Jim
U.S. Army TMDE Support Group
AMXTM - DP
Redstone Arsenal
Huntsville, AL 35898

Mullendore, David
Dayton Scientific, Inc.
92 Westpark Court
Dayton, OH 45459
(513) 433-9600

Nicholson, Rickey
Vitro Technical Services, Inc.
P.O. Box 1898
Eglin AFB, FL 32542-1898
(904) 882-5188

Lee, Larry
Ktech Corp.
901 Pennsylvania N.E.
Albuquerque, NM 87110
(505) 268-3379

Lyman, Charles
Endevco
20 Holmes St.
Mystic, CT 06355
(203) 572-0571

Merritt, James
Boeing Aerospace Ops
FA-56
Kennedy Space Center, FL 32899
(407) 867-3475

Moeller, Al
EG&G Energy Measurements, Inc.
P.O. Box 1912, M/S N-28
Las Vegas, NV 89125
(702) 295-2516

Nappert, Lucien
Defense Research Establishment
2459 PIE XI North
P.O. Box 8800
Courcelette, QUE GOAIRO
(418) 844-4380

Nickless, Steve
Honeywell
1150 Cheyenne Mtn Blvd.
M/S 30007
Colorado Springs, CO 80918
(419) 540-1159

Noyes, Roger
EG&G Energy Measurements, Inc.
P.O. Box 1912, M/S N-28
Las Vegas, NV 89125
(702) 295-2516

Phillips, Van
Nashville State Technical Institute
120 White Bridge Rd.
Nashville, TN 37209

Ralton, John
Applied Measurement AUST/L
Box 159
Oakleigh, Victoria, CANADA 3166
(613) 568-0588

Reed, Bobby
U.S. Army Corps Eng.
Waterways Exp. Sta., WES-JD
Vicksburg, MS 39180-0631
(601) 634-2575

Reid, Dennis
EG&G Energy Measurements, Inc.
P.O. Box 9051, M/S A-5
Pleasanton, CA 94526
(415) 847-1364

Rhodes, Eric
NASA, PT-AST
Kennedy Space Center, FL 32899
(407) 867-2780

Paulson, Wes
NSWSES
Code 4L00
Point Hueneme, CA 93047
(805) 982-3751

Provost, Thomas
AFESC
Tyndall AFB, FL 32401
(909) 283-2960

Rapp, Donald
U.S. Geological Survey, HIF
Bldg. 2101, M/S 1535
Stennis Sp Cen, MS 39529
(601) 688-1535

Reed, Ray
Sandia National Laboratories
P. O. Box 5800, Org. 7116
Albuquerque, NM 87185-5800
(505) 844-6377

Rempert, Lawrence
Allison Gas Turbine
Div. of GM, W2A
P.O. Box 420
Indianapolis, IN 46206
(317) 230-4068

Rogers, Thomas
U.S. Army Airborne & Special
  Operations Test Board
Ft Bragg, NC 28307
(919) 776-8480

Samoian, Ronald
Lawrence Livermore National Labs
P.O. Box 808, M/S L154
Livermore, CA 94550
(415) 422-8814

Shay, William
Lawrence Livermore National Labs.
P.O. Box 808, M/S L-354
Livermore, CA 94550
(415) 422-7044

Sires, Lawrence
Naval Weapons Center
Code 6213
China Lake, CA 93555-6001
(619) 939-7404

Talmadge, Richard
WRDC/FIBGA
Wright-Patterson AFB, OH 45433-6553
(513) 255-5200

Turner, John
Microspec
999 Woodcock Rd
Suite 108
Orlando, FL 32803
(407) 898-3504

Tustin, David
Naval Air Test Center
RDHA
Patuxent River, MD 20670
(301) 863-1609

Schonthal, Ernst
Bruel & Kjaer Instruments, Inc.
185 Forest Street
Marlboro, MA 01752
(617) 481-7000

Shelley, Sidney
Munitions Systems Division
3246 Test WG/TFRL
Eglin AFB, FL 32542
(904) 882-4481

Stein, Peter
Stein Engineering Services, Inc.
5602 E. Monterosa
Phoenix, AZ 85018
(602) 945-4603

Terrell, John
AVL North America, Inc.
P.O. Box 36438
Tucson, AZ 85740
(602) 888-0002

Tussing, Ronald
Naval Surface Weapons Center
White Oak Laboratory - R15
Silver Spring, MD 20903-5000
(202) 394-1187

Walter, Dr. Patrick
Sandia National Laboratories
P. O. Box 5800, Org. 7523
Albuquerque, NM 87185-5800
(505) 844-5226

Watts, David
Air Force Armament Laboratory
AFATL/AGI
Eglin AFB, FL 32542
(904) 882-5375

Whittier, Robert
Endevco Corporation
30700 Rancho Viejo Road
San Juan Capistrano, CA 92675
(714) 493-8181

Xavier, William
EG&G Energy Measurements, AVO
P.O. Box 9051, M/S A-1
Pleasanton, CA 94566
(415) 847-1355

Wheeler, Vernon
Lawrence Livermore National Labs.
P.O. Box 808, M/S L-221
Livermore, CA 94550
(415) 422-7436

Willis, Martha
Rockwell/Rocketdyne Division
6633 Canoga Ave.
Canoga Park, Ca 91303
(818) 710-4864

SESSION 1

CALIBRATION TECHNIQUES

TWARSES-TWO WIRE AUTOMATIC REMOTE SENSING AND EVALUATION SYSTEM

Ernest A. Dahl And Leroy Bates
Naval Ship Weapon Systems
Engineering Station (NSWSES)
Port Hueneme, CA 93043-5007

ABSTRACT

This paper discusses an Automatic Monitoring System (AMS) which provides sensing and monitoring capability to indicate the conditions at any number of sensors at remote location using a common 2 wires which uniquely provides sensor power, sensor identification and sensor performance evaluation. The system consists of a Scanner Display Panel Module (SDPM) panel and up to 144 individual transponders connected by a two-conductor signal bus. Depending on the configuration up to eight transducer parameters can be measured at each location and monitored at the SDPM. The AMS includes Micro Processer Based SDPM which is located remotely from the transponder module and its associated transducer. Capability is available to monitor up to 1152 transducer sensors utilizing a frequency-shift-keyed signal to sequentially interrogate each individual transponder and using FM modulated tone responses to transmit data back to the monitoring module. A display panel provides an LED cell-fault matrix that indicates transducer status and alarm when an out-of-tolerance condition exists. Specific sensor parameter values may be displayed for any selected individual location with the out-of-tolerance parameter identified. The built-in printer provides capability for hard copy location parameters.

SYSTEM DESCRIPTION - AUTOMATIC MONITORING SYSTEM

The Automatic Monitoring System (AMS), Figure 1, provides sensing and monitoring capabilities to indicate sensor conditions for any type data where a sensor (either passive or active) can be installed. The capability to monitor any number of sensor utilizing a Frequency-Shift-Keyed signal to sequentially interrogate each individual location. Modulated tone responses (FM) transmit data back, including out-of-tolerance responses. The system consists of a SDPM, Figure 2, and individual transponder connected by a two-conductor signal bus. The SDPM is remotely located from where the transponder probes are installed. Location of sensors depending on the measurement configuration, up to eight parameters can be measured at each location and monitored at the SDPM.

The SDPM panel display provides and LED cell-fault matrix, Figure 3, that indicates an out-of-tolerance condition at any location. Specific parameter values may be displayed for any selected individual location, with the out-of-tolerance parameter identified.

A built-in-printer provides capability for hard copy of transponder/location parameters.

SCANNER/DISPLAY/PRINTER MODULE

a. Converts line voltage to the required DC voltages for the data processing and display functions.

b. Sequentially interrogates each separate transponder, one transponder for up to eight sensors.

c. Compares the averaged data received from the transponders against established limits and initiates an alarm if the limits are out of specifications.

d. Displays selected parameters and alarm indicators.

e. Prints out data parameters automatically or on command including date and time of day.

The front panel of the SDPM contains a combined power ON/OFF switch. Display matrix for all location and Industrial Readout from any location. Printer and key-board to change data limits and request print out time and other program requirement.

Power supplies, telemeter electronics, data processors, and memories are contained within he metal case. Three connectors provide interfaces for power, signal bus, and remote output including RS-232.

The display, Figure 4, provides both fault monitoring and individual location monitoring with built-in test validation. If one or more individual cell's parameters are out-of-tolerance, and LED will be illuminated in all-cell matrix display. At the same time, a parameter fault light

ABMS SCANNER/DISPLAY

2 WIRE POWER/DATA BUS

SAFTEY STATUS
MODULE

SMOKE DETECTOR
BATTERY VOLTAGE
BATTERY CURRENT
CURRENT DIRECTION
AMBIENT TEMPERATURE

SUMP LEVEL

STATUS MODULES

STATUS MODULES

CELL VOLTAGE
CELL TEMPERATURE
CELL SPECIFIC GRAVITY
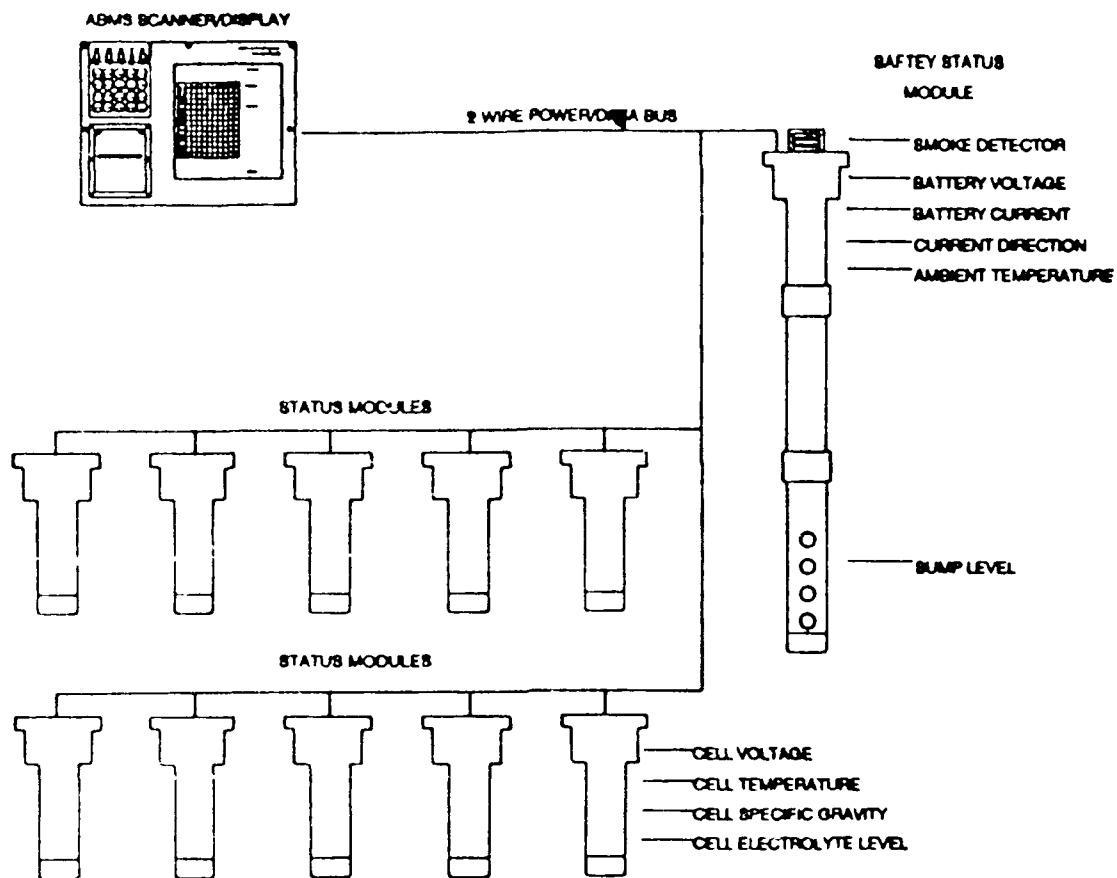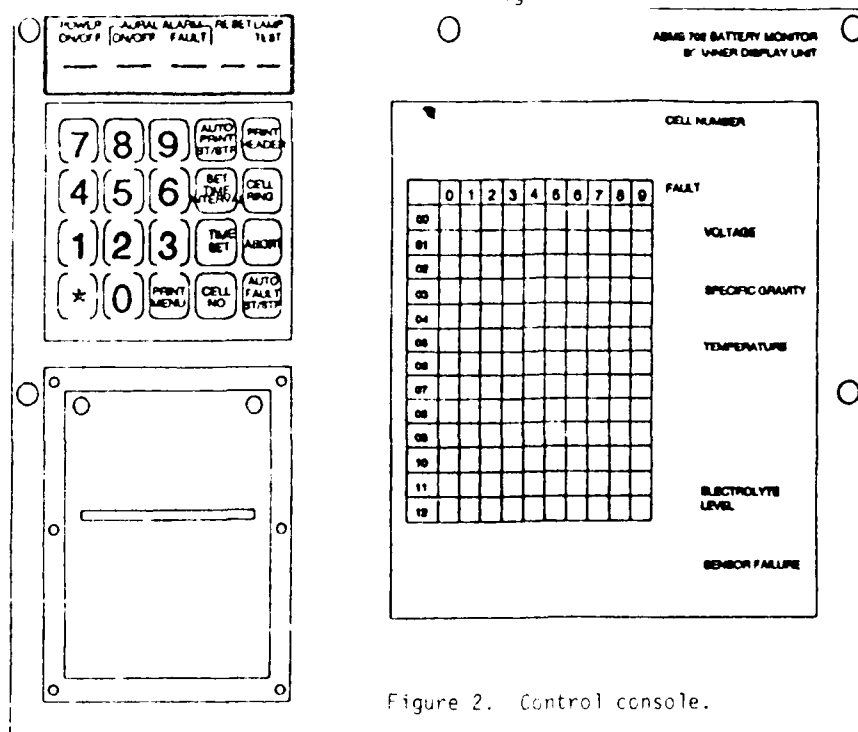CELL ELECTROLYTE LEVEL
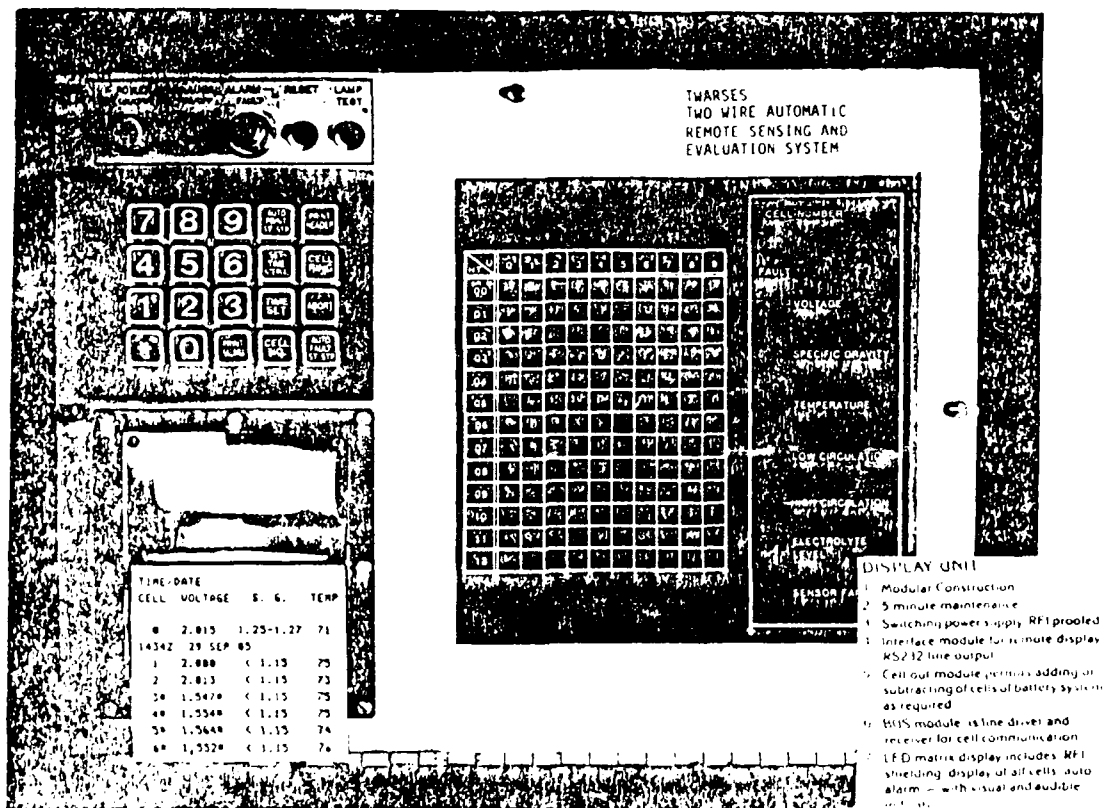
Figure 1

Figure 2. Control console.
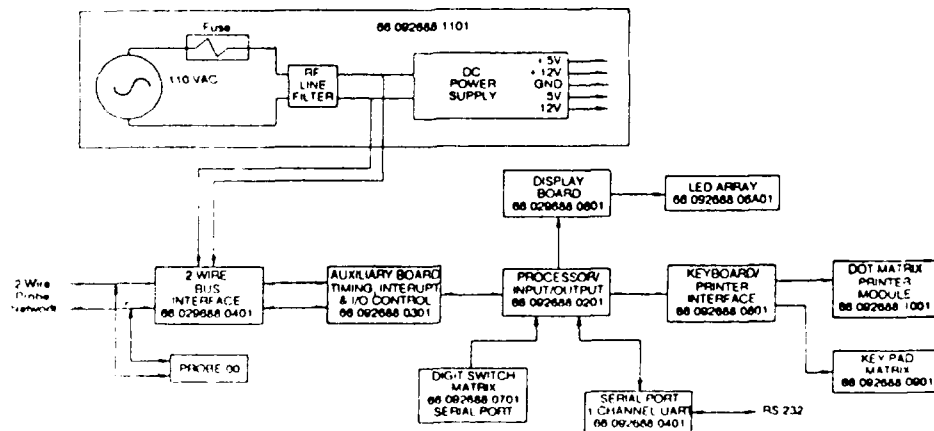
4

Figure 3

Figure 4

will be illuminated in the single location display along with indication of the number of the location being monitored and the parameter values for the sensors at each cell with the fault indicating the specific fault.

The built in printer can be commanded to print parameters for all location or only the selected location being monitored on the single location display. Print can also be programmed for periodic readout and for automatic readout at the time of a fault determination. A plug and interface is provided for RS-232 bus to use either a modem or computer interface.

TRANSPONDER SENSOR MODULE GENERAL DESCRIPTION

The Individual Transponder Sensor Modules and the central unit of the system are connected by a 2-wire signal bus. The Transponder Sensor Modules are wired in parallel on the bus. Communication between the central unit and Transponder Sensor Modules is done according to a cycle that is repeated at regular intervals. The module is shown in Figure 5.

During a communication cycle, the individual Transponder Sensor Modules are sequentially activated and interrogated by means of a frequency-shift-keyed signal (FSK) that is generated by the central unit. Each Transponder Sensor Module responds to a unique address as selected by preset switches. The interrogate command is formatted by the central unit into data between 62.5 kHz and 125 kHz signals. The 62.5 kHz provides the clocking out to the Transponder Sensor Module. The 125 kHz is a digital timing word that includes an identification address, a data parameter request, a data duration request, and a blank time period for returning data.

The data from the Transponder Sensor Module is sent back to the central unit by a frequency modulated signal in the range of 20 to 40 kHz. Technical specifications, description, and operating instructions for the central unit are provided in a separate manual.

TRANSPONDER SENSOR MODULE FUNCTIONAL DESCRIPTION

The TP-129 Transponder Sensor Module has a single circuit board with two functional blocks. The Power, Communication, and Control Block consists of a module, address selection switches, bus isolation transformer, and connector. The Measurement Block consists of a relative humidity sensor, temperature sensor, and low power signal conditioning electronics for both sensors. Figure 6 shows the functional diagram of the module.

Power, Communication, and Control Block

a. The module integrates the following functions in one VLSI chip. The incoming interrogate signal, FSK 62.5 kHz to 125 kHz, is taken off the bus transformer and routed to two rectifiers to produce unregulated 12 VdC. This is used to load two 470 micro Farad capacitors that are connected to the module. These capacitors provide the energy required by the module itself

and by the conditioning electronics circuit. During the time that the interrogate command is off, the capacitor voltage decreases to approximately 8 VDC.

The incoming signal is also decoded and passed to the device address comparator. If the address corresponds to the code preset on the TP-129 switches, the module activates a regulated 6 VDC/2 mA output to power the conditioning electronics. The activation time depends on the instructions coded in the interrogate signal. The module has eight inputs that can interface with the voltage outputs (1-3 VDC) provided by one or several conditioning electronics. In the case of the Standard Missile Sensor Module, only two inputs are being used (humidity and temperature). The remaining six inputs are available on the connector for future use. During a communication cycle, data from the eight inputs is sequentially transmitted back to the bus transformer, according to the instructions of the interrogate command.

Measurement Block

b. The relative humidity sensor is a Rotronic HYGROMER C83 capacitive sensor. The temperature sensor is a Texas Instruments silicon sensor model TMP 100F.

The conditioning electronics circuit is powered with the 6 VDC regulated voltage supplied by the module. The circuit draws a maximum of 2 mA. The two linear DC voltage outputs have a range of 1-3 V, corresponding to 0-100% Relative Humidity (RH) and 40-120 deg.F. The circuit must be powered during 50 to 100 msec to provide correct output signals.

HUMIDITY SENSOR DESCRIPTION

The HYGROMER humidity sensor is a small hygroscopic capacitor that modifies its value as a function of both the water vapor pressure and temperature of the environment. This permits direct measurement of relative humidity after precise calibration of the sensor with National Bureau of Standards (NBS) references.

a. Sensor Design. HYGROMER sensors consist of a thin strip of hygroscopic polymer enclosed between two porous electrodes. This design enables the interchange of water molecules through both surfaces of the sensor. Other capacitive sensors use a non-porous or non-hygroscopic substrate that supports a thin film of polymer and a set of electrodes. Because of this substrate, water molecules are essentially absorbed through only one surface of the sensor.

b. Performance. Both the mechanical design of the HYGROMER sensors and the nature of the polymer used in the sensors, provide faster and more uniform absorption of moisture than in conventional sensors. Improvement of sensor performance is significant, especially at high humidity. Even when operated close to condensation for hours, the HYGROMER sensors do not show a sluggish response or 'creeping up' of the humidity signal. When humidity conditions are reduced, there is no requirement for a recovery period to return the
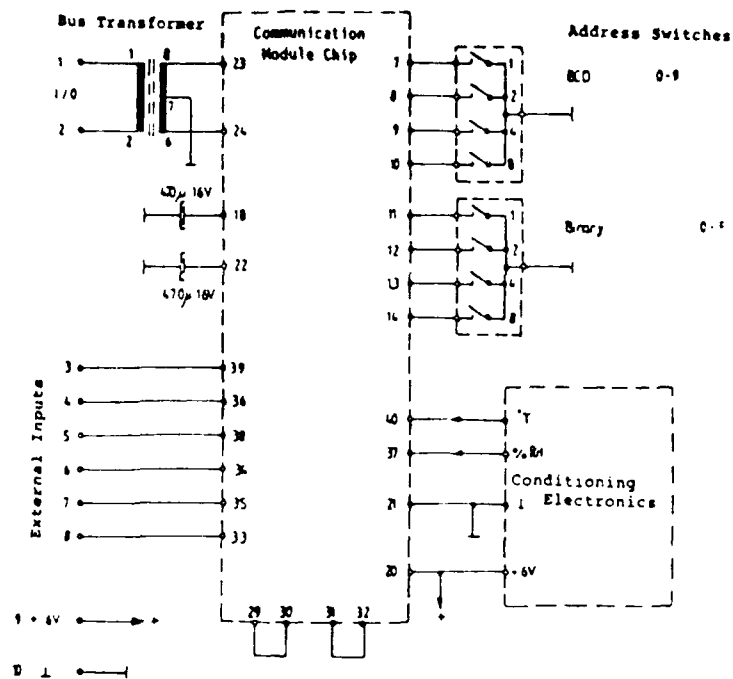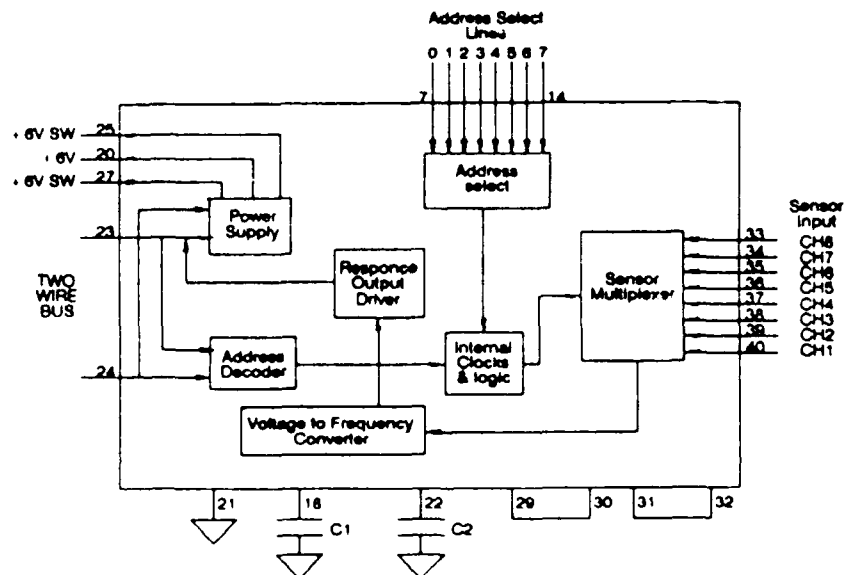
6

Figure 5

Figure 6

7

sensor to its original calibration. As a consequence, sensor hysteresis is exceptionally low and this results in excellent repeatability of measurements.

c. Greater Durability. Careful selection and control of the materials used during manufacturing result in a humidity sensor that resists condensation as well as a wide array of industrial contaminants. Elimination of the substrate used in most conventional capacitive sensors also contributes to greater sensor durability: the film of polymer and the substrate have very different mechanical characteristics and tend to separate under the combined effect of repetitive humidity and temperature cycles. In most applications, the projected lifetime of the HYGROMER humidity sensor exceeds 10 years.

d. Applications. Relative humidity is accurately measured from 0 to 100% RH with only one HYGROMER sensor. Instruments are available that operate at extreme temperatures of -50 to 150 deg.C at the sensor. Advanced filter technology permits use in dusty environments or even in marine environments. In addition, each HYGROMER sensor is fully encapsulated in a membrane filter for protection against dust and accidental contact.

e. Temperature Compensation of the Humidity Sensor. The physical characteristics of the hygroscopic materials (plastic or other) used in a sensor to measure humidity are affected both by humidity and temperature. Temperature also modifies the characteristics of the water molecules absorbed by the sensor. Sensor response to humidity is not the same at all temperatures. As a result, the accuracy of a humidity sensor is affected by temperature to an extent which varies with the level of humidity.

Conventional humidity measuring devices do not incorporate any compensation for the effect of temperature on the humidity sensor. Errors as large as 10% RH or more are quite common when temperature differs from the usual room conditions.

Based on precise sensor measurement at different humidity and temperature conditions, an electronic temperature compensation is employed. The compensation limits the temperature error to less than 3.5% RH over most of the temperature operating range of the sensor.

f. Accuracy. Accuracy of a sensor is a result of such characteristics as linearity, hysteresis, repeatability, temperature error etc. Testing done at NBS in the range of 11-96% RH and -20 to +10 deg.C confirms the basic statements made for linearity, hysteresis, and repeatability of the HYGROMER sensors (see Figure). Additional testing done by four laboratories at temperatures up to 150 deg.C for 120 hrs confirm both the resistance and stability of the sensors.

TEMPERATURE SENSOR DESCRIPTION

The Transponder Sensor Module utilizes a Texas Instruments Metal Insulated Silicon (MIS) ORM sensor.

This sensor is signal condition to provide 1-3V output for 40-120 deg.F. with a accuracy of + 1.5 deg. F. The sensor has long term stability of 0.5 deg.F. or better and provides accurate data within 10 seconds.

CALIBRATION OF THE TRANSPONDER SENSOR MODULE

a. Factory Calibration. Each transponder sensor module is carefully calibrated both for humidity and temperature. Because of the high sensitivity of relative humidity to temperature, calibration is done at room conditions that are stable to within 0.2 deg.C. At 25 deg. C, this provides an accuracy of +/-2% RH or better over the full range of humidity. Special calibration with a stability of 0.025 deg. C at temperatures close to 25 deg. C, is available. In this case, accuracy is +/- 1.5% RH or better over the full range of humidity. Even higher accuracy can be achieved over a limited range.

b. Field Calibration. The transponder sensor module can be calibrated in the field using a hand held battery operated ROTRONIC GT-L indicating probe (or equivalent) which displays both temperature and humidity. Humidity standards, carefully checked against NBS references, are used for rapid and accurate verification of instrument performance. For test and calibration purposes, the conditioning circuit can be permanently powered from an external + VDC regulated voltage source. Two potentiometers permit adjustment of the humidity output signal. The temperature output is adjusted with one potentiometer.

c. Stability. Under most conditions, the long term stability of the units is better than 1% RH and 0.5 deg.F. over a period of one year.

SUMMARY AND CONCLUSIONS

The use of this a common two wire communication bus between a central unit and up to 120 individual transponder sensor modules, using a unique method to provide remote power and the sensing of data requirements and reception of sensor data has been described in this paper. The system uniquely uses a FSK signal to activate the individual transponders and a voltage controlled oscillator for FM transmission of data from active sensors. Each remote transponder sensor unit can be located up to 500 meters from the scanner display unit. The system has been used for a variety of applications including Submarine Battery Monitoring (monitoring 120 battery cells with four or more parameters per cell), Stryker Missile System environmental monitoring, shipboard MX/LW missile container monitoring and shipboard machinery monitoring. Sensor parameters include pressure, humidity, temperature, vibration, specific gravity, and gases. The embedded microprocessor design of the central unit allows for automatic evaluation of the sensor data including out of tolerance conditions indications. A hard copy (paper) print of the data is provided for detailed evaluation by either programmed readout or sensor out of specification alarms.
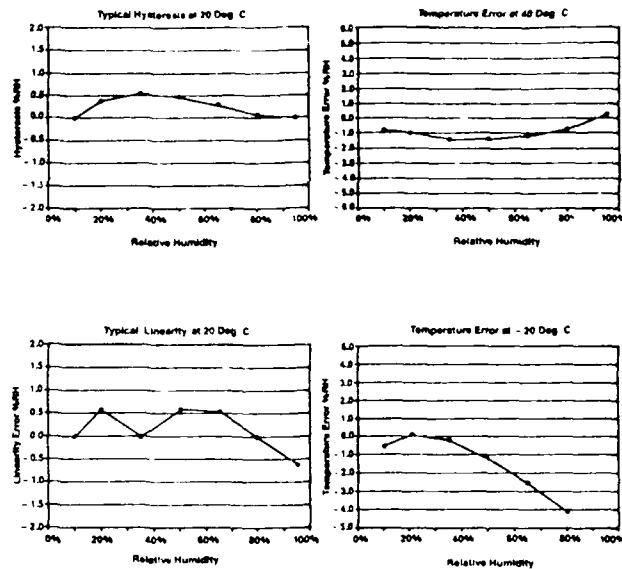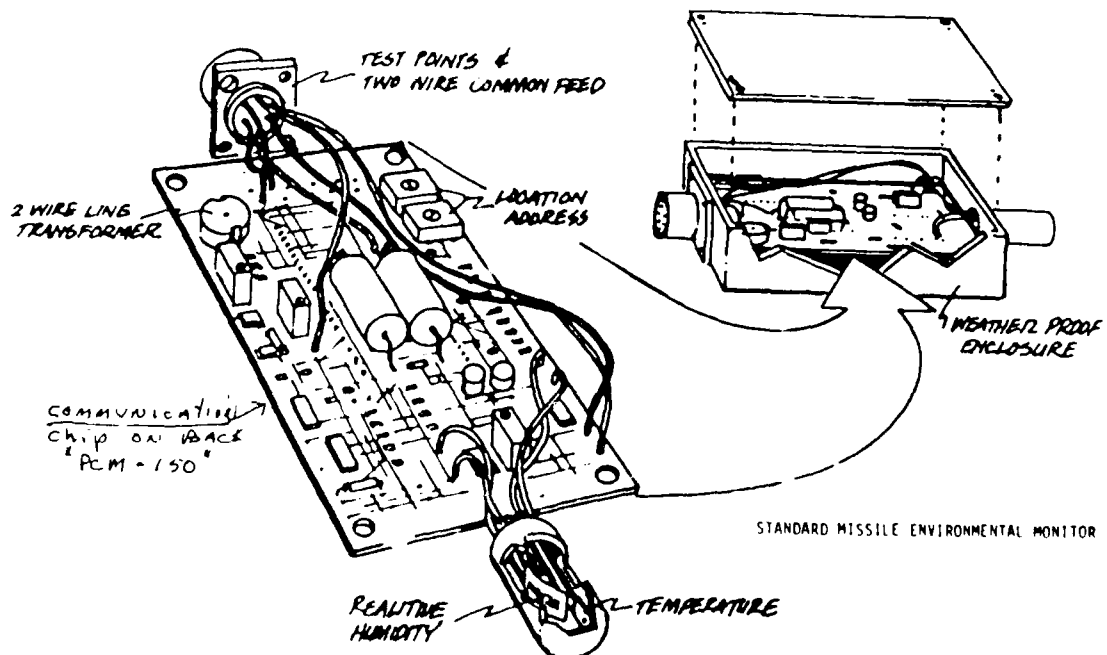
Figure 7. Hygromer sensor/electronics NBS test results.

TWO WIRE AUTOMATIC REMOTE SENSING AND EVALUATION SYSTEM

STANDARD MISSILE ENVIRONMENTAL MONITOR

9

TWO-WIRE AUTOMATIC REMOTE SENSING AND EVALUATION SYSTEM

Q: Steve Baker (Oakridge National Laboratories): The concept looks very novel, do you have any plans to commercialize it or get someone to commercialize it in the private sector?

A: Ernie Dahl: Anybody that wants it for the Navy or the Armed Forces can do anything they would like. The commercial use is undefined as yet because it has so many uses. There are companies in the San Francisco area that make the units and have asked for permission to sell it commercially. We said yes. And they are going to go ahead with it, but there is a license involved. It has an application; a hotel with a fire alarm and smoke system; you just put on two wires and run all the data you want from every area. There are lots of things you can do with it. It's three to four years old from concept to the hardware you see here. Also for Tomahawk containers, a meter is removed and a gas sensor screwed into its place. One of these sensors, by dispersion technique, will measure temperature, humidity and oxygen inside the container. Those are working now. There are standard missile units that measure humidity and temperature. So if you push the button that says cell read, you'll see it read out all six sensors. Each time it takes data, it reads out.

Q: Roger Noyes (EG&G, Inc.): You talked about taking real time data and you talked about making acoustic measurements. Can you talk a little bit about the response time of the system?

A: Ernie Dahl. When we fire a missile, real time data is data that can read off. The way the oscillograph is producing a record it takes a couple of microseconds or longer for the data to reproduce on the paper. That is still real time data. The way this is set now it can be programmed any way, it can be programmed so that when something goes wrong it immediately starts the alarm and does it, otherwise there is a delay of maybe two or three seconds in the data. It depends on how many probes are used and how the microprocessor is configured. There's a piece of paper on the back wall. If you look at that, it shows 128 cells reading out. It takes about 30 seconds to do the whole thing. The time element is restricted by the speed of the printer, not by the speed of the machine. That's why we've gone to a new printer that has five times the speed, prints in both directions and prints a little more data. We're talking about a concept. You can change it any way you want to get data.

EVALUATION OF A DIGITAL DEAD-WEIGHT TESTER

J.R. MILLER III and D. E. Woodliff
U.S. Army TMDE Support Group
Redstone Arsenal, AL 35898-5400

ABSTRACT

Evaluation of a commercially available digital dead weight tester is presented. This pneumatic instrument, using an electrical dynamometer, has been tested over its range and found to be very linear. Several important characteristics were tested such as hystersis, repeatability, temperature effects and vibration sensitivity. Direct dimensional measurements of cross-sectional areas allowed comparison with manufacturer's conversion constants which was within 1.9 or 100 ppm.

I. INTRODUCTION

Why a digital dead weight tester? What's the advantage?

To answer these questions one must be familiar with dead-weight testers--they are accurate standards for pressure measurement; however, they are manual instruments not capable of interfacing to a computer.

Since use of the computer is desired it would be good if a dead-weight tester, dwt, did have a digital output; one has recently been offered[1]. We have bought one of these instruments to see how good it operates.

This paper will present the results of our evaluation.

A simplified description of the instrument is given in the next section.

II. GENERAL DESIGN

The device uses precision piston-cylinders that are closely fitting to establish the cross-sectional area exposed to the pressure to be measured. The force caused by the pressure acting on the piston is measured by an electronic dynamometer (see Figure 1). The dynamometer not only measures the down-ward force, it also maintains the piston in the "float" position. There is a digital display on the front of the device. A small motor rotates the piston relative to the cylinder to eliminate static friction. The device is intended for pneumatic pressure measurements. There were two pressure ranges provided. The dynamometer has a full scale reading of 60,000 counts with a least reading of one count. Further details are given in Table 1.

EQUATION OF OPERATION

Since the dead weight tester equation* is

$$P = Mg\ (1-\rho a/\rho b)/(A_0\ 980.665\ (1+\alpha\Delta T) \qquad (1)$$

and the dynamometer is simply a device to measure the force where

$$F = Mg\ (1-\rho a/\rho b)/980.665 \qquad (2)$$

which when applied produces a number of counts hence

$$P/counts = F/(A_0(1+\alpha\Delta T)) = C/(1+\alpha\Delta T),\ psi/count. \quad (3)$$

Provided with the machine is a set of six 1 Kg weights, Class S2, very accurately known so that periodic checks can be made on the force measuring dynamometer.

III. EXPERIMENTAL RESULTS

A. LOW PRESSURE PISTON-CYLINDER

Using values provided by the manufacturer we compared the instrument (cross floated) with a pneumatic dwt 3905, P534-(21055). See Figure 2. The results were not satisfactory. This lead us on a journey to find out why this difference. The first thought was to check the dynamometer more thoroughly, i.e., check it between the 1 Kg points to make sure it was linear between these points. To do this we used up to 77 weight combinations using the CEC weights and the 1 Kg platters. The results were fit to a straight line using a least squares program. A plot of the residuals from this curve fit would then test the linearity. These results are shown in Figures 3 and 4. There is a peculiar pattern to some of these residuals and some are more than +1 count. This was not expected -- there was either

---
* Terms explained in Appendix.

TABLE 1. CHARACTERISTICS OF DIGITAL DEAD-WEIGHT TESTER

Range

Pressure: Depends on piston-cylinders (0 to 300 psi, 0 to 45 psi)

Force: 0 to 6 newtons

Counts: 0 to 60,000

Piston-cylinder (SN 269) A_o = 1.96106 cm^2 = 0.30396546 in^2 (manufacturer)

Piston-cylinder (SN 3397) A_o = 0.284414 cm^2 = 0.044084258 in^2 (manufacturer)

Temperature coefficient of A_o = 9 ppm/^{o}C

Piston-cylinder materials: Tungsten carbide

Piston-cylinder design: Re-entrant

Deformation coefficient: Insignificant (manufacturer)

A_o determination: Cross-floated (manufacturer)

Error limits $\pm$ (0.005% F.S. + 0.005% of reading) (manufacturer)

Weights: Class 2, true mass values (manufacturer)

TABLE 2. PREDICTED COUNTS VERSUS ACTUAL COUNTS

| Nominal Force	Applied Force, lb_f	Predicted Counts	Actual Counts	Actual-Predicted, Counts
1 lb_f	0.998798	4535.80	4536	0.2
1 lb_f + 1 Kg	3.201085	14536.97	14537	0.03
2 Kg	4.404576	20002.33	20002	-0.33
1 lb_f + 2 Kg	5.403374	24538.14	24538	-0.14
3 Kg	6.606861	30003.49	30003	-0.49
1 lb_f + 3 Kg	7.605659	34539.29	34539	-0.29
4 Kg	8.809148	40004.65	40004	-0.65
1 lb_f + 4 Kg	9.807946	44540.46	44540	-0.46
5 Kg	11.011435	50005.81	50005	-0.81
1 lb_f + 5 Kg	12.010233	54541.62	54542	0.38
6 Kg	13.213727	60005.98	60007	0.02
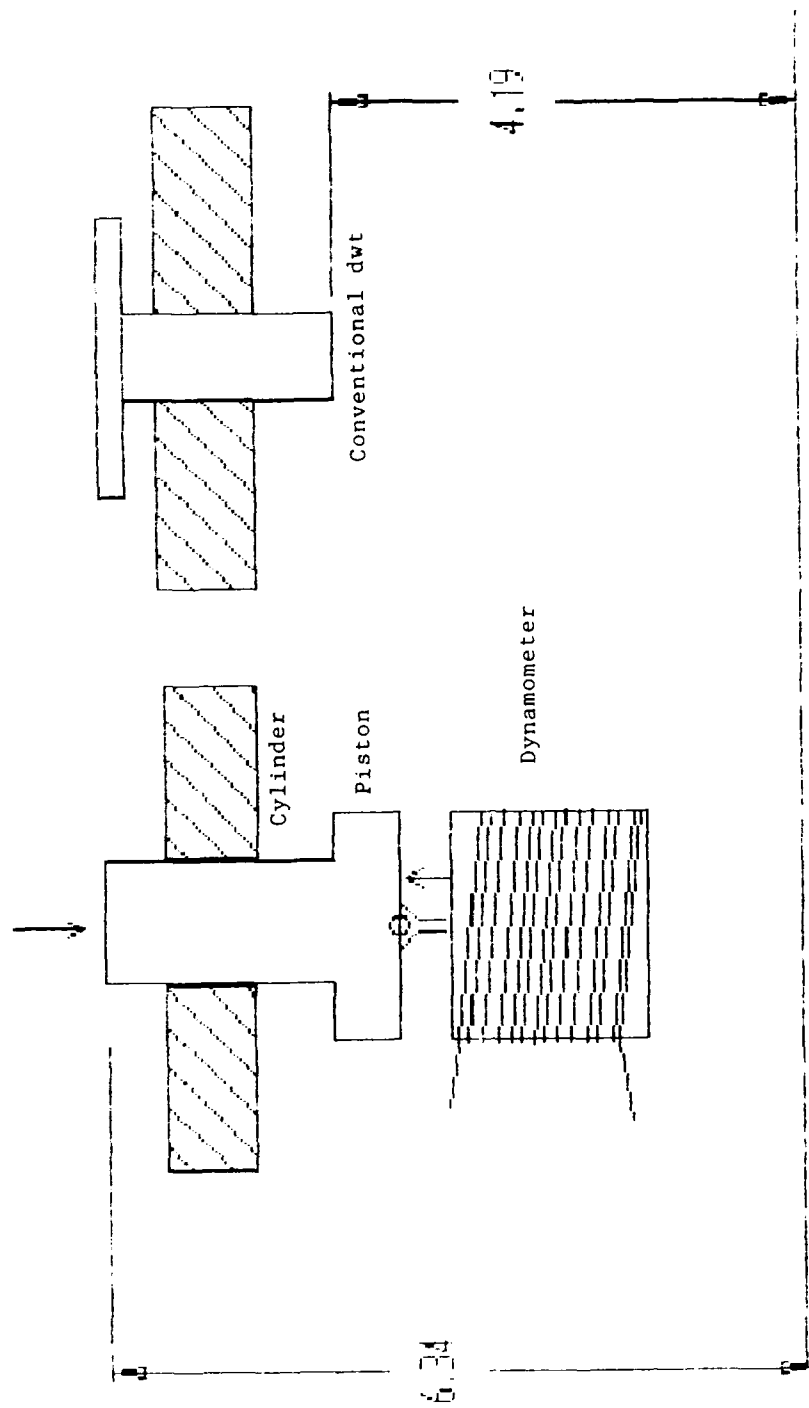
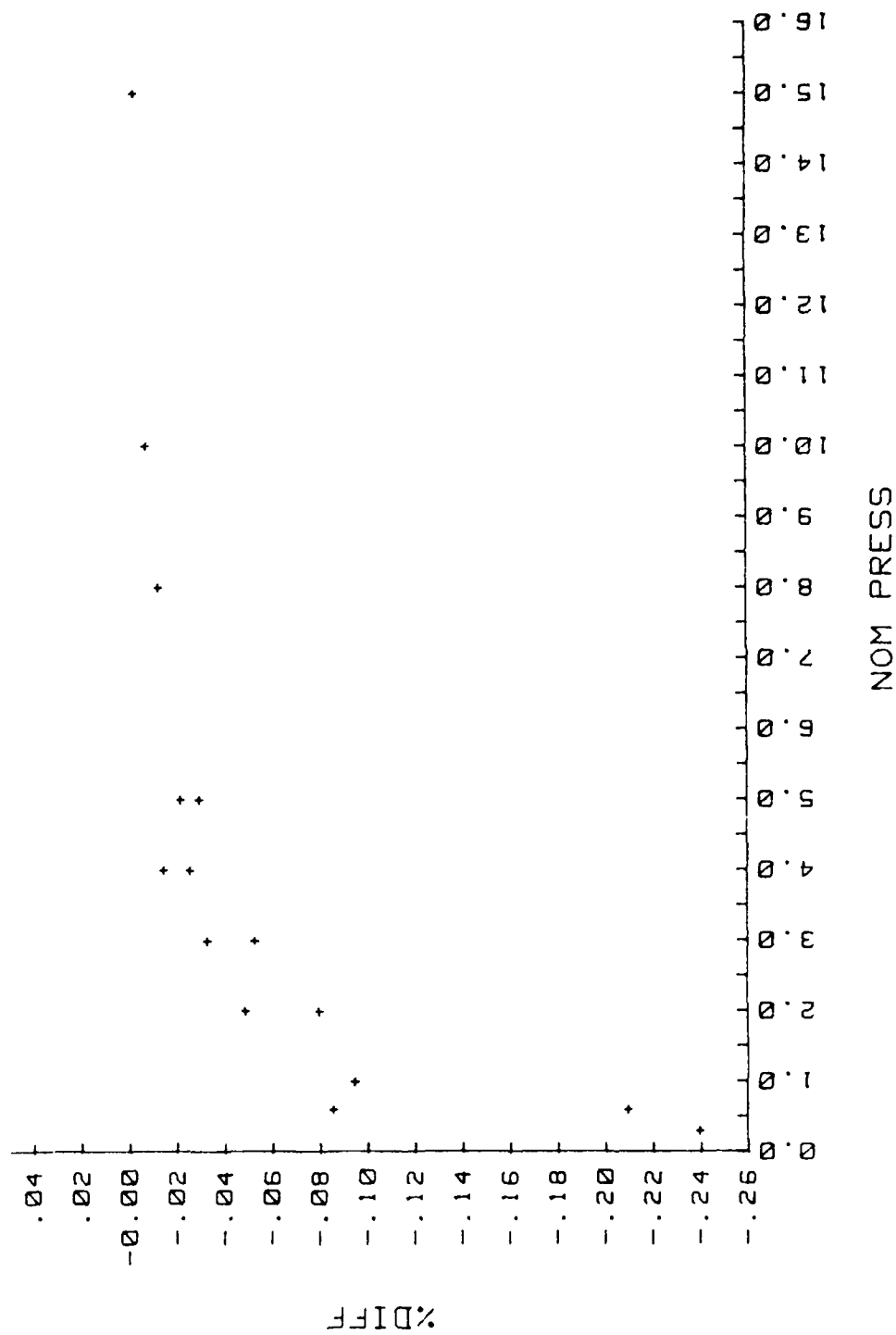Figure 1. Simplified diagram of digital dwt during cross-float.
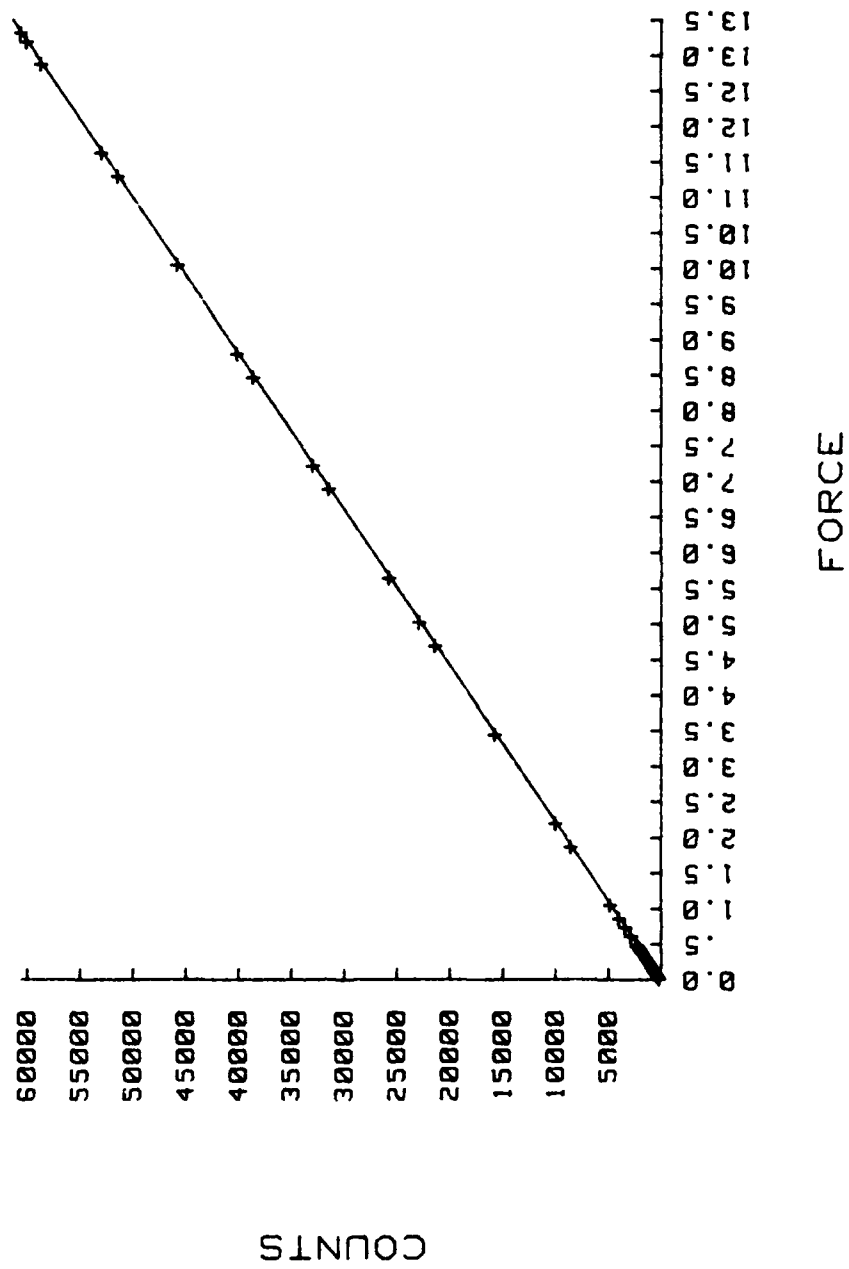
13

Figure 2. DH versus CEC.
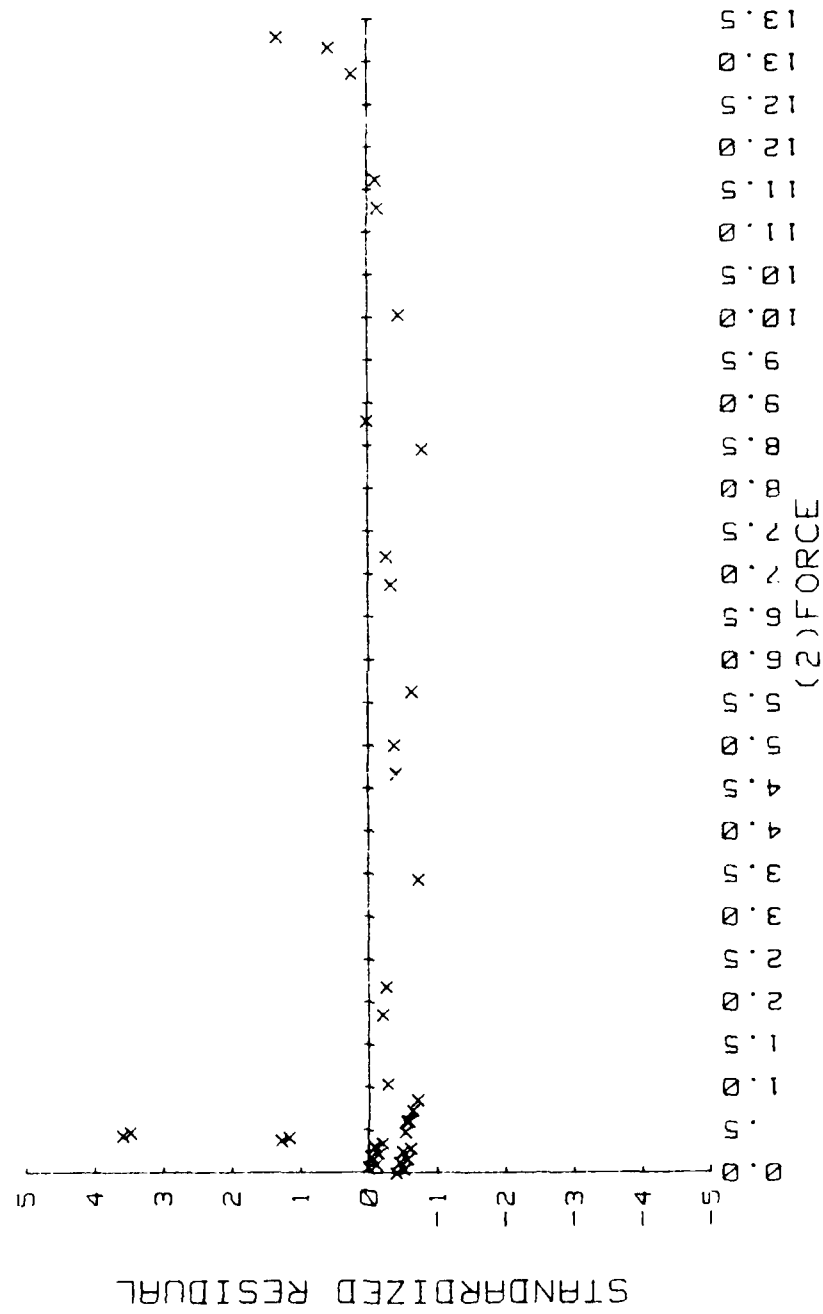
Figure 3. Dynamometer CAL.

15

Figure 4. Dynamometer CAL.

something wrong with the weight values or the analog to digital converter or force transducer in the dynamometer was unlinear.

We designed a weighing sequence to see if the problem was the weights--used six 1 Kg weights and find slope of curve, then insert a weight (the same weight) between each 1 Kg weight, find the residuals and see when the peculiar pattern developed. This idea also had the feature we could use values for the weights independent of the calibration laboratory since

Slope, Δcounts/mass = Counts/ mass = C_2-$C_1/(M_2-M_1)$

the added weight would have a systematic error hence slope would be unaffected.

Another way to ferret out this problem was to presume perfectly linear response and plot each weights response--we tried both these schemes but eventually used the latter.

An application of six Kg mass (apparent mass versus brass, i.e., the buoyancy factor $(1-\rho_a/\rho_b)$ has been allowed for)   produces a force of

$$M(1-\rho_a/\rho_b)g/980.665 = M(1-\rho_a/\rho_b)979.626/980.665 \qquad (4)$$

$= 13.213727$ lbf

which when placed on the dynamometer gave a full scale reading of 60,007 counts. Since the instrument was zeroed with only the weight table on it the slope of the line through these two points gives

4541.2623 counts/lbf

Now using this value one can calculate the predicted counts for a certain applied force. This was done and results are given in Table 2.

During this time it was discovered several problems in the mass calibration lab explained some of the problems with a few of the CEC weights, i.e.,

(a) Some of the weights were weighed on the low 10% portion of a scale.

(b) The 4 oz and 0.3 oz weights taken to another scale showed a surprising disagreement; much larger than the error limit quoted--this undoubtedly contributed to the earlier peculiar results.

Based upon the very good results given in Table 2, we decided to repeat the entire pressure intercomparison with another better calibrated dwt. However before doing this we decided to do a direct measurement of the diameters of piston and cylinder, calculate A_0 and come up with a conversion constant. Table 3 gives the values from which we obtain

$$A_0=(A_p+A_c)/2 = 0.30396546 \text{ in}^2 \qquad (5)$$

which is within 1.9 ppm of the manufacturer value. However note that our ability to measure the dimension is 10 micro inches ($=\Delta D$) hence since

$$A_0 = \pi R^2 = \pi D^2/4$$

$$\Delta A_0 = \frac{\partial A_0}{\partial D}\Delta D \quad (\pi/2) \, D\Delta D \qquad (6)$$

$$A_0 = 9.8 * 10^{-6} \text{ in}^2$$

and the difference in A_0's is 1/10 of this. This means we may have merely been lucky to obtain agreement this close.

Using this value for A_0 (at 20°C), our pressure conversion constant is

$2.2020305*10^{-4}$ lbs/0.30396649 in^2

$= 7.2443579*10^{-4}$ psi/count

The manufacturer gave a conversion constant of $7.244086*10^{-4}$ psi/count which is different by 37.5 ppm--we do not know why this difference.

Comparing to a Ruska Dwt over the pressure range 0.5 to 15 psi with one piston and above this with another piston produces a very good agreement and is entirely satisfactory (see Figure 5). Note the up and down runs provide a hystersis test--and there doesn't appear to be any hystersis, to within the resolution. In all these measurements, all known corrections have been applied, air head, and temperature corrections to each dwt; however, a constant value for the bouyancy effect has been used.

Since the digital output format (and connector) was strange we never did get the device connected to a computer--all data was taken manually.

B. HIGH PRESSURE PISTON-CYLINDER

The other piston-cylinder goes up to 300 psi and has a pressure conversion constant of

$4.99505*10^{-3}$ psi/counts

given by the maker.

Direct measurements of A_0 produces the values given in Table 3, where the agreement is not as close as the other piston, undoubtedly limited by our dimensional measurement resolution.

An intercomparison with the aforementioned Ruska DWT produces the results given in Figure 6. These values are completely within expectations--the only notable thing is the instrument is considerably more sensitive to vibration. By isolating and taking pains with the input pressure line vibration influence has been minimized.

TABLE 3.   Piston-Cylinder Dimensions

Low Pressure Piston-Cylinder

SN 269   Cylinder   Piston

Top   0.62212"   Top   0.62210"

Bottom 0.62212"   Middle 0.62210"

                                               Bottom 0.62210"

A_o = 0.30396546 in^2

High Pressure Piston-Cylinder

SN 3394   Cylinder   Piston

Top   0.23694"   Top   0.23692"

Bottom 0.23694"   Middle 0.23692"

                                               Bottom 0.23692"

A_o = 0.044088974 in^2

_____

$$\frac{A_{oDH} - A_{oarmy} * 100\%}{\text{Nominal}}$$

Low Pressure   = 0.00019

High Pressure = -0.01

18
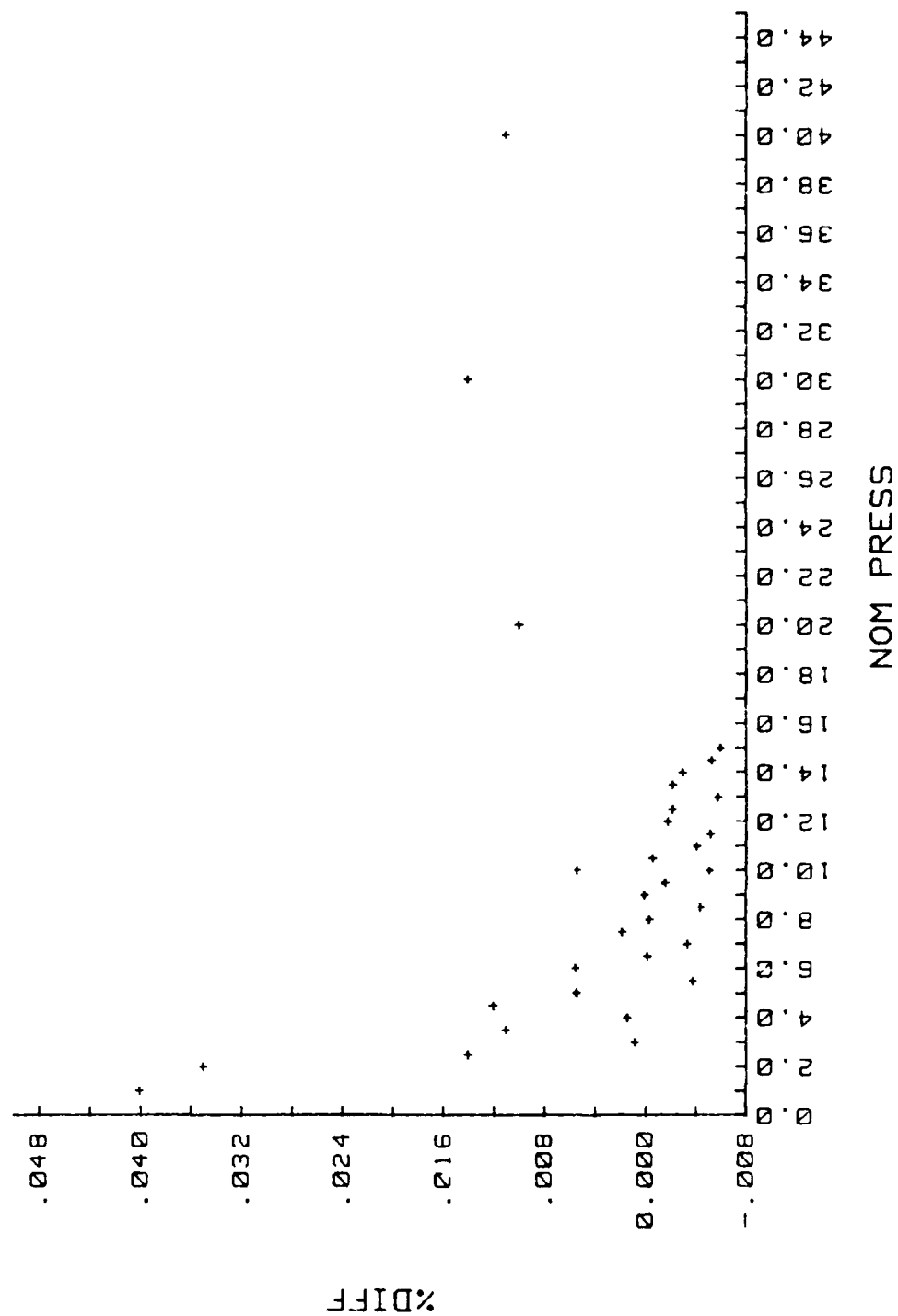
Figure 5. Cr ss-float results, Ruska
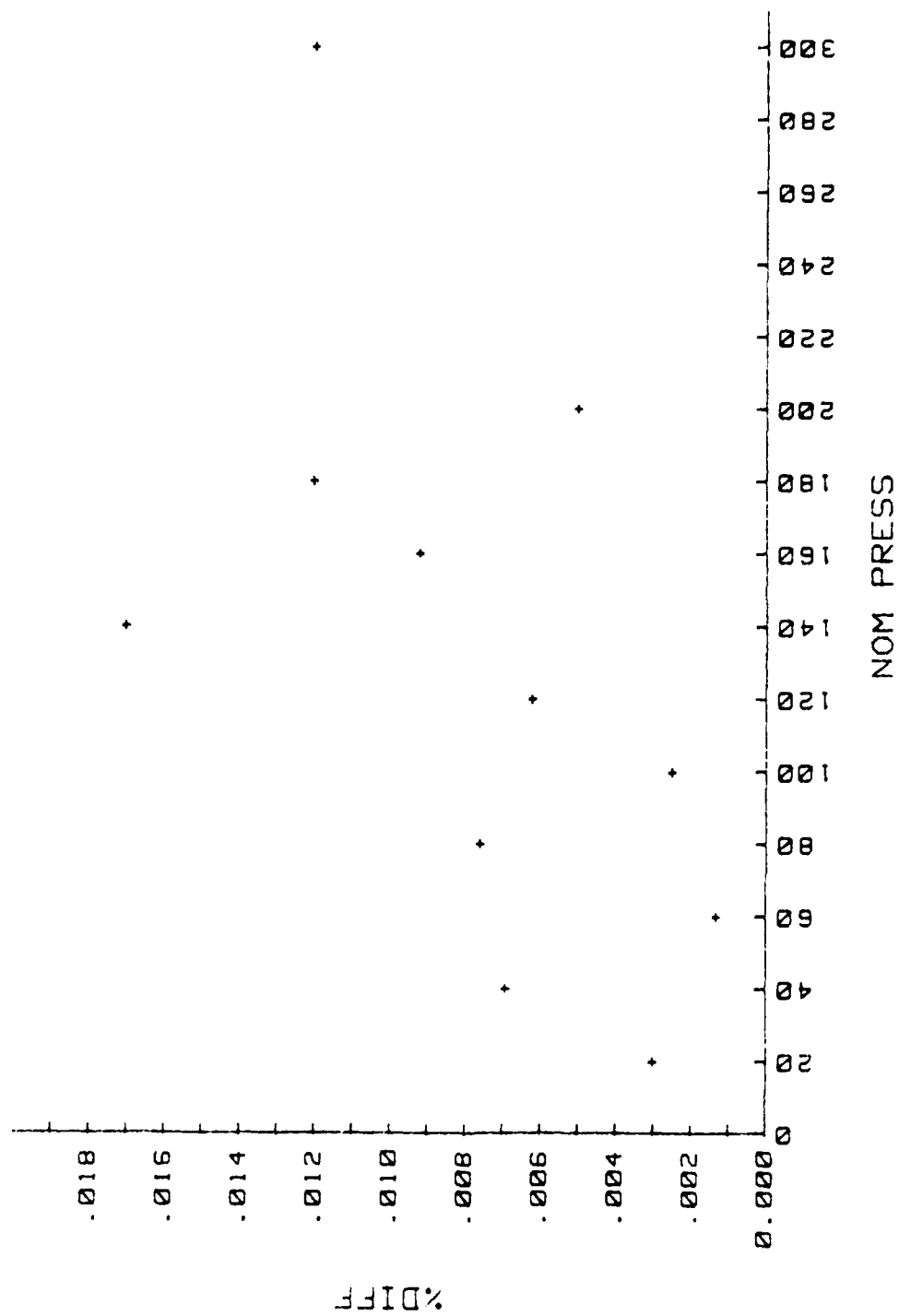
Figure 6. High pressure cross-float results.

Since this piston-cylinder is oil lubricated we tried some lower viscosity oil and even used it with no oil to reduce noisy readings; however, we discovered most of the noisy readings were simply due to vibration from the bench or input pressure line.

C. TEMPERATURE EFFECT

We tested the dynamometer, with a constant load of 4 Kg, in an environmental chamber from 13°C to 33°C to see if it was affected. Figure 7 gives the results. It appears the dynamometer is affected by these temperature changes even though it is supposed to be independent of temperature change.

ACKNOWLEDGEMENTS

It is a pleasure to acknowledge the assisitance David Catlett gave in taking some of the data.

REFERENCES

(1) DH Instrument Co, Tempe, Arizona

APPENDIX

DEFINITION OF TERMS

P = Pressure, psi
M = Mass, lbs
g = Local acceleration of gravity, can/sec^2
ρ_a = Density of air, gam/cm^3
ρ_b = Density of brass, i.4 gm/cm^3
A_0 = Effective cross-sectional area at zero pressure, in^2
α = Temperature coefficient of expansion of piston cylinder, parts per million per degree C
Δ = T-R, temperature of use - Reference temp, $^{\circ}$C
D = Diameter of piston or cylinder, in

Figure 7. On temperature test.

DEVELOPMENT OF A PROTOTYPE SYSTEM
FOR THE
IMPULSE CALIBRATION OF MICROPHONES

David L. Mullendore
Vice President
Dayton Scientific Inc.
Dayton, Ohio

Richard D. Talmadge
Senior Electronics Engineer
Wright Research and
Development Center
Wright-Patterson AFB, Ohio

ABSTRACT

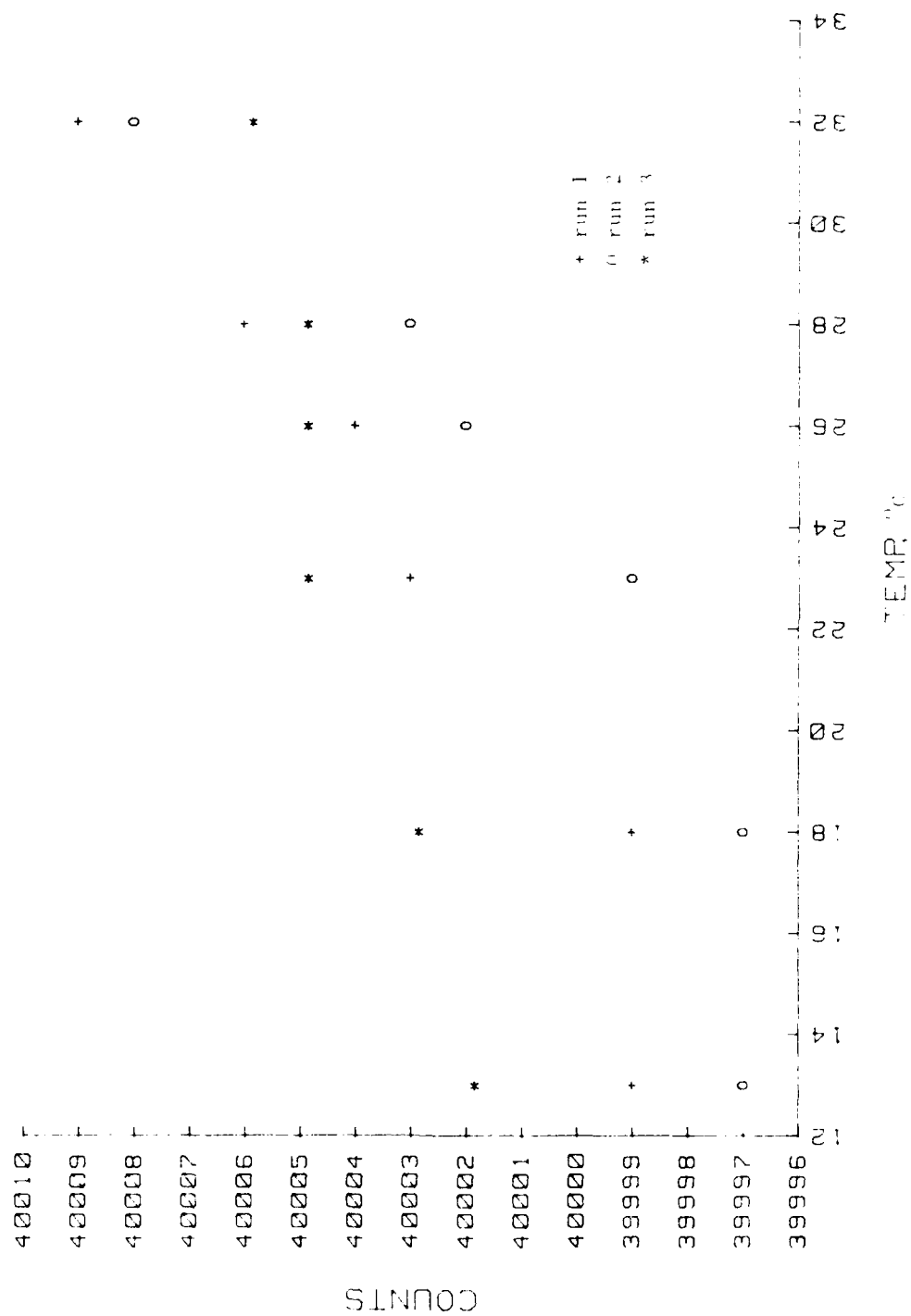Current techniques of microphone calibration are not readily adapted for use in the field and do not produce data on both frequency and phase characteristics. A new technique was investigated for calibrating microphones using a pressure impulse, which will produce calibration of both amplitude and phase and will be adaptable to field use.

INTRODUCTION

The effort described within this document was performed by Dayton Scientific Inc. for the Structural Vibration and Acoustics Branch of the Air Force Flight Dynamics Laboratory, Wright Patterson Air Force Base, under Air Force Contract F 33615-87-C-3220. The Structural Vibration and Acoustics Branch maintains a facility that provides wide-band dynamic data acquisition and analysis capability to support Structural Dynamics Research and Development. These endeavors require an accurate, portable, and simple procedure for calibrating microphones and pressure transducers while being used at remote test sites during field operations.

STATEMENT OF THE PROBLEM

The techniques generally used to obtain the amplitude and phase versus frequency characteristics of microphones and low pressure transducers involve considerable time and require expensive equipment. Conventional calibration methods involve performing a series of sine sweeps at various amplitudes over the frequency range of interest, a procedure that is generally restricted to a laboratory environment. Calibration of microphones at a test site is currently performed with a pistonphone at a single point single level, which results in a check of transducer output but provides no information concerning the transducer's frequency or phase response.

It was the purpose of this contractural effort to develop and validate a technique of microphone

calibration which would use a single pressure impulse as the input to a microphone being calibrated. The response of the microphone to the pressure impulse would then be recorded and Fourier Transform techniques used to determine the frequency and phase characteristics of the microphone. If successful, this technique could be implemented with relatively inexpensive hardware, it would be simple to adapt to field use, and the calibration could be performed quickly.

The primary performance goals of the Impulse Calibration Unit were as follows:

Bandwidth: 10 Hertz to 5000 Hertz
Accuracy: +/- 0.5 dB
Amplitude Range: to 170 dB Sound Pressure
Level (SPL)
Repeatability of Calibration: +/- 0.5 dB SPL

DEVELOPMENT PROGRAM

Design of the Prototype Impulse Calibration Hardware

The initial work on which this investigation is based was conducted by the Structural Vibration and Acoustics Branch of the Flight Dynamics Laboratory, WPAFB, Ohio. The general approach was to create a pressure impulse within a closed cylinder, into one end of which is placed the microphone to be calibrated. The microphone output, in response to the impulse input, is then analyzed using transform techniques to obtain the frequency and phase response of the microphone. A reference microphone whose frequency characteristics are known is also placed in the cylinder.

The pressure impulse is created by striking a suspended piston which occupies the end of the closed cylindrical cavity opposite the microphone. As will be shown later, it is important that the pressure pulse be of relatively short duration so that it will have sufficient high frequency energy content to permit Fourier Transform analysis to be reliable

over the required frequency region, which
includes the range from [...] to five kilohertz.
The pressure pulse will [...] duration if
the mass of the piston [...] small, if
the cavity volume is small, and if the friction
between the piston and [...]
negligible, and it [...] to
minimize leakage [...]

Overall views of [...]
calibration unit are shown in figures 1 and 2. It
consists of a small piston [...]
one end of which [...]

opposite end of the [...]
into which the [...]
that their diaphragm [...]
the cavity. Attached to [...]
on the side opposite to [...]
the photographs, is the [...]
steel ball [...]. An experiment [...]
piston by striking the steel [...] metal
hammer, or by dropping [...]
the piston from a [...]
change its position. In [...]
piston moves under [...]
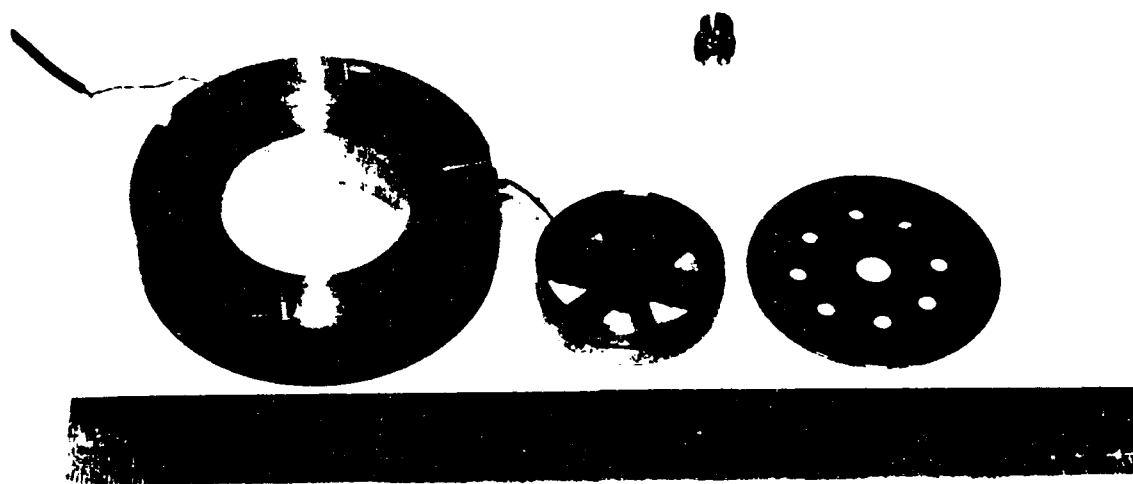cavity, producing [...]
sensed by the [...]

FIGURE 3
VIEW OF CYLINDER AND PISTON DISASSEMBLED

A vacuum chuck whose height is adjustable up to about 15 inches is located above the piston. The vacuum chuck may be used to hold and then drop a steel ball onto the impact button. The vacuum chuck can be seen in Figure 3 attached to the vertical rail above the cylinder assembly.

The Impulse Calibration Unit was designed to have the smallest possible cylinder diameter, so as a very small piston mass, and to have a very small cavity or air gap within the cylinder-piston assembly. In the photograph, Figure 3, the three parts of the cylinder is shown on the left, the piston in the center, and a disk spring which separates the piston to the cylinder is shown on the right. A 1.5-inch diameter piston was originally selected to be the minimum practical diameter consistent with the requirement to hold the impact above a reference microphone which would be located within. The diameter of the cavity diaphragm was further minimized by machining it out of magnesium alloy using EDM (electrical discharge machining) techniques to reduce as much as the material between the walls of the piston. The resulting piston shown in the photograph has a weight of approximately square ounces.

To minimize the friction between the cylinder walls and the piston, the piston bore and the cylinder O.D. were machined to very close tolerances so that the air gap between them was nominally 0.001-inches, or less than a gap of

than 0.0008-inches. Early in the project the piston was kept centered in the cylinder by an air bearing. Later it was discovered that a thin film of synthetic lubricant, Convalube-... worked out as well, plus the lubricant had the added benefit of slightly damping the piston, which minimized high frequency vibrations. The requirement to minimize leakage past the piston was also dictated by these same design criteria.

The prototype Impulse Calibration Unit will provide a peak sound pressure in excess of 170 dB SPL with a peak impact force of only a few pounds. For example, for the force of a 1/4" steel ball in the impact process, the duration of the contact is only an approximately 100 microseconds, with only the impact being of the pressure pulse. Since the impact force is quite good, the duration force in of the cylinder piston assembly is a precise measure of impact force. It was for this reason that a reference microphone included as a standard against which the measurement system is calibrated.

Figure 4 is a block diagram of the prototype instrumentation developed during the development program. The prototype system was instrumented with a force transducer, which was an integral part of the metal hammer, and an ... microphone which was mounted within and along the axis of the cylinder. Both the force

PISTON IMPACT → FORCE TRANSDUCER → SIGNAL CONDITIONER

MODAL HAMMER

WAVEFORMS, DATA TEST RESULTS

PRESSURE IMPULSE → REFERENCE MICROPHONE → AMPLIFIER/LP FILTER (VAR. GAIN & BW) → CH. A

UNKNOWN MICROPHONE → AMPLIFIER/LP FILTER (VAR. GAIN & BW) → CH. B

EXT. TRIGGER

HIGH SPEED MULTI-CHANNEL A/D CONVERTER

200 KHZ THRUPUT

12-BIT RESOLUTION

PERSONAL COMPUTER AT-COMPATIBLE

DATA ACQUISITION AND SIGNAL ANALYSIS SOFTWARE

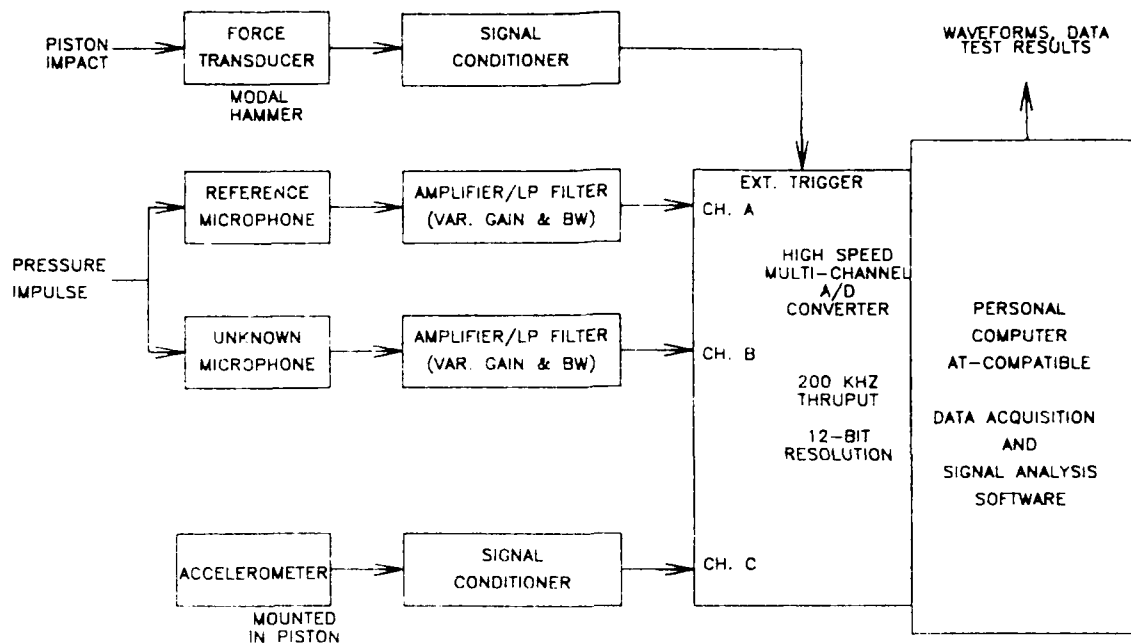ACCELEROMETER → SIGNAL CONDITIONER → CH. C

MOUNTED IN PISTON

FIGURE 4
BLOCK DIAGRAM OF IMPULSE
CALIBRATION SYSTEM INSTRUMENTATION

transducer and the accelerometer were quartz piezoelectric types with an integral unity-gain amplifier. Signal conditioners were used to provide bias current to the transducers and to provide amplification of the transducer output signals.

Since the modal hammer was used as the source of many of the test impacts, the force transducer signal was monitored and could then be analyzed to determine the spectral content of the impulse. Also, the force signal was used as the trigger to initiate the acquisition of microphone signal data during impacts with the modal hammer.

The accelerometer signal was monitored during some test impacts to provide data for analysis of piston motion.

Each microphone channel was provided with an instrumentation amplifier having selectable gain and bandwidth. The gain of each amplifier was generally set to a value which resulted in a peak signal level of 1 to 5 volts at the input to the A/D converter. This permitted maximum utilization of the dynamic range of the A/D converter. The amplifier bandwidth was normally set to 50 kHz.

Each microphone signal was sampled and digitized at a rate of 50,000 samples per second by the A/D converter. The sample interval was set to 0.001 seconds, which resulted in 180 data samples per channel. The resolution of the A/D converter was 12-bits or one part in 4096. After the

microphone data was acquired for each test impact, the data was written to a computer disk file and retained for further analysis. The data acquisition process was controlled from within a commercial software package called SNAPSHOT. The A/D converter hardware consisted of an Analog Devices RTI-860 Data Acquisition board plugged into the PC bus.

Mathematical Analysis and Verification

Figure 5 is a calibration system frequency domain diagram corresponding to the Block Diagram of Figure 4. The frequency domain diagram will be used in the following analysis. A pressure impulse is generated by the impact of a hammer or falling ball on the piston. The pressure impulse I(w) is simultaneously applied to both the reference ("ref.") microphone and the microphone to be calibrated ("unknown" microphone). The reference channel of the system includes the reference microphone having a response function Rr(w) and an amplifier low pass filter having a response function Kr(w). The unknown channel of the system includes the unknown microphone having the response function Ru(w) to be determined, and an amplifier low pass filter having a response function Ku(w).

Now, if the output functions from the reference and the unknown channels respectively are Or(w) and Ou(w), the expressions for the output of each channel are:
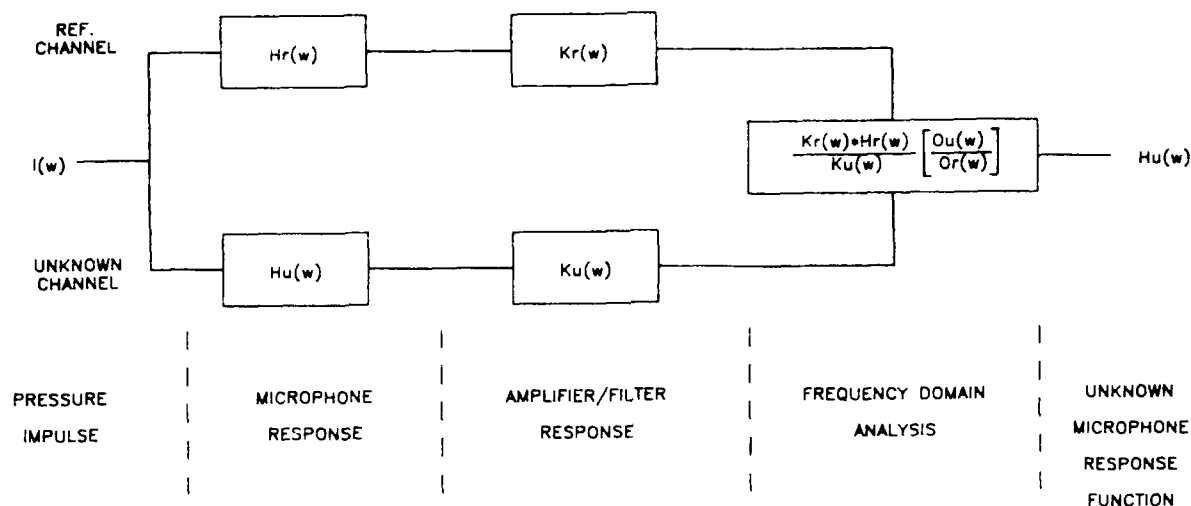
26

FIGURE 5

FREQUENCY DOMAIN DIAGRAM

$$Or(w)=I(w) \cdot Hr(w) \cdot Kr(w) \qquad 1$$
$$Ou(w)=I(w) \cdot Hu(w) \cdot Ku(w) \qquad 2$$

These expressions can be solved for the unknown microphone response, which results in expression (3).

$$Hu(w)=\frac{Kr(w) \cdot Hr(w)}{Ku(w)} \cdot \frac{Ou(w)}{Or(w)} \qquad (3)$$

The first term in this expression consists of fixed quantities which are either known or can be accurately measured. The second term consists of the output of the unknown and reference microphones in response to the pressure impulse. Therefore, if the frequency response of the amplifiers and the reference microphone are known, and if the transforms of the output signals from the two microphones are determined, then the response of the unknown microphone can be calculated. Note that all quantities are complex; that is, they involve both amplitude and phase.

The analysis described above could be performed by a commercially available two-channel signal analyzer. However, since one of the objectives of this program was to develop an inexpensive instrument for field use, the approach taken was to use a personal computer to acquire, digitize, and store the microphone signals; and then to operate upon the recorded signal data with Fast Fourier Transform techniques utilizing a commercially available signal analysis software package. For the purposes of this investigation, the FFT operations were implemented with the commercially available DADiSP signal analysis software package.

The successful application of the impulse calibration technique requires that the frequency response of the reference microphone be accurately known, relatively flat, and repeatable throughout the frequency range of interest. Also, the pressure impulse input to the microphones must have a relatively high frequency content throughout the frequency range of interest. Note however that the impulse transform does not appear in expression (3), which means that the impulse does not have to be perfect nor does it have to be exactly repeatable from test to test.

A typical pressure impulse generated by the prototype calibration unit is shown in Figure 6. The frequency spectrum of this impulse is shown in Figure 7. It will be noted that the spectrum of the pressure pulse has significant energy up to 5 kHz.

The effects of noise on the microphone output signals may be able to be reduced by applying a window function to the time domain signal before taking the frequency transform; and or by averaging the response functions resulting from multiple impacts. A number of different window functions have been suggested in the literature. However for single event impulse-type analysis, a window such as the unity-plus-cosine taper shown in Figure 8 or the exponential taper shown in Figure 9 are recommended. The calibration test results reported in the last section of this paper were obtained using the unity-plus-cosine window (with the cosine taper beginning 600 microseconds into the measurement interval). This window has been found to be preferable to other window functions in this application. Additionally, certain test results were analyzed by averaging the unknown microphone
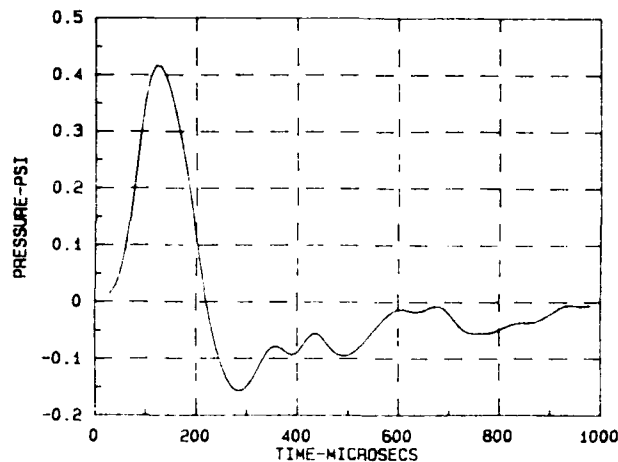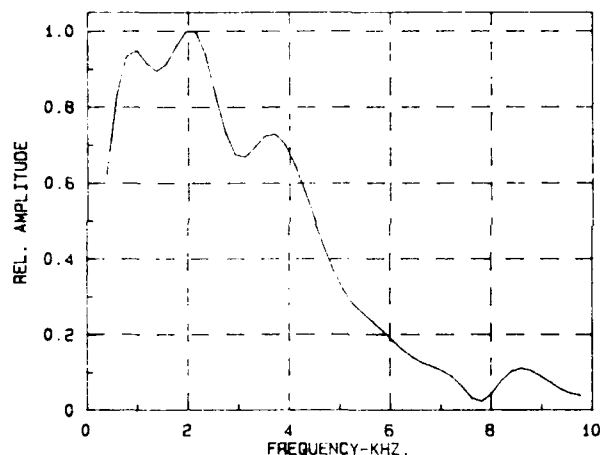
FIGURE 6
TYPICAL PRESSURE PULSE

FIGURE 8
EXAMPLE OF UNITY-PLUS-COSINE WINDOW

FIGURE 7
PRESSURE PULSE SPECTRUM

FIGURE 9
EXAMPLE OF EXPONENTIAL WINDOW

frequency functions from four independent test
impacts, which tends to suppress the effects of
random noise in the microphone signals.

The microphone output signals are conditioned
and/or modified in successive low-pass filtered,
and converted to digital form for computer
processing using required analog to digital
converter (A/D). The signal conditioner and/or
amplifier specially provide transducer biasing,
if required, and amplification of the microphone
signal. The A/D conversion is a sampling process
which introduces the need for the control of
several additional variables, i.e. signal
bandwidth, sampling rate, and sample interval.

The signal data from each microphone was
bandlimited to prevent "aliasing" during the A/D
conversion process. Aliasing results in the
folding of higher frequency energy into the
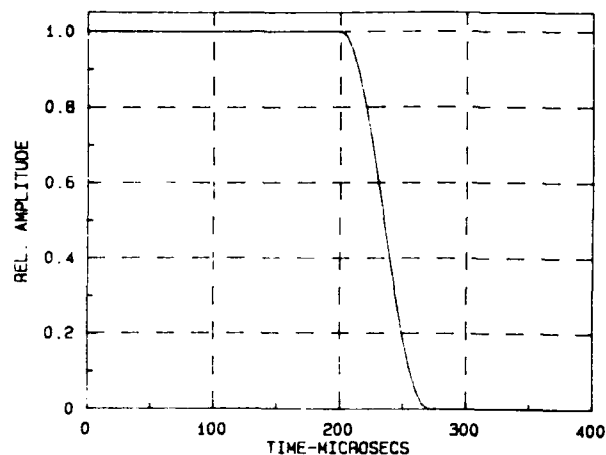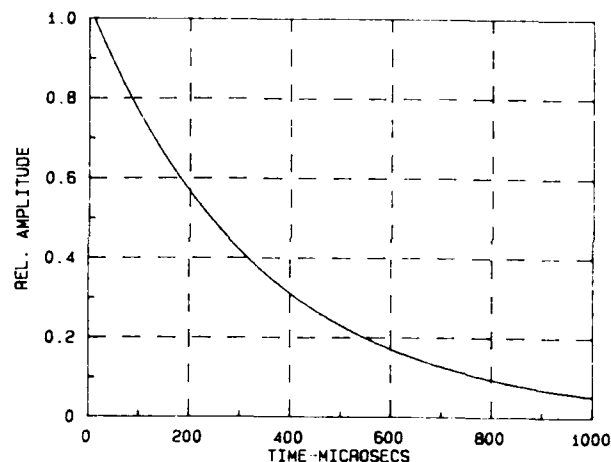frequency band of interest. Aliasing is

prevented by limiting the signal bandwidth before
the A/D conversion process to less than half the
sampling rate.

The microphone signal bandwidth of interest for
calibration purposes is 5000 Hz. Based on the
Nyquist criteria a sampling rate of at least
10,000 samples per second is required. However
to insure computational accuracy all of the
investigations associated with this project have
utilized sampling rates of 50,000 to 100,000
samples per second on each data channel. The
impulse signal from the microphones generally has
a duration of 150 to 200 microseconds. A sample
interval of 1.0 microsecond was used for
acquiring the signal data. With a sampling rate
of 100,000 samples per second and a sample
interval of 1.0 microsecond, 160 samples of data
were acquired from the reference channel and from
the unknown microphone channel during each impact
event.

28

The frequency resolution of the FFT calculation is equal to the inverse of the record length (sample interval). It is also desirable for the record to contain a number of samples which is a power of two. Therefore zeros were added to the data records to make 256 data points or the equivalent of a 2.56 millisecond record, resulting in a frequency resolution of 390 Hz. The pressure rise within the cylinder cavity resulting from an impact can be calculated by considering the change in volume which occurs when the piston is struck. The change in cavity volume is directly related to the displacement of the piston, as shown by expression (4).

$$V_f = V_i - \left[\frac{s}{0.0085}\right] \cdot V_i \qquad (4)$$

where V_f is the final cavity volume,

V_i is the initial cavity volume (which is fixed),

s is the piston displacement after impact, and the constant 0.0085 is the initial cavity gap in inches.

If it is assumed that the temperature of the air in the cavity does not change during an impact, then the pressure change in the cavity resulting from a piston displacement S will be:

$$P = P_i \cdot \left[\frac{s}{0.0085}\right] \qquad (5)$$

where P_i is the initial pressure in the cavity (ambient pressure).

During the program, it was desired to verify that the pressure in the cavity behaved in accordance with Equation 5. Since it was impractical to measure the piston displacement directly, the displacement was calculated by performing a double integration of the accelerometer signal. The resulting piston displacement value was then used in Equation 5 to calculate a peak cavity pressure, which was directly compared to the cavity pressure measured by the reference microphone. It was found that the two values tracked in a predictable manner, with the measured peak pressure generally 20% lower than the calculated peak pressure. This difference is most likely due to inaccuracy in the method used to calculate the piston displacement, since a small error or bias in the acceleration signal will easily contribute to a significant error in the calculated displacement.

General Test Procedure

The procedure used to acquire and analyze test data from the Prototype Impulse Calibration System is indicated by the Flow Chart, Figure 10. The acquisition, display, and storage of microphone signal data resulting from a test impact to the piston was controlled by the SNAPSHOT software package running on an PC/AT compatible personal computer. The acquired data was then imported into the DADISP software

PISTON IMPACT →

GENERATE
PRESSURE
IMPULSE

↓

ACQUIRE MICROPHONE
SIGNALS WITH
SNAPSHOT SOFTWARE

↓

SAVE MICROPHONE
SIGNALS IN
DISK FILE

↓

IMPORT DATA INTO
DADISP SIGNAL
ANALYSIS
ENVIRONMENT

↓

APPLY WINDOW
TO SIGNALS

↓

ADD ZEROS
TO EXPAND SAMPLE
TO 256 POINTS

↓

APPLY FOURIER
TRANSFORM TO REF.
& UNKNOWN MICR.
SIGNALS

↓

APPLY SCALING &/OR
CORRECTION FOR THE
REF. MICR. &
AMPLIFIER/FILTER
RESPONSE

↓

COMPUTE THE
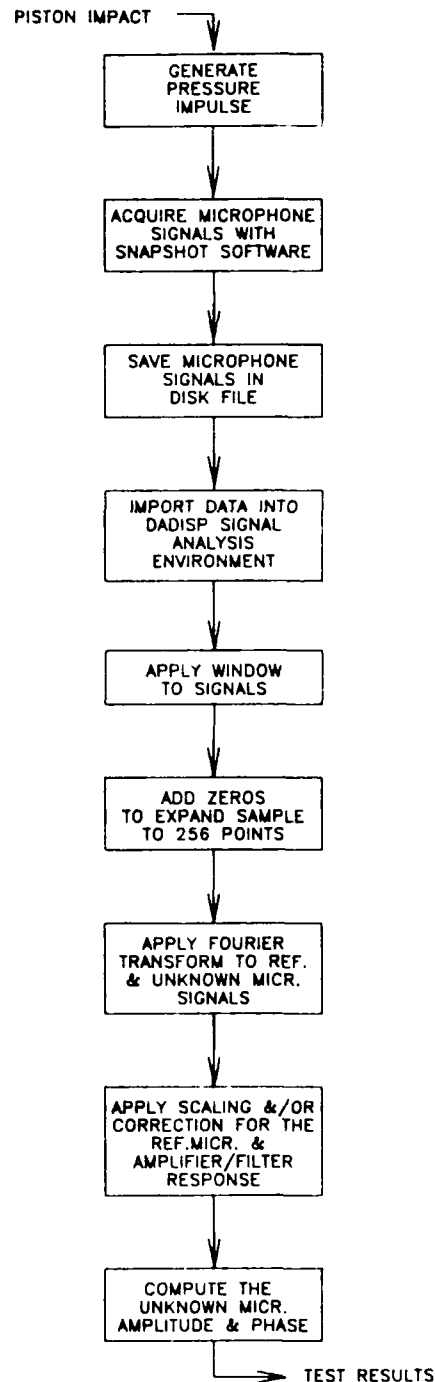UNKNOWN MICR.
AMPLITUDE & PHASE

→ TEST RESULTS

FIGURE 10

FLOW CHART OF GENERAL TEST PROCEDURE

environment for analysis. The DADiSP software provides the capability of applying mathematical functions to the microphone signals for such operations as windowing, scaling, FFT, and complex operations. In general, the operations listed in the Flow Chart, Figure 10 were performed on each dataset. The test results consist of frequency and phase data, which is available either as a table of complex values or as hard copy plots. During the development program, certain of the analysis parameters were varied to arrive at the optimum choice: for example, the best choice of window function.

The general test procedure used during the development program utilized standard software packages because of their flexibility and low cost. The same functionality could be programmed into an appropriately equipped, portable PC for field use: wherein the test procedure would be programmed specifically for the impulse calibration system and would execute automatically.

Test Results

The test results reported in this section consist of several representative plots of an "unknown" microophone whose response function was measured using the Prototype Impulse Calibration System. A second microphone whose characteristics were known was used as the Reference microphone. The "unknown" microphone was a Gulton MVA-2400, S/N nULL. Both microphones were independently calibrated by the Air Force Flight Dynamics Laboratory. The Air Force calibration resulted in a sensitivity of 1.916 volts PSI for the "unknown" microphone.

Figure 11 is a plot of the transfer function magnitude resulting from four impacts using the Prototype Impulse Calibration System, ranging in peak pressures from 0.05 PSI to 0.4 PSI. It can be seen that the data in Figure 11 correlates reasonably well with the Air Force calibration at frequencies above 1000 Hz. Below 1000 Hz, the data is unreliable, for reasons which are unknown at this time. Further data will become available as the investigation continues.
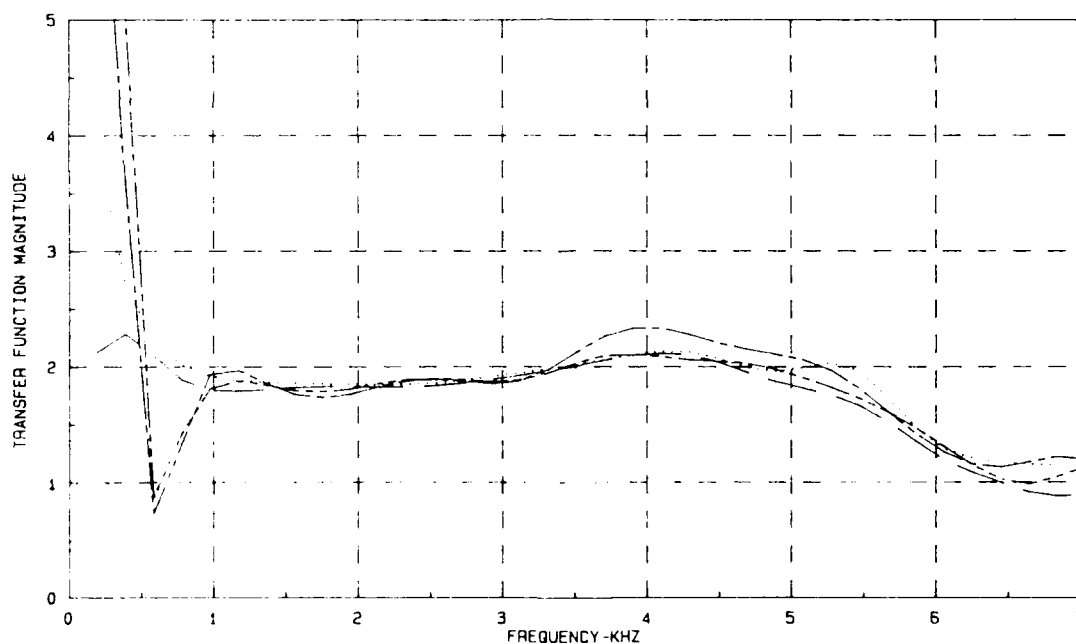

FIGURE 11
TEST MICROPHONE TRANSFER FUNCTION MAGNITUDE PLOTS

REFERENCES

(1)   HEM Data Corporation, "SNAPSHOT Storage
      Scope Version 2.46-A, for Analog Devices,
      Inc. RTI-860 Boards", January 1988, 17025
      Crescent Drive, Southfield, MI 48076

(2)   DSP Development Corp., "The DADiSP Worksheet
      Signal Analysis Software", one Kendall
      Square, Cambridge, MA 02139

(3)   Halvorsen, William G. and Brown, David L.,
      "Impulse Technique for Structural Frequency
      Response Testing," Sound and Vibration,
      November 1977, pp. 8-21.

(4)   Harris, Cyril M., Shock and Vibration
      Handbook, Third Edition, McGrawHill Book
      Company, New York, New York, 1988, pp. 13-1
      to 13-27, 20-4 to 20-7.

(5)   Hewlett-Packard, "The Fundamentals of Signal
      Analysis," Application Note 243, November
      1981.

DEVELOPMENT OF PROTOTYPE SYSTEM FOR THE IMPULSE CALIBRATION OF MICROPHONES

Q: Bill Cardwell (GE, Evandale): On the calibration in the first part of your talk, you talked about putting an accelerometer on which part, on the piston or what?

A: David Mullendore: On the piston.

Q: Bill Cardwell: Did you try putting one on the stable part also to see if there was any reaction that way?

A: David Mullendore: No, that's a good suggestion. We did not try that. We used the accelerometer that was mounted within the piston to try to characterize the movement of the piston. The one set of data we did extract was to do a double integration on the ac   ration to get a mathematical value for piston displacement and then to relate this to the change in pressure within the cavity. It turns out when we did that we were able to correlate the change in pressure with the piston displacement to within about 20% error. That doesn't sound very good until you consider that we achieved this with a double in-tegration of the accelerometer signal. There was some high frequency vibration in the accelerometer signal, as you might expect. When you have an impact, that tends to bias that displacement. We were able to correlate to within 20%. This is over the full range of impacts we're experimenting with which was from about .02 or .05 psi to about 1 psi. But we did not mount an accelerometer on the outer cylinder.

Q: Bill Cardwell: The data that was shown on the final chart, is that with using the modal hammer or the ball dropper?

A: David Mullendore: That was obtained using the modal hammer, we can't see much difference in the data for a given impact level. There seems to be little or no difference between the two techniques as far as the results are concerned.

Q: Bill Cardwell: Your final thought on this; do you think this provides you with an easier way of calibrating in the field other than using the pistonphone?

A: David Mullendore: I think that if it can be shown, and there may be some more work involved here, that the data totally correlates with conventional techniques within the limits that are expected for this type of calibration, which were plus or minus a half a dB, it's a very quick method. In our work, most of the time was spent not with gener-ating the data but with analyzing the data. You generate the data in about two seconds, as long as it takes to pick up the impulse hammer and make an impact, or if you want to make multiple impacts and average the data, that takes a little b t longer. If you would write special software that did the analysis rather than trying to use a standard package which requires some interaction you'd have the results in probably 10 or 15 seconds with a standard AT computer.

From that point of view, I think it does lend itself to field use. The speed with which the results are obtained is one of the things we were after.

Q: **Jim Faller (Aberdeen Proving Ground)**: I'm not totally familiar with the subject, but I had a question about the energy level. You weren't getting enough energy over a broad enough frequency range, and I was wondering what your strategy was to achieve this?

A: **David Mullendore**: The original strategy was to make the impulse as short as possible, and I guess that still is the strategy. We may be up against some fundamental limitations there. I'm not sure we know for sure.

Q: **Jim Faller**: Did I misunderstand the question then originally, that you weren't getting enough output?

A: **David Mullendore**: I think what I tried to emphasize was the distribution of energy throughout the frequency range that we were interested in, which was from essentially 10 hertz up to 5 kilohertz. It's not a question of enough output but the distribution of the output.

Q: **Jim Faller**: So, if you narrow the range you don't have to worry about distribution, is that right? You say the distribution is between two and three kilohertz?

A: **David Mullendore**: If you would accept the one to three and one-half kilohertz range as that in which you were interested then we wouldn't have to go any further, I guess. We're after a broader range than that.

Q: **Jim Faller**: Does the modal hammer influence that in anyway: the construction of the modal hammer, the materials of construction?

A: **David Mullendore**: Yes, as a matter of fact. We did not actually have a direct steel on steel impact. There was about a four mil plastic interface between the modal hammer or the steel ball when we dropped it and the impact point on the piston. Without that we would generate a lot of extraneous vibrations in the piston. They seem to center around 16 kilohertz, which is outside the range of interest. It didn't interfere with the work that we were doing, so the four mil polyester, more like six mils, interface did suppress those. We experimented with other materials and other thicknesses. We're at a point right now where we've kind of optimized that part of it, as far as the weight of the modal hammer and the material, whether it was steel on steel contact or with some kind of a dampening material in between. We probably have some other things we can try there but the results that you see are where we are right now.

Q: **John Judd (Vibrametrics)**: In the last curve you had up there, was that the ratio of the microphones?

A: **David Mullendore**: That was the frequency response of the unknown microphone alone.

Q: **John Judd:** I wondered if you had any coherence data?

A: **David Mullendore:** I did have some coherence data. We did some work with coherence mid-way through the program and the data showed about a .98 coherence up to about four to five kilohertz.

Concurrent Accelerometer Calibration
Utilizing Rigid Body Assumptions

Michael J. Lally
Research Assistant

David L. Brown
Professor

Structural Dynamics Research Laboratory
Department of Mechanical and Industrial Engineering
University of Cincinnati
Cincinnati, Ohio USA

ABSTRACT

The general trend towards increasingly large numbers of channels of sensors has placed tremendous burdens on the calibration aspect of testing. The need to accurately measure rotational degrees of freedom also generates new problems with conventional calibration methods. In an effort to solve these problems, two novel calibration systems are under development at the University of Cincinnati. Utilizing the simplest and most intuitive of all structures, the rigid body, the calibrators can provide quicker calibrations and total motion information. Each calibrator relies on the underlying assumption that the measured sensor outputs must result from motion consisting of some linear combination of the six fundamental rigid body modes. However, beyond this premise, each calibrator uses a different construction and solution method to achieve its end result. The fast concurrent calibration (FCC) method calculates a least squares type estimate for the primary axis of sensitivity for up to 256 Structcel motion sensors at a time. Solving an overdetermined multiple-input multiple-output (MIMO) problem, the total motion calibrator (TMC) uses 24 reference accelerometers and the known geometry of the platform to calculate the exact motion at the location of the test sensors. Thus, a test sensor's output can be calibrated against any or all of the six DOF inputs.

INTRODUCTION

The fast concurrent calibration system provides a quick and economical method for batch processing calibrations. Since only the primary axis of sensitivity is needed in most measurement applications, the calibrator's excitation means and solution algorithm have been optimized to produce single axis calibrations for a large number of sensors in an efficient, cost effective manner. The FCC system functions to transform the measured signals from an array of motion sensors into a best fit rigid body motion (ref 2). The rigid body motion and the sensor's geometric location then dictate the sensor's appropriate sensitivity. Traceable sensitivities are referenced to precision quartz sensors and up to 256 Structcel motion sensors can be calibrated at a single time.

Providing more sensitivity information, the total motion calibrator (ref 3-4) requires a large number of reference sensors and at least six shakers to adequately excite and measure all six degrees of freedom. The TMC functions to transform 24 measured linear accelerations (8 triaxial reference accelerometers) into the primary rigid body accelerations of the platform. A simple geometric transformation then calculates the exact motion at the base of each transducer under test (ref 5). This allows the MIMO estimator to produce the sensor sensitivities.

SYSTEM CONFIGURATIONS

Fast concurrent calibration platform-

The heart of the calibration system consists of a rigid platform which connects to an number of electrodynamic shakers. An aluminum alloy block milled out in a waffle pattern to lighten, yet still retain strength, forms the 12 inch by 12 inch by 2 inch, rigid platform. A number of iterations of finite element analysis provided the basic platform design which has its first resonance at 1200 hz. As stated in the previous section, the calibrator operates on the assumption that all measured motion consists of a linear combination of the rigid body mode shapes. The true rigid body motion frequency range extends to about half of the first resonant frequency. Hence, the useable frequency range of the present design extends to just about 600 Hz. Future designs of the platform will include ultra-stiff, light-weight composites to greatly extend the useable rigid body frequency range.

Providing mounting for the Structcel motion sensors (ref 6-8), a grid of 256 mounting sockets occupy the surface of a printed circuit board. The two layer board, which is rigidly laminated to the platform with epoxy, conveniently routes the large number of signal leads (3 per sensor x 256 sensors) from the mounting sockets to multi-pin connectors at the edge of the board. The array of motion sensors report the measured motion which will be used to determine actual combination of the rigid body modes. The entire platform rides on soft springs with a system resonance of less than 10 hz. Sixteen ribbon cables carry the signals from the edge connectors on to

the Data Harvester which provides the necessary signal conditioning (power, gain and low pass filtering) for the Structcel motion sensors.

Four electrodynamic shakers attach at the corners to vertically excite the platform. Each shaker can be set in phase or 180 degrees out of phase in order to create the different forcing vectors needed to guarantee a solution. With only vertical excitation, the motion of the platform must consist of vertical translation and the two rotations in that plane. Accordingly, a minimum of three independent forcing vectors must be applied to guarantee a calibration solution. We assume that the sensors do not measure in the other directions thereby focusing only on the primary axis of sensitivity.

Total motion calibration platform:

A 6 inch cube constructed of a balsa-graphite laminate then filled with structural foam provides the mounting platform for this system. Lighter in weight than the aluminum platform, the cube behaves as a rigid body to nearly 1 Khz, but has a much smaller surface area for mounting test sensors. The symmetric geometry of the cube makes it much more suitable for uniform excitation in all degrees of freedom.

In order to measure the complete motion of the block, at least 6 reference sensors are needed. Since we will use only translational accelerometers, these must be spatially distributed and oriented in a manner that allows measurement of all three rotations. One possible configuration is to measure triaxial acceleration at one point, biaxial acceleration at another point in directions perpendicular to the line between these two points, and a uniaxial acceleration at a third point in a direction perpendicular to the plane containing the three points. This represents the minimum configuration needed for all 6 DOF. These accelerometers will be called the reference accelerometers, because they act as calibration standards for the calibration process, and they are therefore calibrated by standard means prior to use on the platform.

Housed in the corners of the cube, the use of 8 triaxial accelerometers gives 24 reference accelerometers on the platform, four times the minimum requirement. The resulting redundancy in measuring the motion of the platform provides two advantages: it allows averaging of the 24 measurements in calculating the six degrees of freedom of the platform's motion, and it allows deletion of one or more reference accelerations from the process in the case that the corresponding measurement channels are not functioning properly at the time of the calibration. The calibration algorithm uses a least-squares method for the averaging. This averaging provides the usual benefits of a finer resolution of the motion, a reduction in random errors, a correlation coefficient that indicates the reliability of the inherent assumptions in the method, and greater confidence in the computed results.

The excitation method varies depending on the measurement technique utilized. When testing with conventional broad band techniques, six shakers driven with uncorrelated random noise are connected in pairs on mutually perpendicular faces. This drives the cube into random vibration along all three translational axes and about all three rotational axes. The random noise sent to the exciters is chosen so that each of these six degrees of freedom of motion have approximately uniform vibration over the calibration bandwidth.

Utilizing the spatial sine testing system, the shaker configuration remains the same, but excitation occurs at a single frequency. The shakers must apply a minimum of 6 independent forcing vectors at each frequency step to guarantee sufficient information for a solution. Practically, additional forcing vectors increase the data set information and provide a statistically more precise answer.

MATHEMATICAL DEVELOPMENT

The same equation forms the basis for each of the calibration solution algorithms. The measured signals, scaled by some sensitivity vector, must equal the active modes times the modal participation factors.

$$[X]\{S\} = [G]\{k\} \qquad (1)$$

where, $[X]_{n \times n}$ = diagonal matrix of measurements

$\{S\}_{n \times 1}$ = transducer sensitivity vector

$[G]_{n \times 3}$ = rigid body mode shapes $(G_z \ G_{\theta x} \ G_{\theta y})$

$\{k\}_{3 \times 1}$ = modal participation factors

n = number of measurement channels

In expanded form for N measurement sets,

$$
\begin{bmatrix}
X_1 & G & 0 & 0 & \dots & 0 \\
X_2 & 0 & G & 0 & \dots & 0 \\
X_3 & 0 & 0 & G & & 0 \\
& & & & & \\
X_N & 0 & 0 & 0 & \dots & G
\end{bmatrix}
\begin{Bmatrix}
S \\
k_1 \\
k_2 \\
k_3 \\
\vdots \\
k_N
\end{Bmatrix} = 0 \qquad (2)
$$

The benefits from working with a rigid body result in the simplification of the G matrix. The translational rigid body modes can be described with zeros and ones while the rotational rigid body modes need only the x,y,z geometry with plus or minus one weighting functions. Furthermore, the calibration range is not limited to the rigid body frequency span of the platform. If so desired, analytical estimates of the first flexible modes can be adjoined to the G matrix to extend the calibration frequency range.

Currently, two algorithms have been developed to solve the basic equation for the FCC system. The first algorithm develops a Rayleigh quotient and reduces the equations to a directly solvable eigensolution. The second algorithm implements an iterative least squares technique to perform the eigensolution. Both algorithms assume that the platform receives vertical excitation from a number of shakers. Exciting only three rigid body modes (translation and two planer rotations), this configuration allows for maximum input along the sensitive axis and reduces the overall calculation by requiring only three modes in the G matrix.

Using basically the same equations as the iterative technique, the IMC incorporates the known sensitivities of the reference accelerometers and calculates the best rigid body with a direct transformation in all 6 DOF. A second geometric transformation provides the exact motion at the base of the test sensor. Finally, the algorithm employs a multiple-input/multiple-output frequency response estimator to determine the sensor's output response sensitivities to each of the 6 calculated inputs.

FCC direct solution:

Reformulating this so that there is the minimal number of equations for the number of unknowns ({S} and {k}),

$$
\begin{bmatrix}
X_1 & G & 0 & 0 \\
X_2 & 0 & G & 0 \\
X_3 & 0 & 0 & G
\end{bmatrix}
\begin{Bmatrix} S \\ K_1 \\ K_2 \\ K_3 \end{Bmatrix}
= \begin{Bmatrix} E_1 \\ E_2 \\ E_3 \end{Bmatrix} \qquad (3)
$$

where, the subscripts indicate the measurement and associated modal participation factors for the respective forcing pattern. (This represents the minimum number of measurements needed to solve for the sensitivities. There must be at least one equation for each rigid body mode excited. More measurements may be used and will result in a least squares type estimate).

The error terms in the above equation arise from the inconsistencies in the sensitivities between the various data sets. These should be minimized in order to obtain the best fit of the best of sensitivity vector for the given measurement set. Minimizing the error term with respect to a solution matrix, M, and the modal participation set equal to the identity matrix we have,

$$
\sum \qquad (4)
$$

the norm of the respect to an arbitrary Mass weighting matrix and

$$
\sum \qquad (5)
$$

the Euclidian norm of k. By minimizing the error with respect to K, we can set up a Raleigh Quotient type problem such as,

$$
\min \left| \frac{|E|^2_M}{|K|^2} = \frac{\begin{bmatrix} S^H & K^H \end{bmatrix} \begin{bmatrix} A & B \\ B^H & I \end{bmatrix} \begin{bmatrix} S \\ K \end{bmatrix}}{\begin{bmatrix} S^H & K^H \end{bmatrix} \begin{bmatrix} 0 & 0 \\ 0 & I \end{bmatrix} \begin{bmatrix} S \\ K \end{bmatrix}} \right| \qquad (6)
$$

where,

$$
A = \sum_{i=1}^{n} X_i^h M X_i
$$

$$
B = \begin{bmatrix} X_1 MG I & X_2 MG I & \dots & X_n MG I \end{bmatrix}
$$

$$
I = [G]^T [G]
$$

The physical interpretation of this is to minimize the strain energy while maximizing the kinetic energy. Since we know that the structure is a rigid body in the frequency range which we are exciting, this minimization technique should result in the best fit of the data.

The kinetic energy term is strongly related to K (the modal participation factors of the rigid body modes) due to the fact that the Euclidian Norm of K is a direct function of the coordinate system's velocity squared (unity mass or symmetric mass).

In order to view the error terms in relation to the internal strain energy, we must look at the error term in a different perspective. As was stated earlier, the error terms are the result of inconsistencies in the sensitivities. Alternatively, this error vector could be thought of as the result of unaccounted mode shapes. These unaccounted mode shapes would not be rigid body modes and therefore result in internal strain energy, which currently shows up as an error term.

Given these physical interpretations, minimizing the Rayleigh Quotient tends to make sense since under normal operating circumstances the structure used for calibration should have no internal strain energy.

Reformulating the above Raleigh Quotient problem into a standard Eigenvalue problem,

$$
\frac{|E|^2_M}{|K|^2} = \frac{\begin{bmatrix} S^H & K^H \end{bmatrix} \begin{bmatrix} A & B \\ B^H & I \end{bmatrix} \begin{bmatrix} S \\ K \end{bmatrix}}{\begin{bmatrix} S^H & K^H \end{bmatrix} \begin{bmatrix} 0 & 0 \\ 0 & I \end{bmatrix} \begin{bmatrix} S \\ K \end{bmatrix}} = \lambda \qquad (7)
$$

$$\begin{bmatrix} S^H & K^H \end{bmatrix} \begin{bmatrix} A & B \\ B^H & 1 \end{bmatrix} \begin{bmatrix} S \\ \overline{K} \end{bmatrix} = \begin{bmatrix} S^H & K^H \end{bmatrix} \begin{bmatrix} 0 & 0 \\ 0 & 1 \end{bmatrix} \begin{bmatrix} S \\ \overline{K} \end{bmatrix} \lambda \qquad (8)$$

The solution of the Raleigh quotient problem is now to solve the above Eigen-problem for the minimum Eigenvalue and its associated Eigenvector. As can be seen, this is a very large Eigen-problem and must be reduced. By expanding the equations we have,

$$[A]\{S\} + [B]\{K\} = \{0\} \qquad (9)$$

$$\{S\} = -[A]^{-1}[B]\{K\} \qquad (10)$$

and,

$$(-[B]^H [A]^{-1}[B] - [1])\{K\} = \{K\} \lambda \qquad (11)$$

which reduces to,

$$-[B]^H [A]^{-1}[B] = [1]\{K\} = \{K\} \lambda \qquad (12)$$

The above Eigen-problem now is reasonably small (9x9) and the solution for the minimum Eigenvalue and its associated Eigenvector can be determined using one of the several Eigensolution methods. The solution of this subset results in the Eigenvalue which is not used, and the Eigenvector which is the set of modal participation vectors for each set of measurements. To solve for the sensitivities the modal participation vector is back substituted into equation number 9.

FCC iterative solution:

Equation number (2) can be represented in the form of,

$$[A] \begin{Bmatrix} S \\ K \end{Bmatrix} = 0 \qquad (13)$$

Setting up the equation in least squares form which minimize the error

$$[A]^H[A] \begin{Bmatrix} S \\ K \end{Bmatrix} = 0 \qquad (14)$$

and let,

$$[A]^H[A] = \begin{bmatrix} B & C \\ C^H & D \end{bmatrix} \qquad (15)$$

The problem is now to find the eigensolution for the $[A]^H[A]$ matrix where

$$[B] = \text{diagonal} \sum [X]^2$$

the diagonal matrix containing the measured signals for N different forcing sets and,

$$[D] = \text{block diagonal} \left[[G^T G] \right]$$

with equal blocks containing the geometry of the rigid body modes. Also we know,

$$[C] = \left[\left\{ X_1 G \right\} \left\{ X_2 G \right\} \dots \left\{ X_N G \right\} \right]$$

which is the measured signal for each forcing condition times the rigid body mode geometries. Now expanding equation (14) into two equations,

$$[B]\{S\} + [C]\{k\} = 0 \qquad (16)$$

$$[C^H]\{S\} + [D]\{k\} = 0 \qquad (17)$$

and rearranging equation (17),

$$\{k\} = -[D]^{-1}[C]^H\{S_n\} \qquad (18)$$

where n is the nth estimate of the sensitivity vector. Also rearranging equation (16),

$$\{S_{n+1}\} = -[B]^{-1}[C]\{k\} \qquad (19)$$

Substituting equation (18) into equation (19), the iterative equation is,

$$\{S_{n+1}\} = ([B]^{-1}[C][D]^{-1}[C]^H\{S_n\}) / \{S_n\}_1 \qquad (20)$$

where the sensitivity is normalized to the first element of the S vector. Though inverse calculations of large matrices can be complex, the matrices in equation (20) are very simple because B is diagonal and D is a block diagonal matrix with 3 by 3 blocks. The addition of a weighting matrix to remove "bad" sensors prevents a measurement error from corrupting the best fit solution. Setting initial sensitivities to one and using three iterations to determine the basic sensitivity, the algorithm zeros out any sensor with a correlation coefficient of less than 95 percent. A final 12 iterations then converge very quickly delivering a stable calculation of the sensor sensitivity.

TMC calibration algorithm:

The total motion algorithm also begins with the rigid body equation (1). However in this case the reference measurements can be scaled directly due to the calibrated triaxial accelerometers in each corner of the cube. The left hand side of the equation can be condensed as a vector, R, consisting of the measured

reference translational accelerations. Including all six rigid body modes instead of just three, G is still a function of geometry. The k vector includes the modal participation factors (which are the six principal rigid body accelerations for a rigid body). Thus equation (1) becomes,

$$\{R\} = [G]\,\{k\} \tag{21}$$

where, $\{R\}_{24 \times 1}$ = translational ref accelerations

$[G]_{24 \times 6}$ = rigid body mode shapes (6 DOF)

$\{k\}_{6 \times 1}$ = principal rigid body accelerations (modal participation factors)

To end up with the principal accelerations at the base of the test sensor, the geometry is input with the origin located at the base of the test sensor. Setting up a normal equation of a least squares solution to utilize the over determined measurement set,

$$[G]^T\{R\} = [G]^T[G]\,\{k\} \tag{22}$$

$$\{k\} = \left[[G]^T[G]\right]^{-1} [G]^T\{R\} \tag{23}$$

Note that equation (23) is essentially the expanded version of equation (18) with known sensitivities and three extra degrees of freedom. The TMC algorithm mirrors the first loop of the iterative solution and directly determines the values for k.

Clearly, a weighting matrix could be applied to the left hand side to judiciously eliminate any questionable measurement channels. All matrix operation can be performed prior to testing such that a single transformation matrix, T, would exist to calculate the principal accelerations.

$$\{k\} = [T]\{R\} \tag{24}$$

where, $[T] = [W]\left[[G]^T[G]\right]^{-1} [G]^T$

and, $[W]$ = weighting matrix

Once the principal accelerations have been determined, the estimated accelerations at any point can be calculated by using a geometric transformation from the original point. This allows for the formulation of error functions for the reference accelerometers and also concurrent calibrations.

Using the calculated principal accelerations at the base of the test sensor as inputs, a six-input/multiple-output estimator determines voltage sensitivities to each DOF.

EXPERIMENTAL RESULTS

As published in a previous paper (ref 9), plots 1 and 2 examine the comparability of the rigid body calibration method to a standard single sensor calibration and also examine the effect of different permutations of subsets of large number of forcing vectors. Both plots are normalized to use channel 2 as the reference. Plot number 1 displays first 32 relative sensitivity values for the hand held calibrator and the rigid body calibrator, as well as their differences. As can be seen by the plot, the normalized calibration value for the two different methods are very comparable. In fact, the first 16 channel are within one-half percent while the next 16 channels are within two percent.

In order to check the stability of the data reduction technique when using different forcing vectors, the original set of five forcing vectors (for one run) was used as a base set. This base set was permutated in such a way that the data reduction algorithm received different combinations of three forcing vectors (required for a unique solution). This resulted in 13 different force vector sets from the original 5 forcing vectors. Plot number 2 displays the normalized calibrations for the analysis set which included all permutations. The top of the lower traces indicates that the difference between the sensitivity vectors generated by the permutations is generally less than four percent. This indicates that the eigensolution is not overly dependent on any particular set of forcing vectors or amount of additional sets over the required three. Any set of three or more independent forcing vectors provides a reasonable data base for sensitivity analysis, but as usual a large set of forcing vectors provides better statistical confidence in the results. (Channels 45-48 were inoperative due to hardware difficulties).

Plot 3 reports new investigation into the repeatability of calibration values. Two tests performed a day apart with the sensors in the same locations each time demonstrate a repeatability of less than a percent. A following test was conducted removing all sensors and randomly replacing them in the platform geometry, but still referencing to the same sensor as before. The maximum variation between this trial and the two previous was about four percent with most less than two percent.

Each of these tests has used the iterative technique for a solution algorithm. To compare this with the direct solution algorithm, a mathematical simulation was created in a PC mathematics program and executed on the raw data from the previous tests. A variation of around two percent in average sensitivity causes some concern when the algorithms should deliver nearly identical values. One possible reason for the discrepancy may be the lack of a weighting matrix in the current direct solution implementation. Two bad sensor channels were averaged into the solution, possibly causing the difference in calibration values.
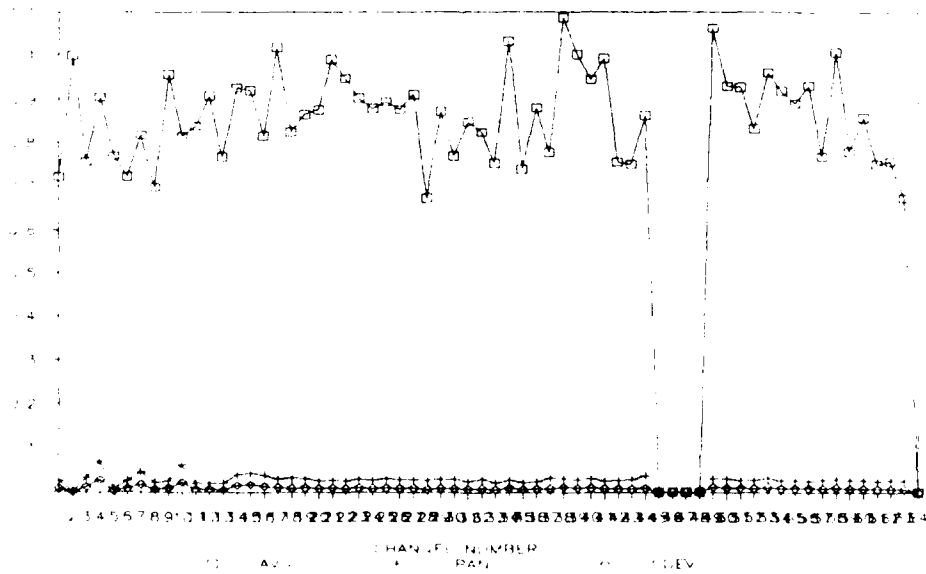
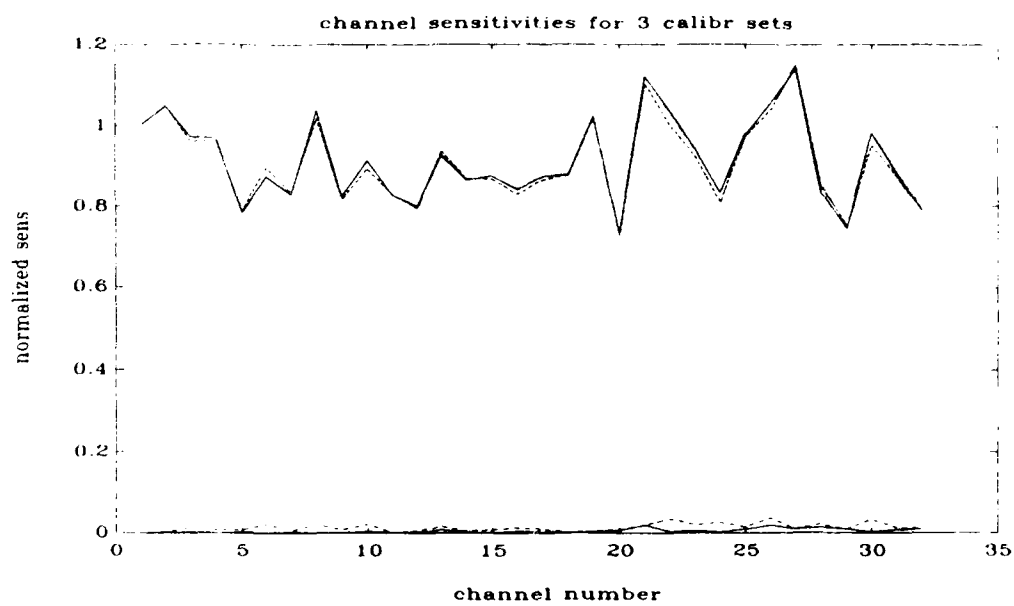SENSITIVITY — 64 STRUCTURE
HANDHELD CALIBRATOR VS GROUP CALRS
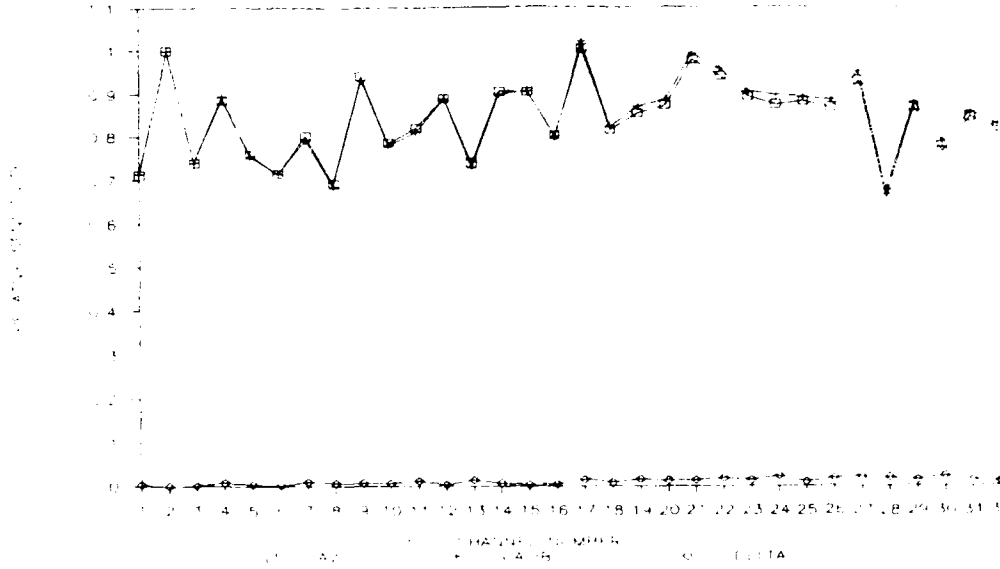
PLOT NO. 1

PERMUTATIONS OF FORCE VECTORS

PLOT NO. 2

40

channel sensitivities for 3 calibr sets

PLOT NO. 3

41

Experimental results from the total motion calibrator can be found in reference 3. Unfortunately, the lack of signal conditioning for the standard ICP type sensors used in the TMC prohibited further evaluation with the recently developed spatial sine testing methods. These tests will be the next examinations as adequate equipment becomes available.

Conclusions

The FCC method of calibration appears to be an accurate way to quickly calibrate a large number of Structcel motion sensors. Due to the convenience, users with large installations of Structcel's can use the calibrator not only to perform initial calibrations, but also to verify calibrations after a test is performed. This check gives further insurance that all sensor channels are operating properly during the critical data acquisition phase. Money will also be saved by shortening calibration time, expediting tests and ensuring accurate data.

A excellent candidate for further research, the total motion calibrator exhibits great potential for future benefits. A smaller scale concurrent calibration could provide all 6 DOF sensitivities for a number of sensors. Translational and rotational sensors could be tested for cross sensitivities in the manufacturing process and fine tuned to provide higher performance sensors. Self calibration could also be performed by considering one of the reference sensors as the test sensor. Under the presumption that most of the reference sensors are already well calibrated, the TMC could verify the reference sensitivities one by one.

Lastly, the benefits of computer aided testing are rapidly surfacing in the testing world. Large amounts of time and money are saved by automating calibrations. Other research topic include automated information management tools like barcoded serial numbers, and archived sensitivity data bases. Many of the advances are presently being integrated in to the spatial sine testing system under development at the University of Cincinnati.

BIBLIOGRAPHY

(1) "Calibration Methods for Modal Testing" Lally, R. W., Brown, D. L., Proceedings of the Sixth International Modal Analysis Conference, Lueven, Belgium., 1988

(2) "System Support for Spatial Sine Testing" Lally, M. J., Severyn, A.J., Brown, D. L., Proceedings, International Modal Analysis Conference, 9 pp., 1988.

(3) "Calibration System for Rotational Transducers" Severyn, A. J., Zimmerman, R., Proceedings, 11th International Seminar on Modal Analysis, Katholieke Universiteit Leuven, Belgium, 9 pp., 1986.

(4) "Six Axis Dynamic Calibration of Accelerometers", Severyn, A. J., Zimmerman, R., Proceedings of the Fifth International Modal Analysis Conference, London, England., 1987.

(5) "Dual Input Estimation of Frequency Response Functions for Automotive Structures", Allemang, R. J., Rost, R. W., SAE Technical Paper Series, No. 820193

(6) "A Low Cost Transducer System for Modal Analysis and Structural Testing", Lally, R.W., Poland, J. B., Sound and Vibration, January 1986.

(7) "An Evaluation of a Low Cost Accelerometer Array System, Advantages and Disadvantages", Poland, J. B., Master of Science Thesis, University of Cincinnati, Dept. of Mechanical and Industrial Engineering., 1986.

(8) "STRUCTCEL - A New Instrumentation System", Lally, M. J., Brown, D L, Fourteenth Transducer Workshop, Colorado Springs, Colorado., June 1987.

(9) "Benefits and Behavior of a Simultaneous Multiple Sensor Calibrator", Lally, M. J., Barney, P. S., Proceedings, International Modal Analysis Conference, 12 pp., 1989.

CONCURRENT ACCELEROMETER CALIBRATION UTILIZING RIGID BODY ASSUMPTIONS

Q: **Jim Faller (Aberdeen Proving Ground):** This is a minor point, but when you were referring to a six-axis calibrator system, I couldn't help thinking that using that term was somewhat inaccurate. Isn't it six degrees of freedom, with three axes and three rotations. Why the six axis designation?

A: **Michael Lally:** It just turns out to be the term that people adopted. Someone wanted it to be the kinetic array calibrator; some say six degrees of freedom. It has gone through a number of terminologies. That's the slang term that held in our lab.

Q: **Jim Faller:** Let me ask you this; are you employed by the Government working on a Master's Thesis?

A: **Michael Lally:** I am not employed by the Government.

Q: **Jim Faller:** Oh, you are with the University of Cincinnati?

A: **Michael Lally:** I am with the University of Cincinnati, and I also work with PCB. I should say Dick Talmadge has an ongoing contract to develop that six degree of freedom calibrator. But it had been dragging. There was a very small company that it was contracted through and actually the president of the company passed away recently, so that development may come back into our lab just as a general project; hopefully, to wrap it up. It was dragging on equipment costs and things like that.

Q: **Ray Reed (Sandia National Laboratories):** I had a question about the potential for increasing the frequency range of the six degree-of-freedom test. I think that you had indicated that you are able to maintain rigid body conditions up to about 500 Hz?

A: **Michael Lally:** Yes, 500 Hz.

Q: **Ray Reed:** Do you have any feel for what the range is; how far you may be able to extend this someday?

A: **Michael Lally:** This is something that we are currently working on. We've got the SDRC IDEAS work stations in our laboratory and have personnel up to speed on this so that we can produce our models rather quickly now. One man just went through the design of a shaker table stand for NB Dynamics, which was a couple of feet across, and they were working with frequencies around 2100 Hz, but they kind of fudged it a little by saying that their accelerometers were going to be mounted at the center, and the first mode has a node line across the center. So they cheated a little bit and said "That's not going to affect it." We are hoping that with the advanced composites (exotic carbide graphite), and things like that coming out; I would like to get up to a couple of thousand Hz. Again, being that we are working with a complex structure, that is going to be one of our major limitations on the frequency range. Just with the aluminum block, we are hoping that we can get beyond aluminum or maybe switch to magnesium, or something like that, up to a thousand Hz range.

Q: **Tom Rogers (Airborne Test Board, Fort Bragg):**   Is your linear force actually eliminated or is it such a small value that it is insignificant to your testing?

A: **Michael Lally:**   Linear.....I am not clear on your question.

Q: **Tom Rogers:**   In your slide you said that you had eliminated the linear force on the vibration testing?

A: **Michael Lally:**   Now what we are doing is exciting with six shakers on the six degrees of freedom and measuring the resultant upward motion of the block.   There are both linear forces and rotational forces. We are putting it in motion, using linear force in all degrees of freedom and then we are measuring the rigid body motions of the block with reference accelerometers.   We are determining the translational measurements and applying a geometrical transformation to get our rigid body rotations, and then we are saying that this is the motion of the block.   I don't know if that clears it up but we are not measuring any forces on it.

Comment: **Pete Stein (Stein Engineering):**   One of the fringe benefits that you get from the proposal using a sine wave and being able to slow down the rate of frequency change as you approach your resonance, and almost totally avoid the so-called swept frequency effect, where you would get wrong data at your resonance if you swept through it too fast.

A: **Michael Lally:**   We are using a step sine approach.   We are discretely stepping through a frequency.   We can adaptively control all of the aspects.   It helps so that we don't destroy whatever we are testing.   We can reduce our levels.

LARGE HIGH EXPLOSIVE DRIVEN FLYER PLATE TECHNIQUE
FOR THE VALIDATION OF
STRESS AND MOTION INSTRUMENTATION

Joseph D. Renick
Gordon M. Goodfellow
Lt. Leah E. Flores

Weapons Laboratory
Kirtland AFB, New Mexico
(505) 846-7204

20 - 22 June 1989

INTRODUCTION

There has been a long-standing need for a means by which the response of stress and motion instrumentation designed for fielding in cratering and groundshock experiments can be experimentally validated. A high quality validation would require that the instrumentation be embedded in a geologic material of interest and subjected to stress and motion fields representative of those in which the instrumentation is to be fielded. In addition, a true validation would require that there be some independent means for relating some measurable standard to the actual stress and motion fields produced in the validation experiment.

It is generally accepted that if there is an overall consistency and agreement among many gages of different kinds (stress and motion gages as well as different kinds of stress gages and different kinds of motion gages) fielded over a range of environment levels in a test event, then one can establish a good level of confidence in the results (especially if they agree with someone's prediction calculation). This internal consistency feature of the results provides a kind of validation. This approach is appropriate and is an essential part of any posttest analysis. In general, however, traceability to a true standard (other than time base) is not available. Thus, the credibility of the results is always subjective and the degree of subjectivity is dependent on the consistency of the results - which is not always good. Pretest validation experiments in which traceability to a standard is provided would add greatly to the credibility of the instrumentation systems fielded in weapons effects experiments. This would not necessarily eliminate inconsistencies between gages but it would allow one to evaluate and analyze results against the knowledge that a

particular gage type had been validated in a well-controlled validation experiment.

The Weapons Laboratory (WL) has developed the large explosively-driven flyer plate technique for evaluating and validating the response of stress and motion instrumentation in a variety of geologic materials. Thus far, the technique has been applied to dry soil and rock geologies. The technique for dry soils is very well developed and several validation experiments have been conducted. The technique for rock geologies is under development and several small scale exploratory experiments have been conducted.

This paper will: (1) describe the flyer plate experimental technique, (2) describe the theoretical model for the dry soil flyer plate technique and, (3) present selected results of dry soil flyer plate experiments.

DESCRIPTION - SOIL FLYER PLATE EXPERIMENTAL TECHNIQUE

The experimental configuration for the dry soil flyer plate technique is shown in Figure 1. The primary diagnostic instrumentation in the experiment are time-of-arrival (TOA) pins located immediately above the soil test bed surface for determination of flyer plate impact velocity, TOA switches for the determination of shock velocity as a function of depth in the soil, and soil strain cans for the determination of peak strain as a function of depth in the soil test bed. The explosive charge is initiated with a multipoint firing system where the spacing between initiation points is not greater than the charge thickness. The quantities of explosive needed to produce the desired plate velocities were determined using Gurney equation (Ref 1,2) predictions and the results of a series of plate velocity calibration experiments using small plates. A polystyrene foam buffer is placed between the explosives and the flyer plate to prevent spallation of the plate. In our experimental program, we have determined that it is important to obtain a good seal between the concrete support ring and the flyer plate to prevent blow-by gases from triggering TOA switches prematurely. An air
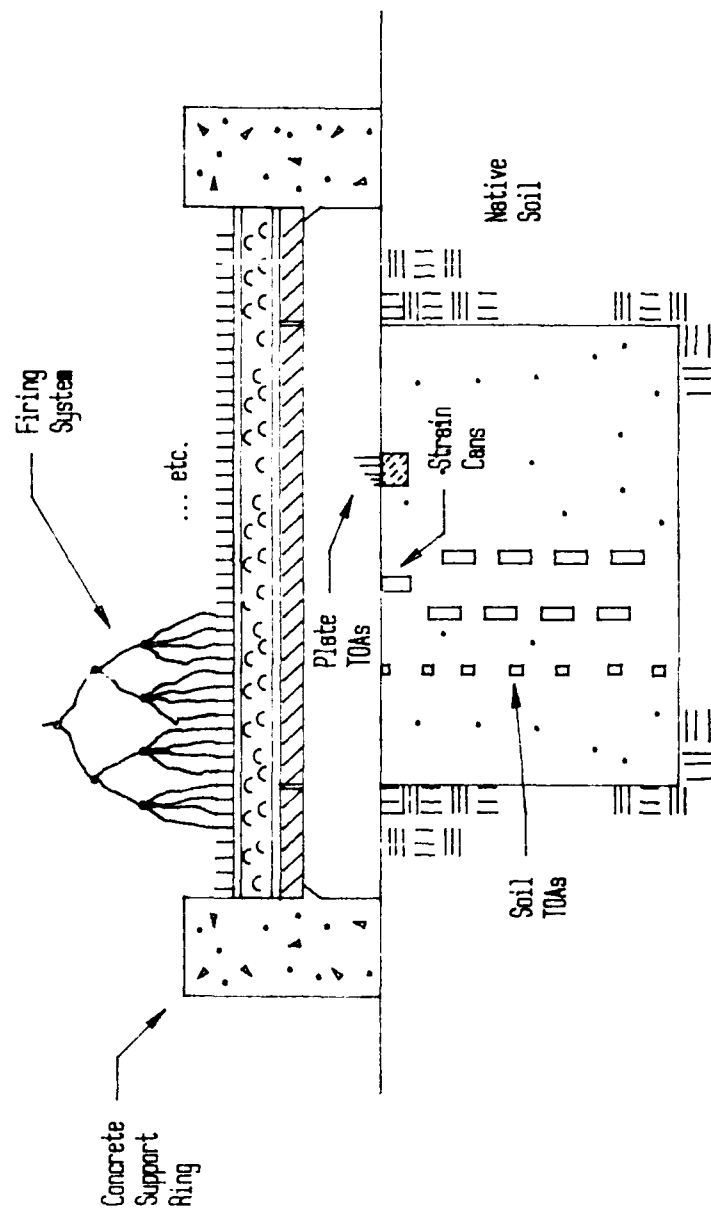
Large HE Flyer Plate Technique

FIGURE 1

shock, which is driven by the flyer plate, is compressed to high pressure due to reverberations between the plate and test bed surface and a precursor is produced in the soil. However, calculations by Southwest Research Institute (SwRI) and our own studies (Ref 3,4) indicate that the precursor is significant only in the first few centimeters of the soil, after which, it is overtaken by the main shock generated by the impact of the flyer plate with the soil.

One problem encountered was that following each experiment, the plate would be found with the outer portion bent upward. Bending occurred because of the reduced loading from the explosives around the outer portion of the plate caused by edge rarefactions. This situation was remedied by adding a guard ring around the plate which prevented coupling of shear and bending loads to the center plate. This technique was successful in eliminating the bending problem.

THEORETICAL MODELING - SOIL MATERIAL

The nomenclature for development of the theoretical model for a dry soil testbed is described in Figure 2 where conditions before and after impact are defined. We treat only the one-dimensional aspects of the phenomenology in the theoretical development, i.e., edge effects are ignored. In the actual experiment design, consideration must be given to two-dimensional flow effects induced by the edge effect to insure that the assumptions made in the one-dimensional modeling are still applicable. Results of two-dimensional calculations performed by SWRI (Ref 3) indicate that in the central portion of the soil test bed, out to approximately one-half the plate radius, the flow field remains essentially one-dimensional, even to late times. This is due primarily to the confining effects of the native soil outside the test bed. Thus, the primary design consideration for determining plate diameter is that it must be large enough so that all the instrumentation in the soil can be conveniently placed inside a circle that has a radius of one-half that of the plate and is centered in the soil test bed.

The total momentum per unit area of the flyer plate is simply the mass per unit area of the plate, M_f, times its impact velocity, V_f. Using conservation of momentum and assuming a locking soil model (no strain recovery), the momentum per unit area at some time after plate impact can be expressed as

$$M_f V_f = (M_f + \rho_s x) u \qquad (1)$$

where

ρ_s is the soil preshocked density,

x is the shock position in the soil relative to the impact surface, and

u is the soil particle velocity behind the shock

Solving for u in Equation (1)

$$u = \frac{M_f V_f}{M_f + \rho_s x} \qquad (2)$$

Note that through Equation (2), u(x) can be determined by knowing only the preshock soil density and the plate impact velocity. Through soil shock TOA data, $t_a(x)$, or soil strain data, $\epsilon(x)$, or by knowing the soil model in terms of shock velocity, c, versus particle velocity, u, the remaining parameters that characterize the stress and motion field in the soil can be determined. Any two sets of data will provide a solution, thus, for the four data sets there are six independent solutions

Solution 1 using $V_f + t_a(x)$ data sets

Solution 2 using $V_f + \epsilon(x)$ data sets

Solution 3 using $V_f + c(u)$ data sets

Solution 4 using $t_a(x) + e(x)$ data sets

Solution 5 using $t_a(x) + c(u)$ data sets

Solution 6 using $\epsilon(x) + c(u)$ data sets

The remaining equations required to completely describe the stress and motion field are

$$I_s = \rho_s x u \qquad (3)$$

$$I_g = \rho_s (x - x_g) u \qquad (4)$$

$$\sigma = \rho_s c u \qquad (5)$$

$$\epsilon = \frac{u}{c} \qquad (6)$$

$$\sigma_s = \frac{\rho_s c u M_f}{M_f + \rho_s x} \qquad (7)$$

$$\sigma_g = \frac{\rho_s c u (M_f + \rho_s x_g)}{M_f + \rho_s x} \qquad (8)$$

where

x_g is a gage location,
I_s is impulse at the soil surface,
I_g is impulse at a gage location,
σ is soil stress at the shock front,
ϵ is soil strain at the shock front,
σ_s is soil stress at the impact surface, and
σ_g is soil stress at a gage location.

The locking soil model is the key to the simplicity of this technique. This model assumes that the soil is compressed to its maximum strain state by the shock wave and that only an insignificant amount of strain is recovered during and after unloading. A result of the locking soil model assumption is that every soil particle behind the shock front, as well as the flyer plate, is moving at the same velocity. The time at which a stress and motion state exists at any point in the test bed is determined explicitly through
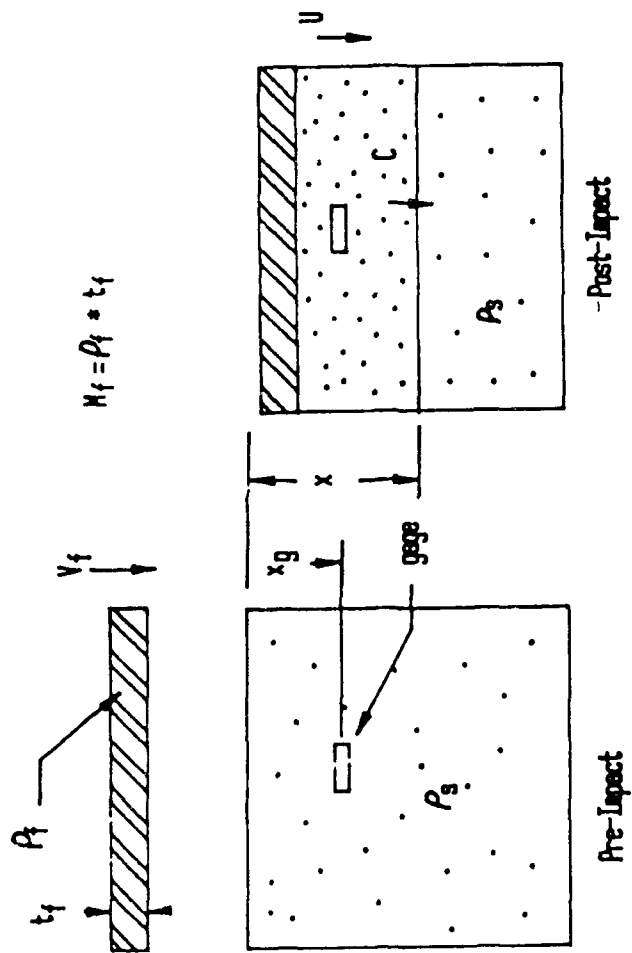
47

$M_f = \rho_f \cdot t_f$

V_f

ρ_f

t_f

x_g

gage

ρ_s

Pre-Impact

U

C

ρ_s

x

-Post-Impact

Figure 2. Flyer Plate/Soil Interaction Model

48

the TOA data, or, if that is not available, $t_a(x)$ generated through any two sets of the other data (such as plate velocity and soil strain data).

A review of strain versus depth data collected in numerous dry soil flyer plate experiments suggested that the variation was linear. We assume the linear relationship shown in equation (9) where C_0 and C_1 are constants.

$$\epsilon = C_0 + C_1 x \tag{9}$$

We now derive the functional form for $t_a(x)$ based on Equation (9). Substituting for u in Equation (6) from Equation (2), equating with Equation (9) and then solving for c, we obtain

$$c = \frac{M_f V_f}{(M_f + \rho_s x)(C_0 + C_1 x)} \tag{10}$$

or as expressed in reciprocal form

$$\frac{1}{c} = \frac{dt_a}{dx} = \frac{(M_f + \rho_s x)(C_0 + C_1 x)}{M_f V_f} \tag{11}$$

Integrating Equation (11), we obtain

$$t_a = \left(\frac{C_0}{V_f} \right) x + \left(\frac{C_1 M_f + C_0 \rho_s}{2 M_f V_f} \right) x^2$$

$$+ \left(\frac{C_1 \rho_s}{3 M_f V_f} \right) x^3 + \text{constant}$$

$$t_a = B_0 + B_1 x + B_2 x^2 + B_3 x^3 \tag{12}$$

where

$B_0 = 0$ (arbitrary constant)

$B_1 = \frac{C_0}{V_f}$

$B_2 = \frac{C_1 M_f + C_0 \rho_s}{2 M_f V_f}$

$B_3 = \frac{C_1 \rho_s}{3 M_f V_f}$

Equation (12) is simply a third degree polynomial whose coefficients can be determined explicitly in terms of the parameters indicated or by use of a polynomial regression program applied to the TOA data.

A more detailed development of the theoretical model as well as a full development of the scaling relationships are presented in Reference 5.

EXPERIMENTAL RESULTS — DRY SOIL GEOLOGY TESTBED

Eight 1.22-m, four 2.44-m and one 3.05-m diameter flyer plate experiments were conducted during the development phase of this program. The objectives of these experiments were to develop the flyer plate launch technique, develop diagnostic instrumentation for the measurement of plate impact velocity,

soil shock wave time-of-arrival and soil peak strain, to develop methods for placing the soil in the test bed in a controllable, repeatable manner and to validate gages. Experiment FP 8-3 was the third 2.44-m (8-ft) diameter test and the first to be extensively instrumented with a full compliment of diagnostic instrumentation. In addition, several types of stress and motion gages were placed in the test bed for purposes of evaluation and calibration. MIPV data from the FP 4-10 experiment were also selected to show it's comparison with the model. Posttest measurements of two MIPV records from FP 4-10 and the results of Solution 4 are plotted in Figure 3 and show very good agreement. The rest of the brief analysis presented here describes the results of the FP 8-3 experiment and compares those results with the theoretical model presented above. Diagnostic instrumentation fielded in FP 8-3 is described in Reference 6. Data obtained with the diagnostic instrumentation resulted in a good determination of flyer plate impact velocity (474 m/s), shock front time-of-arrival versus depth and peak soil strain versus depth. The nominal soil density was 1653 kg/m³ and the steel flyer plate was 4.572 cm thick.

Ground shock time-of-arrival versus depth data are shown in Figure 4 with a third-degree polynomial fit to the data. The soil strain versus depth data are shown in Figure 5 with a linear fit to the data. All data shown in Figures 4 and 5 are for gage locations within a radius of 0.61 m from the centerline of the test bed.

Since three independent sets of data were obtained $(V_f, t_a(x), \epsilon(x))$, there are three independent solutions for determining the stress and motion fields in the test bed. The solution data sets used will be referenced, as before, in the following way:

Solution 1 using $V_f + t_a(x)$ data sets

Solution 2 using $V_f + \epsilon(x)$ data sets

Solution 4 using $t_a(x) + \epsilon(x)$ data sets

Solutions 3, 5 and 6 involve $c(u)$ which was not determined independently in this experiment.

Figures 6, 7, 8 and 9 describe the stress and motion field in the test bed for the three solutions indicated. Figures 6 and 7 show the attenuation of peak particle velocity and stress with depth. In Figure 6, solutions 1 and 2 are identical for velocity versus depth. The higher velocity indicated by solution 4 should be treated with less confidence than solutions 1 and 2 which are determined directly from the momentum equation. In Figure 7 at depths below approximately 0.10 m (stress below 600 MPa), very good agreement is observed between all three solutions. Soil particle velocity versus time is shown in Figure 8. The time history of particle velocity at some depth, for instance at a velocity gage location, can be determined by
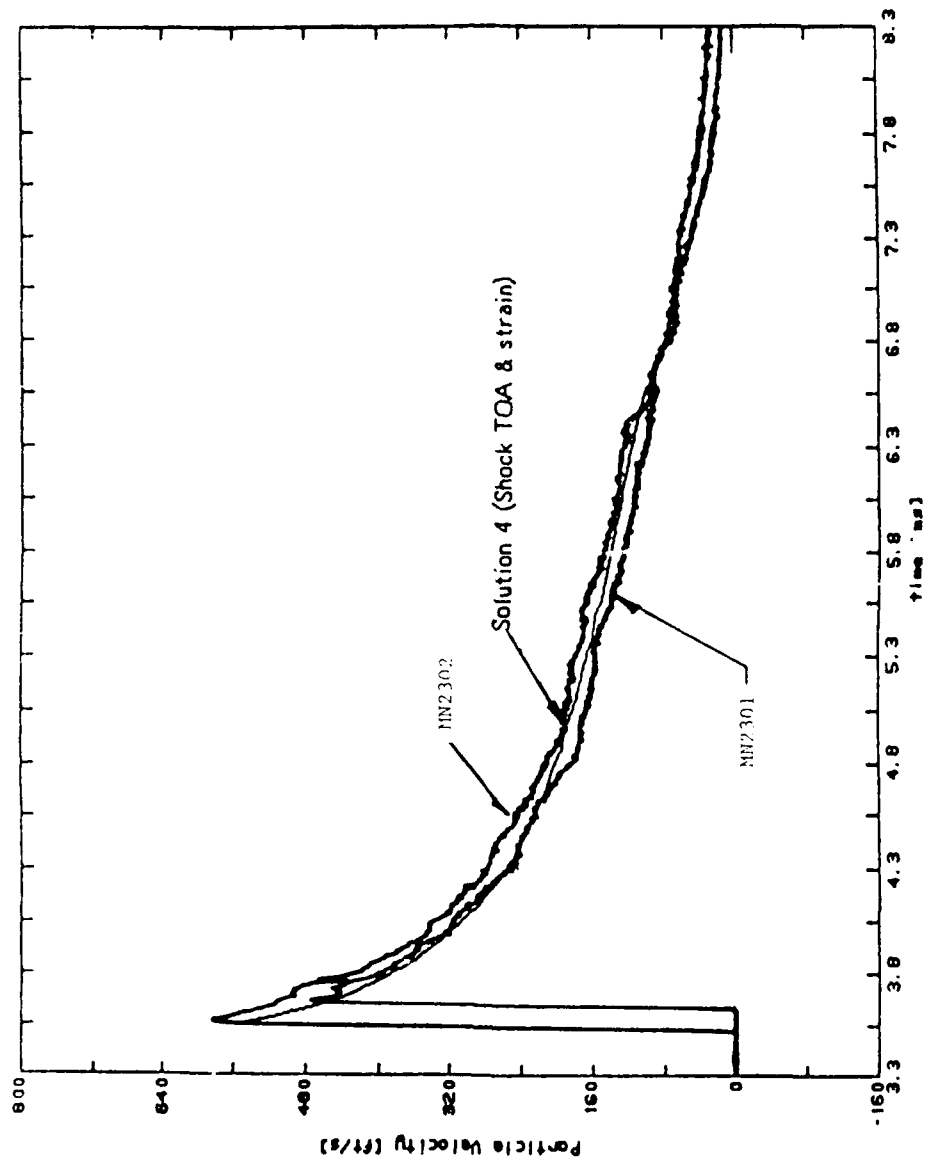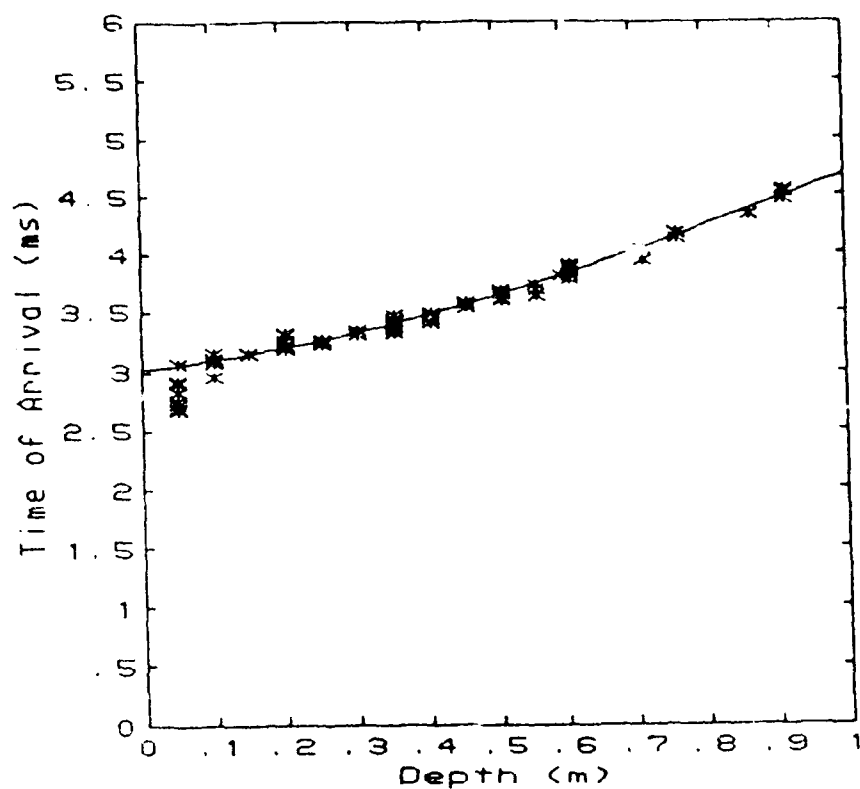
FIGURE 3 MIPV Data

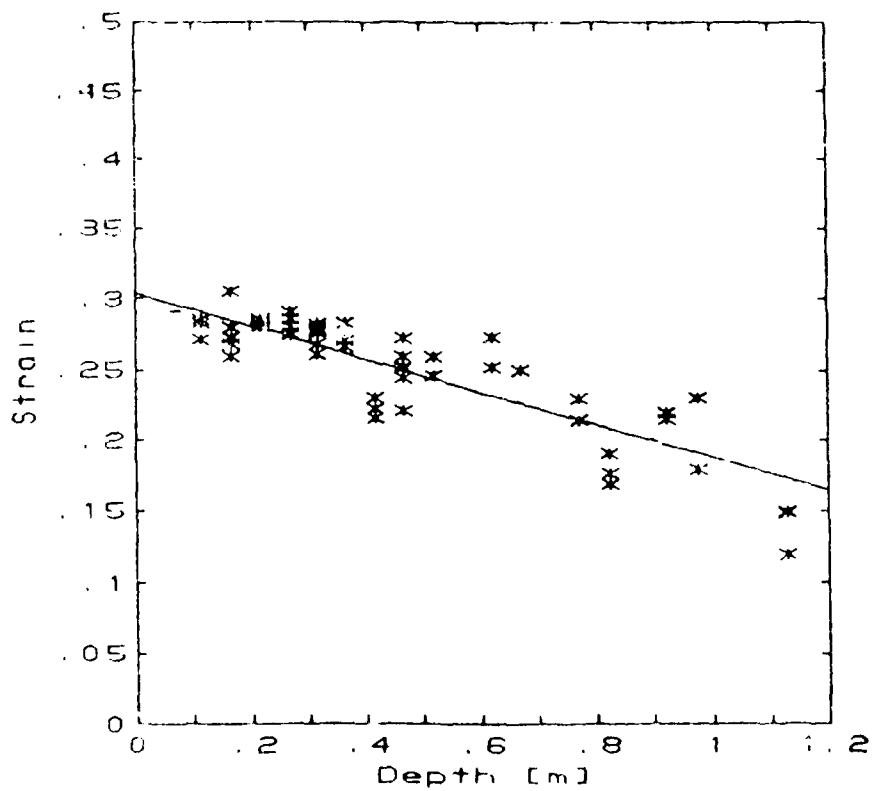FIGURE 4. Ground Shock Time-of-Arrival vs. Depth, FP 8-3

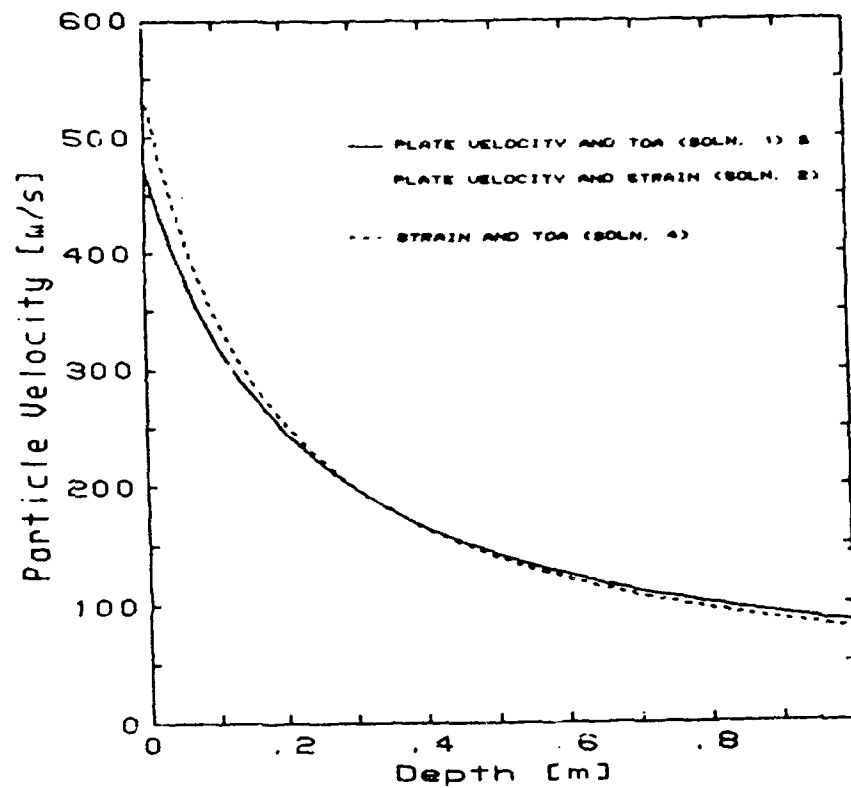FIGURE 5. Peak Strain vs. Depth, FP 8-3
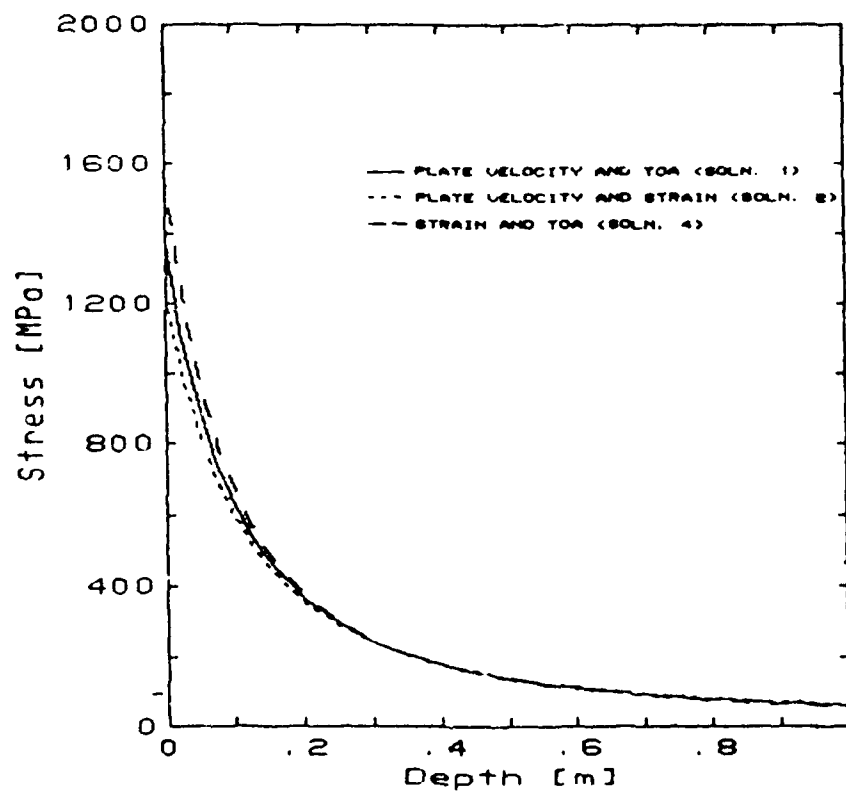
FIGURE 6. Peak Particle Velocity vs. Depth, FP 8-3

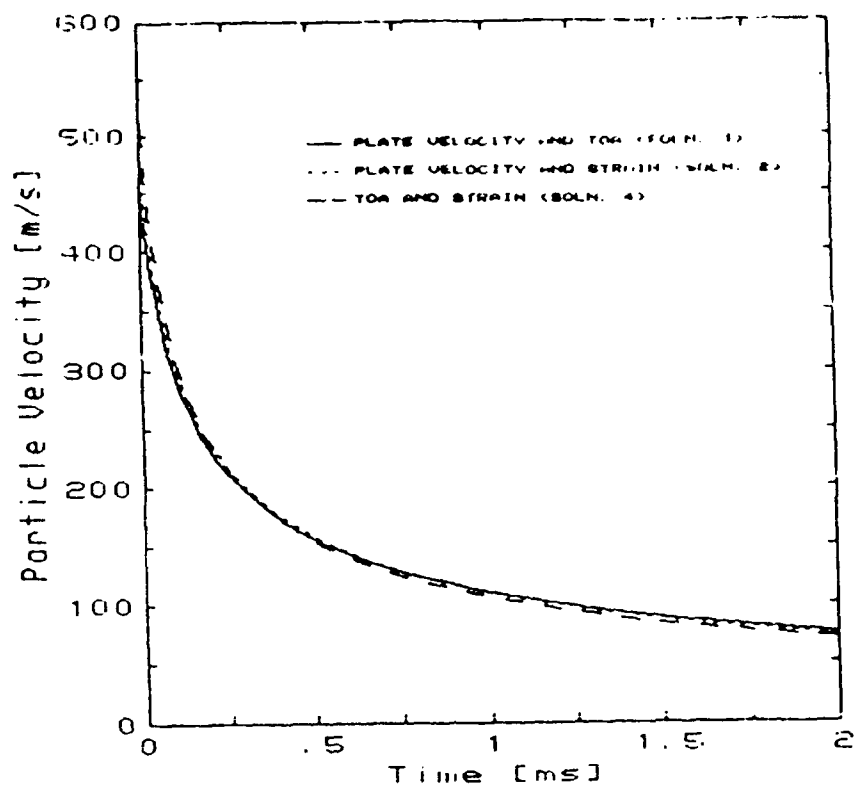FIGURE 7. Peak Stress vs. Depth, FP 6-3
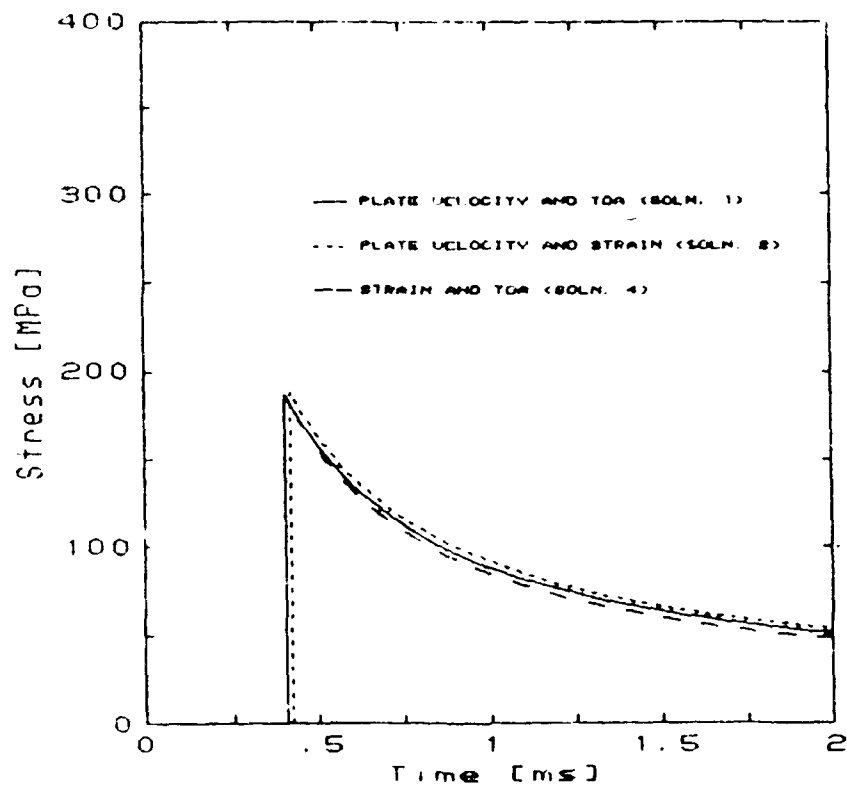
FIGURE 8. **Particle Velocity vs. Time, FP 8-3**

FIGURE 9. **Soil Stress vs. Time at x_g = .381 w, FP 8-3**

simply noting the arrival time of the shock front at that depth. Again, below approximately 0.10 m in depth, the three solutions are in very good agreement. Note that since the soil is considered to be in rigid body motion behind the shock, motion in the test bed is completely described by Figure 8.

Soil stress versus time is shown in Figure 9 for a gage depth of 0.381 m which corresponds to the depth at which flatpack stress gages were placed. Note that there is very little difference in the stress waveforms for the three solutions if the time-of-arrival shift is accounted for.

Posttest analysis calculations and corresponding stress records are shown in Figures 10, 11 and 12 for one HRSE gage and two CBS gages placed at 0.91 m depth. The peak values agree extremely well. Because these gages were relatively deep, the calculation values become increasingly unreliable shortly after the peak value is reached.

FLYER PLATE TECHNIQUE - ROCK MATERIAL

The simple analytic method developed for the dry soil flyer plate technique is not applicable for the rock matching grout geology since this material cannot be adequately described by a locking soil model. A more elaborate analysis methodology has been developed (Ref 7) for these materials which requires the measurement of particle velocity at several depths in the test bed. The velocity data is used with preshock density and TOA data in a Lagrangian analysis to determine the stress and motion fields in the testbed. An important result of this analysis technique is the determination of the material response from which a model may be generated. The model is then used in a one dimensional Lagrangian calculation of the flyer plate experiment. If the calculated motion fields agree well with the experimental velocity data, then it is concluded that validation criteria have been satisfied. As before, the flyer plate impact momentum is the validation standard.

Exploratory development tests and preliminary results for rock geology tests are discussed in References 8 and 9.

SUMMARY

The high explosive driven flyer plate technique for validating the response of stress and motion instrumentation has been successfully demonstrated in a dry soil and rock like geologies. The technique for dry soil is well developed and several instrumentation validation experiments have been conducted. The technique for rock like geologies is in development. However, the results of initial exploratory experiments are very encouraging. We is planning to perform a 2.44 m diameter flyer plate experiment on a rock-matching grout test bed in FY 90 pending appropriate support.

REFERENCES

(1) Gurney, R.W., "The Initial Velocities of Fragments from Bombs, Shells, and Grenades," U.S. Army Ballistic Research Laboratory Report 405, 1943.

(2) Kennedy, J.E., "Explosive Output for Driving Metal," Behavior and Utilization of Explosives in Engineering Design, 12th Annual Symposium ASME, Published by The New Mexico Section ASME, March 2-3, 1972.

(3) Anderson, C.E., Jr., O'Donoghue, P.E. and O'Kelley, D.E., A Methodology for the Calibration of Soil Stress and Motion Instrumentation for Dry Soils, AFWL-TR-87-70, Air Force Weapons Laboratory, Albuquerque, New Mexico, June 1988.

(4) Renick, J.D., Anderson, C.E., Jr., O'Donoghue, P.E., O'Kelley, D.E. and Felice C., "A Methodology for the Calibration of Stress and Motion Instrumentation for Dry Soils," J. App. Phys. 63(5), 1 Mar 1988.

(5) Renick, J.D., Goodfellow, G.M. and Flores, L.E., "Large High Explosive Driven Flyer Plate Technique for the Calibration of Soil Stress and Motion Instrumentation," Proceedings of the Conference on Instrumentation for Nuclear Weapons Effects Testing, 6-8 October 1987, DASIAC-SR-88-220-VI-PT-2, September 1988.

(6) Jarpe, J.S., Flyer Plate 8-3 (#10) Data Report, Report No. NMERI/CERF WA9-240, New Mexico Engineering Research Institute, Albuquerque, New Mexico, October 1987.

(7) Seaman, L., Lagrangian Analysis for Stress and Particle Velocity Gages, SRI Project PYU-8179, SRI International, Menlo Park, California, August 1984.

(8) Jarpe, J., Rock Flyer Plate Tests, FFP Tests, Test Report, Report No. NMERI/CERF WA7-02(1), New Mexico Engineering Research Institute, Albuquerque, New Mexico, January 1989.

(9) Goodfellow, G.M. and Renick, J.D., "Large High Explosive Driven Flyer Plate Technique for the Validation of Rock Stress and Motion Instrumentation," Proceedings of the Conference on Instrumentation for Nuclear Weapons Effects Testing, 6-8 June 1989, to be published.
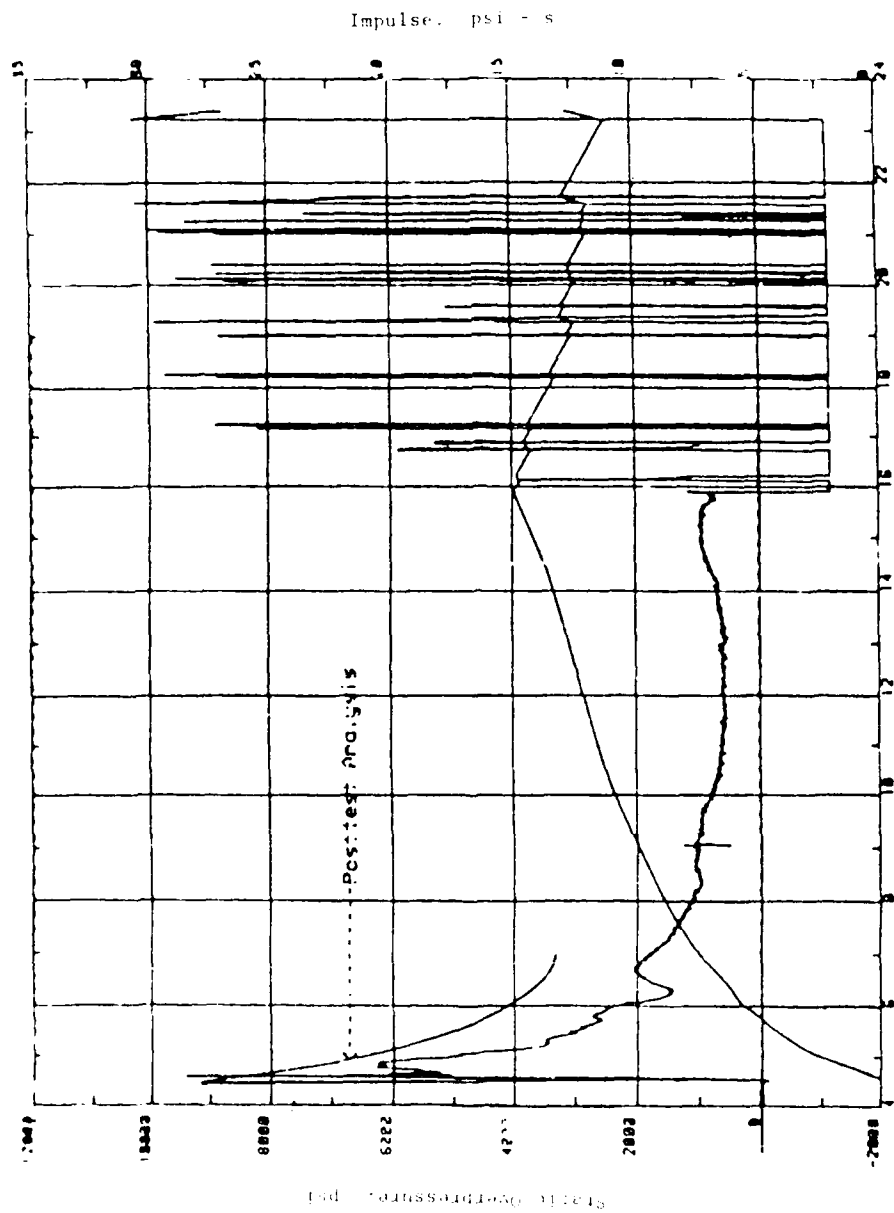
Impulse. psi - s
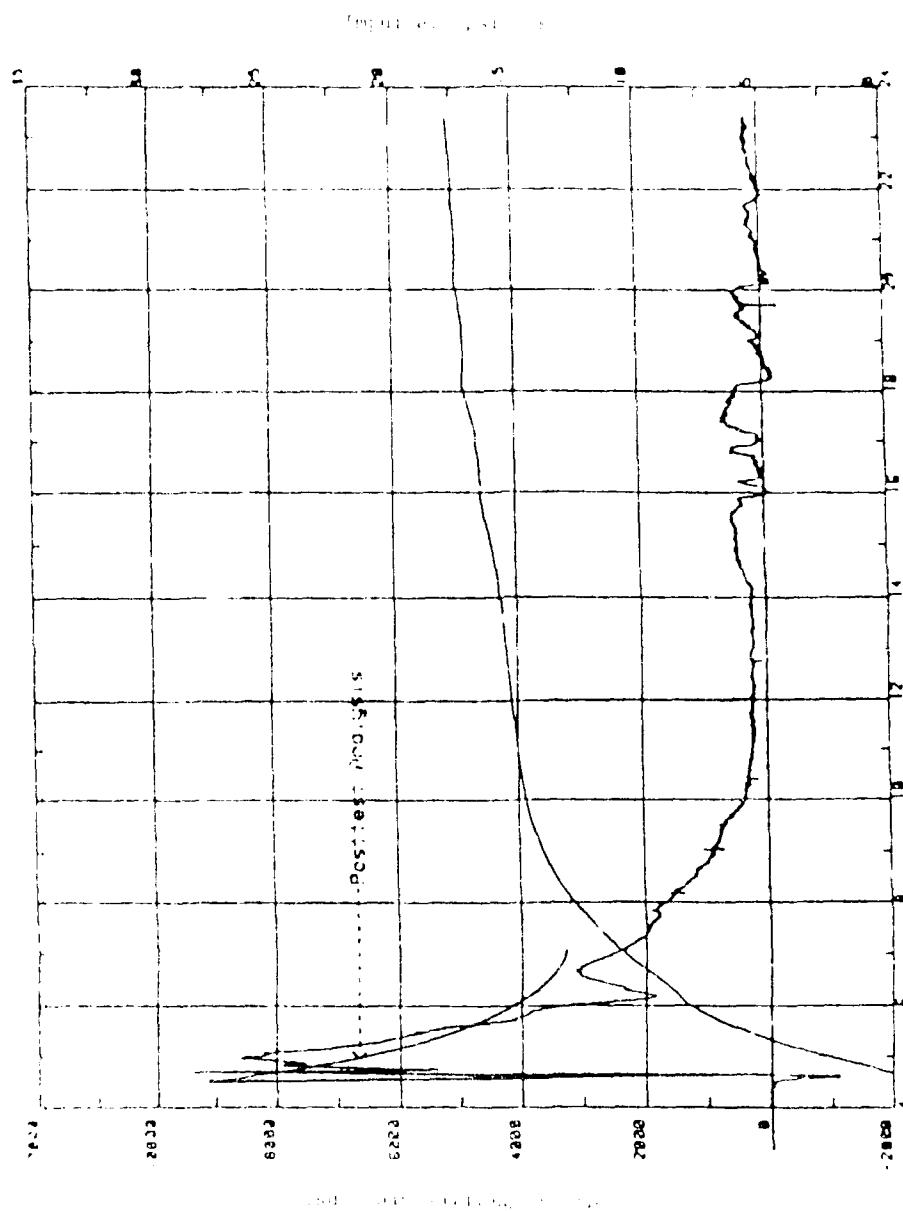

FIGURE 10 FLYER PLATE 8-3 HRSE 8393884 E18/A/07/V1x8781

Static Overpressure, psi

Posttest analysis

FIGURE 1: FLYER PLATE 8-3 CBS.517 E10/A/81/W165001

Impulse, psi - s

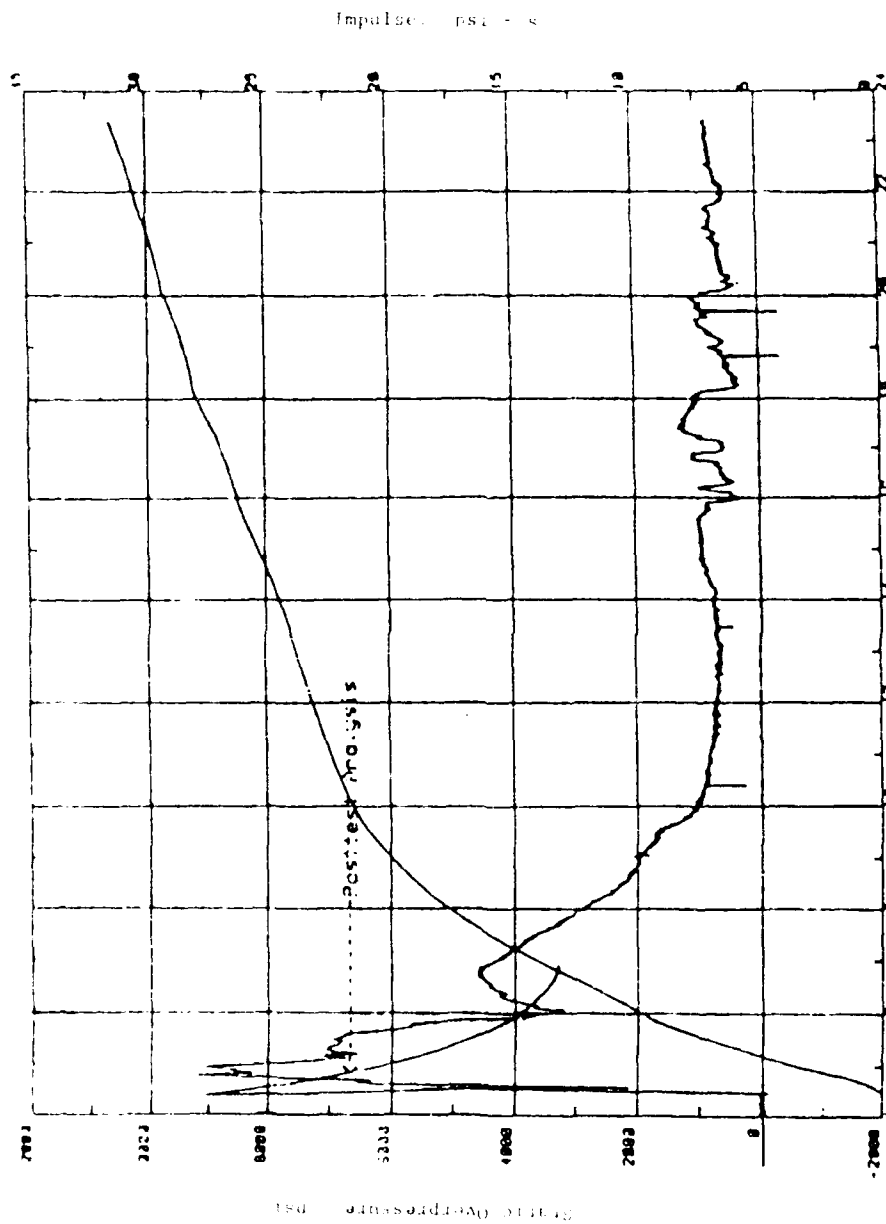FIGURE 12 FLYER PLATE 8-3   CBS-539   E10/A/03/W1#5082

"Performance Evaluation of Piezoelectric Accelerometers Using a FFT Based Vibration Transducer Calibration System"
Ernst Schonthal and Torben R. Licht

Verification (calibration) of the useful frequency range of a piezoelectric accelerometer, are traditionally performed by the point-by-point method or by the swept sine excitation method.

With the point-by-point method time restraints normally permit only a limited number of points to be verified, whereby irregularities in the sensitivity versus frequency are easily missed. With the swept sine excitation method limitations in penand sweep speed may result in poor resolution and important information may be lost.

PERFORMANCE EVALUATION OF PIEZOELECTRIC ACCELEROMETERS USING FFT BASED VIBRATION TRANSDUCER CALIBRATION SYSTEM

Q: **Ray Reed (Sandia National Laboratories):** The part I missed in your talk - you are applying the FFT - how were the accelerometers excited and to what G level; were they excited by impulse, or were they excited by random excitation?

A: **Ernst Schonthal:** Random excitation and at about 2 g's.

SESSION 2

APPLICATIONS

AN INCREASED ACCURACY, DUAL CHANNEL,

TELEMETRY ACCELEROMETER

Robert Hartzell   Robert Catchel
Marketing Manager   Design Engineer
Inertial Products Group
Columbia Research Labs., Inc.
Woodlyn, PA

ABSTRACT

A major problem in transmitting analog
data over an FM telemetry data link has
been the inherent resolution of the link
itself. A typical link might have a
received output of 250 counts per 5
volt transducer span, thereby having a
maximum resolution of ±1 count on 250 or
±0.4%. A technique has been developed at
the cost of only one additional data
channel, which magnifies the data between
individual counts by a factor of 16 to 1
and represents this data as a separate 0
to 5 Volt telemetry input. When the two
pieces of data are recombined at the
receiver, there will be an increase in
the overall data accuracy from 0.4% to
0.025%.

INTRODUCTION

The technique employs the use of a CMOS
digital loop similar to the methods used
in autoranging voltmeters. Columbia's
Model DCT-521209 incorporates a force
rebalanced linear accelerometer inside
the enclosure. The transducer is factory
rangeable to the user's specific
requirements. This method can also be
readily implemented and function with any
transducer (i.e. temperature, pressure,
displacement, vibration, etc.) that has a
0 to 5 Volt output span.

DESCRIPTION OF A FORCE REBALANCED LINEAR ACCELEROMETER

The servo (or force rebalanced)
accelerometer senses acceleration by
means of a force rebalanced pendulum.
The pendulum's position is detected with
respect to the case. As the pendulum
begins to deflect due to an acceleration,
the position error is fed to the input of
a servo amplifier and the pendulum is
restored to its null condition by means
of a torque motor. The motor torque
current is directly proportional to the
applied acceleration. Accelerometers are
usually mechanized by means of linear
translational mass or a pendulum. The
mass (or pendulum-bob) is the element on
which the acceleration acts. Newtons
second law of motion states that force
is proportional to a mass which is being
accelerated. For a given mass, if the
acceleration increases, the force (or
torque, in the case of the pendulum)
increases proportionally and vice versa.
Let us investigate the case of the
pendulous accelerometer. If we suspend
a pendulum in a structure and accelerate
the structure, the pendulum will tend
to stay fixed in inertial space (Newtons
first law of motion). The displacement
angle traversed by the pendulum is
directly proportional to the magnitude
and direction of the applied acceleration.
The servo accelerometer has a restoring
means for the translational mass or
pendulum. A torque generator (D.C.
motor) is incorporated with the spring
mass system which maintains the pendulum
in a fixed or reference position. As the
system is accelerated, the magnitude and
direction of the restoring torque is
directly proportional to the applied
acceleration. The restoring phenomenon
is in effect an electrical spring. We
now have an equivalent mechanical element
which is electrically controllable.
Damping can also be electrically
introduced into the system by means of
an electrical "lead term" in the servo-
amplifier frequency characteristic. By
selecting the torque motor parameters,
changing amplifier gain/frequency
characteristics and pendulousity
(pendulum parameters), there is
substantial leeway in that overall range,
bandwidth and damping requirements can be
accomplished. The damped spring mass is
readily modelable as a spring mass system
(ref. Fig. 1). The inherent performance
characteristics of this type device is
many times greater than the accuracy of a
data link. Typical performance is listed
in the data sheet contained in the
appendix.

DESCRIPTION - PREAMPLIFIER/DIGITIZER

The signal conditioning circuitry of the DCT-521209 provides the two telemetry channel outputs; the step output, which yields the whole G increments in steps of 0.156 V/G and the vernier channel, which yields the magnified, fractional G levels which vary from 0 to 5 V, depending on the step level and accelerometer signal.

The operational sequence of the DCT signal conditioning circuitry begins at the servo accelerometer, described earlier. The output of the accelerometer is fed through a buffer/inverter with a gain of -1. The buffer effectively isolates the conditioning circuitry from the servo section and performs a voltage inversion necessary for proper operation of the difference amplifier. See Figure 2 for functional block diagram.

The difference amplifier consists of a summing node at the inverting input of a low noise operational amplifier. The signals to be summed are the inverted servo output and the non inverted step channel output. The difference voltage generated at the input of the difference amplifier is magnified by a factor of 16. This amplified difference signal represents the vernier output of the DCT. The amplifier is biased such that if the servo input and the step output are exactly equal, the output of the amplifier is 2.500 V. When the servo voltage increases to a maximum +1G level above the step output, the difference voltage of .156V is amplified by 16 and added to the 2.500 zero bias, yielding a 5.000V full scale output. Conversely, when the servo output voltage increases to a maximum -G level below the step output, the difference voltage of 0.156 is amplified by 16 and subtracted from (or algebraically added to) the 2.500 V zero bias, yielding a 0 V output.

The output of the difference amplifier (vernier output) is fed to the input of the window comparitor. The window comparitor actually consists of two distinct voltage comparitors, one referenced to 5.00 V and the other referenced to "near ground" potential. When the vernier output reaches a 5.00 V level, the output of the 5 V comparitor goes from a normally "high" state to a low state. When the vernier output falls below the 5.00 V trigger level, the output of the 5 V comparitor returns to its "high" state. Similarity, the operation of the 0 V comparitor is exactly the same as that of the 5 V comparitor.

The output of the window comparitor is fed to the logic section. The 5 V comparitor output is fed to the up line of the logic, while the 0 V comparitor output is fed to the down line. When the count up line of the logic section is made low by the action of the window comparitor, a free running astable multivibrator clock is fed to the count up section of a 5 bit, full binary counter. The action of the count down line is similar to that of the up count line; when the 0 V comparitor goes low, the clock pulses are routed to the down count line of the counter.
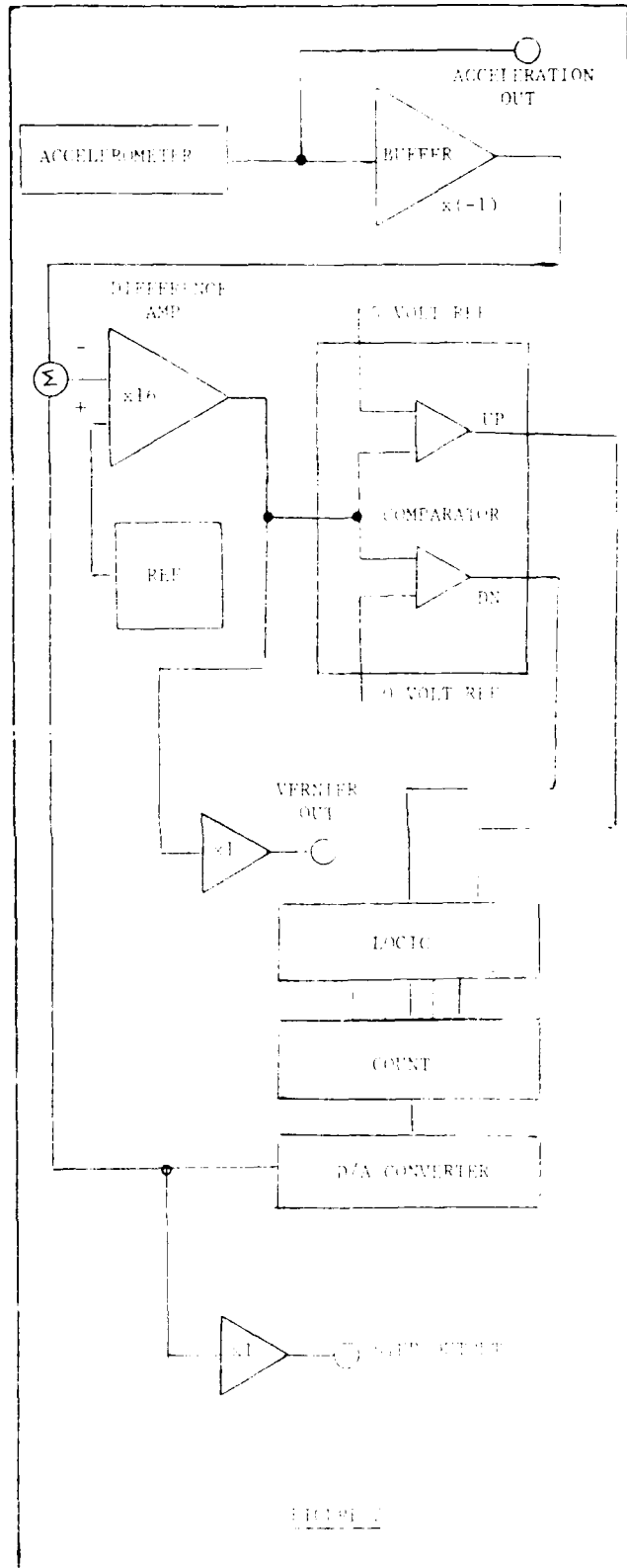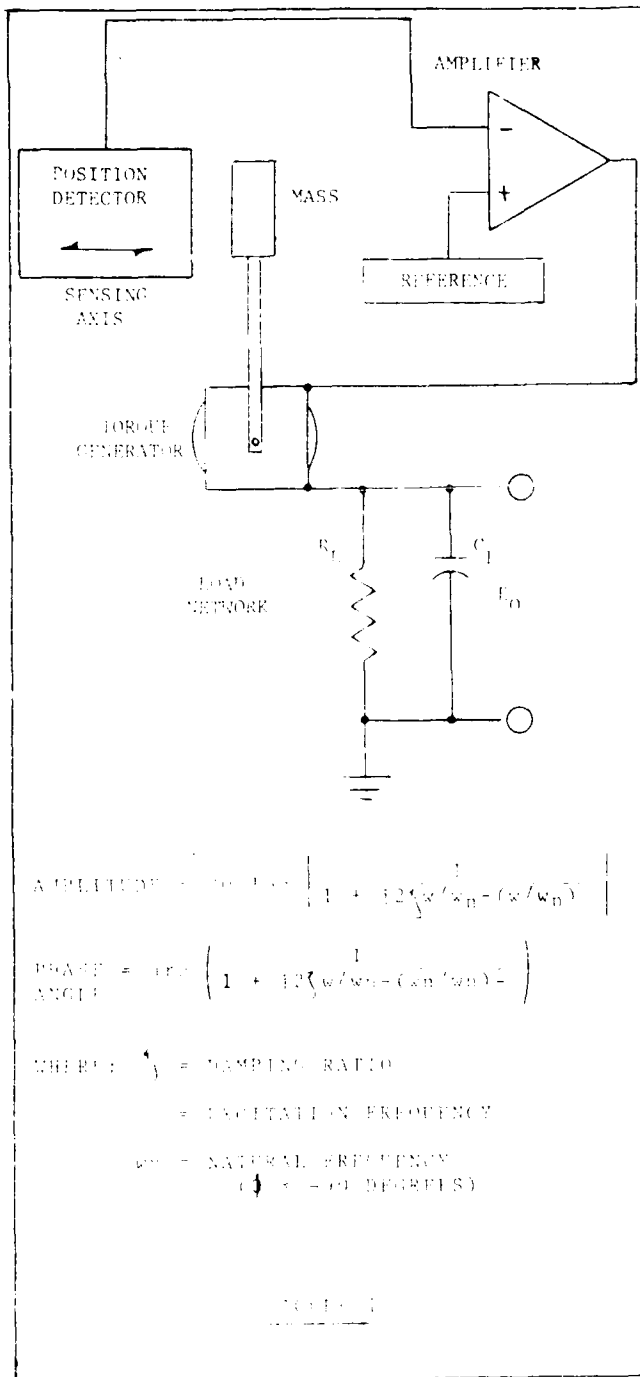
The binary word of the counter is fed to the input of the Digital to Analog converter which generates a voltage corresponding to the binary output word of counter section. The output of the DAC can range from a high of 5 V to a low of 0 V, in a series of 32 discrete levels or steps or 0.156 V/step. This DAC output voltage represents step output signal.
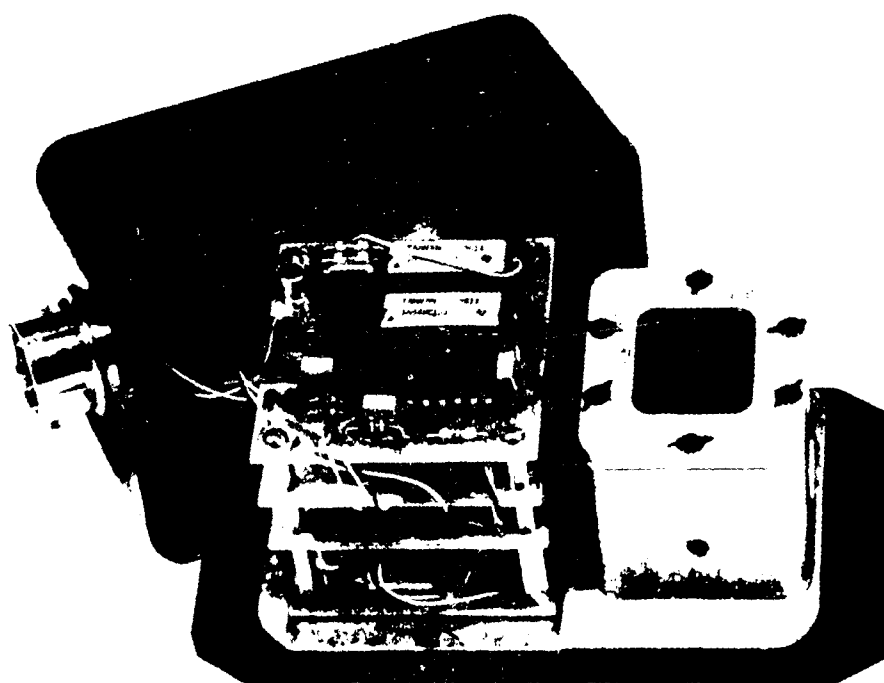
The overall function of the window comparitor, counter and the DAC is to quantize the servo accelerometer output into discrete 0.156 (1g) steps. The quantized servo accelerometer output is fed back to the summing node of the difference amplifier, thus completing the loop.

SUMMARY

Columbia Research Laboratories, Inc. has devised and implemented a method of reclaiming inherent transducer accuracy in a telemetering system. Attached in the appendix is a specification sheet which defines the system as applied to a linear acceleration transducer. This particular device has been fully qualified for use in military missile systems where ruggedness, inherent reliability and environmental stability are essential to mission success.

The technique can be readily applied to any transducer that has a zero to 5 Volt output span.

AMPLIFIER

POSITION
DETECTOR

MASS

SENSING
AXIS

REFERENCE

TORQUE
GENERATOR

LOAD
NETWORK

R_L

C_1

E_o

$$\text{AMPLITUDE} = \ldots \left| \frac{1}{1 + j2\zeta(w/w_n) - (w/w_n)^2} \right|$$

$$\text{PHASE} = \tan^{-1} \left(\frac{1}{1 + j2\zeta(w/w_n) - (w/w_n)^2} \right)$$

WHERE: ζ = DAMPING RATIO

= EXCITATION FREQUENCY

w_n = NATURAL FREQUENCY
($\phi = -90$ DEGREES)

FIGURE 1

ACCELERATION
OUT

ACCELEROMETER

BUFFER

$x(-1)$

DIFFERENCE
AMP

Σ

$x16$

5 VOLT REF

UP

COMPARATOR

REF

DN

0 VOLT REF

VERNIER
OUT

$x1$

LOGIC

COUNT

D/A CONVERTER

$x1$

FIGURE 2

COLUMBIA
DUAL CHANNEL ELEMETER SYSTEM
MODEL DCE-1200
RANGE

PN

APPLICATION		REVISIONS			
NEXT ASSY.	USED ON	LTR.	DESCRIPTION	DATE	APPROVED
		-	DOCUMENT RELEASE	3 8⁷	
		A	REVISED FOOT DIMENSION P.4	-29.99	
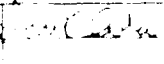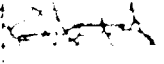
OUTLINE

AND

SPECIFICATION

FOR

DCT 521269

DUAL CHANNEL TELEMETRY SYSTEM

1	2	3	4	5	6	7	8	9	10	11	12	13	14	15	16	17	18	19	20	21	22	23	24	25	26	27	28	29	30	31	32

REVISION STATUS OF SHEETS

UNLESS OTHERWISE SPECIFIED DIMENSIONS ARE IN INCHES TOLERANCES FRACTION .DEC. ANGLE

MATERIAL:

DWN.	
CKD.	
ENG.	
QA	

⚲ COLUMBIA RESEARCH LABS., INC.

DUAL CHANNEL TELEMETRY SYSTEM

MODEL DCT 521269

	PROJ APP		SIZE	CODE IDENT NO	DRAWING NO
			A	07571	
			SCALE ~		SHEET 1 OF ~

SYSTEM SPECIFICATION:

ACCELERATION RANGE (base channel)	-24g to +8g (0 to 4.8VDC)
(vernier	±1g (0 to 4.8VDC)
INPUT POWER	+25VDC to +31VDC 300 mA Max.
BASE CHANNEL SCALE FACTOR	0.1563 Volt Steps/g
BASE CHANNEL BIAS	3.75VDC @ 0g
VERNIER SCALE FACTOR	2.50 Volts/g
VERNIER BIAS	2.50VDC @ 0g
ANALOG CHANNEL SCALE FACTOR	0.1563 Volts/g
ANALOG CHANNEL BIAS	3.75VDC @ 0g
ALIGNMENT	±1°, Case To True Sensitive Axis
ACCURACY	±0.2% Full Range (Exclusive Of Temperature)

ACCELEROMETER SPECIFICATION:

RESPONSE	0 To Full Scale, 0.01 Sec Max
DAMPING RATIO	1.0 Of Critical, Min
HYSTERESIS	±0.02% FR Max
RESOLUTION	±0.0001% FR Max
NON-REPEATABILITY	0.01% FR Max
OUTPUT NOISE	2.5 mVrms Max (0 to 100HZ)
CROSS AXIS SENSITIVITY	0.002g/g Max
TEMPERATURE SENSITIVITY	+0.005% FR/°F (68°F + 25°F) +0.010% FR/°F (-40°F to + 200°F)

	SIZE	CODE IDENT. NO.	DRAWING NO.:		REV.
COLUMBIA RESEARCH LABORATORIES, INC. Woodlyn, Pa 19094	A	07571	DTD-3477		
	SCALE: ~			SHEET: 1 OF 4	

ENVIRONMENTAL SPECIFICATION:

TEMPERATURE, OPERATING	$0^{O}F$ to + $170^{O}F$
TEMPERATURE, STORAGE	-$40^{O}F$ to + $200^{O}F$
VIBRATION	14g pk 5 to 2000HZ
SHOCK	60g pk, 5.5 msec rise time, 11 msec duration
ALTITUDE	+5 ATM to 150,000 ft.
RF INTERFERANCE	Per MIL-STD-826
OPERATING LIFE	200 Hrs Min
STORAGE LIFE	0.1% FR max/yr, 3 yr min.

PIN	FUNCTION
A	VERNIER OUT
B	STEP OUT
C	ANALOG OUT
D	ACCELERATION OUT
E	SIGNAL RET.
F	ACCELERATION TEST
G	SIGNAL GROUND
H	+28 VDC IN
I	+28 VDC RET.
K	CASE GROUND

J2 PIN FUNCTIONS

SIZE	CODE IDENT. NO.	DRAWING NO.:	REV.
A	07571	DTD-3477	

SCALE: ~   SHEET: 3 of 3

─.209 DIA.
3 PLS.

LABEL

2.30
MAX

1.400

4.200

4.60 MAX.

─ST1H-13-1GP
(J2)

2.30
MAX.

.25

.25

.030

─.49 ─
TYP.

COLUMBIA
RESEARCH LABORATORIES, INC.
Woodlyn Pa.19094
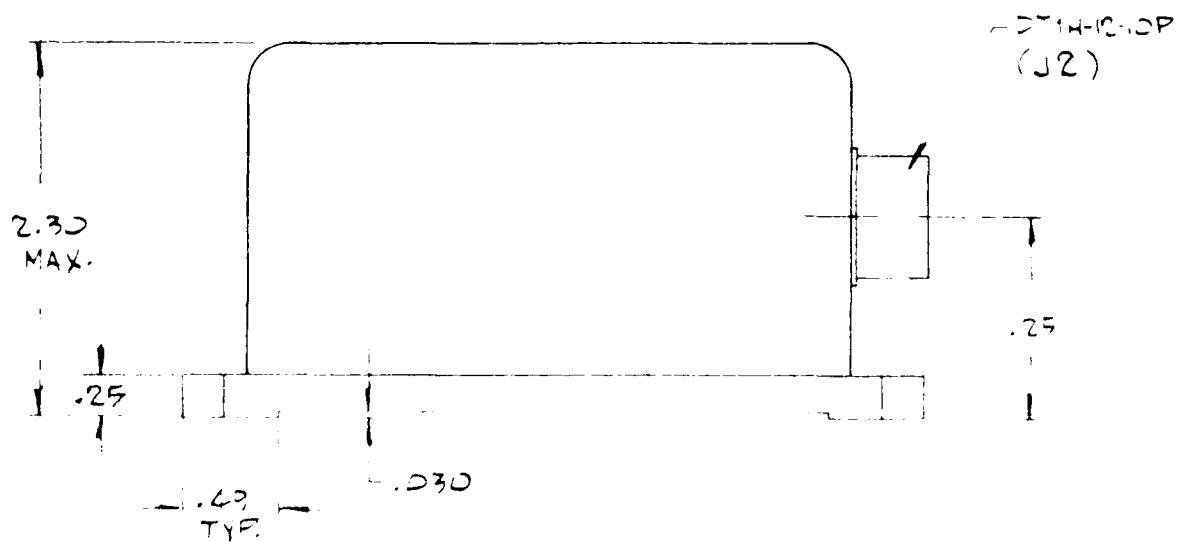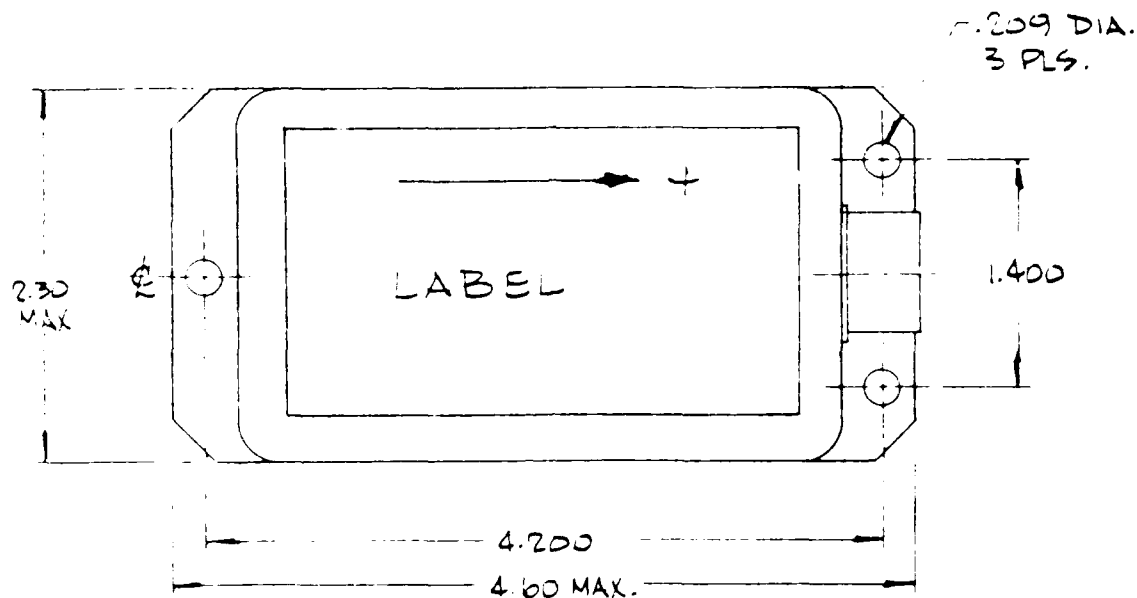
SIZE	CODE IDENT. NO.	DRAWING NO.:	REV.
A	07571	DTD-3477	
SCALE: FULL			SHEET: 4 OF 4

AN INCREASED ACCURACY, DUAL CHANNEL TELEMETRY ACCELEROMETER

Q: **Wes Paulson (NSWSES):** I think you've answered my main question, that is, you do have one accelerometer but two outputs?

A: **Robert Hartzell:** Right.

Q: **Wes Paulson:** Okay and that's to protect yourself. The noise source that you're protecting yourself from isn't any non-linearity in the accelerometer but it would be in the transmission channels?

A: **Robert Hartzell:** Right, it's the link itself that's causing the error or not allowing the inherent accuracy of the accelerometer in the first place.

Q: **Wes Paulson:** What's the approximate dynamic range of the link itself that's causing the error or not allowing the inherent accuracy of the accelerometer in the first place?

A: **Robert Hartzell:** The link that the Army was using was 250 counts full range, so it was like 138 millig's of inherent accuracy and this technique takes you down to about eight millig's and 32 g's full scale. And again that's not the limit of the accelerometer itself. That was the test data that they needed. The accelerometer we used in the system has an inherent accuracy less than 3 millig's.

Q: **Roger Noyes (EG&G):** When you mean accuracy, perhaps do you really mean resolution?

A: **Robert Hartzell:** Well, resolution and accuracy basically is a function of the suspension of the mechanism. Different manufacturers use different mechanisms and that's what they market.

Q: **Roger Noyes (EG&G):** I'm referring more to pure terms than your particular unit because it sounded to me like you were increasing your resolution thereby increasing your accuracy based on the inherent accuracy of your device. But it really sounded to me like you were only increasing your resolution of the system?

A: **Robert Hartzell:** That's correct. You're not increasing the resolution of the accelerometer.

Q: **Peter Stein (Stein Engineering):** That system ought to be applicable to other transducers and accelerometers as a general principal, do you have any plans?

A: **Robert Hartzell:** We offer the technique, in the paper we say that we haven't done it yet. But it is as I mentioned, anything that would have a zero to five volt span will be applicable. And Columbia, I'm sure, would be willing to offer the box for a nominal fee.

A MICROWAVE TRANSDUCER FOR MEASURING PISTON AND PROJECTILE

VELOCITIES IN A TWO-STAGE LIGHT-GAS GUN

L. Nappert
Defence Research Establishment
Valcartier
Québec, Canada, GOA 1RO

ABSTRACT

A microwave transducer has been developed and incorporated to a Michelson type microwave interferometer system. The instrument enables the simultaneous measurement of the velocity of the piston and projectile in the pump and launch tubes of a two-stage light-gas gun (LGG). The transducer is used to couple the microwave energy in and out of the pump and launch tubes, without interfering with the projectile motion. The development of the microwave transducer, its working principies, as well as its important electrical and mechanical characteristics are discussed. The signal conditioning performed and the data acquisition system used with the transducer on the two-stage LGG of the Defence Research Establishment Valcartier (DREV) are described. Typical experimental signals recorded during firings of the LGG are shown. The piston and projectile velocities calculated by processing these signals are presented. It is shown that these results correlate well with data obtained from different transducers (pressure and strain) mounted on the LGG.

INTRODUCTION

The Defence Research Establishment Valcartier (DREV) is equipped with a 250/105-mm two-stage light-gas gun capable of accelerating kilogram-class projectiles to velocities exceeding 5 km/s. This facility is currently used for studying hypervelocity impact and penetration phenomena under controlled conditions. Recently, a detailed mathematical model describing the physical phenomena associated with the internal ballistic cycle of two-stage light-gas guns was developed. To validate this mathematical model and its related computer program, an experimental program was undertaken whose objective was to measure gun performance during firing.

The displacement and velocity of the piston and projectile inside the pump and launch tubes of two-stage light-gas guns are important data that characterize their internal ballistic cycle. Microwave interferometry provides a useful method for observing the motion of the piston and projectile during their travel through the pump and launch tubes respectively. One of the most important components of a microwave interferometer sys-

tem for interior ballistic measurements is the microwave transducer used to couple the microwave energy in and out of the pump and launch tubes.

First, this paper briefly explains the operation of the DREV two-stage light-gas gun. Then the experimental arrangement setup to obtain simultaneously the dynamics of the piston and projectile is described. Afterwards the design of the microwave transducer is explained in detail and its electrical performances are presented. Finally some experimental results are shown and the correlation with other data obtained from different sensors mounted on the gun is briefly discussed.

PRINCIPLE OF OPERATION OF THE LIGHT-GAS GUN

The DREV two-stage light-gas gun is schematically illustrated in Figure 1. The pump tube is about 12 m long with an inner diameter of 256 mm. The launch tube is roughly 21 m long with an inner diameter of 110 mm. The principle of operation of a two-stage light-gas gun is explained in detail in the literature (1) and can be demonstrated by describing a typical launch cycle.

The operation starts with the ignition and burning in the combustion chamber of solid gun propellant (first stage). The hot gases generated from this combustion process drive the piston into the pump tube (second stage), which, in turn, compresses a light gas, usually helium. A diaphragm is used to isolate the projectile from the light gas. When the light gas is compressed to a given pressure, the diaphragm ruptures and the compressed gas accelerates the projectile down the launch tube. The piston is stopped in the area-change section between the tubes. The high velocity is achieved by the increased speed of sound in the light gas at the higher temperature. The physical limits to projectile velocity are set by the speed of sound in the gas and dissipative losses in the flow. The engineering limits are set by the stresses in the projectile, in the combustion chamber and in the area-change section.

The performance of the launch cycle is controlled by varying the amount of gun propellant, the mass of the piston, the initial pressure of the helium, the diaphragm rupture pressure, and the mass of the projectile.
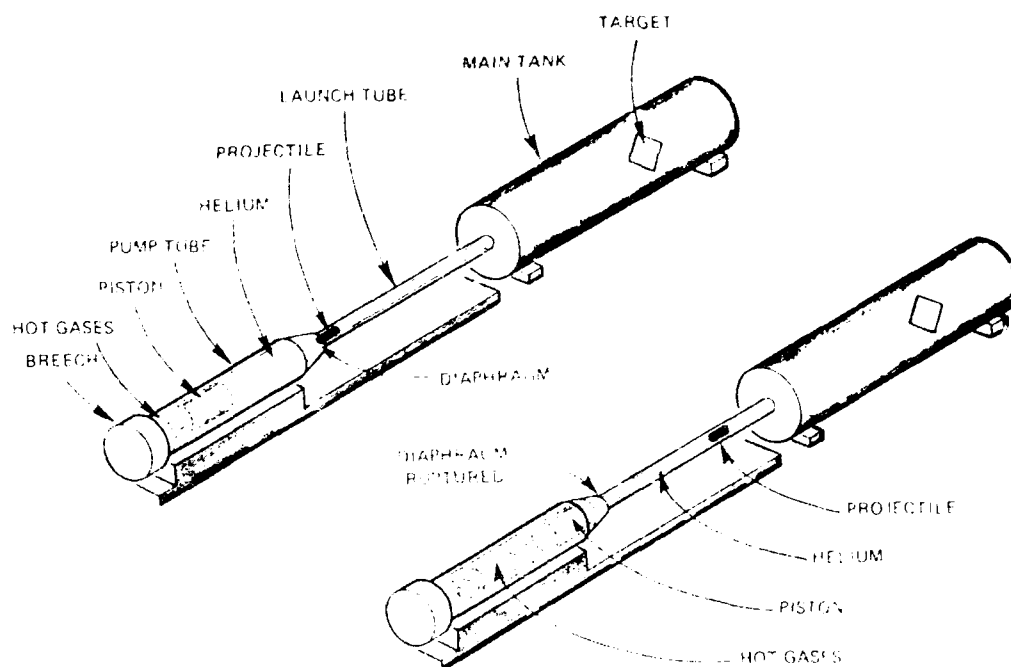
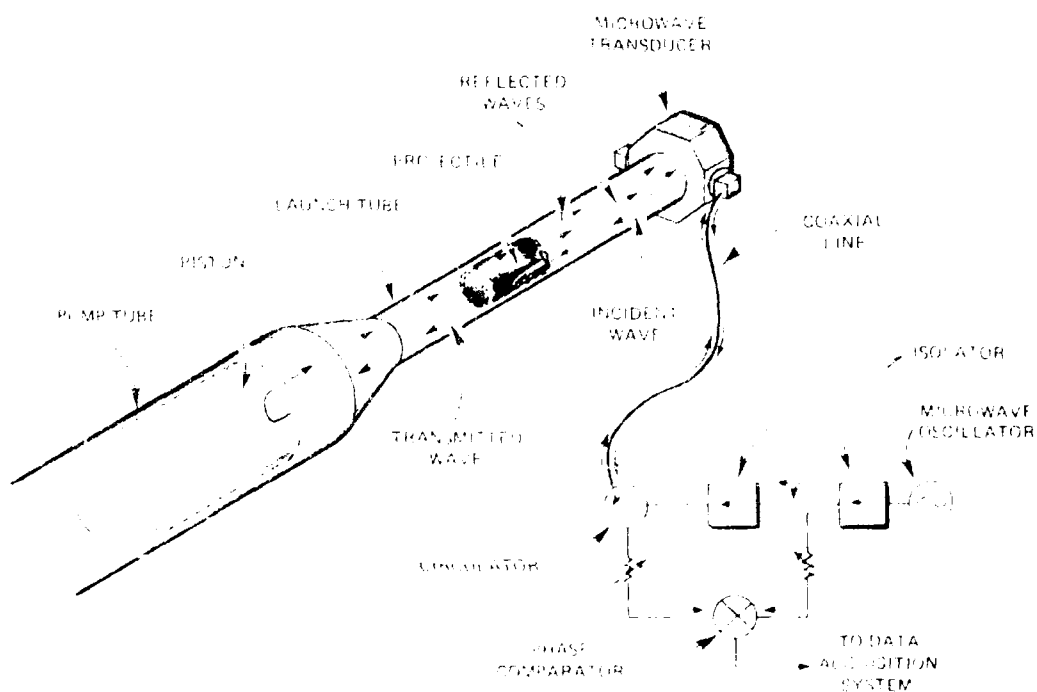FIGURE 1 - Schematic of the operation of the DREV two-stage light-gas gun

FIGURE 2 - Schematic drawing of the application of a microwave interferometer
for interior ballistic measurements

INTERIOR BALLISTIC MICROWAVE INTERFEROMETRY

The idea of using microwave interferometry to measure the interior ballistics of light-gas guns is not new. In the late 1950s, Pennelegion (2) used a microwave technique to measure piston displacement and velocity in a hypersonic gun tunnel. Since that time, several laboratories (3, 4) have reported microwave measurements of projectile kinematics inside the launch tube of light-gas guns. At DREV, a microwave interferometer has been deployed in its Terminal Ballistics Facility since 1982 (5).

Figure 2 illustrates schematically the experimental setup used at DREV to measure simultaneously the kinematics of the piston and projectile during their acceleration in the pump and launch tubes respectively. In the arrangement shown, both tubes must be viewed as waveguides of circular cross section, and the piston and the projectile as moving boundaries inside the waveguides.

The operation of this interferometer can be summarized as follows: The output power of the microwave oscillator is split into two waves, one is kept as reference and the other is used for measurement. The later is sent to a microwave transducer which excites an electromagnetic wave in the launch tube. This incident travelling wave propagates down the launch tube where it is partially reflected by the projectile which is designed to be semi-transparent to microwaves. This semi-transparency is necessary in order to observe the motion of the piston in the pump tube simultaneously with that of the projectile. The transmitted wave in the projectile propagates in the pump tube where it is almost totally reflected by the piston which has its front face coated with a thin aluminum foil.

It must be noted that the path length of the two reflected waves changes as the piston and the projectile move. Furthermore these two reflected waves combine by addition to form a single wave that is picked up by the microwave transducer and mixed with the reference wave of the interferometer. The reference wave is a fraction of the original output of the microwave oscillator and this wave always travels a fixed path length.

The output signal of the interferometer is given by a phase comparator which detectes the instantaneous phase difference between the mixed waves. From the theory of guided electromagnetic waves, this output signal is ideally composed of the sum of two sinusoidal functions. The argument $\theta(t)$ of each sinusoidal function is given by (6)

$$\theta(t) = \frac{4\pi}{\lambda_g} \cdot z(t) - \theta_0 \qquad [1]$$

where $z(t)$ represents the position of the piston or the projectile as a function of time and λ_g is the guide wavelength in the pump tube or the launch tube. θ_0 is the phase angle at the rest position of the piston or the projectile. Equation [1] indicates that $\theta(t)$ shifts by 2π each

time the piston or the projectile moves by half a guide wavelength. This is due to the geometrical arrangement of the measuring setup. The instantaneous frequency $f(t)$ of each sinusoidal function is obtained by differentiating [1] with respect to time (7)

$$f(t) = \frac{1}{2\pi} \cdot \frac{d}{dt}\theta(t) = \frac{2\dot{z}(t)}{\lambda_g} \qquad [2]$$

where $\dot{z}(t)$ represents the velocity of the piston or the projectile. This equation is the well-known Doppler relation. Its shows that it is possible to calculate the velocity of the piston and the projectile by extracting the instanteneous frequency of each sinusoidal function from the interferometer output signal. This is done with a signal processing technique that estimates the spectral content of the interferometer signal. This technique is explained later in this paper.

One of the critical aspects of the microwave interferometer measurement technique is the design of the microwave transducer used to couple the energy in and out of the launch tube. The problems of exciting waves in waveguides and of absorbing their energy are usually not simple problems. Our approach for solving these ones will now be described.

MICROWAVE TRANSDUCER DESIGN CRITERIA

The design of a microwave transducer involves the selection of a number of electrical parameters and its intented use in a gun environment imposes certain conditions on its mechanical design. The first two electrical parameters to select are

1) the propagation mode of the guided electromagnetic wave in the launch and pump tubes,

2) the frequency of the electromagnetic wave.

The TE_{11} propagation mode is the dominant or fondamental mode in waveguides of circular cross section. That means that it has the lowest cutoff frequency f_c of all possible modes in a circular waveguide, which gives the best spatial resolution at a given frequency. Furthermore the attenuation rate of the TE_{11} mode is generally lower than that of other usable modes (principally the TM_{01} mode) and its energy pattern is well distributed over the waveguide cross section. For these reasons, the TE_{11} mode has been widely used in interior ballistics microwave interferometry (8, 9).

As the frequency of the excited TE_{11} wave in the launch tube increases, the spatial resolution of the microwave interferometer also increases which is a desirable feature. However, as the frequency increases, the launch tube becomes capable of propagating other modes than the desired TE_{11} mode. The practical problems raised by multimode propagation are higher losses and distortion of the interferometer output signal produced by the different phase velocities of the several propagating modes. In certain cases, this distortion may be

severe and could greatly complicated the analysis of the interferometer output signal. In order to guard against multimode propagatio , the frequency f_0 of the electromagnetic wave is chosen lower than the cutoff frequency f_c of the TE_{21} mode which is the second possible TE propagation mode. In other words, the frequency f_0 is chosen in the following frequency band

$$f_c \ (TE_{11}) < f_0 < f_c \ (TE_{21}) . \qquad [3]$$

This relation could be expressed in term of the radius r_ℓ of the launch tube (10)

$$\frac{0.293}{r_\ell \ (\mu \varepsilon)^{\frac{1}{2}}} < f_0 < \frac{0.485}{r_\ell \ (\mu \varepsilon)^{\frac{1}{2}}} \qquad [4]$$

where μ and ε are respectively the permeability and permittivity of the medium filling the launch tube (air). For a tube with an inner diameter of 110 mm, [4] gives

$$1.6 \ GHz < f_c < 2.6 \ GHz \qquad [5]$$

Because the radius of the pump tube is larger than the radius of the launch tube, [4] indicates that multimode propagation is possible in the first one even if only the TE_{11} mode exists in the launch tube. These higher modes, if present, will be generated by the discontinuity created by the area-reduction section between the tubes.

The third electrical parameter to consider in the design of the microwave transducer is

   3) the microwave energy coupling efficiency of the transducer.

An efficiency of 100% means that all the energy available from the microwave oscillator is coupled by the transducer into the launch tube and that all the energy is contained in the TE_{11} wave. Several factors could affect the coupling efficiency of the transducer. One of the most important is the kind of method used to excite the TE_{11} wave in the launch tube from the TEM wave in a coaxial line. It is evident that some physical arrangement is more efficient than the others because of the compatibility between their electric and magnetic field patterns. Furthermore some arrangement would lead to more simple impedance matching of junctions between the launch tube and the coaxial line. But above all it is imperative that the arrangement selected be compatible with the interior ballistic measurements, that is the intended use of the transducer.

From a mechanical point of view, the intended use of the transducer requires that

   1) the transducer configuration and placement be such that neither the projectile nor any significant part of the transducer be damaged during the firing of the light-gas gun, and

   2) the transducer be rugged enough to withstand the pressures and accelerations due to the gun.

The transducer that was designed with the above criteria in mind will now be described.

MICROWAVE TRANSDUCER DESCRIPTION

Various transducer configurations were devised from which some prototypes were build and tested in laboratory or on the gun. However most of them were rejected because they did not meet one or more of the required criteria. For example the simplest transducer is obtained by employing a rod at right angle to the longitudinal axis of the gun tube and placed in or just in front of the muzzle opening. In this position the rod coincides with a line of electric field intensity for the transverse electromagnetic wave and this type of wave alone can be excited in the tube. The rod may be fed from a coaxial line and its length adjusted to obtain a maximum energy transfer into the gun tube.

This simple transducer was tested during firings of the light-gas gun and as expected it does not demonstrate the required mechanical characteristics. It was destroyed at each firing of the gun by the shock wave preceeding the projectile, preventing the measurement of the velocity of the projectile during the final part of its travel in the launch tube. Furthermore the mechanical vibrations propagating in the launch tube wall were transmitted to the transducer. These vibrations introduced large amplitude low frequency fluctuations in the interferometer output signal, thereby reducing the quality of the processed data. For these reasons a more sophisticated transducer was needed.

The basic design retained is schematically illustrated in Figure 3. In this design, two identical rectangular waveguides propagating the dominant TE_{10} wave are used to excite the two polarizations of the TE_{11} wave in the launch tube. The wide dimension of each rectangular waveguide is parallel to the longitudinal axis of the gun tube and the two rectangular waveguides are perpendicular to each other. This shunt coupling between rectangular and round waveguides is possible and efficient because of the compatibility between the electric and magnetic fields at the junction between the waveguides (11). Furthermore, from a mechanical point of view, the geometrical arrangement between the rectangular waveguides and the launch tube presents no obstruction to the projectile motion.

Commercially available type N coaxial-connector-to-waveguide adapters are used to excite the TE_{10} wave in the rectangular waveguides. In these adapters, the center conductor of the coaxial line extends only part way into the guide (Fig. 4). In order to protect the center conductor from being destroyed by the shock wave in front of the projectile or by the hot gases behind it, the rectangular waveguides are completely filled with polye-
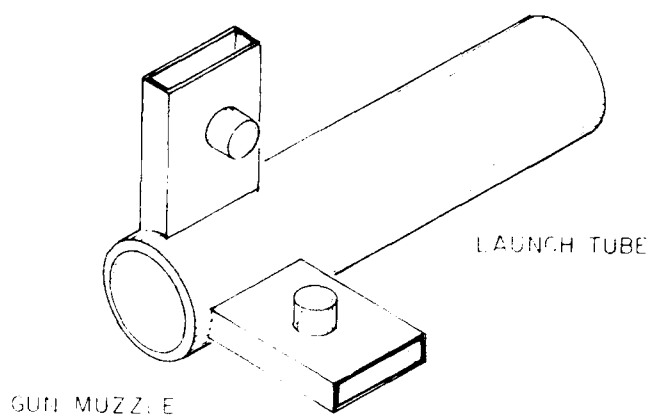
RECTANGULAR WAVEGUIDES

LAUNCH TUBE

GUN MUZZLE

FIGURE 3 - Transition from two rectangular wave-
guides to launch tube

FIGURE 6 - Normalized power propagating inside the
launch tube versus frequency

COAXIAL LINE

DIELECTRIC

RECTANGULAR
WAVEGUIDE

FIGURE 4 - Schematic drawing of a coaxial-
connector-to-waveguide adapter
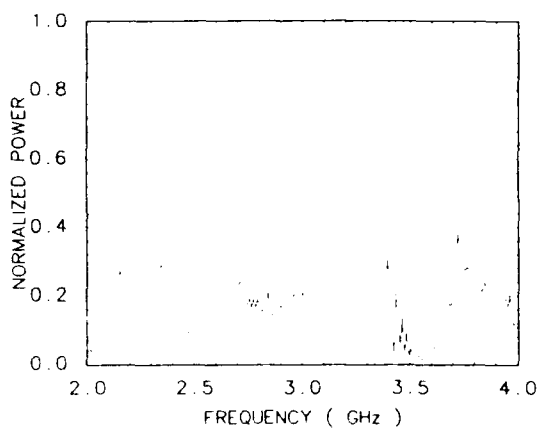
FIGURE 7 - Normalized power radiated outside the
launch tube versus frequency

FIGURE 5 - Voltage standing-wave ratio versus fre-
quency at a coaxial input port of the
transducer
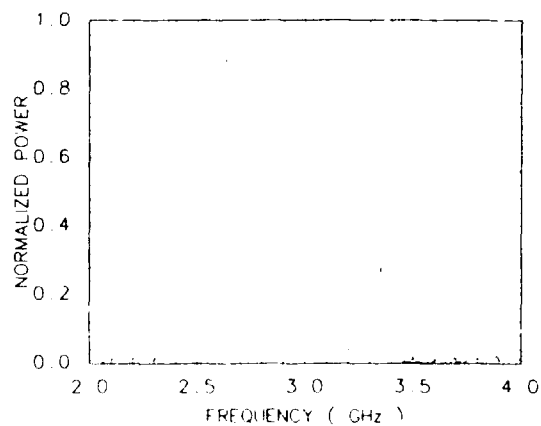
FIGURE 8 - Normalized power coupled between the
rectangular waveguides versus fre-
quency

76

thylene. This arrangement results in a simple, rugged and accurate method of supporting the center conductor. There is an additional benefit gained by filling the rectangular waveguides with polyethylene. The cutoff frequency f_c of the TE_{10} wave in a rectangular waveguide is given by (12)

$$f_c = \frac{c}{2a \ (\mu_r \epsilon_r)^{\frac{1}{2}}} \qquad [6]$$

In this equation c is the speed of light, a is the wide dimension of the waveguide and μ_r, ϵ_r are respectively the relative permeability and relative dielectric constant of the medium filling the waveguide. In order to have the same f_c, equation [6] shows that the ratio between the wide dimension of a rectangular waveguide filled with a dielectric material to the wide dimension of a waveguide filled with air must be equal to $1/(\epsilon_r)^{\frac{1}{2}}(\mu_r = 1)$. In reducing the required wide dimension of the rectangular waveguide by filling it with polyethylene, the thickness of the transducer is also reduced which means a reduction of its weight.

High order modes are set up in the rectangular waveguides by the coaxial line to waveguide adapter but all these modes are beyond cutoff. The lenght of the rectangular waveguides is chosen such that all these modes are attenuated sufficiently at the junction between the rectangular waveguides and the launch tube. The lenght of the rectangular waveguides sets the diameter of the transducer.

Conventional impedance matching techniques compatible with the intended use of the transducer were studied to maximize the transfer of energy from the microwave oscillator into the launch tube. Once coupled into the launch tube, it is desirable that the energy propagates in the TE_{11} mode toward the pump tube instead of being radiated outside the launch tube by the muzzle opening. Furthermore, the two rectangular waveguides are not stricly independent for there will be some energy coupling from one to the other. The coupling factor between the two waveguides must be as low as possible.

In order to determine the best matching arrangement among those tried, the following electrical parameters were measured as a function of the frequency:

- the dominant propagating mode of the microwave energy in the launch tube,

- the voltage standing-wave ratio (VSWR) at the coaxial input ports of the transducer,

- the power travelling inside the launch tube compared to the power radiated outside, and

- the coupling factor between the two rectangular waveguides.

These parameters were determined from the measurement of the scattering coefficients S (13) at the different input ports of the transducer with a six port automatic network analyser (14).

The best results were obtained by giving to the opening of the rectangular waveguides at the junction with the launch tube the configuration of a wide slot. The optimum dimensions of the slot were determined experimentally. Furthermore, from a mechanical point of view, this configuration presents the advantage of reducing the pressure of the gas on the rectangular waveguides.

It was determined for this transducer configuration that the TE_{11} mode is the only mode presents in the launch tube from 2.0 to 2.6 GHz. From 2.6 to 3.6 Ghz, the TE_{11} mode is still present but most of the energy is propagated in the TE_{21} mode. From 3.6 to 4.0 GHz, higher order modes are dominant.

Figure 5 gives the voltage standing-wave ratio (VSWR) at one of the coaxial input port of the transducer. A VSWR of 1.7 (4.6 dB) is obtained in the neighbourhood of 2.16 GHz which is in the frequency band for which only the TE_{11} mode exists in the launch tube. A slightly better VSWR is reached at 3.72 GHz but at this frequency there is more than one modes propagating in the launch tube.

Figures 6 and 7 enable the comparaison between the power propagating inside the launch tube and the power radiated outside by the muzzle opening. At 2.16 GHz there is approximately 1.5 more power propagating in the launch tube than radiated outside. At some other frequencies, the contrary is observed particularly at 3.72 GHz which is the frequency at which the VSWR is minimum.

The last performance curve of the transducer is shown in Figure 8. It indicates a relatively low coupling between the two rectangular waveguides at 2.16 GHz. It also shows that there exists a strong coupling at some other frequencies.

Figure 9 shows two photographs of the microwave transducer on which we can see the two coaxial input ports and the wide slot in the rectangular waveguide opening. The transducer is screwed onto the muzzle of the launch tube as shown in Figure 10. The most favorable operating frequency for the transducer is 2.16 GHz.

DATA ACQUISITION AND PROCESSING

The nature of the interferometer output signal dictates the design and performance requirements of the data acquisition system. For projectile velocities up to 2.5 km/s with 2.16 GHz microwave excitation, the data are contained in an AC signal whose frequency increases from zero to nearly 25 kHz in an interval of less than 20 ms.

Figure 11 shows the microwave interferometer schematically illustrated in Figure 2. The output signal of the interferometer after amplification and analog low-pass filtering is digitized in real time by a 12-bit analog-to-digital converter (LeCroy model 8212A). The sampling rate of the
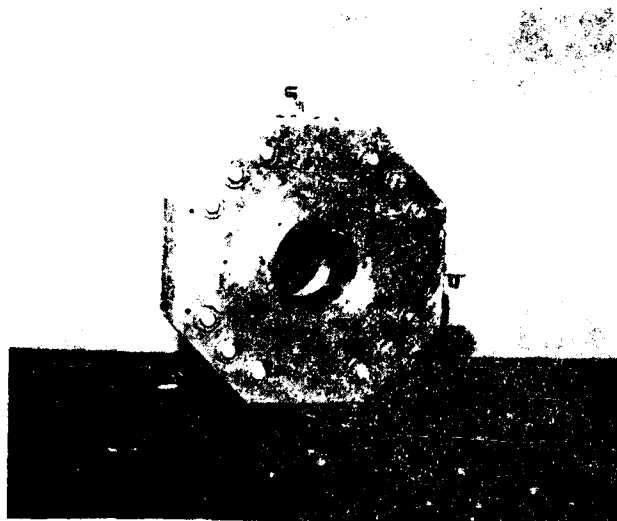
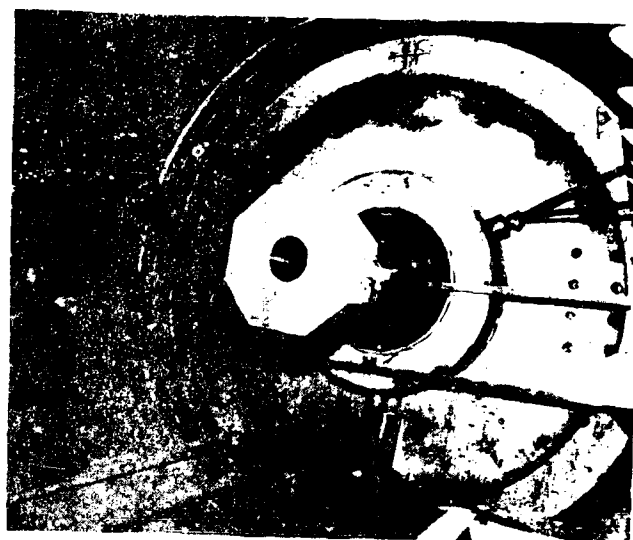FIGURE 9(a) - Front view of the microwave trans-
ducer

FIGURE 10 - Close-up view of the microwave trans-
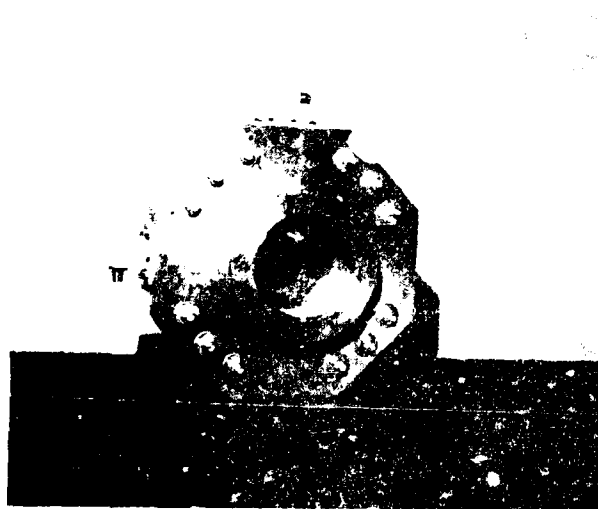ducer mounted on the light-gas gun

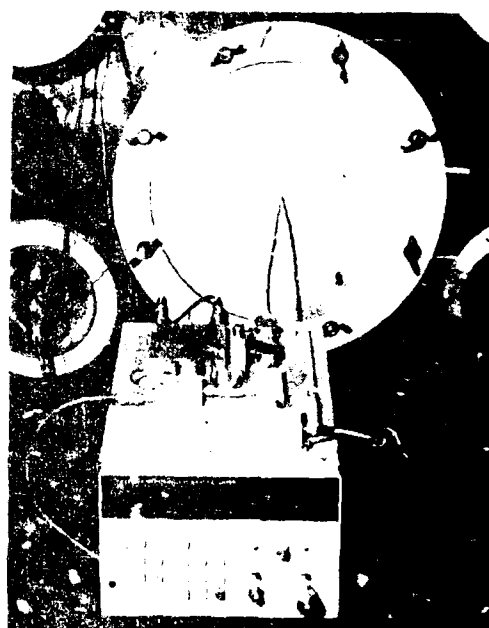
FIGURE 9(b)   Back view of the microwave trans-
ducer

FIGURE 11   Experimental microwave interferometer
for interior ballistic measurements

digitizer is chosen equal to 3 to 4 times the maximum expected Doppler frequency which is determined by the muzzle velocity of the projectile. The digitized data are transferred to an HP 9000 series 320 computer for processing. Because of the great importance and the high costs associated to LGG firings, the amplified interferometer output signal is also recorded on a Racal Store-7D analog tape recorder in the case of a digital equipment malfunction.

The data processing is based on high resolution spectral analysis of the interferometer output signal. In the method selected, called the Welch periodogram method (15), the interferometer signal is divided into overlapping segments of equal length and an estimate of the spectral content of each segment is obtained by applying an FFT algorithm (16). The velocity of the piston and the velocity of the projectile are extracted from the peak positions in each spectral estimate and are calculated with [2]. The displacement versus time curve is obtained by integrating the velocity versus time curve.

EXPERIMENTAL RESULTS

A series of firings of the DREV two-stage lightgas gun operating in its ordnance (low) velocity range were recently performed with the transducer mounted on the launch tube. For each firing, the projectile launched was a 1.90 cm steel cube supported by a sabot made of polycarbonate. The 0.91-m-long piston was made of high-density polyethylene with lead inserts to increase its mass to the desired value. Its front face was coated with a thin aluminum foil in order to increase its microwave reflectivity.

A typical output signal from the microwave interferometer is reproduced in Figure 12. This signal was digitized at a 100-kHz sampling rate during one firing of the light-gas gun. The microwave interferometer signal clearly shows the initial movement from the rest of the piston some 25 ms after the firing pulse of the gun. The increasing frequency indicates the acceleration of the piston down the pump tube. In this illustration, the Doppler sine wave from the projectile is only evident during the final part of the interferometer signal. The large amplitude fluctuations at the end of this signal are due to the passage of the projectile assembly through the opening of the microwave transducer. The small amplitude modulation observed on the interferometer signal is generated by the presence in the pump tube of microwave propagating modes other than the TE_{11} mode. These higher order modes are generated in the discontinuity created by the tapered section between the launch tube and the pump tube. Mechanical vibrations which propagate in the wall of the launch tube are transmitted to the microwave transducer. These vibrations are responsible for the low-frequency fluctuations observed.

The signal depicted in Figure 12 was processed as described in the previous section. The results obtained for the velocity time histories of both

the piston and the projectile are shown in Figure 13. The piston shot start time was determined from a careful examination of the analog data record of the interferometer signal. The projectile shot start time comes from a first-order polynomial fitted by the least squares method to the velocity versus time data. Figure 13 illustrates how the piston is rapidly accelerated by the hot propellant gases, later decelerated by the high-pressure light gas, and finally brought to rest before entering the area-reduction section. The discontinuities in the velocity-time curve of the projectile correspond to the arrival of shock waves, which propagate in the light gas, at the sabot back face. This curve also indicates that the projectile assembly exits the launch tube with a velocity of about 2.2 km/s.

Displacement-time histories of both the piston and the projectile assembly are obtained by integrating numerically the corresponding velocity-time curve. The results are shown in Figure 14 along with other pertinent information gathered from analysis of the waveforms produced by different sensors mounted on the gun. The crossdots on the figure represent the arrival times of the shock waves propagating in the light gas at three pressure gauge measuring positions on the pump tube and at two strain gauge measuring positions on the launch tube. The first dot at each strain gauge position represents the estimated arrival time of the projectile at these stations. We could see that there is a good correlation between the data obtained from the analysis of the microwave interferometer signal and the data extracted from different sensors mounted on the gun.

The overall accuracy of the data presented so far has not yet been determined precisely and depends, among other things, on the accuracy with which the waveguide wavelength in the pump tube and in the launch tube is known. Of all the parameters determining the waveguide wavelength, only one may vary significantly during the interior ballistic cycle. It is the refractive index of the medium immediately in front of the piston and the projectile. The wavelengths used in the processing of the data presented in this paper have been calculated with a refractive index equal to 1.

CONCLUSIONS

This paper has described the development of a microwave transducer which is incorporated to a microwave interferometer used for interior ballistic measurement. The microwave transducer excites an electromagnetic wave in the launch and pump tubes of a light-gas gun without interfering with the projectile motion.

The experimental results presented are examples of the data that have been obtained with the microwave interferometer and its associated transducer at the time of firings of the DREV light-gas gun. The performance of the transducer during these firings indicates its ability to withstand the pressures and accelerations characteristic of an installation on a gun.
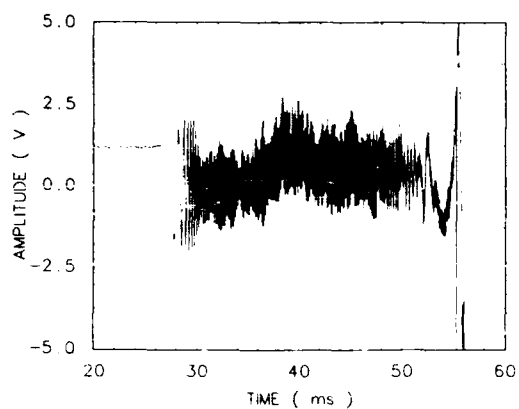
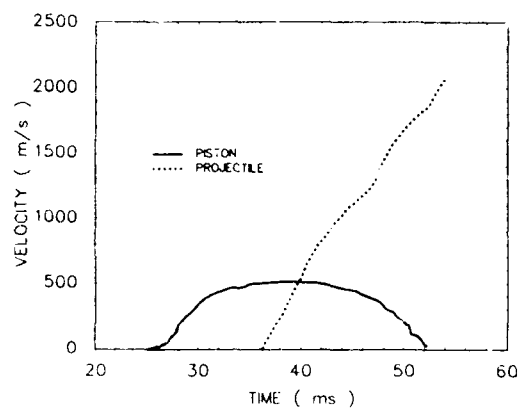FIGURE 12 - Typical microwave interferometer out-
put signal

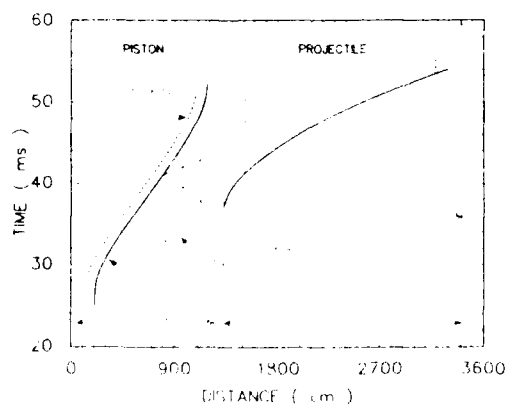FIGURE 13 - Piston and projectile velocity-time
histories

FIGURE 14 - Piston and projectile displacement-
time histories

It is believed that by using the same design principles than those presented in this paper, similar microwave transducers could be developed for light-gas guns with different bore diameters.

REFERENCES

(1) Seigel, A.E., "Theory of High-Muzzle-Velocity Guns", in "Interior Ballistics of Guns", AIAA, Progress in Astronautics and Aeronautics, Vol. 66, pp. 135-175.

(2) Pennelegion, L., "A Microwave Method of Determining the Displacement and Velocity of a Piston in a Hypersonic Gun Tunnel", Nature, Vol. 183, No. 4656, 1959, p. 246.

(3) Knapp, R.E., Hendrix, R.E., "Experimental Projectile Kinematic Studies in a Two-Stage Light-Gas Gun", AEDC Technical Report 65-60, March 1965.

(4) Hruby, R.J., Sander, R.C., Berggren, R.E., "Microwave Technique for Measuring Projectile Time History in Light-Gas Guns", Proc. of Second International Congress on Instrumentation in Aerospace Simulation Facilities (IEEE), Stanford University, August 1966.

(5) Bourget, C., Gladstone, D.H., Drouin, G., Cayouette, J.F., Robertson, W.J., "The DREV Terminal Ballistic Facility", DREV Report 4364/85, April 1985.

(6) Ramo, S., Whinnery, J.R., Van Duzer, T., "Fields and Waves in Communication Electronics", Wiley, New York, 1965, p. 32.

(7) Lathi, B.P., "Communication Systems", Wiley, New York, 1968, p. 212.

(8) Loder, R.K. "On In-Bore Microwave Interferometry", Proc. of Sixth International Symposium on Ballistics, Orlando, USA, October 1981, pp. 400-411.

(9) Fuller, P.W.W., "Small Calibre In-Bore Dynamics", Proc. of Ninth International Symposium on Ballistics, Shrivenham, UK, April-May 1986, pp. (7-287)-(7-296).

(10) Ramo, p. 431.

(11) Ehlers, F.E., "Lowest Mode in Waveguide Transitions", in "Microwave Transmission Circuits", MIT, Radiation Laboratory Series, Vol. 9, 1948, pp. 351-369.

(12) Ramo, p. 425.

(13) Ramo, pp. 603-605.

(14) Bosisio, R.G., "Etude Expérimentale sur des Méthodes Non-Obstructives d'Excitations de Modes Hyperfréquentiels dans l'Ame d'un Canon", Contract No. 8SD84-00187, December 1986.

(15) Marple, S.L., "Digital Spectral Analysis with Applications", Prentice-Hall, New Jersey, 1987, p. 154.

(16) Jain, V.K., Collins, W.L., Davis, D.C., "High-Accuracy Analog Measurements via Interpolated FFT", IEEE Trans. on Instrumentation and Measurement, Vol. IM-28, No. 2, June 1979, pp. 113-122.

A MICROWAVE TRANSDUCER FOR MEASURING PISTON AND PROJECTILE VELOCITIES IN A TWO-STAGE LIGHT-GAS GUN

Q: Steve Nickless (Honeywell Solid State Electronics): What's the material of the launch tube and does it have an effect on the performance of the transducer?

A: Lucien Nappert: As for the launch tube, what kind of steel I don't know. The transducer is aluminum. Up to now we fire the gun with this transducer mounted on it only in its slow velocity range. The maximum velocity we have obtained is 8,000 feet per second. We have not yet fired the gun at 15,000 feet per second with this transducer on it. We will have to do some measurement before that because we don't know how the transducer will affect the function of the gun at this very high velocity.

Q: Jim Faller (Aberdeen Proving Grounds): Sometime ago I had some, I would say, minimum exposure to the gas-gun. There was some infrared technique that was being used. Are there other competitive technique that can be applied to the measurement of the velocity once the projectile exits? I just wondered with what are you competing with out there in terms of making this kind of measurement?

A: Lucien Nappert: These measurements were made to validate computer code, that was the problem. You could use other techniques to take measurements for internal ballistic measurement like laser interferometry or something like that. But with laser interferometry you will have very high resolution at the start of the projectile but the doppler effect frequency is increasing so rapidly that you will have some problem to recall the data and also with this technique I think it's the first time we've measured the velocity of the piston and the projectile simultaneously. That could not be done with other types of measurements, like laser interferometry or something like that.

Q: Jim Faller: You call attention to the light gas-gun. Is there such a thing as a heavy gas-gun that this technique would not be adapted to?

A: Lucien Nappert: We've used this technique to measure the internal velocity of an ordinary gun; but we didn't do it with this transducer, we used a much lighter transducer.

Q: Bill Cardwell (GE, Cincinnati, Ohio): Have the projectiles that you are using on this been metallic or have you done any investigating with nonmetallic projectiles?

A: Lucien Nappert: The projectile in this case was a one inch steel cube supported by a sabot made of polycarbonate and the diameter of the sabot was 110mm and the steel cube is glued in the front of the polycarbonate sabot. The polycarbonate is semitransparent to the microwaves. Some part of the energy is transmitted to the polycarbonate and some is reflected back.

Q: Bill Cardwell: Your system has to have some sort of metallic object to reflect the .....

A: **Lucien Nappert:** Not necessarily, only the polycarbonate sabot will be okay. If you have some metallic object, you will increase your reflectivity but you must make a compromise between the transmitted energy and the reflected if you want to see the projectile and the piston simultaneously.

Q: **Bill Cardwell:** Then the amount of reflected energy you have would effect the accuracy of your measurement, is that correct?

A: **Lucien Nappert:** Yes, I think that in this case we have a better accuracy on the piston velocity than on the projectile velocity because there is much more reflected power of the piston. We put on the piston front face a thin aluminum foil to increase its reflectivity.

Q: **John Kalnowski (EG&G):** In equation of state work we have a material which we impact with the piston, as you call it, so we can study the effect of the material under high pressures. I would imagine we would like to know what the input velocities were, and so, I'm wondering if we put a target just aft of your microwave system if that target would affect your reading and if it would be valid or invalid?

A: **Lucien Nappert:** Yes, we have a target in front of the gun, maybe ten feet from the muzzle of the gun so the target has no effect on the measurement technique. But if you put your target very close to the muzzle of the gun, you will have some effect because of the radiated power outside of the gun and in fact we followed the projectile for a few feet outside the barrel. Because the radiated power outside of the gun is taken back by the transducer.

BUILT-IN MECHANICAL FILTER IN
A SHOCK ACCELEROMETER

Anthony Chu
Project Engineer
Endevco
Rancho Viejo Rd
San Juan Capistrano, CA 92675

ABSTRACT

Isolating the sensing element of a transducer from high frequency transient attacks appears to be one of the most effective design improvements in shock accelerometers. An experimental transducer design with integral mechanical filter has allowed the experimenter to record close-range shock excitation without zeroshift, a common linearity error in pyroshock measurement. This piezoelectric accelerometer prototype features both an input mechanical filter and an electronic low-pass filter in order to maximize usable bandwidth. Calibration data indicate flat frequency response to 10kHz with 24 dB per octave roll-off thereafter. Field test results are also shown in this paper.

INTRODUCTION

With all the advances in digital data acquisition equipment and signal processing techniques, the acceleration transducer (accelerometer) is still the weakest link in a pyroshock measurement chain. Current design approaches in accelerometers, such as electronic filtering and high resonance, can not always guaranty the experimenters with repeatable performance and believable results.

The core of the problem has been identified to be the sensing element of the transducer. All sensing mechanisms are vulnerable to high-g excitation at frequencies far above our point of interest. These high frequency, high-g transients, although "invisible" to many recording systems, are present in all close-range pyrotechnic events and metal-to-metal impact testings which are common in many qualification requirements.

The advantage of using a mechanical filter as an isolator is discussed. Isolating the sensing element (piezoelectric or piezoresistive) from high

frequency transient attacks appears to be one of the most effective design improvements in shock accelerometer. A shock transducer design with an integral mechanical filter has allowed the experimenter to record pyroshock time history without zeroshift, a common linearity error of the sensor in pyroshock measurement. This piezoelectric accelerometer prototype features both an input mechanical filter and an electronic low-pass filter in order to maximize usable bandwidth. Calibration data indicate flat frequency response to 10kHz with 24 dB per octave roll-off thereafter. A comparison of this unique design with commercially available mechanical filters is also presented. The survivability of transducers in high-g environments has greatly increased due to shock isolation provided by these filters.

PROBLEM IDENTIFICATION

All spring-mass type accelerometers have a finite seismic resonance. To obtain linear response from such a transducer, one must be certain that the input spectrum always stays within its recommended bandwidth. As a general rule-of-thumb, the maximum m̲ ̲asured frequency for an undamped accelerometer to be less than one fifth of the transducer resonance. This rule is generally well observed in the vibration-test community.

Unfortunately, the term maximum measured frequency are often misinterpreted as the upper band of the Shock Response Spectrum in shock measurement. Since most Shock Response Spectra stop at 10kHz or 20 kHz, accelerometers with resonance in the neighborhood of 100 kHz are usually considered adequate for these applications. It is however important to remember that the input spectrum of most high-g shock measurements contains frequency components way above 100 kHz, well be-

yond the capability of our modern recording devices. These high frequency components are often unnoticeable until something occurs during data acquisition; eg. aliasing of a digital recorder. The most commonly used wide-band analogue tape recorder can only capture time history up to 80 kHz (running at 120 ips), out-of band information is therefore naturally attenuated and "invisible" on playback.

The problem is further confused by the issue of the damage potential of high frequency. It is known that shock inputs above 10 kHz seldom cause any damage to the test article, and they are routinely ignored in most data analysis. These high frequency components, although posing no danger to the article, seriously affect the linear operation of any spring-mass type accelerometer.

Recently, a few papers and articles have been published [1] [2] concerning the effect of ultra-high frequency impulses on shock measurements. This out-of-band transient phenomenon is referred to in the papers as "Pre-Pulse". There are two types of shock simulations capable of generating near true-impulses:

a) Close-Range Pyrotechnic Shock

The process of explosion involves chemical reactions in a substance which convert the explosive material into its gaseous state at very high temperature and pressure. Most explosives, such as Flexible Linear Shaped Charge and pyrotechnic bolts, do not contain as much energy as ordinary fuel, but generate extremely high rate of energy release during explosion. The response of the structure near the immediate region can actually approach a true impulse due to the instantaneous velocity change at the explosive interface. As a result, measuring at the area surrounding a pyrotechnic explosion has always been a nightmare for engineers and scientists.

Depending on the explosive location and the point of measurement, the amount of high frequency energy reaching the transducer is inversely proportion to the distance between them. In a remote sensing location where the shock wave has to propagate through a long path or many joints of dissimilar materials to reach the transducer, high frequency components can be significantly attenuated.

b) Close-Range Metal-to-Metal Impact

Most pyroshock simulation devices, such as drop towers and pneumatic hammers, rely on high velocity metal-to-metal impact to generate the required shock spectrum. When the point of contact allows very little material deformation (like in all reusable machines), the acceleration response of the structure can also approach a true impulse. Again, the response spectrum is highly dependent upon the accelerometer location relative to the point of impact.

EFFECTS OF NEAR TRUE-IMPULSES ON ACCELEROMETER

There are two types of commonly use shock accelerometers, piezoresistive and piezoelectric devices. Each reacts differently under the attack of near true-impulses. Three common failure modes are observed:

a) Sensor Failure

Recent new designs in piezoresistive accelerometer have tremendously improved their usable bandwidth and rigidity. One type of commercially available PR sensor exhibits seismic resonance above 1 MHz [3], leaving quite a margin of safety for the general rule-of-thumb. Under the attack of delta function liked impulses, however, the sensor can still be set into resonance (at 1 MHz) due to the nature of the input signals. Since the gage mechanism is practically undamped, displacement of the elements goes out of control at resonance and eventually cause gage breakdown. The result of this type of failure is complete loss of data.

Piezoelectric sensors are more robust under the same condition. But they fail in other fashions:

b) Zeroshift

This subject has been well examined in many technical papers [4] [5] [6]. A piezoresistive accelerometer generally does not exhibit zeroshift until the gage mechanism has been damaged or is in the process of deterioration. Piezoelectric sensors, on the other hand, account for most of the zeroshift phenomena associated with transducers.

When a piezoelectric element is set into resonance, two things can happen:

1. Relative displacement of the seismic mass can exceed 100 times of the input. The crystal material is overstressed and produces spurious charge outputs due to domain switching. The result of this type of failure is DC offset in the time history.

2. The crystal material is not overstressed but a huge amount of charge output is generated which saturates or damages the subsequent electronics. The result of this type of malfunction is loss of data or gross DC offset in the time history.

Slight amount of zeroshift in the time history can yield unrealistic velocity and displacement during data reduction. The real danger remains that, although data with gross DC offsets are generally discarded, the minor one are accepted as good measurements.

c) Non-Linearity

The output of a transducer at resonance is sometime non-linear and not repeatable. The response of a saturated charge converter is also non-linear and not repeatable. The result of this type of malfunction is poor repeatability in SRS, leading to incorrect definition of the shock environment.

SOLUTION TO THE PROBLEM -- MECHANICAL FILTER

Mechanical Filter

An obvious solution to the accelerometer resonance problem is to isolate the sensor from the high frequency signals. When an appropriate material is placed between the structural mounting surface and the transducer, a mechanical low-pass filter is formed. The filter slope of such an arrangement approaches 12 dB per octave. In order to make the filter effective, the -3 dB corner must be set at a frequency far below the accelerometer resonance to insure adequate attenuation.

There are three critical design parameters in a mechanical filter:

a) First, the filter/accelerometer combination must be robust enough to withstand high level shocks. Many "isolators" rely solely on the strength of spring/damping material to keep the accelerometer in place.

b) Secondly, the Q (amplification) of the mechanical filter must be very low. Otherwise the linearity of the passband data will suffer. Damping characteristic is a critical consideration in matching the accelerometer to the mechanical filter.

c) Thirdly, the relative displacement between the transducer and the mounting surface must not exceed the linear range of the spring/damping material. When the accelerometer "bottoms out", its high frequency isolation characteristic of the filter is lost, and the protection to the sensor fades.

Existing Designs

Although there many shock isolators on the market for machine vibration isolation, they are not designed with linearity in mind, and their applications are quite different. A few foreign and local private institutions have built some experimental devices for their own shock measurements, but none are commercially available. These prototypes were made out of exotic materials, such as rosewood and cloth, for their unique damping and stiffness properties; reliability and repeatability of these external filters are questionable. One of the accelerometer manufacturers does offer an external mechanical filter especially tuned for its own brand of transducers, but it is really intended for a general vibration environment.

One common problem facing external mechanical filters is the resonance of the filter itself. Even with careful selection of spring and damping materials, critical damping is rarely achieved. Any small amount of amplification factor (Q) in an imperfectly damped filter will produce substantial degree of amplitude distortion from a shock input. This distortion manifests itself as ringing (at the filter's corner frequency) superimposed on the accelerometer output signals.

Another problem has to do with accelerometer matching. The corner frequency and the Q of a external filter is highly sensitive to the mass of the attached transducer. Minor deviation on size and weight can result in significantly different response.
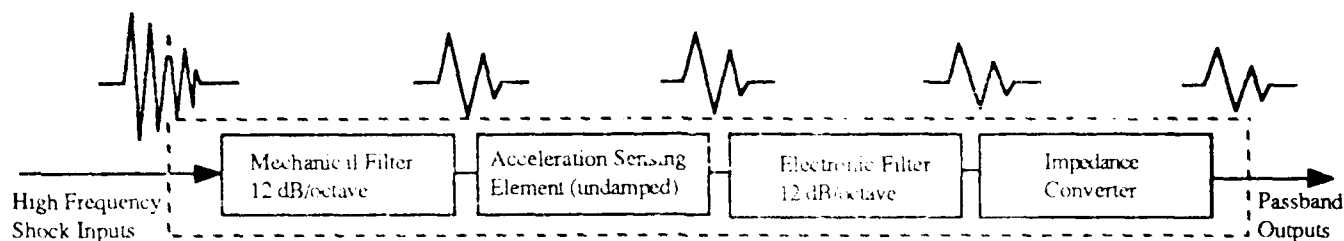
ACCELEROMETER WITH BUILT-IN FILTERS

Figure 1

Given the physics of the problem discussed above, it seems obvious that if one can design a shock accelerometer to incorporate a tuned internal mechanical filter for sensor isolation, and match it with a built-in electronic low-pass filter to remove unwanted residual ringing of the mechanical filter, many transducer problems in pyroshock measurement can be avoided. A block diagram in Figure 1 depicts this concept.

Built-in Mechanical Filter

An experimental accelerometer with both mechanical and electronic filters was successfully built in our Engineering Lab.

Based on a well established piezoelectric shock sensor, this accelerometer featured a captive mechanical filter arrangement. Compared to the model of an external filter (Figure 2a), this unusual scheme provided the transducer/filter system with added rigidity. (see Figure 2b) The transducer's external housing, which served as an enclosure for the sensor and the isolation material, kept the "guts" together in case of excessive shock input.

The light-weight sensor assembly housed the piezoelectric element and the hybrid microelectronics. The internal electronic filter, a two-pole Butterworth low-pass, provided another 12 dB per octave roll-off after the mechanical filter. The spring/damping material was meticulously chosen and matched to react with the mass of the sensor in a synergistic fashion. This combination yielded a mechanical filter with a damping coefficient of .20 to .15, and a resonant frequency of 15 kHz.

To attenuate the ~5 dB rise at 15 kHz, the corner of the 2-pole low-pass filter was purposely set at 10 kHz
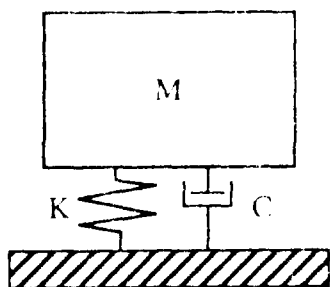
Figure 2a
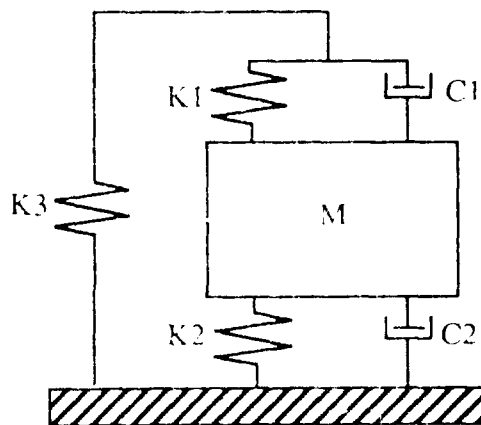
Figure 2b

MECHANICAL FILTER MODELS

87

in order to compensate for this unwanted peak. The end result is shown in Figure 3 where the solid line represents the combined frequency response of the accelerometer; the single dotted line represents the mechanical filter response, and the double dotted line denotes the electronic filter response. This combination offered a 24 dB per octave roll-off beyond 10 kHz which effectively isolated the piezoelectric element and subsequent electronics from any high frequency transient. Built-in electronics also allowed impedance conversion taking place inside the transducer, a desirable feature for signal transmission.

Accelerometer Performance

A frequency response calibration is shown in Figure 4. The accelerometer has an effective linear amplitude response from 1 Hz to 10 kHz within ±1 dB. Sensitivity of the unit is .11mV/g which equates to a full scale dynamic range of >50,000g. Cross-axis sensitivity up to 50,000 g is less than 5%, and the resonance of the crystal element itself is larger than 130 kHz. The accelerometer weights 3.8 grams and operates from a constant current source.

One of the major concerns regarding the performance of the transducer has been temperature response. Since the material used for damping was basically a polymer, frequency characteristics varied with temperature. An experiment was conducted to investigate the effect of temperature using transient inputs from a Hopkinson bar. The input transient was defined to be about 100,000 g peak, and the corresponding pulse width was ~70 μS. Repeatability of the pulse shape was quite acceptable, but the shock level had a standard deviation of 5,500 g.

Figure 5 compares the transient responses of the accelerometer at 75°F and 45°F. The peak response at 75°F is measured to be 86,000 g, and 78,100 g at 45°F (these are median data selected from samples at approximately the same level). The peak level is considerably less than 100,000 g due to filter attenuation. Taking the variability of input level into account, the indicated peak g at 45°F is 9.2% lower than at room temperature.

Figure 6 shows the transient responses at 75°F and 120°F. Here the indicated peak g at 120°F is 83,000 g, and 79,000 g at 75 °F, a +5.0% increase in amplitude response.

Pushing the physical limit of the damping material, the same test was conducted at 150°F. Figure 7 shows the transient responses at 75°F and 150°F. At 150°F, the peak response indicates 100,700 g while the 75°F shows 84,000 g, a +19.9% increase in apparent response.

Our data seems to indicate that, within ±30°F from ambient temperature (75°F), the mechanical filter displays a small amount of variation. Above 120°F, however, some correction factor may be necessary.

Design Limitation

Apart from the temperature constraint mentioned in the preceding section, the accelerometer has another physical limitation. Referring to Figure 2b. The mass M, in our design, is the sensor of the accelerometer, and the mounting surface becomes the boundary of this second order system. The confined springs/dampers are represented in this model by K1, K2, C1 and C2; the stiffness of the outer case is represented by K3. As long as the transmitted force F to the sensor does not cause excessive travel in K1 and K2, the system will behave in a predictable manner. The practical displacement limit of the existing system is estimated to be > 0.01".

The equation which relates dynamic range of the mechanical filter to the maximum linear travel of the spring material is:

$$\frac{t}{\ddot{\chi}} = \frac{1}{\omega_n{}^2 \sqrt{\left[1-\left(\frac{\omega}{\omega_n}\right)^2\right]^2 + \left(2\zeta\frac{\omega}{\omega_n}\right)^2}}$$

where

t = maximum travel of spring

$\ddot{\chi}$ = maximum input acceleration

ζ = damping factor

ω = input frequency

ω_n = resonant frequency of mechanical filter

A maximum input shock spectrum derived from this equation (based on 0.01" spring travel) is shown in Figure 8. The weakest spot is understandably at 15 kHz where the filter resonates.

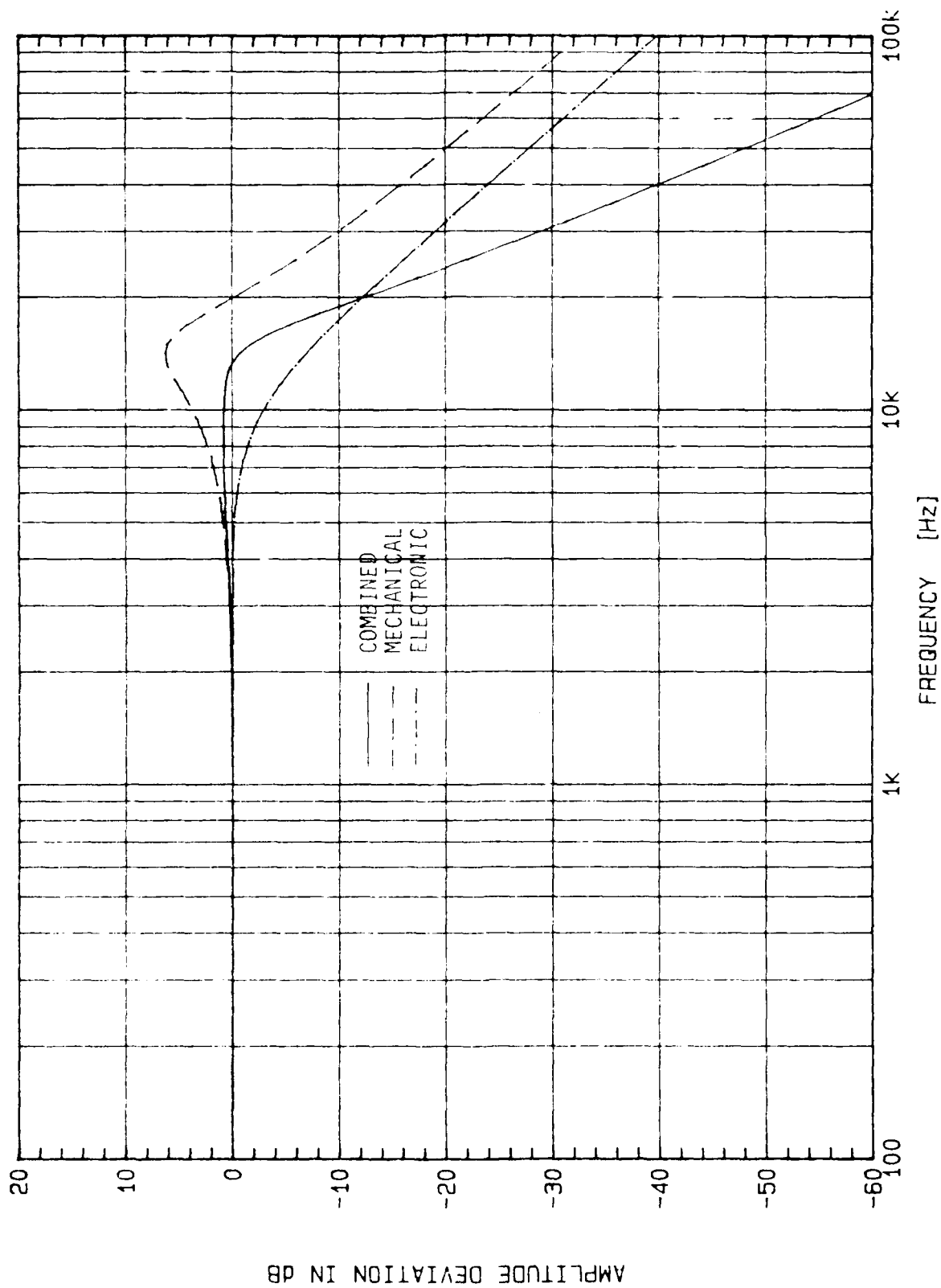# COMBINED FILTER CHARACTERISTICS

ACCELEROMETER FREQUENCY RESPONSE

FREQUENCY [Hz]

FIGURE 3

AMPLITUDE DEVIATION IN dB

89

Model Number 7255-01 Serial Number XA23

Sensitivity: 0.088 (mV) pC/g @ 100 Hz

System 80 Acceleration Level: 2.0 g pk

Frequency Limits: 100 Hz to 50K Hz

Vertical Scale: 10 db per major division

Cal. by: A.C. Date: 2/24/88

FREQUENCY RESPONSE CALIBRATION

FIGURE 4

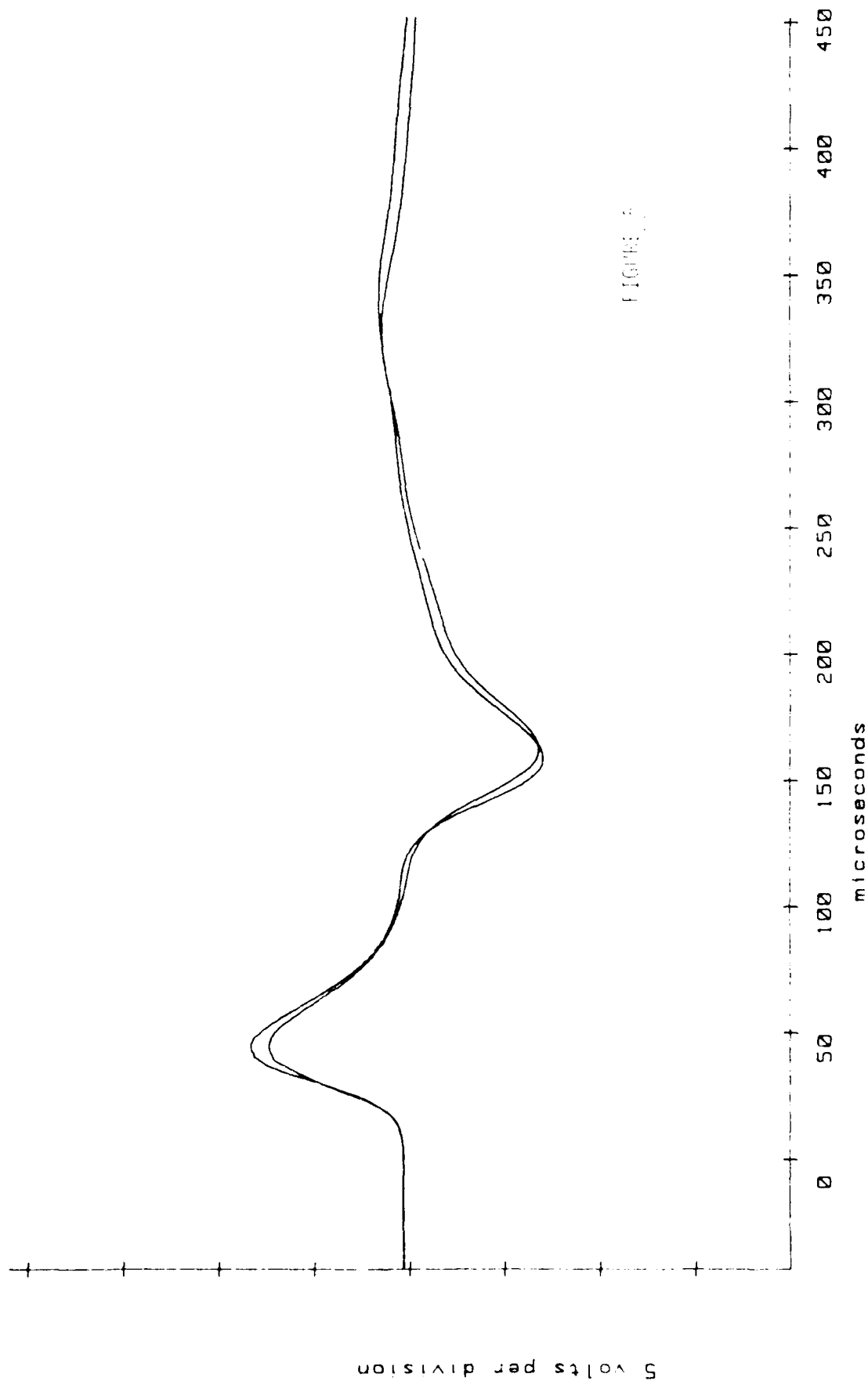MODEL ✦ 7255

SERIAL ✦ PY04

REPORT ✦ 45 deg F

DATE: 5-20-88

5 volts per division

microseconds

TRANSIENT RESPONSE AT TEMPERATURE

FIGURE 5

MODEL # 7255

SERIAL # PY04

REPORT # 120 deg F

DATE: 5-20-88

FIGURE 6

microsecond's

TRANSIENT RESPONSE AT TEMPERATURE

5 volts per division

92
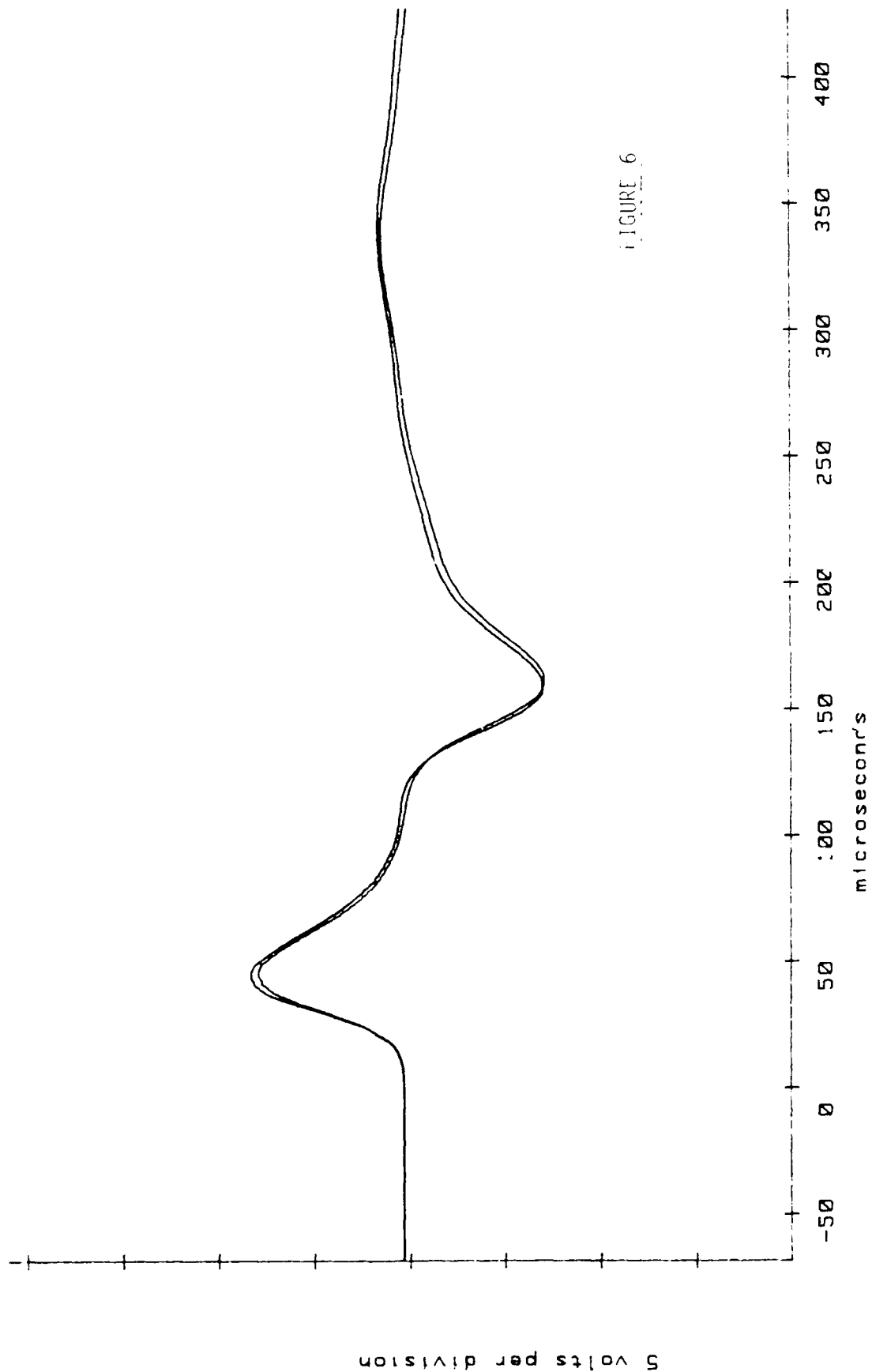
MODEL # 7255

SERIAL # PY04

REPORT # 150 deg F

DATE: 5-20-88

FIGURE 7

microseconds

TRANSIENT RESPONSE AT TEMPERATURE

5 volts per division

93
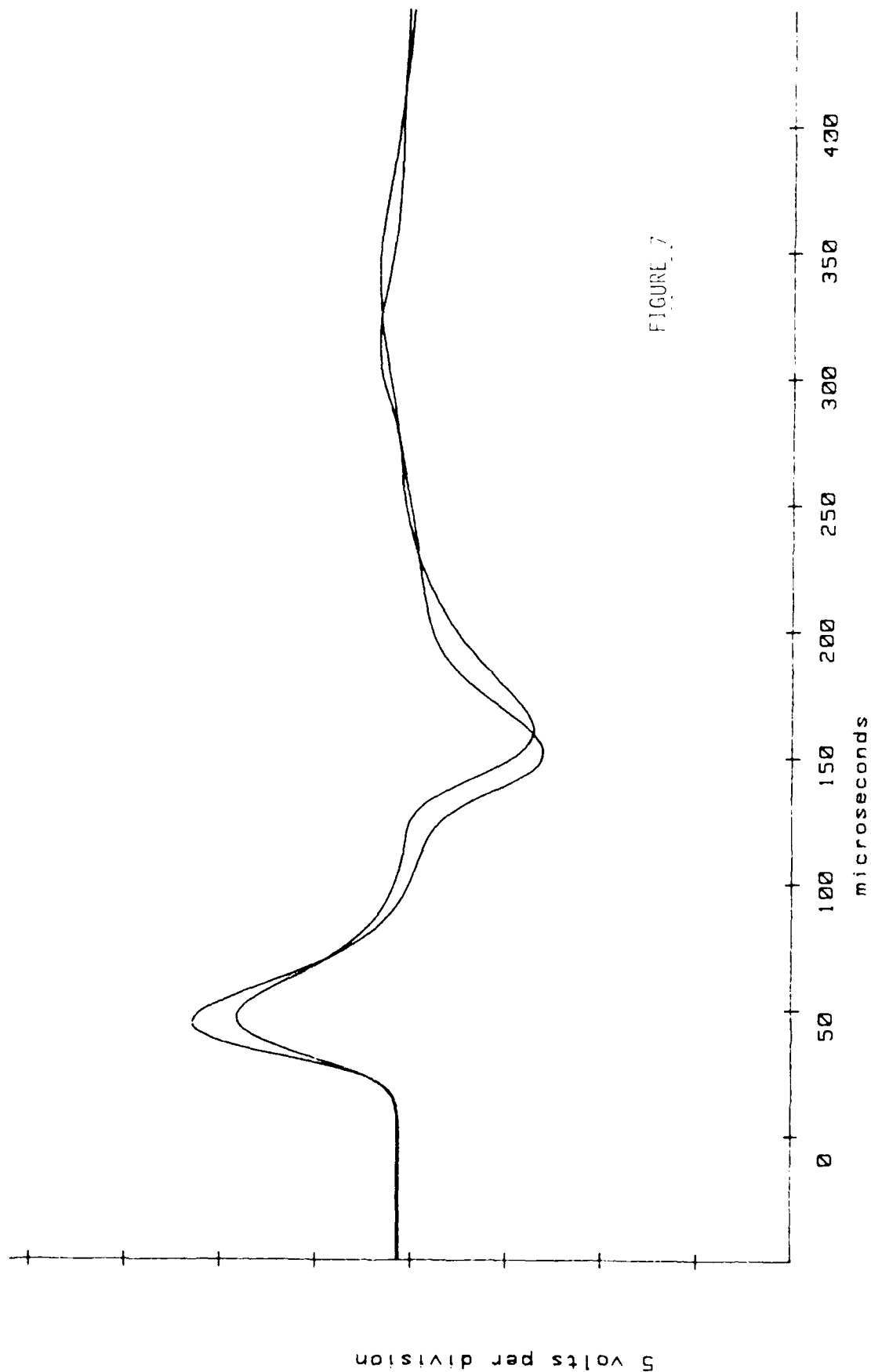
MAXIMUM INPUT SPECTRUM
BUILT-IN FILTERS

FREQUENCY

FIGURE 8

MAX. PEAK ACCELERATION IN g's

94
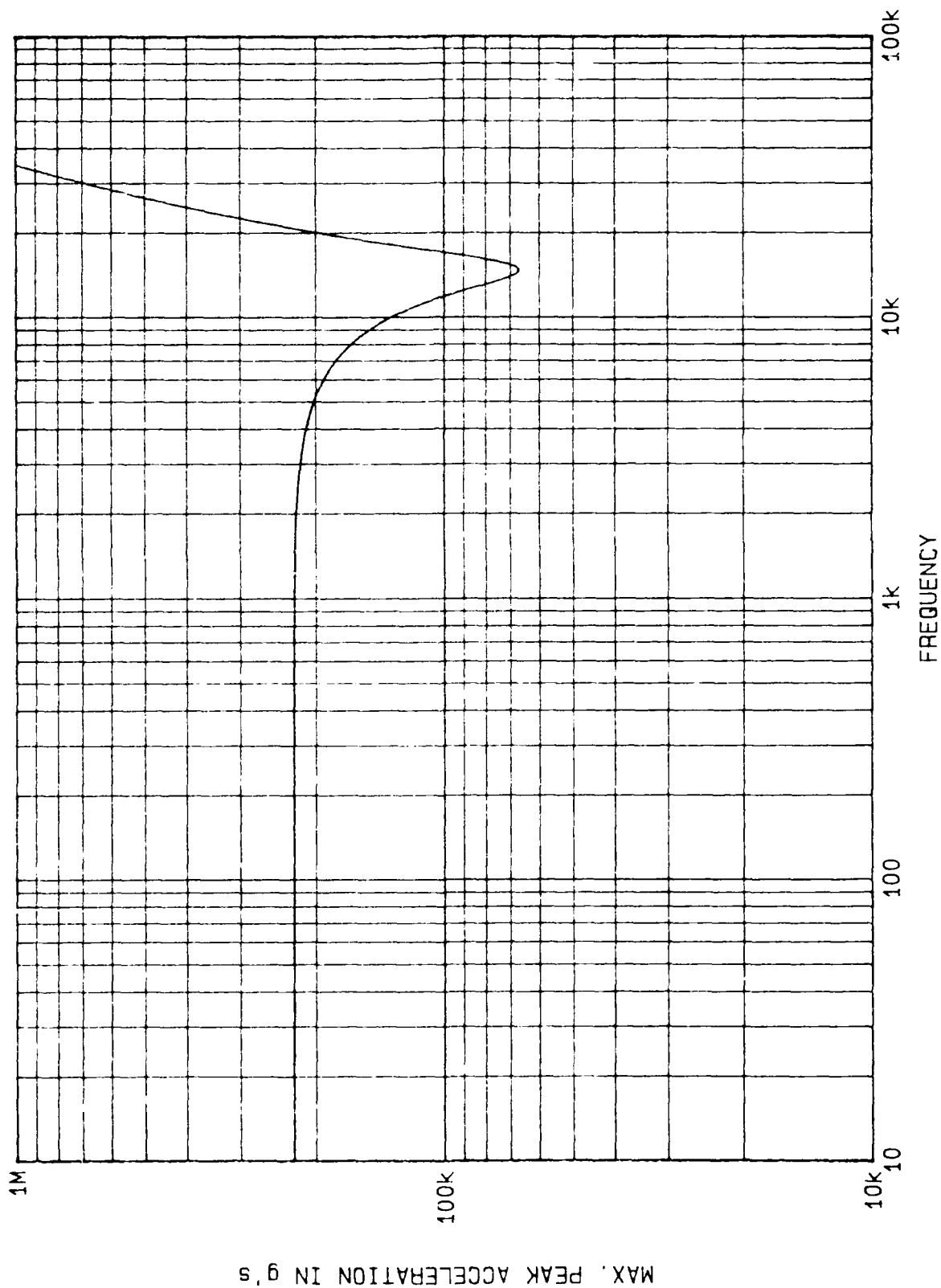
The maximum allowable level at that frequency is 67,000 g. Above 67,000 g, the mechanical filter loses its effectiveness (eg. bottoms out), and protection to the sensor ceases.

TEST RESULTS

Several prototypes were sent out for field evaluation. The first group were tested at the U.S. Army Combat Systems Test Activity, Aberdeen Proving Ground, Maryland. The evaluation set-up was a classical close-range shock measurement [7] which involved a 18" x 18" x 1.5" steel plate. All the test transducers were hard mounted on one side (in the middle), while the impacts occurred directly on the other side of the plate. Types of excitation used for shock generation ranged from ball bearing impacts, blasting caps, to C-4 detonation.

Figure 9 shows a comparison between the shock responses of a 200,000 g piezoresistive type accelerometer and the prototype with built-in mechanical filter. A 2" ball bearing was used to strike the plate and produced the input acceleration. The dotted line shows the response of the prototype at about 1,100 g peak, whereas the PR accelerometer shows almost double the peak g level due to its wider bandwidth (1 MHz). Figure 10 shows the same event except that the PR transducer output has been filtered at 10 kHz. Note the closed agreement between the two accelerometers. (the phase shift could be due to different filter characteristics)

Figure 11 shows the response of a typical shock accelerometer measuring the excitation from a DFP-2 non-electric type blasting cap (.05 gram). A classical zeroshift occurred 2 milliseconds after the blast-off. Figure 12 shows the response of the prototype under the same excitation condition; no DC offset was noted.

Figures 13 and 14 show the differences in amplitude response of a typical shock accelerometer and the prototype with mechanical filter. Input excitation was the detonation of a M7 blasting cap (.9 gram) directly behind the sensors. Again the transducer without mechanical filter exhibited a huge amount of DC offset.

Figure 15 shows the killer -- 1 oz. of C-4 detonated on the plate. The experimenter reckoned that the

input transient could well be in excess of 1 million g. Here the prototype survived the blast, but the DC level has shifted; apparently the mechanical filter bottomed out. In similar tests, other piezoresistive accelerometers had been destroyed due to the high frequency energy content.

Another field test was conducted at McDonnell Douglas, St. Louis, Missouri where three prototypes were mounted on a test article with 28 feet of 18 grain/ft PETN mild detonating cord. This test exhibited tremendous amount of high frequency energy in certain directions. Figure 16 shows the response of one of the prototypes in a mild direction. The Shock Response Spectrum and the velocity were said to be believable.

Figure 17 shows the response in the vicious direction. Although the time history seems normal, integration indictes unrealistic velocity. Note also the rising low end of the SRS due to latent zeroshift. To analyze the data further, the Fourier Spectrum was calculated and is shown in Figure 18. Here an obvious spike dominates the FFT plot at 15 kHz, indicating that the filter is resonating.

FUTURE DEVELOPMENT

There are still many problems to overcome in making a perfect shock accelerometer. Within its limitation, however, this experimental transducer is one step closer to the reality. A patent recently has been applied for this shock transducer design concept , and production units may be available in the near future.

Future development of this experimental accelerometer may include refinement of the mechanical filter for better linearity and higher dynamic range. Different types of sensing elements will be investigated in search of wider frequency response and reduction of sensor non-linearity. Improvement in temperature response of the mechanical filter can also be expected.

IMPACT: 2 IN. BALL BRNG
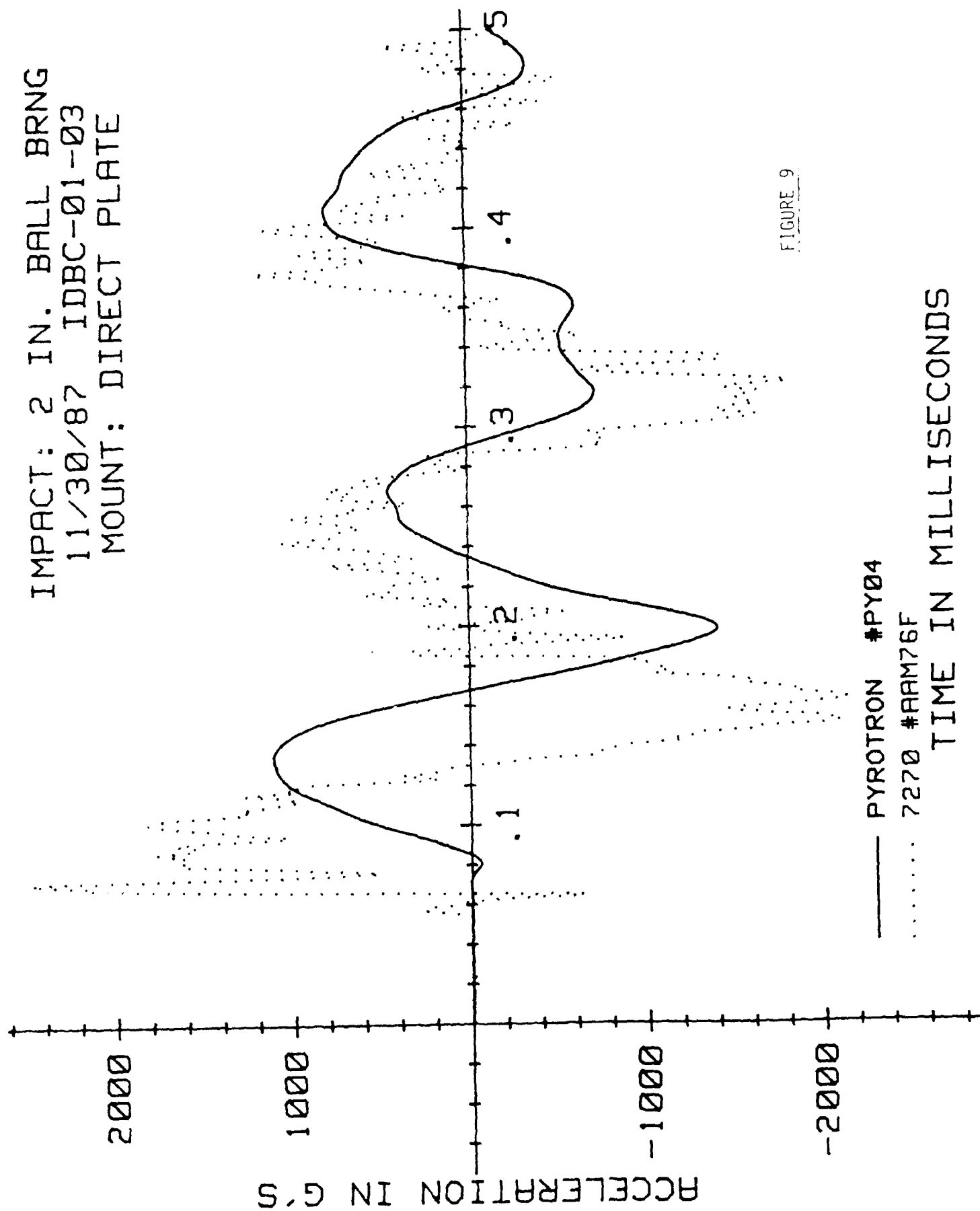11/30/87 IDBC-01-03
MOUNT: DIRECT PLATE

PYROTRON #PY04
7270 #AAM76F

TIME IN MILLISECONDS

ACCELERATION IN G'S

FIGURE 9

IMPACT: 2 IN. BALL BRNG
11/30/87 IDBC-01-03
MOUNT: DIRECT ON PLATE

PYROTRON #PY04
7270 @ 10 KHz

TIME IN MILLISECONDS

ACCELERATION IN G'S

FIGURE 10

97
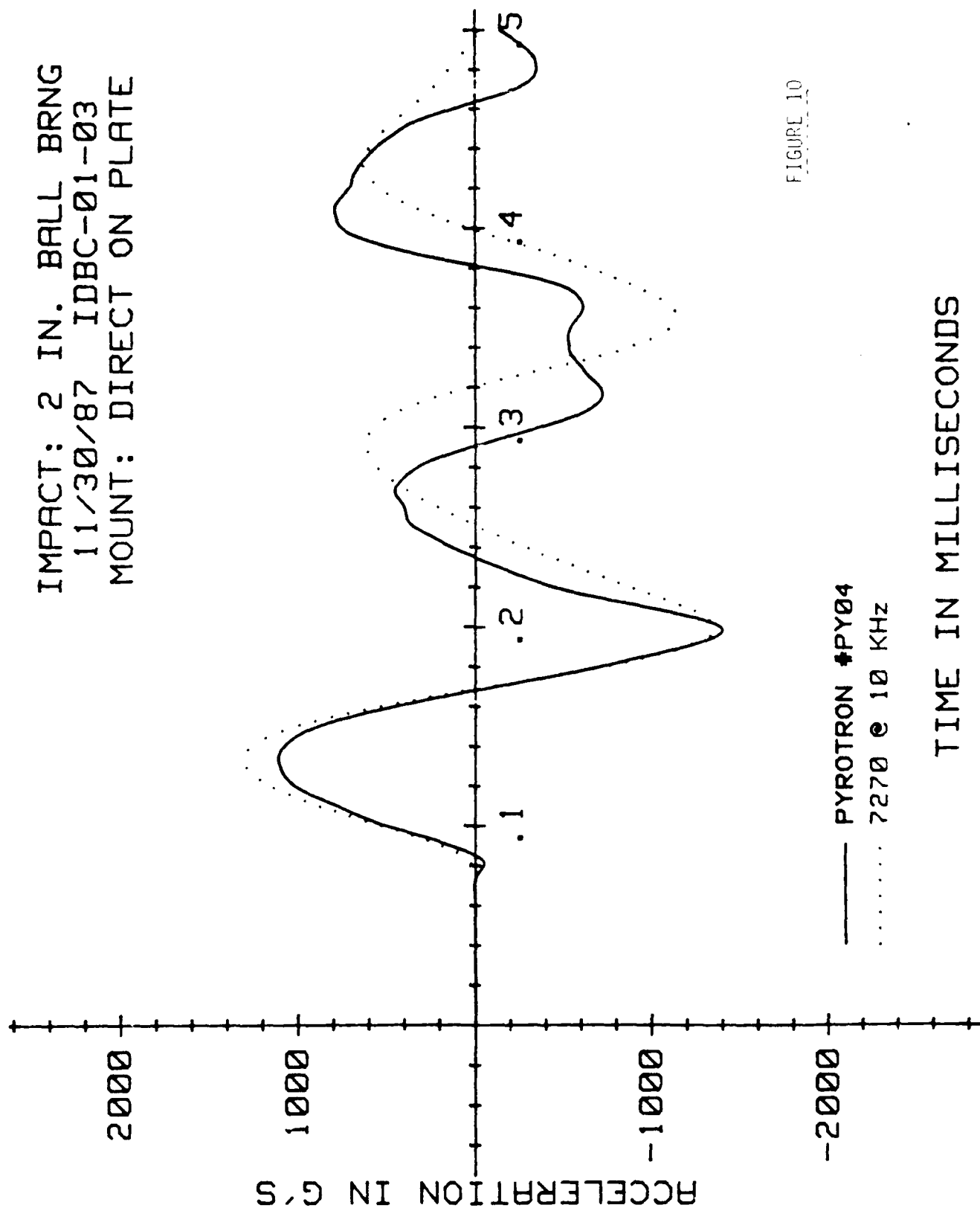
@ 10KHz

RND#7 12APR88 014-05

DFP-2 CENTER

FIGURE 11

ACCELERATION IN G'S

TIME IN MILLISECONDS

98
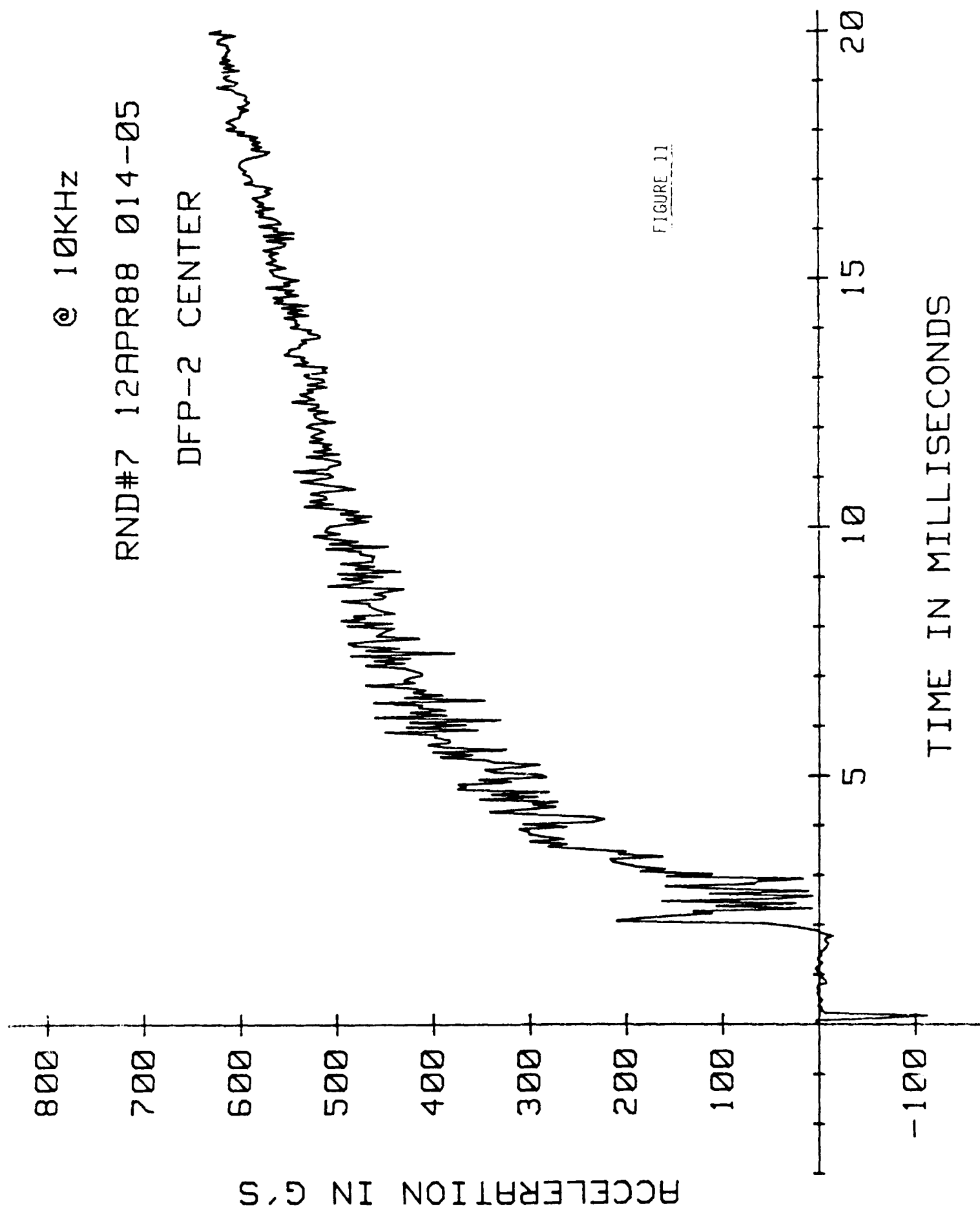
7255 ACCEL DIRECT MOUNT
RND#02 13APR88 012-20
DFP2 CENTER

FIGURE 12

TIME IN MILLISECONDS

ACCELERATION IN G'S

600 400 200 -200 -400 -600

35 30 25 20 15

RND# 9 12APR88 014-07   @ 10 KHz

M7 CENTER

FIGURE 13

ACCELERATION IN G'S

TIME IN MILLISECONDS
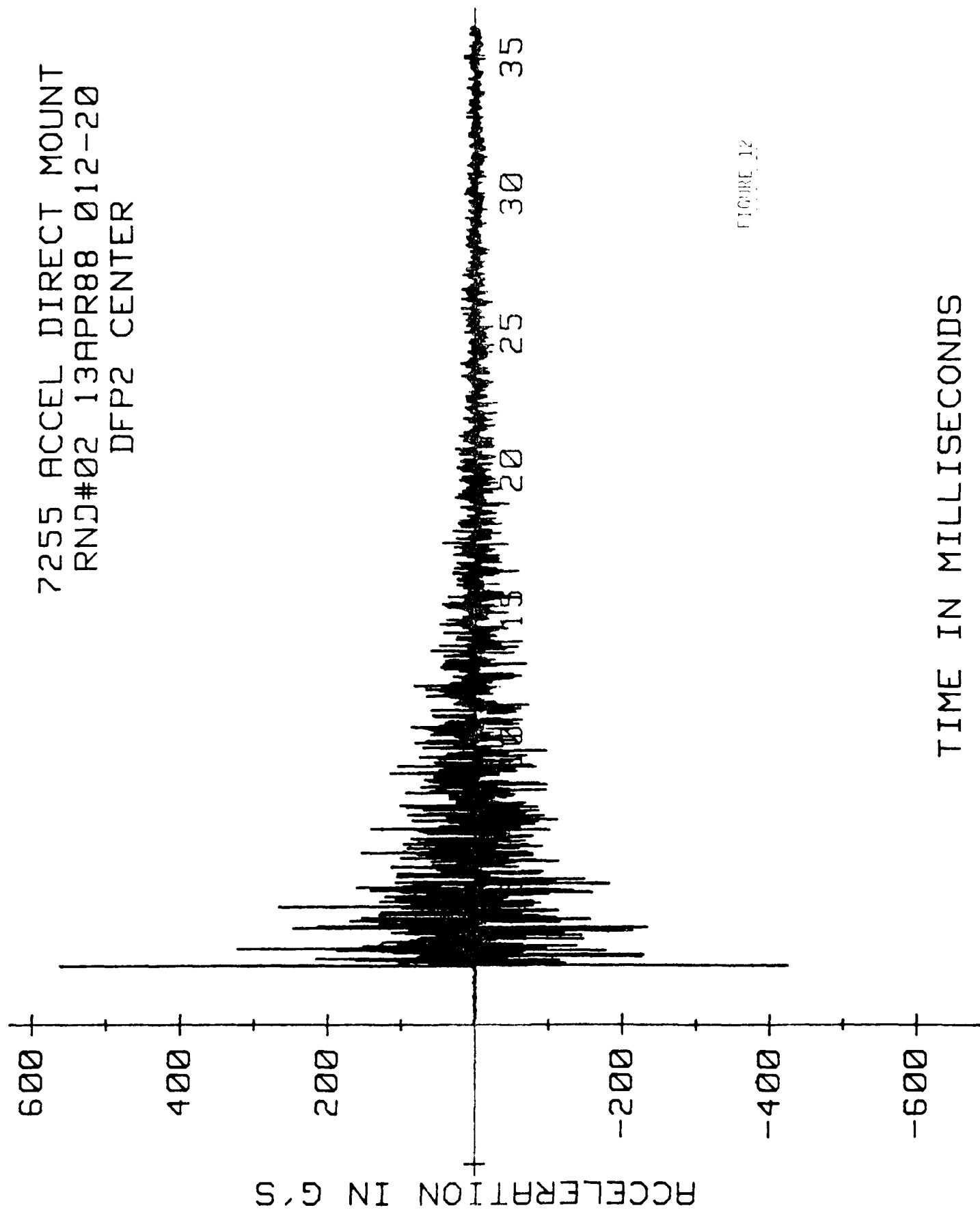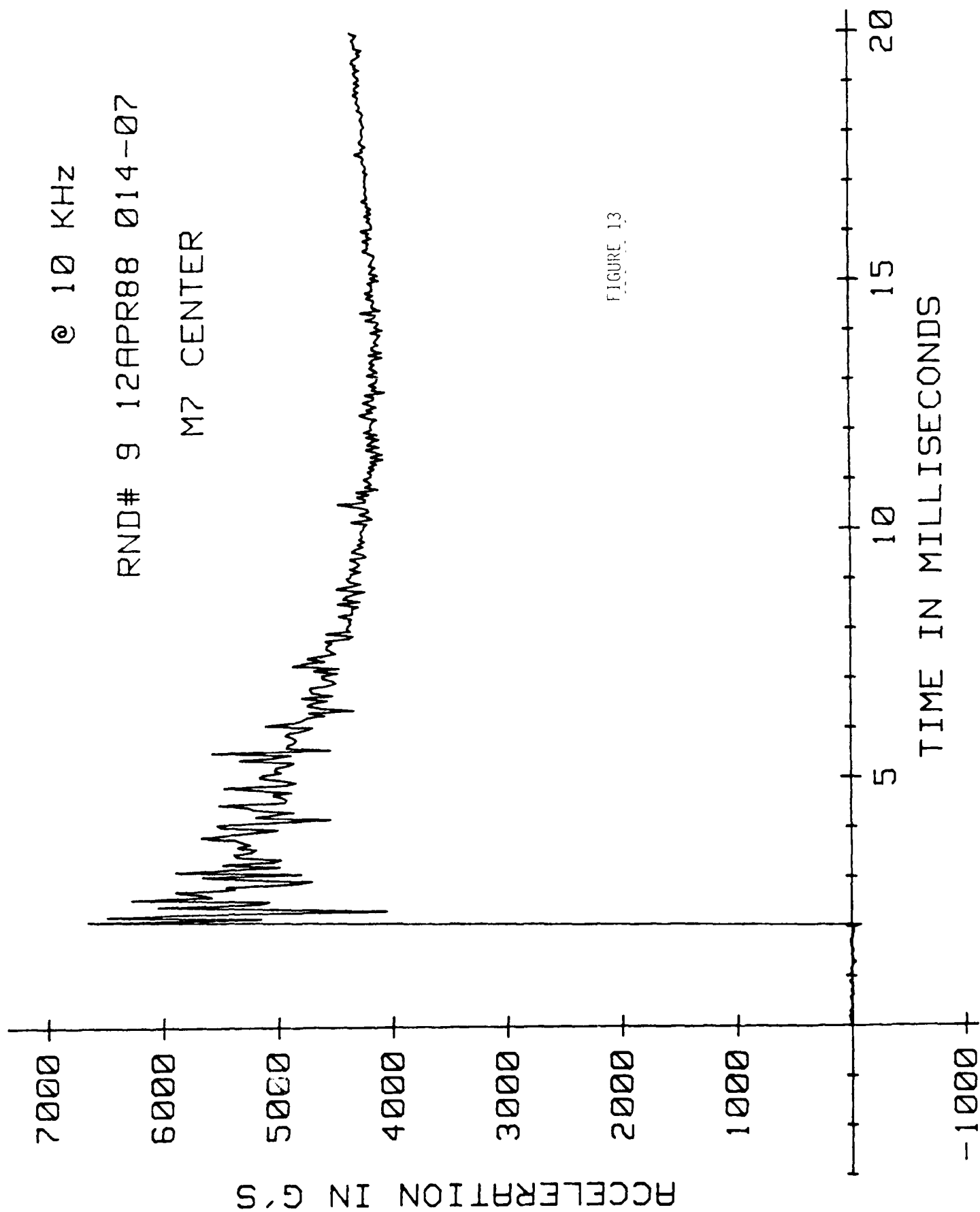
7255 ACCEL DIRECT MOUNT
RND#3 13APR88 017-01
M7 CENTER
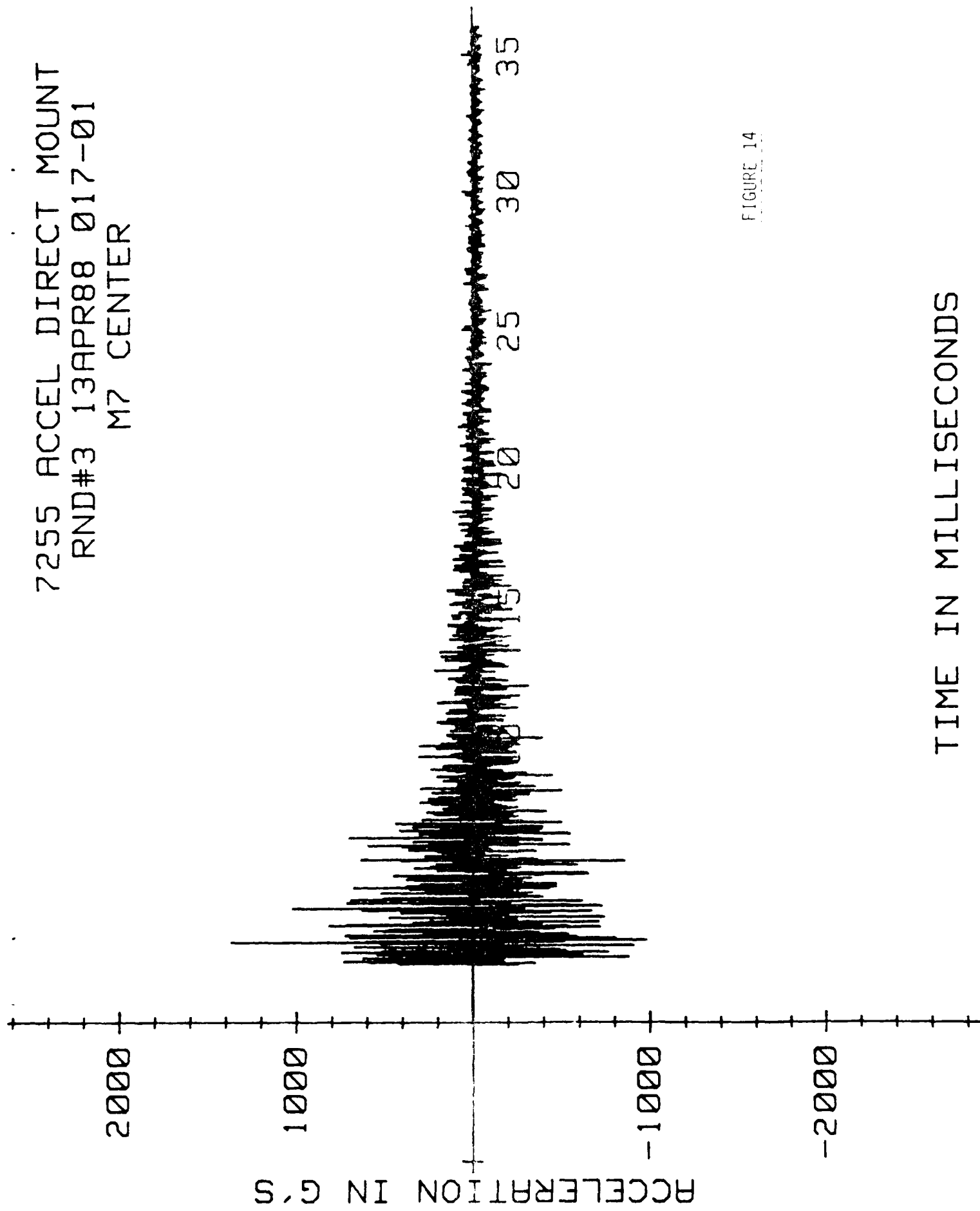
FIGURE 14

TIME IN MILLISECONDS

ACCELERATION IN G'S

2000   1000   -1000   -2000

35   30   25   20   15

101

C-4 DETONATION

FIGURE 15

MILLISECONDS

FIGURE 16

103

EO14X_C61SSE.SRS   C= 10.0

PLUS AND MINUS SPECTRUM - G

FREQUENCY - HZ

ACCEL - G ,10³

VELOCITY - IPS

TIME - SEC ,10-3

FIGURE_17

104

FOURIER SPECTRUM
OF FIGURE 17
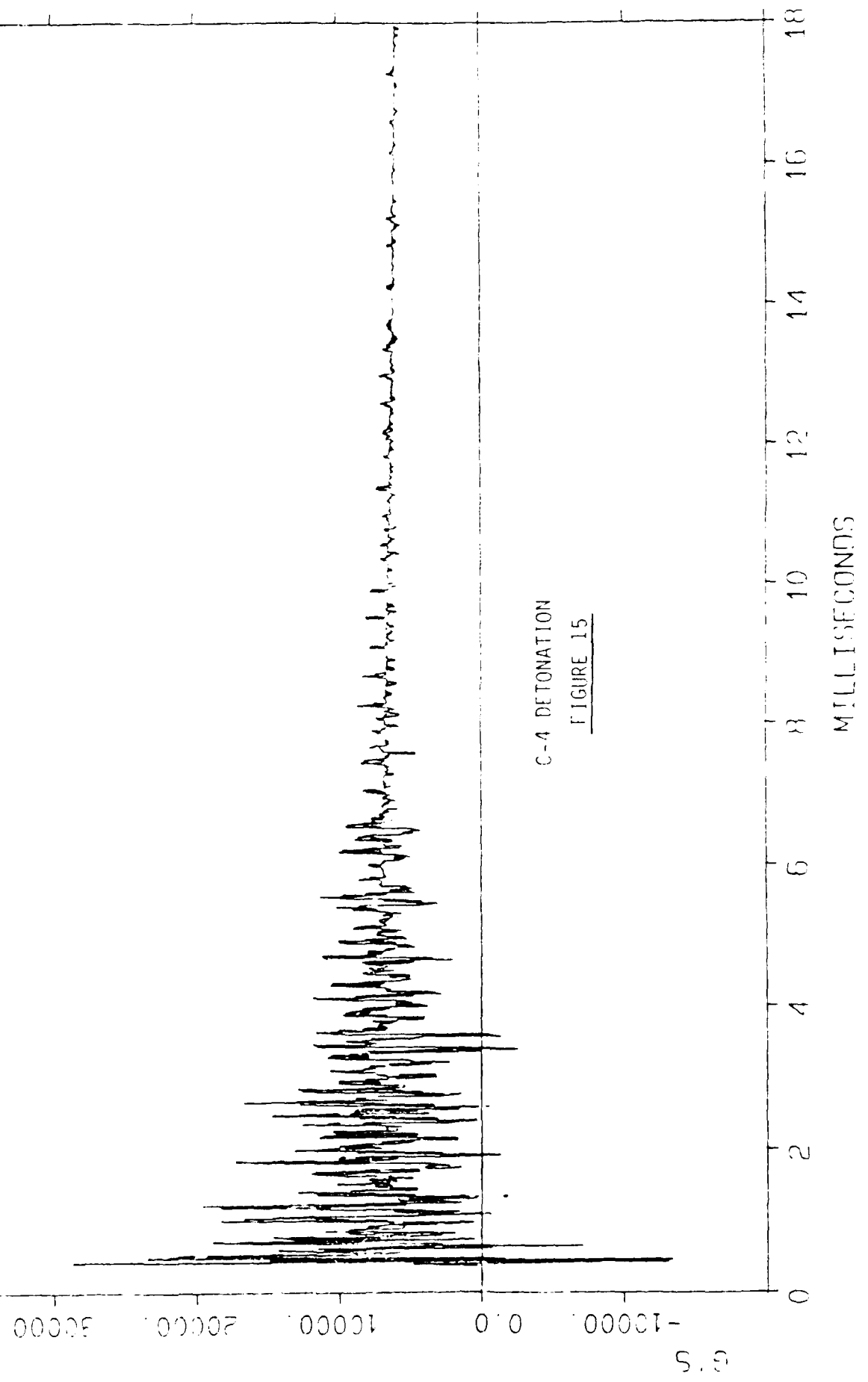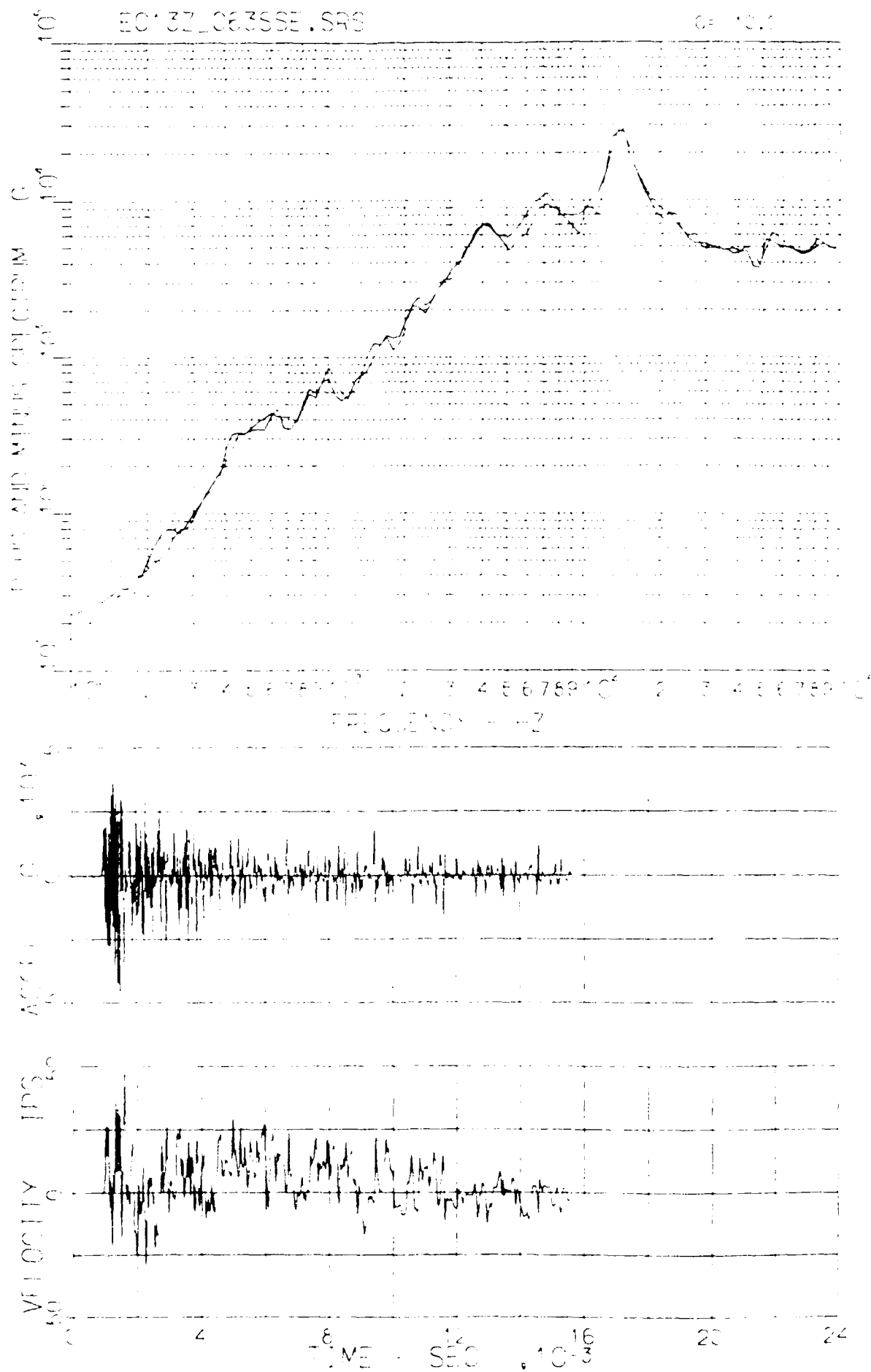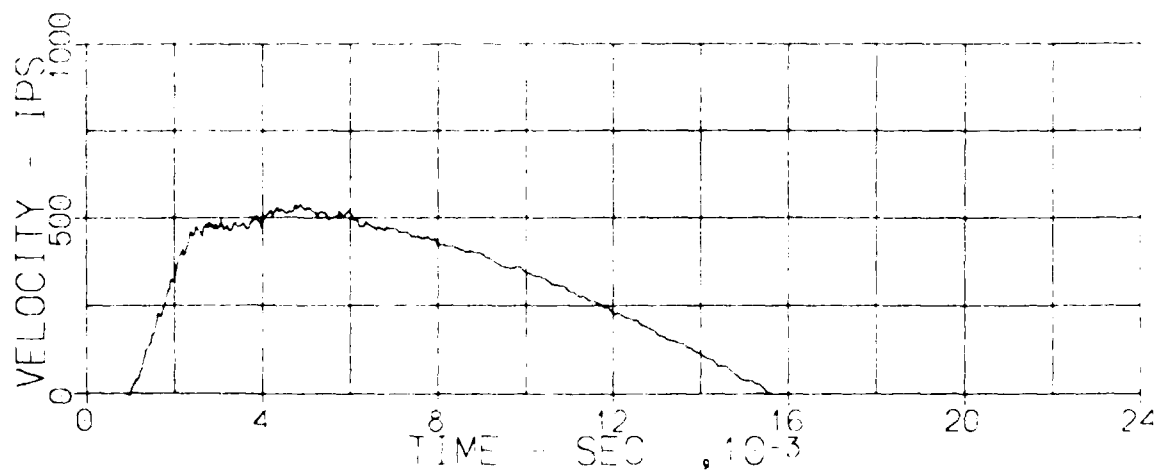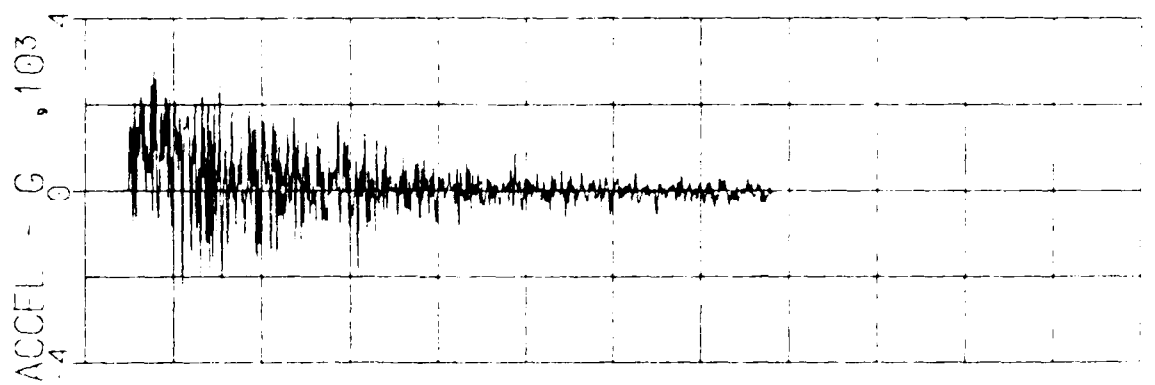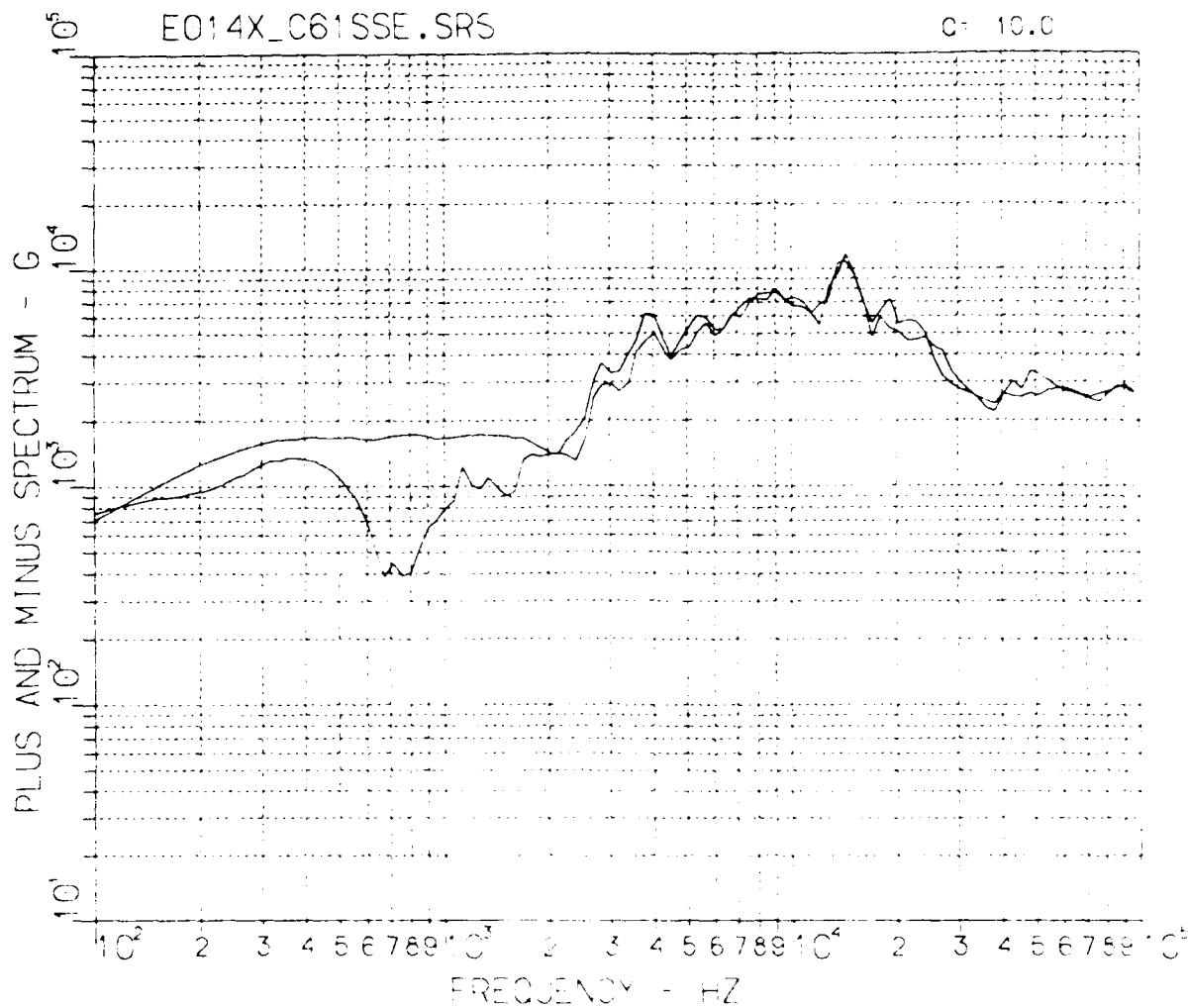
FIGURE 18
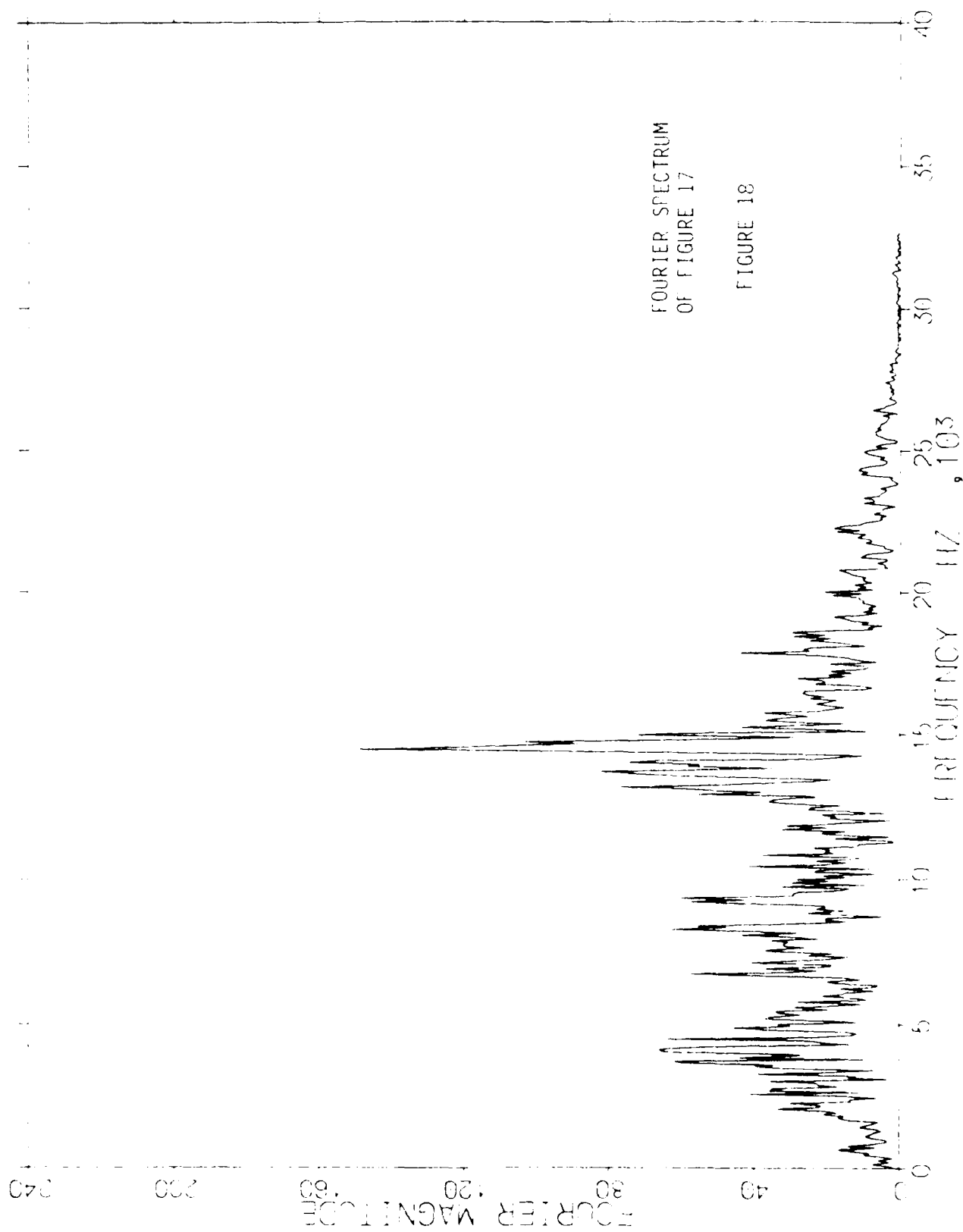
REFERENCES

1. A. E. Galef, "The Pre-Pulse in Pyroshock Measurement and Analysis", Bulletin, 56th Shock & Vibration Symposium, Part III, 1986.

2. A. E. Galef, "Zero-shifted Accelerometer Outputs", Bulletin, 56th Shock & Vibration Symposium, Part III. 1986.

3. R. D. Sill, "Shock Calibration of Accelerometers at Amplitudes to 100,000g Using Compression Waves", Proceedings, 29th International Instrumentation Symposium. ISA, 1983.

4. R. H. Plumlee, "Zeroshift in Piezoelectric Accelerometers", Sandia Corporation Report, SC-RR-70 755, 1971.

5. D. B. Davis, "Investigation of Zero Shift in Piezoelectric Ceramic Accelerometers", Sandia Corporation Report, 71-631.

6. A. S. Chu, "Zeroshift of Piezoelectric Accelerometers in Pyroshock Measurements", Bulletin, 57th Shock & Vibration Symposium, Part I, 1987.

7. W. S. Walton, "Dynamic Response of Armor Plate to Non-Penetrating Projectile Impact", Bulletin, 56th Shock & Vibration Symposium, Part I, 1986.

BUILT-IN MECHANICAL FILTER IN A SHOCK ACCELEROMETER

Q: **Jim Faller** (Aberdeen Proving Grounds): I'm familiar a little bit with the individual who did this test and Endevco now manufactures both piezoresistive and piezoelectric accelerometers, am I right? So do you now consider this an improvement over your existing line of products?

A: **Anthony Chu:** For pyro-shock close range metal to metal impact, yes.

Q: **Jim Faller:** That comparison test was between another Endevco gauge?

A: **Anthony Chu:** Yes, that was the 7278. That's correct.

Q: **Jim Faller:** Now what emerges from that test? Was one gauge to be believed more than the other, because even though you didn't call attention to that differential and amplitude; it was, I would imagine, from one stand point substantial. Is there any way of determining which gauge gives the better measurement?

A: **Anthony Chu:** At that g level, I don't think there's a significant difference, but that was just a ball bearing dropped onto a plate and he had some more vicious tests that the 7278 simply didn't survive because the cantilever would break. You excite resonance of the one megahertz sensor that resonates and it breaks, so its a matter of survivability.

Q: **Jim Faller:** You're also saying this is 67,000 g's versus one million g's for the other one? The other one is capable of going a million or more?

A: **Anthony Chu:** No, I didn't say that.

Q: **Jim Faller:** I thought they they were measuring a million or more?

A: **Anthony Chu:** No, the test that he shifted the one with the mechanical filter was at about one million g's.

Q: **Jim Faller:** Is this now an available new product?

A: **Anthony Chu:** Yes, this is an available new product.

Q: **Jim Faller:** What is the option a person will have? What is going to be recommended? In other words, your standard line or is this new product is going to be considered superior?

A: **Anthony Chu:** If you are measuring really close to the source, that's the only way that I can see it, at this point.

"A Pressure Transducer to Measure Blast-Induced Porewater Pressure in Water Saturated Soil"

Dr. Wayne A. Charlie

This paper describes our use of a modified commercial pressure transducer (ENDEVCO Model 8511A-5K-M1) to experimentally measure the transient water pressure in water saturated cohesionless soils. A series of controlled laboratory and field tests were conducted which subjected water and water-saturated soils to a high amplitude stress waves induced by impact and explosives. The results of our study and the response and calibration of the porewater pressure transducer will be presented and discussed. The results of our research indicate that the transducer can measure the porewater pressure in water saturated gravels, sands and silty sand.

A PRESSURE TRANSDUCER TO MEASURE BLAST-INDUCED POREWATER PRESSURE IN WATER SATURATED SOIL

Q: Bill Cardwell (GE Electronics, Evandale):   You mentioned you had capability of cold and hot water in the tank. Was there a reason that you wanted to go up to higher temperature and what temperature did you reach?

A: Wayne Charlie: The reason we went to warm temperatures is that it's very difficult to saturate soil. We ran de-aired water through for two weeks and we couldn't saturate the sample. We have something like 50 tons of soil we're trying to saturate so we ended up having to go to hot water. We used the hot water to de-air the soil. We ran warm water up and as it was coming through it would be cooling down. We actually ran the test at the normal air temperature, we let it cool down first. But it was just to get the air out of the soil so that we're actually running truly saturated tests.

Q: Ron Tussing (Naval Surface Weapons Center):   I talked to John Ainsworth from Endevco and they make a special gauge for Germany, although it may be made in England, I don't recall which it is, but it's made for underwater use. What you have works fine, but the Germans in the Baltic found that the oil did wash out of the gauge so they had to go to this special Endevco. So there is a gauge although I'll have to look it up when I get home. Did you consider using something like an underwater pressure gauge since you're essentially underwater there, something like a tourmaline gauge from PCB or something like that?

A: Wayne Charlie: No, we did take the plate off and on and tried it under water. We did correlate those back to Kohl's underwater explosive shots at the same pressure. His correlates with distance and charge size within probably 10% of that data.   We have not used another gauge on this shot, so there's some potential. On the acceleration data that we have, when we integrate that particle velocity for the peak particle velocity and convert it to what we're seeing on the pore pressure, the shape is the same on the early part of the curve and the stress that you would calculate from the acceleration or the particle velocity integrated from the acceleration is also within 10% of what we're seeing on the peak shots, although on our later shots we lost our acceleration.   The lab calibration looking at the projectile velocity etc., all ran within 10% of what we expected from the transducer, and it wasn't just on one side, it was on both sides. We also measured independently at another site, particle velocity, but we were further away and that also correlated with the pore pressure.

DIFFICULTIES/REMEDIES IN PRESSURE MEASUREMENTS
WITH PIEZORESISTIVE SENSORS

S. Nickless and R. Maglic
Honeywell Solid State Electronics
Colorado Springs, Colorado 80906

ABSTRACT

Resistors implanted into single crystal of thin Silicon diaphragms have their resistance stress sensitive. When measured fluid pressure causes this stress, the resistance measurement allows an accurate assessment of pressure in question. Although this sounds simple, the resistance change R depends on factors other than just stress: temperature, direction of the resistor in the crystal, impurities on the surface and definitely the quality of P-N junction bordering the piezoresistor; in this paper we show how the sensor current leakage I_L, results from defects in the P-N junction. Some of these defects are crystalographic and some are impurity related.

We describe here first a pressure-sensing IC-structure and how the leakage current is observed. Next, we describe how stacking faults are introduced in the "Front End" of the IC wafer processing (example a); other types of defects are introduced during subsequent die/sensor processing (examples b).

Example a. Stacking Fault introduced into P-N junction area during Front End processing provides a leakage path for current I. The leakage path is completed however, only if subsequently deposited "N-Cap" layer is very conductive. Computer simulation of resistor/N-Cap implant predicted formation of peculiar P-type islands influencing the leakage.

As examples of type b we discuss the effect of high-pressure water scrub on the current leakage of a piezoresistor: this popular processing step (clean) can introduce defects in the same sensitive area of the piezoresistor mentioned above. Great yield improvement results when it is eliminated/controlled.

Finally, the origin of defects induced by the scrubbing is examined.

INTRODUCTION

Electron/hole conductivity in single crystal silicon depends on energy barriers a carrier "sees" for particular direction of propagation; electron/hole energy bands are stress sensitive in silicon leading to well known empirical expression for change in resistance

$$\Delta R \approx \pi(\theta).R.\sigma$$

where σ, psi is stress at the resistor site and θ angle of propagation -in respect to say [100]-direction. $\pi(\theta)$ is piezoresistive coefficient and $\pi.\sigma$ is of the order of 1% for Si. If fluid pressure is to be measured P, psi, a silicon diaphragm is etched out of a solid wafer of single crystal silicon and a resistor is implanted into it; usually a P-type wafer (Boron diffused into silicon) is used and an N-type epitaxial layer (N-Epi) is deposited on it. The N-Epi serves as an etch stop when manufacturing the diaphragm - it defines diaphragm thickness. Figure 1 shows a pressure sensor die after an N-Epi was grown on the P-type wafer. SiO2 is the passivation layer; the diaphragm is formed by etching away P-type silicon.
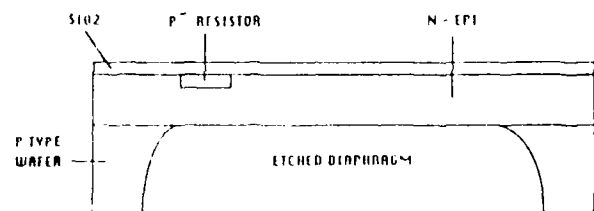

FIGURE 1. SILICON DIE AFTER ETCHING, P⁻ IMPLANT, AND SIO2 DEPOSITION

After a resistor implant (light implant, P⁻) a heavy P-implant insures connection between resistors and "outside world" (P⁺ implant). Finally, an N-implant is made ("N-Cap") over the resistors providing protection against electro-static field in the environment, Figure 2.

Boundary between P⁻ resistors and N-Epi makes an N-P junction - electrical isolation of the resistor. P-type area is always held on lower potential than the N-Epi is. When a current leakage problem occurs a current between
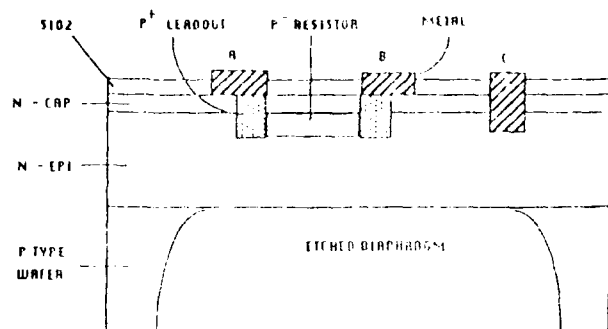
FIGURE 2: P⁻ RESISTOR WITH N-CAP AND CONNECTIONS

contacts C&B is non-negligible; if the P-N junction fails totally I_L may go to microamperes for positive voltages applied to terminal C (reverse bias conditions).

After the wafers have been processed through the front end, the junction integrity must be maintained during the cavity formation and subsequent sensor packaging operations. As an example, a high pressure water scrub was pinpointed as contributing greatly to junction leakage. The measurement of the leakage, failure analysis to characterize the cause of the leakage, and the impact of junction modifications are discussed.

I. FRONT END LEAKAGE CONSIDERATIONS

1. JUNCTION LEAKAGE

Note, on Figure 2, that the P⁻ resistor is surrounded by several different P-N junctions: P⁻/N-Epi, P⁻/N-CAP and P⁻/P⁺ (junction J_1, J_2 and J_3 respectively). Our detailed studies showed that P⁻/N-Cap is the most sensitive junction. Partly, because implant energies and doses for P⁻ and N-Cap layers are such to make J_2 junction depths only .4μm. (J_1 junction depth was measured to be ~ 1μm.) This puts N-Cap junction (J_2) close to SiO_2/Si interface and very sensitive to environmental conditions.

In silicon pressure sensor technology it is a well known fact that depth of J_2 has to be optimized. If X_{j2} is small so that reverse voltage bias depletes N-Cap completely (to wafer surface), no leakage occurs. There are no carriers in the depleted zone (DZ) then. The sensor is unstable at this time however, because impurities on the wafer surface feel the electric field of the DZ. This results in a drift.

In the opposite case when X_{j2} is large DZ in N-Cap doesn't reach the wafer surface and then leakage is possible if J_2 is weak. Consequently, by increasing phosphorous implant dose (N-Cap) the leak monotonically increases.

Two dimensional crystalographic defects (stacking faults in Si) have been observed near J_2-junction and correlated with leaking units.

Opposite is true also, by eliminating stacking faults (high temperature oxidation) current leakage was reduced significantly.

2. CATS WHISKERS

Current leakage path, as described above, leads from electrode C (Figure 2) through Epi and through N-Cap above P⁻ to resistor via P-N junction J_2. Then the path leads out through piezoresistor and P⁺ lead out. We assume that junction J_2 doesn't deplete to wafer surface.

The leakage path may be broken however, at the resistor edge by formation of "Cats Whiskers" -regions of P-type material going from a buried resistor to wafer surface, through N-Cap. Figure 3 shows a possible whisker formed on one side only.
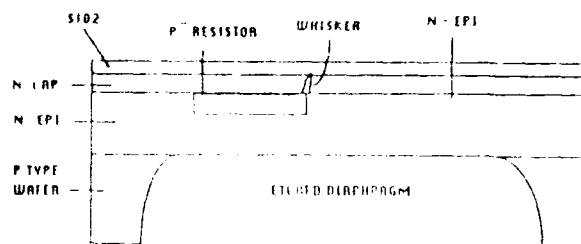

FIGURE 3 CROSS SECTION OF RESISTOR TO SHOW WHISKER.

If a complete whisker forms along both edges of the resistor, the leakage path is broken. Note on Figure 4a, b and c various cases that can happen in whisker formation. Case 4c has, like Figure 3, a complete whisker formed. Figure 4b shows curious P-type islands formed near wafer surface. This latter case however, would allow leakage.

Figure 4 results were obtained by computer calculation, calculating in two dimensions (x axis perpendicular to wafer surface) of Boron and Phosphorous implant density N_B, N_P. Boron is implanted through a SiO_2 mask (Figure 5). Since SiO_2 is thinned down at the end, N_B distribution may result. Boron at a corner is

$$N_B = \frac{1}{\sqrt{2\pi} \, S_1} \, e^{\frac{(r-A_1)^2}{2S_1^2}}$$

with $r^2 = x^2 + y^2$ and A_1 being Boron range for the given implant energy; S_1 is "implant struggling" quantity.

N-Cap is deposited after SiO_2 mask has been removed with some constant concentration (B_0) at the surface where top expression holds for $x < A_2$; the bottom one for $x > A_2$. Constant C determines Boron/Phosphorous dose ratio. (See Figure 6) For points x,y where $N_B/N_P > 1$,

```
0    0 0 0 0 0 0 0 0 0 0
2    0 0 0 0 0 0 0 0 0 0
3    0 0 0 0 0 0 0 1 0 0
4    0 0 0 0 0 0 1 1 0 0
5    0 0 0 0 0 0 1 1 1 0
6    0 0 0 0 0 1 1 1 1 0
7    0 0 0 0 1 1 1 1 1 0
8    0 0 0 1 1 1 1 1 1 1
9    1 1 1 1 1 1 1 1 1 1
10   1 1 1 1 1 1 1 1 1 1
```

(a)

```
1    0 0 0 0 1 1 1 0 0 0
2    0 0 0 0 1 1 1 0 0 0
3    0 0 0 0 1 1 0 0 0 0
4    0 0 0 0 0 1 0 0 0 0
5    0 0 0 0 0 0 0 0 0 0
6    0 0 0 0 0 0 0 0 0 0
7    0 0 0 0 1 0 0 0 0 0
8    0 0 0 1 1 0 0 0 0 0
9    1 1 1 1 1 0 0 0 0 0
10   1 1 1 1 1 1 0 0 0 0
```

(b)

```
1    0 0 0 0 1 1 1 0 0 0
2    0 0 0 0 1 1 1 0 0 0
3    0 0 0 0 1 1 1 0 0 0
4    0 0 0 0 1 1 1 0 0 0
5    0 0 0 0 1 1 0 0 0 0
6    0 0 0 0 1 1 0 0 0 0
7    0 0 0 1 1 1 0 0 0 0
8    0 1 1 1 1 1 0 0 0 0
9    1 1 1 1 1 1 0 0 0 0
10   1 1 1 1 1 1 0 0 0 0
```

(c)

Figure 4. CAT'S WHISKERS CALCULATION: Dx = .5, Dy = 1. AND OTHER PARAMETERS

	a	b	c
A_1	8	6	6
C_1	2	2	2
A_2	1	3	3
S_2	1	1	1
B_0	1	.25	.25
C	.5	.5	.3
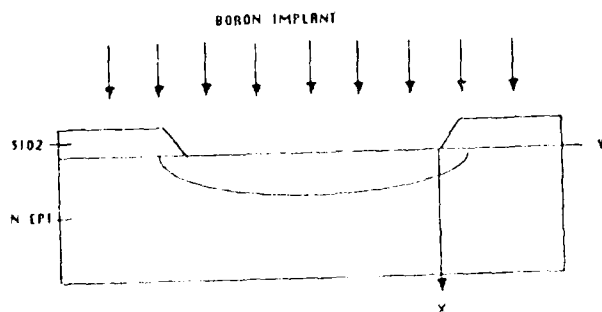
FIGURE 5. BORON IMPLANT WITH A SILICON DIOXIDE MASK THINNED DOWN NEAR OPENING
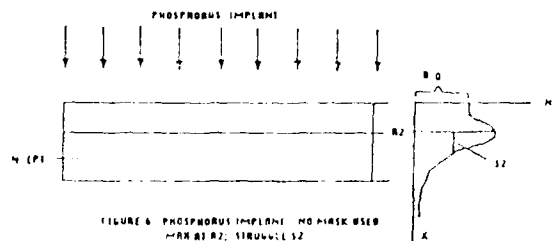
FIGURE 6. PHOSPHORUS IMPLANT - NO MASK USED MAX AT A2, STRUGGLE S2

$$N_P = \begin{cases} C\left[\dfrac{B_o}{\sqrt{2\pi}\,S_2} + \dfrac{1}{\sqrt{2\pi}\,S_2}\,e^{-\frac{(x-A_2)^2}{2S_2{}^2}}\right] \\[2em] C\left[\dfrac{1}{\sqrt{2\pi}\,S_2}\,e^{-\frac{(x-A_2)^2}{2S_2{}^2}}\right] \end{cases}$$

computer prints 1-digit; 0 for the opposite case. Note: above calculation was done only qualitatively, but with realistic magnitudes. Second, no depletion width is added anywhere.

Finally, we add that etch patterns allowed us to observe, experimentally, Cat's Whiskers on some units that did not leak.

II. BACK END LEAKAGE CONSIDERATIONS

1. HIGH PRESSURE WATER SCRUB
Completed wafers through the front end must next have backside etch processing to form the diaphragm which creates the pressure sensitivity. The diaphragm formation along with other packaging operations are stressful and can cause junction degradation and current leakage.

As an example, a high pressure deionized water scrub operation which is used to remove ink residue from the wafer surface is analyzed. The scrub machine operates by sweeping a high pressure nozzle across the surface of a spinning wafer. The result of this scrub is a wafer which has good adhesion characteristics which are needed in the next step of the process. The negative effect of the scrubber on the sensor are discussed in the following sections.

2. MEASUREMENT OF LEAKAGE
The final device leakage is kept in the nA range with 5v applied at 25°C to achieve device performance. Several wafers were measured for leakage before a high pressure deionized water scrub and then again immediately following the scrub. Table 1 defines the leakage change on the same die after receiving the high pressure scrub. Notice the change in the I-V characteristic which shows a "soft" junction, evidence of a damaged or contaminated junction. (See Figure 7)

Wafer #1

PRE HP SCRUB			POST HP SCRUB		
.7nA	20.9nA	.3nA	121nA	41nA	2.7nA
.7nA	TD	.6nA	.5nA	TD	9.2nA
.4nA	.7nA	.7nA	1200nA	.5nA	143nA

Wafer #2

PRE HP SCRUB			POST HP SCRUB		
.5nA	.6nA	1.5nA	.5nA	42nA	8.5nA
32nA	TD	.3nA	529nA	TD	.5nA
103nA	.5nA	.7nA	436nA	32nA	316nA

Wafer #3

PRE HP SCRUB			POST HP SCRUB		
1.1	0.7	0.9	2700nA	18.2nA	1290nA
2.3	TD	1.3	8250nA	TD	5300nA
1.7	30.2	0.7	585nA	54.7nA	39.9nA

Table 1:
Junction Leakage Measurements

Vs = 5V applied from C to B in Figure 2.
TD = Test Die (Used as measurement position reference)

POST HIGH PRESS. SCRUB

PRE HIGH PRESS. SCRUB

Figure 7. Scrubber Junction Damage
I-V Curve

3. FAILURE ANALYSIS

The leakage location was pinpointed using light emission photodetection equipment. The defect area emitted low levels of light due to electron trapping and discharge allowing these areas to be mapped and a decorative Wright etch was performed in the vicinity of the leakage area. SEM analysis of the post etched wafers showed that microdefects were present in the implanted resistor regions at the location of the leakage. It is therefore believed that these defects are responsible for the leakage experienced on the device and are created by the high pressure scrubber. See Figure 8 for SEM photographs of the decorated defects.

4. HIGH PRESSURE SCRUBBER EFFECTS

The high pressure deionized water scrubber creates defects in various forms of processed or unprocessed silicon. Unprocessed wafer starting material was subjected to a 1650 psi scrub and a defect count showed 135 defects/cm^2. Since the final device has a thin layer of thermal oxide for circuitry protection, a study was completed to determine the amount of damage created as a function of oxide thickness. The increase in thermal oxide was inversely proportional to the defect density showing that one possible protection should be thermal oxide (see Figure 9). This study conflicted with the defect densities found in the implanted resistor
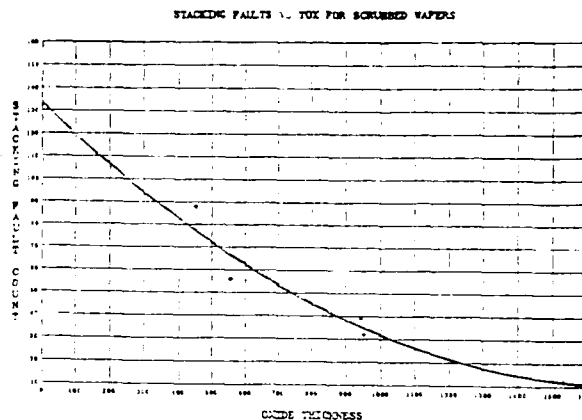
Figure 8. SEM Photos Of Defects

Figure 9: Oxide thickness vs. defects

HPS unit, by Eaton Corporation, produces a high pressure water beam by forcing water at $P_{H2O} \sim$ 1000 - 2000 psi through a small hole (diameter d $\sim$ .005in.). We measured amount of H_2O collected, in say 30sec, coming out of the orifice; this, with tube cross section measurement, gave jet velocity of 145m/sec. Pressure the jet exerts p at the exit of orifice is p $\sim \rho v^2$ = 2.9kpsi with water density being ρ. Pressure p at the wafer was measured to be 700psi, and this is the value we used in subsequent calculations. Difference in two pressures results from beam widening (.015mil at the wafer) and velocity variation across the jet diameter. Before we propose a model for defect origin, we examine here some auxiliary tests done to eliminate other, unrelated sources of defects.

•Electrostatic Discharge (ESD) of charges accumulated on the wafer by DI water (isolating, deionized water) can produce crystal defects. We changed DI-water to normal, conducting water and grounded HPS tube and wafer chuck. Etch pits remained- the damage was only slightly decreased.

•Direct stressing of wafers with $\sigma \sim$ 2Kpsi produced no etch pits after etch.

•SiO_2-formation: If H_2O from HPS penetrates Si-wafer regions (damage) of SiO_2 could form. To reveal these, a SiO_2 etch was used. No etching took place.

In a "companion" experiment free H_2O inside wafer after scrub was searched using IR-radiation. With known IR-absorption sensitivity, we found that if any water got inside the wafer, it must be less than 200 H_2O molecules per Si-cell square.

•If indeed the defects were crystalographic in origin high T anneal would decrease the damage. We indeed found etch pit density decreased by about a factor of 4 after a scrubbed wafer was annealed at 950°C for 30 min. Electrical

areas of processed wafers which have a thin oxide. Processed wafers had 224 def/cm^2 in the resistor areas. The greater sensitivity to defects in the resistor area could well be attributed to an imperfect latice in the areas which previously received an implant, therefore, on actual devices the thin oxide is not enough to protect the circuit from defects.

5. ORIGIN OF CRYSTALOGRAPHIC DEFECTS
Previous analysis showed that high pressure scrub (HPS), with water, often causes current leakage of pressure sensors due to P-N junction degradation. Both micro-defects (impurity related) and dislocations are possible candidates.

leakage test showed however, wide spread leakage over the wafer, after the anneal.

• Kinetic energy of an impinging H_2O molecule was calculated to be 2meV. This kinetic energy is insufficient to move a Si atom from an equilibrium site but is well within phonon energies of the Si crystal.

Analysis of Laue spots (X-rays) didn't show crystalographic defects however, due to insufficient resolution.

RESUME: We conclude from above tests that dynamic stress produced by water jet creates a crystalographic defect.

Theoretical model coming out of these tests is suggested: Crystalographic defects (probably dislocations) are formed after HPS. Since wafer's top surface is (100), the slip direction is [001] and, since this is also leaking direction, we conclude that the Burger's vector (b) is parallel to dislocation axis. This narrows down the dislocation type to the Screw Dislocation (SD).

The SD of the defect originates on wafer surface (N-Cap) passes through DZ of J_2 and probably reaches to the other side of the diaphragm h ~ 100μm.

We can now estimate total energy the SD contains

$$E_{SD} = \frac{Gb^2h}{4\pi} \log_e \frac{R}{r_o}$$

where r_o ~ 1nm, is SD core radius. By taking R ~ 30μm for outer circle radius (diaphragm radius) we get E_{SD} = 7aJ or 43.5eV/(at plane); for silicon Young modulus E the shear modulo G is G ~ E/3 = 5.3•10^{10}Pa for [100]-direction and b = .543μm. The total energy contained in a SD is
$$E_{SD} \simeq 8MeV$$
assuming SD straight, stretching from inside diaphragm surface to the outside one.

The important question now is if the HPS jet can produce this much energy. Since diaphragm strain is $\epsilon = \frac{\Delta l}{l} = \frac{p}{E}$ we have
ϵ = .44•10^{-6} using p and E numbers for HPS and Si already quoted. Since active volume of a diaphragm in
$$V = \frac{\pi}{4} D^2 h,$$
we have V = 1.1•10^{-11} m^3 with D .015mil (water jet cross section radius). The elastic energy below the jet is

$$E_{EL} = \frac{1}{2}\sigma \epsilon V = \frac{E}{2}\epsilon^2 V = 10^{10}eV$$

Clearly, the water jet produces macroscopically enough energy to generate 1250 dislocations on

10^{-3}cm^2; not all available energy is used for dislocation generation.

Finally, let us mention again that no clear identification of dislocations have been made. Other types of defects may be playing the key role here; idea of dislocations is attractive however, because once created it may split into two partials (Shockley) that would encircle a stacking fault. The latter were observed.

On the other hand, micro defects are, strictly speaking, surface defects; N-Cap thickness dependence of leakage (that was observed) would be in wrong direction when assuming them. Strongest evidence against dislocations playing the key role here is weak directional properties the etch pits reveal.

6. DEVICE CHANGES TO "HARDEN" JUNCTION
As previously mentioned, one of the primary delicacies of the sensor configuration is a dual layer junction structure to confine the resistor in an equapotential envelope. The envelope forms two junctions, one at 0.4 μm and one at 1.0μm. (See Figure 2.) The shallow nature of the top junction along with the relatively high n-type doping, as compared to the p-type resistor, make it very susceptible to leakage. The upper junction structure was removed to study the effects of the scrubber. Samples with only the deep (1.0μ) junction showed improved reverse breakdown characteristics (45v rather than 14.5 on standard structure) and did not have the leakage problem after scrub. Only 3/188 die degraded without the upper junction where 49/188 degraded on the dual junction structure. Since the equapotential envelope is critical for device performance, the upper junction was re-introduced but at a lower dose allowing the depletion region to extend all the way to the thermal oxide on the surface, as shown by the calculation and diagram, Figure 10.
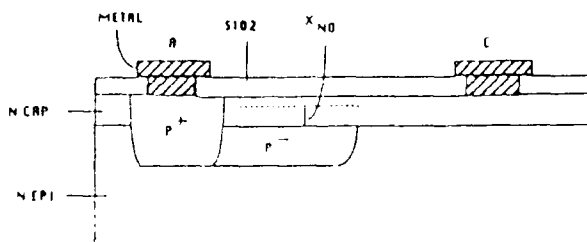

FIGURE 10. DEPLETION REGION IN N-CAP

Standard depletion width:[3]

$$X_{no} = \left\{ \frac{2\epsilon V_o}{q} \left[\frac{N_a}{N_d \ (N_a + N_d)} \right] \right\}^{1/2}$$

n-cap $= 0.1 N_a$

p resis $= N_a$

$X_{no} = 0.129 \mu m < 0.4 \mu$ junction depth

Reduced n-cap:
     n-cap $= 0.01 N_a$

p resis $= N_a$

$X_{no} = 0.428 \mu m > 0.4 \mu$ junction depth

The extension of the space charge region to the oxide surface severs the leakage path caused by a damaged junction. This was experimentally verified on a wafer which had only 10/188 die degrade where the dual junction structure had 45/188 degrade after the scrub.

CONCLUSION

To provide efficient conversion from pressure to electrical signal on a piezoresistive sensor, current leakage must be minimized. The creation of cats whiskers and modifications to the surface (N-Cap) junction are the primary tools to control the leakage levels in the front end. These modification also effect the sensitivity of the device to back end operations which can introduce defects into the resistor regions. An understanding of the back end operation's mechanisms creating defects allows one to control/eliminate the degradation to the sensor.

ACKNOWLEDGMENT

REFERENCES

[1] Ravi, K.V.,"Imperfections And Impurities In Semiconductor Silicon", John Wiley & Sons, New York 1981.
[2] Hull, D., "Introduction To Dislocations", Pergamon Press 1975, Oxford p.91
[3] Streetman, B., "Solid State Electronics Devices", Prentice Hall 1981

"The PVF2 Piezoelectric Polymer Shock Stress Sensor - Some Techniques for Application Under Field Test Conditions"
R. P. Reed and J. I. Greenwoll

The basic design and some fundamental characterisitics of PVF2 shock stress transducer elements were described by two papers at the 14th Transducer Workshop. Since that meeting, the sensor has become more readily available. It has been applied in many additional varied applications under severe laboratory and field test conditions and calibration has been extended to both lower and higher peak stresses over the range from 2 psi to more than 6 million psi (46 GPa).

The exceptional versatility and application range of this measuring element allow it to be used in diverse circumstances. Many of these present distinct sets of measurement problems. Successful measurement with PVF2 sensors in many practical situations requires that response of the entire measurement system be considered with the sensor being only one critical component involved in the measurement. This is particularly true of experiments where stress waves generated by explosion are to be measured under field test conditions. A hybrid combination of hardware and software tools must be applied in both prediction of the voltage waveform that must be recorded and also in the the reduction of that experimental voltage record to the desired accurate measure of applied transient stress.

Contrary to normal application of piezoelectric sensors as pressure sensors or accelerometers, the conditions of field use often require that the PVF2 stress transducer be applied in a manner that is in neither of the traditional ways: charge mode or current mode. Rather, application must often be in a well-defined intermediate mode.

This paper was unavailable for printing at press time.

THE PVF2 PIEZOELECTRIC POLYMER SHOCK STRESS SENSOR - SOME TECHNIQUES FOR APPLICATION UNDER FIELD TEST CONDITIONS

Comment: **Wayne Charlie (Colorado State University):** This sounds like an application where you can use fiberoptics to take your signal out.

A: **Ray Reed:** Well it is possible to use fiberoptics, and fiberoptics are coming into use but at some level you always have signal distortion. What you are saying is that you need higher bandwidth. It would be nice to have higher frequency recorders as well. This deals with a situation where you don't have access to those and demonstrates a very practical technique that works to get you out of a situation that you prefer not to be in. Peter Stein would tell you immediately that you always want to deal with systems that linearly scale and have adequate bandwidth and are not therefore frequency creative. Frequency creation in this situation simply means you have distorted the signal; it doesn't mean that you have lost the information but you do have to treat it properly. An essential to treating it properly is the proper characterization of that specific real situation as it exists in the field.

Q: **Pete Stein (Stein Engineering):** How sensitive is the process to the individual specific cable? Do you have to check each particular cable over several 100 or 1000 feet or can you determine for a particular catalog number of a cable, a procedure?

A: **Ray Reed:** Because cables get damaged in the field, the catalog specification is not adequate nor is the mathematical model of the cable. They are perfectly fine for prediction of the distorted wave form so that you can go ahead and signal condition a..d record. But, they are not adequate for unfolding accurately.

Comment: **Ron Tussing (NSWC):** I can further comment on that. We have our low-noise, low tribo-electric effect cable made for us, and it is available to other people too. Every batch we get is different and is quite a bit different, and is supposedly the same; but for instance, the capacitance per foot will vary between 30 to 40 picofarads and averages around 35. This is supposedly made for the Government through specification; buy if you want the cable, you buy it. you take it the way it comes, and so, we do different things, as Ray has said, but we would match each batch for each length of cable.

A: **Ray Reed:** Not only do cables vary from batch to batch but they vary from place to place. In field installations, people have frequently matched and put two or three cables in sequence. They have gone through breaks for gas blockings; and so, you always want to do the characterization, if for no other reason, to assure yourself that you have what you think. But if you are going to characterize it, it is absolutely mandatory that you do this sort of thing. With regard to Ron's comment--somebody said butterflies are free, charge is too. In a piezoelectric circuit, and particularly used open circuit, you will learn very quickly how much free charge there is around from piezoelectric sources and just hanging around from some change of temperature or a variety of things: and that's again, why we have always been driven in the field to use these gages in the current mode, although in theory, they can perfectly well be used in a charge mode. I

point out that we are using neither current nor charge mode. At the last meeting, I made the strong assertion that you must use them one way or the other, or don't know what you've got, and I promptly went off and did this which is neither fish nor fowl, it is somewhere in the middle. I point out, there are other applications to this technique. I give this paper in the context of the application of PVF2. The techniques are perfectly general when applied to any measurement system.

Q: **John Kalnowski (EG&G):** What type of cable do you use in the field?

A: **Ray Reed:** A variety of things. On the last field experience, we used RG22 which I preferred, because it is a balanced cable and avoids some noise problems. On the other hand, when you use it with physically available equipment; you have problems because that equipment is almost always single ended; and so, matching that cable to regular carters is a problem. Since then we're using combinations of cables ranging from, I think, an RG55, which is one I wasn't familiar with, RG213 going then to RG214 in one continuous run. And so, you have all of these things stacked together plus gaps in the system where you have to make the transition from one to the other.

Q: **John Kalnowski:** On your RG22 did you have to use a cable equalization?

A: **Ray Reed:** In this peculiar situation, you don't want to equalize because you're throwing away gain. We started that way, and it finally dawned on us, that the cable is partially integrating for us. If we just throw another little capacitor on there, we'd complete the integration, and we'd be half way home. All you've got to do then is complement that with this digital filter and proceed on your way. You have got high signal to noise and the data as well.

PIEZOELECTRIC POLYMER SHOCK GAUGE APPLICATIONS

L.M. Lee, D.V. Keller,
E.S. Gaffney, and D.A. Hyndman
Ktech Corporation
Albuquerque, NM

L.M. Moore
Sandia National Laboratories
Albuquerque, NM

F. Bauer
Institute Saint Louis
Saint Louis, France

ABSTRACT

Many investigators have contributed to development of piezoelectric polymer shock gauge during the last fifteen years, with the main emphasis being on polyvinylidene fluoride (PVDF). The PVDF shock gauge offers numerous advantages over currently available piezoelectrics (single crystals and ceramics). Specific advantages offered by the PVDF stress gauge include ruggedness, ability to make unobtrusive measurements in thin sections (10-25 microns), high time resolution, large stress range application, large charge output per unit stress, and enhanced adaptation to specific transducer designs. Early PVDF studies produced results that indicated material could not be fabricated reproducibly enough to be used as a shock transducer. Because a sensor that functions under shock loading is usually destroyed in use, these applications require a high degree of reproducibility in material constants. Recent studies of PVDF film by Bauer have shown that conventionally available piezoelectric films do not exhibit sufficient reproducibility for shock applications. However, PVDF film processed to precise specifications and poled with the Bauer method achieves the desired level of reproducibility. During the last three years, a standardized transducer that can respond to shock loading over a large stress range (10^{-1} to 10^{5} [?]) has been demonstrated, with the polymer material source and operational treatment based on the work by Bauer. Shock attenuation data have shown that standardized gauge can be produced at different facilities utilizing the same material and poling process. The purpose of this paper is to describe applications of the Bauer PVDF stress gauge in shock loading applications including gas gun impact, pulsed ion beam, pulsed laser, explosive and gas shock tube loading conditions. In addition to experiments conducted at atmospheric and reduced pressures, the standardized Bauer high stress gauge has been successfully used in underwater shock measurement. The wide range of applicability of the gauge is limited primarily by the requirement for calibration. However, certain fundamental procedures must be followed in respect of gauge fabrication and mounting if consistently detailed results in both of these areas are presented in this following paper.

INTRODUCTION

It has been known for many years that appropriately treated polyvinylidene fluoride (PVDF) exhibits piezoelectric properties suitable for a wide variety of applications. Some of these applications require a high degree of reproducibility in material constants because a sensor which functions under shock-compression loading is destroyed in use. Various studies of PVDF film by Bauer [1-4] have shown that conventionally available piezoelectric films do not exhibit sufficient reproducibility for shock applications. However, PVDF film processed to exacting specifications and poled with the Bauer method achieves the desired level of reproducibility.

A cooperative effort has been pursued between Institute Saint Louis (ISL) and Sandia National Laboratories, Albuquerque (SNLA) to provide a stress gauge for widespread use in shock measurements. SNLA has been receiving technical support from Ktech Corporation to develop the Bauer poling process in the United States, while ISL has been working with Metravib Corporation in France to develop a commercial source for the standardized PVDF gauges. Initial efforts in the cooperative program, which was started in 1982, showed agreement of independent shock wave measurements made at the two laboratories on PVDF gauges fabricated by ISL [5]. The initial work was in the stress range from 1.0 to 2.2 GPa. Later work involved setting up specific material film specifications and the Bauer poling process in the United States and the Metravib Laboratory [6]. Further work showed agreement over a larger stress range. An exacting, controlled impact technique for evaluating PVDF stress gauges has been developed [7].

The ISL laboratory was the only source for PVDF gauges produced by the Bauer method until recently. As a result of the cooperative effort between our laboratories, gauge fabrication facilities have been developed in both the United States and France that can produce standardized PVDF shock compression gauges based on the patented Bauer process. The essential ingredients of the standardized gauge are a uniform high quality biaxially stretched PVDF film and the

Bauer electrical poling process. The Gauge Fabrication section of this paper reports on our gauge standardization effort.

The purpose of this paper is to demonstrate the use of the Bauer PVDF gauge in different shock loading-unloading applications. Applications described include gauges loaded in gas gun, explosive, pulsed ion beam, pulsed laser and gas shock tube experiments. Gas gun applications have achieved stresses up to 48 GPa, while gas shock tube applications have achieved stresses as low as 10 KPa.

GAUGE FABRICATION

Material

The PVDF film used in the United States and France was extruded and biaxially stretched by Rhone Poulenc films in France from polymer pellets obtained from kurena, Japan. The special film has a nominal thickness of 26 μm. Enough of the PVDF film has been procured for many years of gauge development and applications. This particular film was chosen because of the documented successful poling by Bauer of similar PVDF batches, where shock wave measurements on standardized gauges made from different PVDF lots have shown close agreement. Other PVDF films are available, but they are different from the Rhone Poulenc material and none have been subjected to such extensive testing as this material. An essential part of any shock transducer development project is a material with well defined characteristics to ensure that proper processing can achieve the required end result.

GAUGE ELECTRODING

The standardized stress gauge electroding process was developed after evaluating a number of metallization techniques and mask designs. Magnetron sputtering of gold or aluminum over platinum produced electrodes with very good adhesion. No metal was removed using the scotch-tape peel test and there was no evidence of film overheating during electroding. Other sputtering and vapor deposition techniques have shown that overheating the film results in detrimental effects on the gauge electrical properties. The electrode and masking used to construct the standard gauge is shown in Figure 1. The sensor area, located where the two electrodes overlap is clearly the most important region of the gauge. It is essential to have sharp edge definition for the total electroded area because accurate sensor area measurement is required for accurate shock wave measurements. Masking techniques have been developed which produce the required sharp edge definition at 100x magnification and also reduce the tendency of the PVDF to wrinkle during deposition. [8].

POLING PROCESS

The purpose of the poling process is to induce reproducible piezoelectric polarization in the PVDF and to remove any trapped space charge. Many static, field discharge, and cyclic methods have
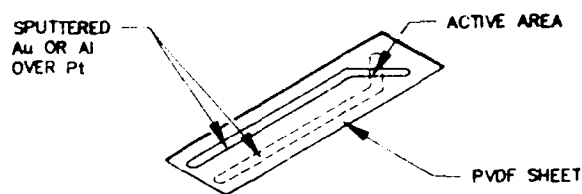
Figure 1. Standardized PVDF Shock Gauge Configuration.

been tried over the past few years, but only the Bauer process with a specific cyclic poling schedule has been proven by shock-compression tests to condition the PVDF for accurate reproducible output. The poling process incorporates the essential features as described in Bauer's U.S. patent and in the open literature [9].

The Bauer poling procedure is specifically tailored to create a transducing element that produces charge under stress only, from the piezoelectric effect and under temperature change only, from the pyroelectric effect. The process aligns crystallites, orients dipoles, and migrates ions and space charges out of the film homogeneously throughout the poled region.

A Bauer process poling facility has been developed in Albuquerque, New Mexico, and has been shown to produce routinely high quality gauge elements with high polarization. The remanent polarization of PVDF shock gauges produced with the United States system is the same as produced in France at Isl and Metravib, nominally 9.2 + 0.2 μC cm².

The joint program of PVDF gauge development has resulted in a set of quantitative specifications describing the standardized stress gauge. Specifications relative to material, electroding and poling parameters that must be achieved to produce a repeatable, high fidelity, shock wave sensor are shown in Table 1. The normal hysteresis loop listed in Table 1 is shown in Figure 3 for gauges produced at the three different facilities. The excellent agreement in remanent polarization and hysteresis loop characteristics shows the reproducibility of PVDF gauges made to exacting standards.

Table 1. Standardized PVDF Gauge Specifications

Material	Biaxial stretched 26 μm Rhone Poulenc
Electrode	Sputtered 2000 Å gold over 500 Å platinum
Poling	Is used less strip sensitive area. Remanent polarization 9.2 + 0.2 μC cm². Normal hysteresis loop.
Physical-Geometric	Quantitative definition of all parameters

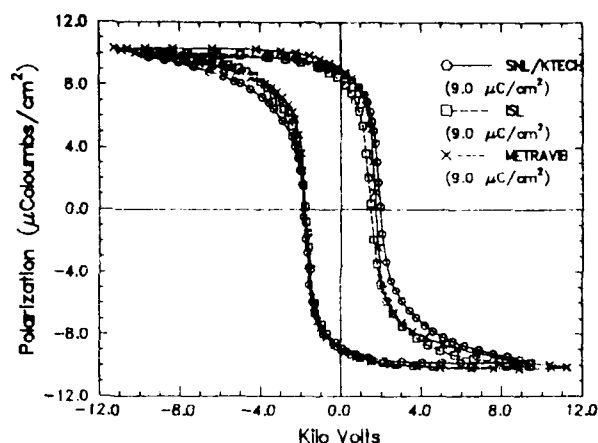Figure 2. Hysteresis Loop.

The electrical currents produced upon impact from electrode areas of about 0.1 cm² range from about 1 to 30 amperes in the most recent experiments. Current-viewing resistors with resistances between 0.025 and 0.2 ohm are connected to the gauge electrodes to reduce the signal levels to acceptable values for the digitizers. Further signal level reduction, if desired, is accomplished with microwave dividers placed at the inputs to the digitizers.
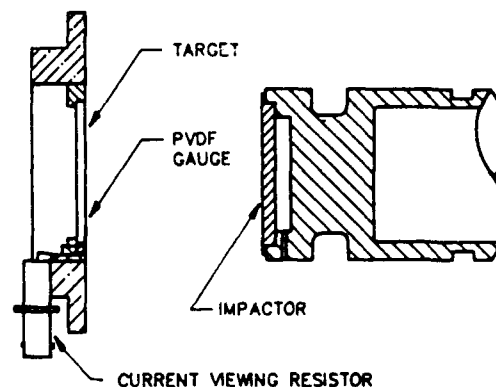
TARGET ASSEMBLY   PROJECTILE

Figure 3. Impact Loading Configuration for Controlled Shock Loading of Standardized PVDF Gauges.

SHOCK MEASUREMENTS

Gas Gun Methods

A standard impact loading experiment for PVDF has been developed for the SNLA 25-meter compressed gas gun which has been used for many previous studies involving precisely controlled impact loading, including quartz and lithium niobate piezoelectric gauge work. The gauge element is placed directly on the impact face of a target of either kel-F, Z-cut quartz, Z-cut sapphire or tungsten carbide as shown in Figure 3. The impactor is the same material as the target; hence, the equilibrium particle velocity is known to the precision of the impact velocity measurement, 0.1 percent. The gauge elements are subjected to unusually well behaved shock and release stress pulses because the Z-cut quartz and sapphire target and impactor materials remain elastic up to about 13 and 20 GPa, respectively. The response to release waves can be carefully studied by the use of thin impactors in this arrangement. Tungsten carbide is used for stress greater than 20 GPa with 25 μm thick FEP Teflon film on either side of the gauge to provide electrical insulation. Kel-F is used because of its lower mechanical impedance for stress less than 3 GPa [10].

Various electronic recording arrangements have been investigated. High speed digitizers provide the best records for ease in data reduction. A high digitizing rate is required to track the detail in the PVDF response because of the very fast loading achieved. LeCroy 6880 digitizers which sample at a rate of 0.742 ns per point and have a recording window of 7.4 μs were used. The experiment used two separate low-loss coaxial cables to provide recording of the signals at different sensitivities rather than a single cable with a parallel connection to two digitizers.

Although the program is ongoing, the results to date over a wide range of parameters relative to gauge area and shock stress are shown in Table 2. Of primary importance in Table 2 is the fact that the same remanent polarization, which has been shown in previous work to be critical to producing a repeatable shock transducer, has been achieved in the three different laboratories using essentially the same gauge fabrication processes. Also shown in Table 2 is a wide range of shock-compression loading to which the gauges have been exposed. This dynamic range is an order of magnitude larger than any previously available piezoelectric shock gauge.

A comparison of results from different gauges shock loaded using the controlled impact technique is shown in Figure 4 [11]. The shock compression data shown in Figure 4 were generated at SNLA ("KTECH DATA" and "SANDIA DATA") and ISL. The results indicate minimal scatter, with similar responses being obtained for the gauges produced in France and the United States. Limited data of this type have been obtained previously; however, in the current study the applicable stress gauge range was expanded up to 46 GPa where the gauge is still functioning properly. The ability to produce repeatable PVDF shock transducers in the different laboratories to exacting specifications now provides the general availability of shock transducers for reliable measurement application.

122

Table 2. PVDF Gauge Parameters

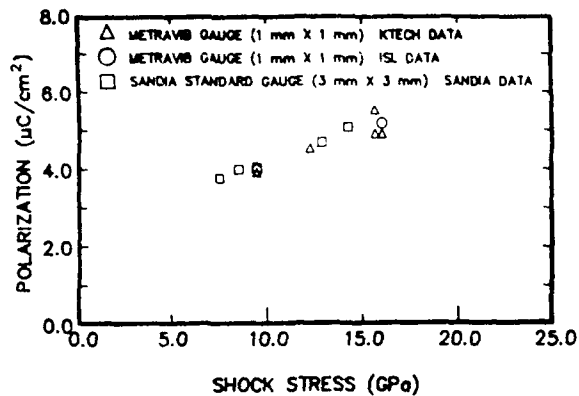| Gauge Fabrication	Gauge Area (cm²)	Remanent Polarization (μC/cm²)	Controlled Shock Loading (GPa)
ISL	0.01 1 mm x 1 mm	9.1	7 – 15
SNLA/Ktech	0.09 3 mm x 3 mm	9.1	0.3 – 46
Metravib	0.01 1 mm x 1 mm	9.1	0.7 – 35

Figure 5. PVDF Gauge and Target Configuration.

Figure 4. PVDF Gauge Charge as a Function of Shock Stress. (preliminary data, detailed data analysis in process).

Some gauges were studied with the negative electrode on the impact surface to investigate the influence of gauge electrical orientation on output current. Data reported here were obtained with the standard orientation used by Bauer in which the positive electrode is placed on the impact surface. It appears there is an electrical polarity effect which has not yet been fully evaluated.

Pulsed Laser and Ion Beam Methods

Standardized PVDF gauges have been utilized in pulsed laser experiments which allowed stress measurements to be made within 30 μm of the deposition region which flows ranging to 10^8 W/cm². A typical PVDF gauge and target configuration for pulsed laser and ion beam experiments is shown in Figure 5. Two PVDF records from these experiments are shown in Figure 6. The large signal to noise ratio combined with the ability to make small sensor areas in the range of 0.01 cm² and the inherent flexibility of the PVDF shock sensor allow data to be obtained in an extremely harsh electrical environment, which further illustrates the reliability and utility of the PVDF gauge.

Figure 6. PVDF Stress Gauge Data From Pulsed Laser Experiments (SPRITE).

Representative data from a pulsed ion beam experiment are shown in figure 7. Again the desirable large signal to noise ratio resulting from the PVDF charge output characteristic is evident. Unambiguous (amplitude and recording time) shock wave measurements in these environments could not be made without the PVDF output due to the large, electrically noisy, pulsed power accelerators used to generate ion and photon fluxes.

Gas Shock Tube Methods

PVDF transducers have seen successful application for measuring low amplitude shock in gas (air) shock tubes. The gauging requirements were easily met due to the versatility of PVDF, permitting air shock measurements with a time resolution previously not obtainable. Experimentation at the Ktech shock tube facility has established the usefulness of PVDF as an air shock transducer. PVDF transducers were bonded onto a shock tube insert as shown in Figure 8. A reference gauge (PCB model 102A02, a quartz element gauge with a resonant frequency of 275 kHz, and a sensitivity of about 7.5 mv/Pa over a range from 0 to 800 kPa) was used to determine equilibrium pressure after the initial air shock reflected from the shock tube insert.

Air shocks were initiated in the tube producing reflected pressures between 8 and 800 kPa. The signal from the PVDF was recorded by a LeCroy 9400A digital oscilloscope. The PVDF output was recorded in the charge mode, with the signal sent directly to the scope input ($10^6 \Omega$) over 2 meters of cable [12]. A typical data record is shown in figure 9, which shows the excellent time resolution that can be obtained with these transducers. The data obtained during this series of shock tube experiments is shown in Figure 10, suggesting a uniaxial strain calibration factor of

$$d_{ux} = 15.7 \pm 0.7 \ pC/N$$

for the low-overpressure air shock response of PVDF. A linear response to air shock is expected up to pressures of approximately 100 MPa (1 Kbar).

Air shock measurements with PVDF were complicated by thermal effects. The pyroelectric response of PVDF is quite large, with the charge density per degree kelvin being equivalent to pressures of about 10 kPa. Even at the lowest pressures used, the temperature in the air shock was a few degrees above ambient. A substantial effect was observed when the heat from the air shock reached the active area of the transducer. The characteristic time for diffusion of heat through the sputtered leads is on the order of 1 μs, correlating to the signal degradation seen for an unprotected transducer. A thin film of castor oil was placed over the active area of the transducer in order to slow the diffusion of heat through the electrodes. This expedient solution removed the thermal effects during the controlled shock tube experimentation. In field applications, thermal effects could be best controlled by protecting the PVDF transducer with a thin film of Teflon or other suitable covering.
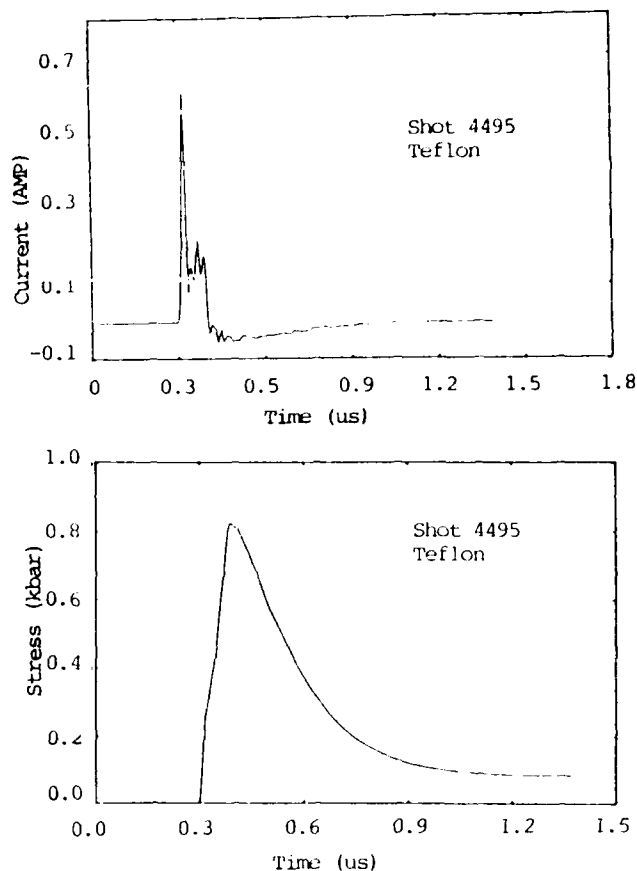

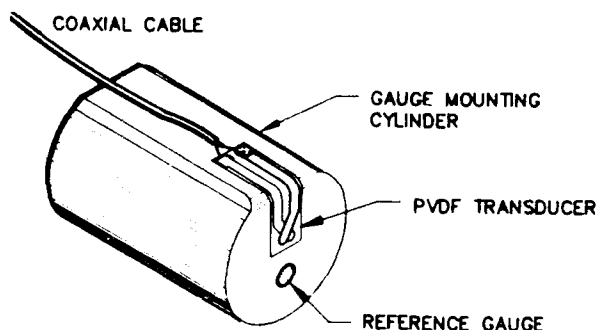Figure 7. PVDF Stress Gauge Data From Pulsed Ion Beam Experiments.

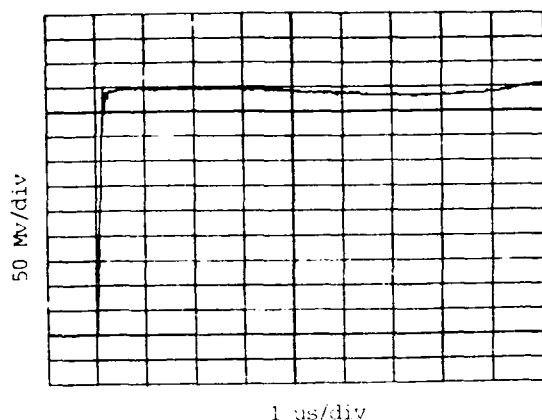Figure 8. Mounting Configuration for PVDF Air Shock Experimentation.

124

Figure 9. Typical PVDF Air Shock Response.

Figure 10. Low-Overpressure Air Shock Data.

Although this air shock experimentation was conducted in a small (76 mm) compressed air shock tube, the feasibility of PVDF air shock measurements in other experimental environments is amply demonstrated. This gauging technique is immediately applicable to explosively driven shock tubes, large and small high-explosive simulations, and explosive ordinance experimentation.

Underwater Shock Methods

Recent experimentation at Sandia National Laboratories and Ktech has demonstrated the feasibility of underwater shock measurements with PVDF. Two styles of PVDF underwater shock gauges were fielded to record shocks 10 cm from small explosive detonators (RP-1). The first style gauge was very similar to the air shock arrangement discussed above, consisting of a 1 mm² PVDF transducer bonded to a poly-carbonate plug. The transducer was covered with a thin Teflon film and suspended into the test chamber on a brass rod. This type gauge was intended to measure the reflection or stagnation of the water shock on the plug face. The second style water shock gauge consisted of a 1 mm² PVDF transducer mounted on the end of a thin rod, as depicted in Figure 11. This probe gauge was intended for free field water shock measurements. Both gauges were recorded in the charge mode over approximately 60 feet of 50 Ω cable. A typical data trace for each gauge is shown in Figure 12.

These records show the rapid and robust PVDF response to water shock. The difference in output is due to the larger active area used in the probe gauge and slight differences in placement with respect to the detonation. The short period (150 ns) noise seen in both records was correlated to ringing in the cables. Although this is preliminary data, and exact calibration of PVDF response to water shock requires further effort, the ability to measure shock in fluids is clearly demonstrated.
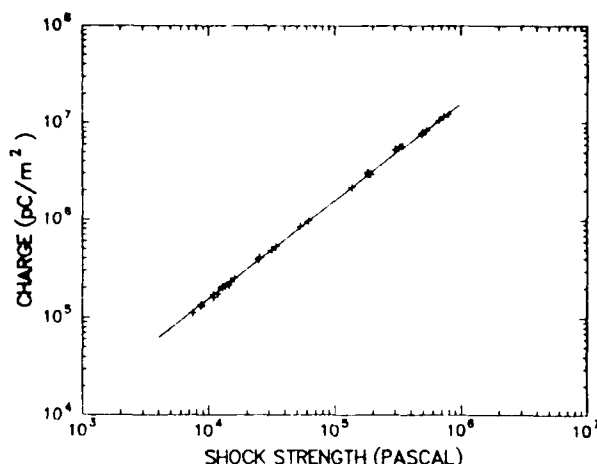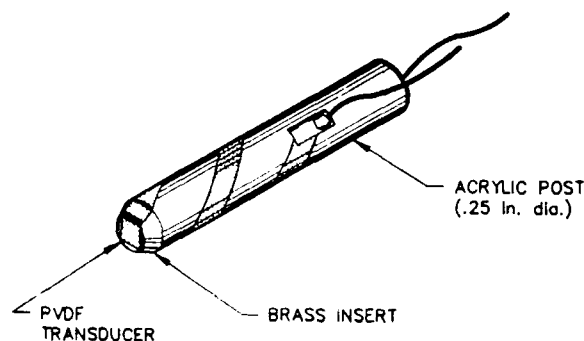
Figure 11. Probe Type Water Shock Gauge.
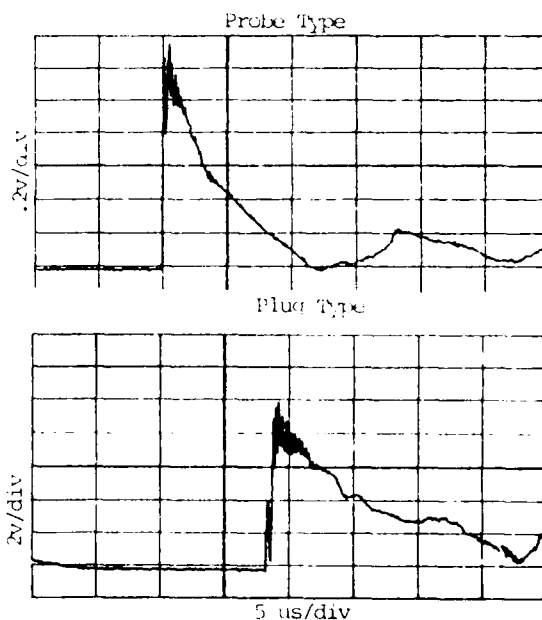
Figure 12. Typical Data From PVDF Water Shock Gauges.

125

SUMMARY

PVDF has many applications in shock measurements. Recent advances in stretching and poling techniques have resulted in a reproducible shock transducer which can respond to fast-rising (ns) shock waves. Attention to quality control requirements of production and details of calibration tests leads to identical response for gauges produced at separate facilities in France and the United States. These transducers have been used at stresses as high as 40 GPa. Lower stress calibration (10 KPa) of similar transducers using a gas shock tube have also been reported. The wide range of PVDF gauge applicability is limited primarily by the experimentalist's imagination.

REFERENCES

(1) Bauer, F., "Behavior of Ferroelectric Ceramics and PVF$_2$ Polymers Under Shock Loading," Shock Waves in Condensed Matter - 1981, eds. W.J. Nellis, L. Seaman, R.A. Graham, Amer. Inst. Phy., 1982, p. 251.

(2) Bauer, F. "Piezoelectric and Electric Properties of PVF$_2$ Polymers Under Shock Wave Action: Application to Shock Transducers," Shock Waves in Condensed Matter - 1983, eds. J.R. Asay, R.A. Graham, G.K. Straub, North Holland, 1984, p. 225.

(3) Bauer, F., "PVF$_2$ Polymers: Ferroelectric Polarization and Piezoelectric Properties Under Dynamic Pressure and Shock Wave Action," Ferroelectrics, Vol. 49, 1983, p. 231.

(4) Bauer, F., "Properties and High Pressure Shock loading Response of Poled Ferroelectric PVF$_2$ Polymer Gauges," Techniques and Theory of Stress Measurements for Shock Wave Applications, eds. R.B. Stout, F.R. Norwood, M.E. Fourney, Amer. Soc. Mech. Eng., 1987, pp. 19-28.

(5) Lee, L.M., W.D. Williams, R.A. Graham, and F. Bauer, "Studies of the Bauer Piezoelectric Polymer Gauge (PVF$_2$) Under Impact Loading," Shock Waves in Condensed Matter, Y.M. Gupta, ed., Plenum Press, New York, 1986, p. 497.

(6) Engelson, D.J., L.M. Lee, D.W. Gilbert, W.R. Conley, R.A. Graham, R.P. Reed, and F. Bauer, "Fabrication of Standardized Piezoelectric Polymer Shock Gauges by the Bauer Method," Shock Waves in Condensed Matter - 1987, Elsevier Science Publishers, B.V., 1988, p. 619.

(7) Graham, R.A., L.M. Lee and F. Bauer, "Response of Bauer Piezoelectric Polymer Stress Gauges (PVDF) to Shock Loading," Shock Waves in Condensed Matter - 1987, Elsevier Science Publishers, B.V., 1988, p. 619.

(8) Reed, R.P., "Recent Developments in Piezoelectric Polymer Stress Gauges," Proceedings The Range Commanders Council, Instrumentation/Transducer Committee, 14th Transducer Workshop, ed S.F. Kuehn, Colorado Springs, CO, 16-19 June 1987.

(9) Bauer, F., "Method and Device for Polarizing Ferroelectric Materials," U.S. Patent # 4,611,260, 9 September 1986.

(10) LASL Shock Hugoniot Data, Stanley P. Marsh ed., University of California Press, Berkeley, CA, 1979.

(11) Lee, L.M., J.P. Berhault, J.P. Chambard and F. Bauer, "PVDF Applications in Shock and Vibration Measurements and Control," 39th ARA Meeting, Albuquerque, NM, 10-13 October 1988.

(12) Reed, R.P., J.I. Greenwoll, "The PVDF Piezoelectric Polymer Shock Stress Sensor: Signal Conditioning and Analysis for Field Test Application," SAND88-2907-UC-37, May 1989.

PIEZOELECTRIC POLYMER SHOCK GAUGE APPLICATIONS

Q: **Steve Baker (Oakridge National Laboratory):** I noticed that the rise time is very fast on this device. What is the frequency band width?

A: **Larry Lee:** The gauge is responding to the stress difference between the two faces of the transducer, if it's properly bonded and properly fabricated into a mechanical matching backing. It has a transient time at about four nanoseconds. So consequently, you're usually limited by the recording device.

Q: **Steve Baker:** This is flip side to what you're doing. You're measuring very high pressure levels, large stress. What about on the other end? Could you use it in the very low pressure end since it has more gain than other types of piezoelectrics?

A: **Larry Lee:** What do you mean by low pressure?

Q: **Steve Baker:** Down to a few psi or lower.

A: **Larry Lee:** The lower pressure data that I showed down to 10^3 and 10^4 pascals, I think, one psi is 7×10^3 pascals. So those data were taken down to a fraction of a psi.

Q: **Pat Walter (Sandia Labs):** On the pressure time, the shock tube data, you didn't specifically say it, but I just inferred from your preamble that the backup material to your gauge in that was teflon?

A: **Larry Lee:** That was actually plexiglas, and when we look at the shock response down at very low pressures the teflon, the plexiglas, the Kel F; there are differences but they are not as noticeable as the chart I showed, which went up to a 100 kilobites.

Q: **Pat Walter:** You showed some at least one piezoelectric constant up there. What do they know about the other piezoelectric constants? Like the shear constants D13.

A: **Larry Lee:** Not near enough, everything I've talked about has been in a condition of one dimensional strain shock loading. When we want to record the milliseconds, and we want to use this gauge in other arenas, if you will, there has to be work done in that area. One piece of work that's been done now, is using the PVDF in a spilt Hopkinson bar configuration, where it was between steel bars. The only good news out of that is the fact that the gauge behaved in basically the same manner. The output was shifted, not shifted markedly so you were getting more output, because we think you're getting contributions from the others.

Comment: **Pat Walter:** The reason I asked about the other constants and just concluding the discussion, if you ignore the high-stress application you might infer that the material is not particularly exciting for one reason, it just has a large pyro-electric output so you have a lot of thermal-drift associated with it. But in Anthony's talk ("Built-in Mechanical Filter in a Shock Accelerometer") he eluded to the problem of zero shift, which you always get in fero-electric

127

ceramics at high levels. Just because you get some misorientation of the dipoles since that material seems to be attuned to working at the high-stress level that might be a candidate material for pyro-electric type shock accelerometers.

A: **Larry Lee:** Very well could be.

Comment: **Ray Reed (Sandia National Labs):** Larry I'd like to make some comments to what you've just said. First with regard to the band width, this group customarily thinks in terms of bandwidth other than being a shock reverberation, you do not. The gauge has a peculiar characteristic that probably most of you are not accustomed to thinking in terms of. Namely that when you're interested in looking at very short duration, fast rise shocks, the gauge response in one manner, it responds in the fashion that Larry described as looking at the stress difference between opposite faces. So on each reverberation it's behaving as a thick quartz gauge. Through that process depending on the nature of loading, you ring up to equilibrium state very quickly over about ten cycles. So in about 15 nanoseconds you've rung up to the peak amplitude. So the inverse of that you might think of as the bandwidth. It is responding in like a 10^9 hertz. Second comment, was in regard to Pat's question regarding the transverse coefficients, while neither of us said so, one of the favorable characteristics of the gauge, in a sense, is that it does have a hydrostatic response, which means that the normal directional loading is not completely compensated for by transverse loading. The D31 coefficient that you asked about Pat is not a shear coefficient, it's a transverse coefficient and both 31 and 32 are not zero but they're not at all well known for this particular material and we have work in process on that. But with regard to your question about shear response, fortunately, this material does not have a shear response. That is one of the coefficients that is null in the sensitivity matrix. Beyond that—the comment with regard to the pyro-electric response is an open question right now. This material is extremely pyro-electrically sensitive, it's a better temperature sensor than it is a stress sensor in fact. And so, there is a question that we're trying to deal with is, "What is the interaction?" In the paper that I presented here last time, I made the comment because of the way those coefficients interact—it is quite possible that what we're seeing as a stress calibration is in fact a combination of stress loading and shock heating. Because of the way the experiments have been done to this point, it does not allow you to separate those two effects. I believe, Larry, you've had a number of results or at least a few where not only have you been able to track the rise time but also the release path all the way back to the base line. And that's the indication that at least in those particular experiments that we have at very high stress. The heating was not a problem, because that would have remained while the stress vanished.

Comment: **Larry Lee:** We would expect it not to begin to come back to the baseline if the heating was having the kind of effects we typically think of.

"Selected Time Histories and Power Spectral Densities of Environmental Data Taken on the Smart Radar at the Army Proving Grounds Yuma, Arizona During March 1988"
Wesley Paulson

Twenty-six shots were fired during the test of the SMART RADAR (4 calibration and 22 evaluation). Immediately after each shot, the data were examined and were found to be of good quality. This "near real time" examination also showed a general increase in the various responses (pressure, acceleration and strain) as the test progressed (as the SMART RADAR was moved closer to the gun). Some differences were seen between those tests where the radar was facing the gun and those tests where the radar was orthoginal to the gun. These differences seemed most pronounced in the case of the strain data.

SESSION 3

TUTORIALS

GROUNDING & SHIELDING

FOR

INSTRUMENTATION

SYSTEMS

GORDON DEAN
PACIFIC INSTRUMENTS, INC.
215 MASON CIRCLE
CONCORD, CA 94520
(415) 827-9010

131

GROUNDING & SHIELDING

DIRECT EFFECT-ACCURACY/PERFORMANCE

EQUIPMENT & FACILITY LIMITATIONS

UNDERSTAND & VISUALIZE

PROBLEMS ARE "MYSTERIOUS"

INSTRUMENTATION SYSTEM

MEASURE LOW-LEVEL SIGNALS

REJECT NOISE-COMMON MODE

TRANSITION GROUND ENVIRONMENT
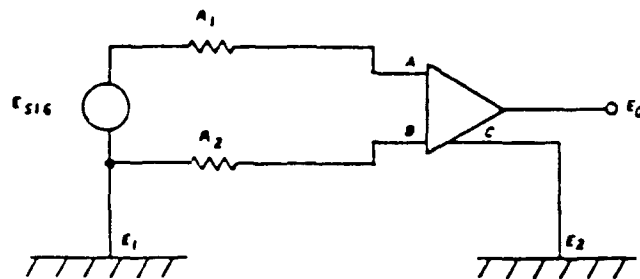
FIGURE 1 DIFFERENTIAL INPUT
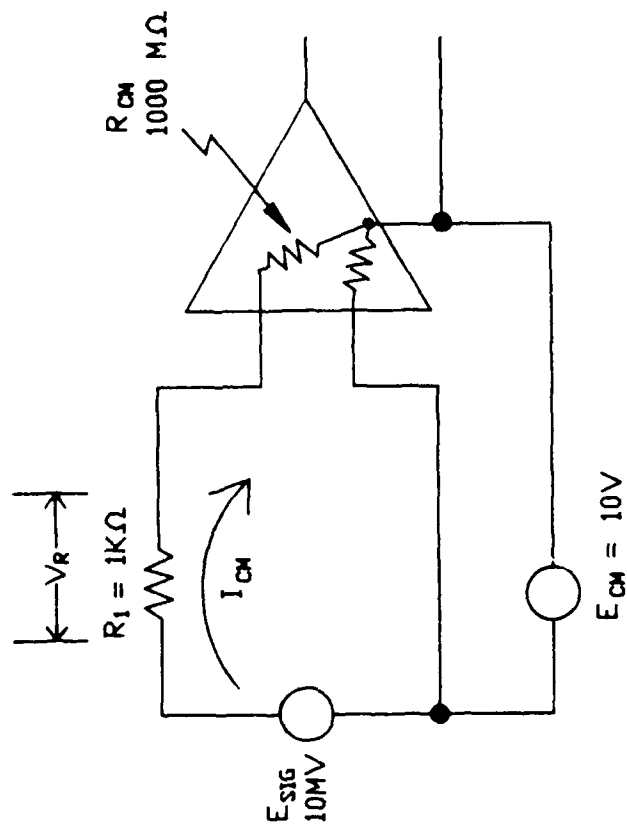
$$I_{CM} = \frac{E_{CM}}{R_{CM}} = \frac{10}{1000 \text{ M OHMS}}$$

$$= 10 \times 10^{-9} \text{ A}$$

$$V_R = I_{CM} \times R_1$$

$$= 10 \times 10^{-9} \text{ A} \times 1000 \text{ OHMS}$$

$$= 10 \times 10^{-6}$$

$$= 10 \ \mu V$$

$$ERROR = \frac{10 \ \mu V}{10 MV} \times 100 = 0.1\%$$

FIGURE 3 DIRECT COUPLED - 10 VOLT

FIGURE 4 DIRECT COUPLED - 300 VOLT

134
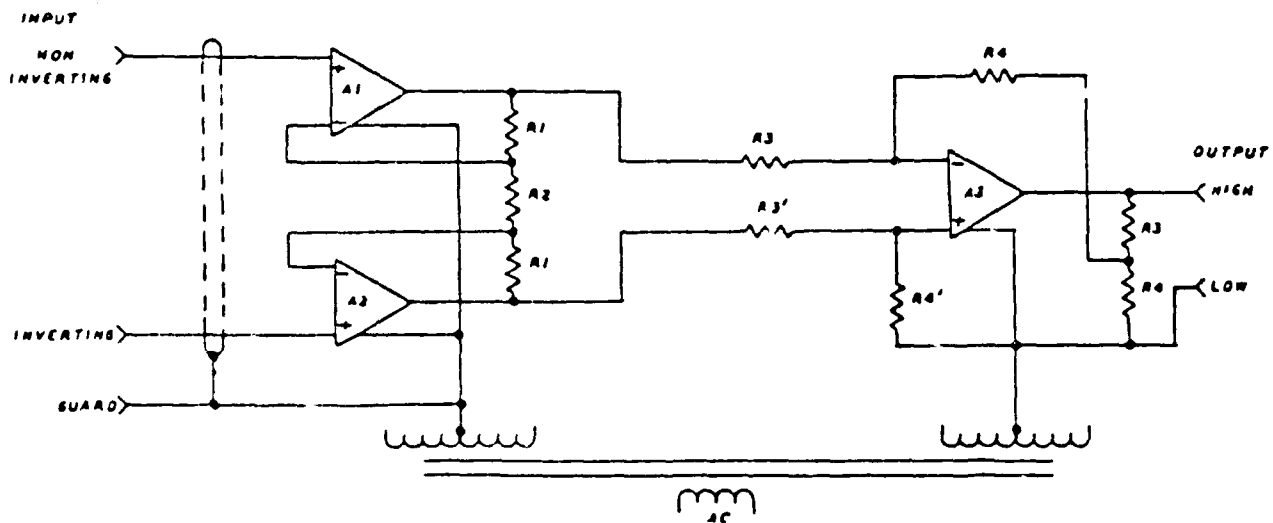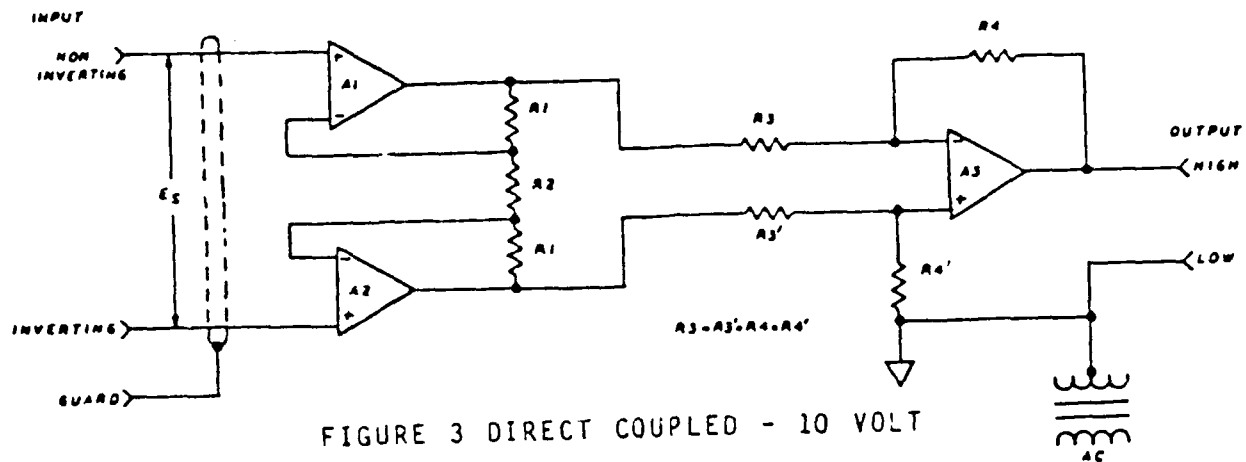
INPUT CABLE

PHYSICAL CONSTRAINTS

ELECTROSTATIC SHIELDING

    A) MYLAR/FOIL

    B) BRAID

ELECTROMAGNETIC PICKUP

    A) MINIMUM LOOP AREA

    B) MAGNETIC SHIELDING

    C) INTER-8-WEAVE CABLE

BEST RESULTS

TWISTED PAIR

MINIMUM LOOP AREA

FOIL SHIELD-HIGH COVERAGE

CONTINUOUS SHIELD THROUGH INTERFACES

AVOID HIGH MAGNETIC FIELDS

GUARD SHIELD RULE

SIGNAL CONDUCTORS & ELEMENTS MUST BE
ENCLOSED IN AN ELECTROSTATIC SHIELD
& NOT CONDUCT ANY SHIELD, GROUND OR
OTHER NON-SIGNAL CURRENTS.
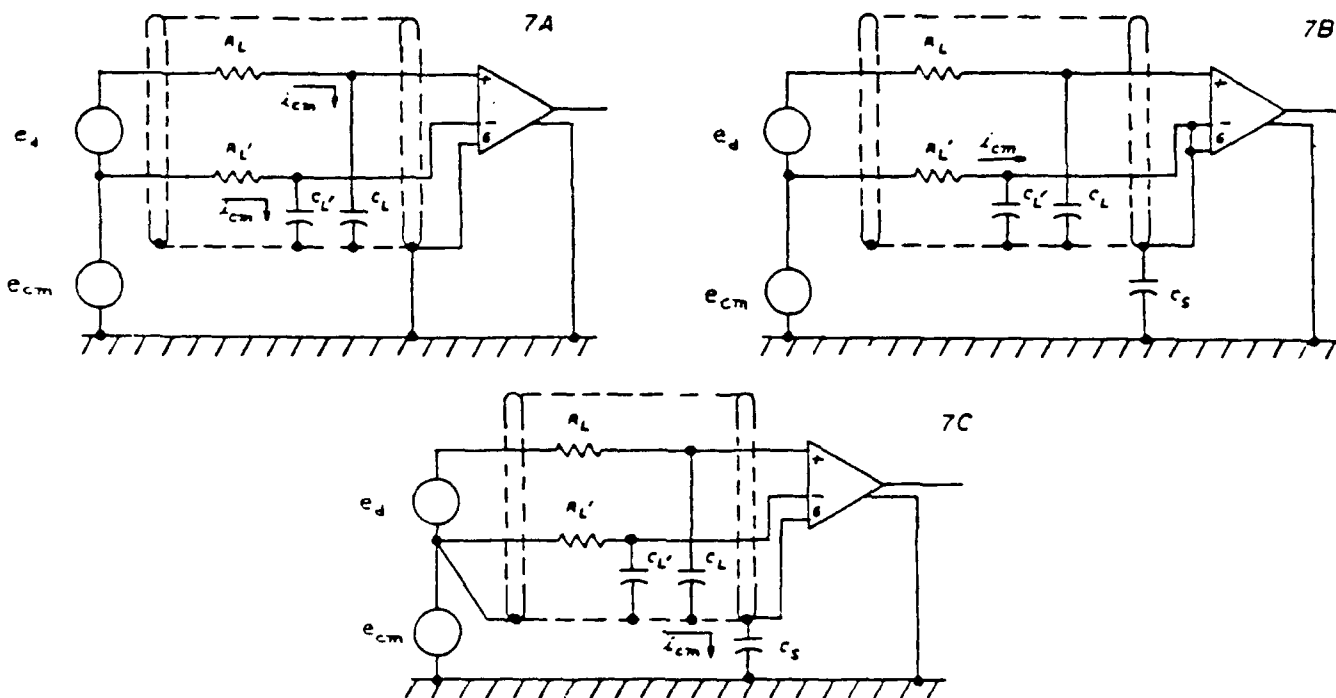
FIGURE 7   INPUT (GUARD) SHIELD

$R_L = 350$ OHMS

$R_L' = 0$

$C_{(L)} = 25$ PF/FOOT

CABLE LENGTH = 1000 FEET

$E_{CM} = 2V$ P/P @ 60HZ

$$I_{CM} = \frac{E_{CM}}{1/2\pi FC_L}$$

$$= \frac{2}{1/2 \times \pi \times 60 \times 25pf \times 1000}$$

$$= 18.8uA$$

ERROR $= 18.8uA \times 350$ OHMS

$= 6.6MV$

138

COMMON MODE SIGNALS

DC TO RF-POWER FREQUENCY

MILLIVOLTS TO 1000 VOLTS

TRANSIENT
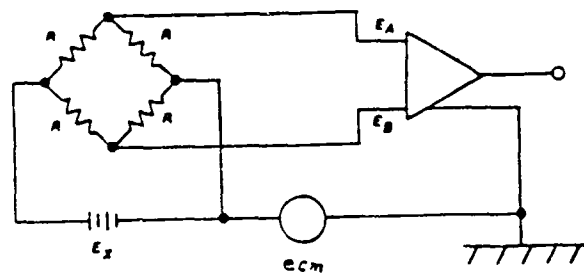
$$\frac{E_A + E_B}{2} = e_{cm} + \frac{E_x}{2}$$

FIGURE 9 BRIDGE COMMON MODE
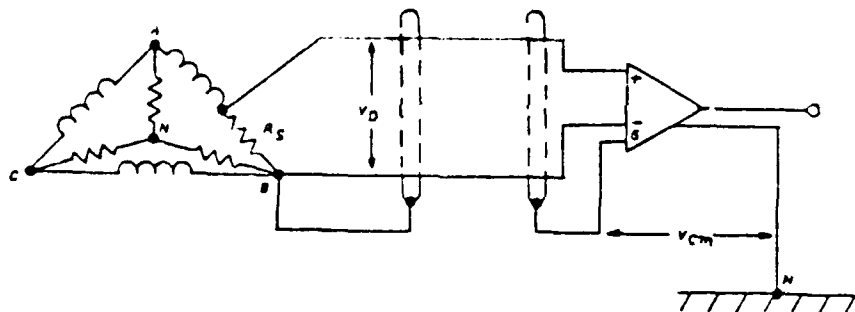
FIGURE 16 CURRENT SHUNT IN DELTA CONNECTED LOAD

SOURCE CURRENT

GENERATES COMMON MODE VOLTAGES

REQUIRES OHMIC RETURN TO OUTPUT COMMON

RETURN PROVIDED THROUGH GUARD
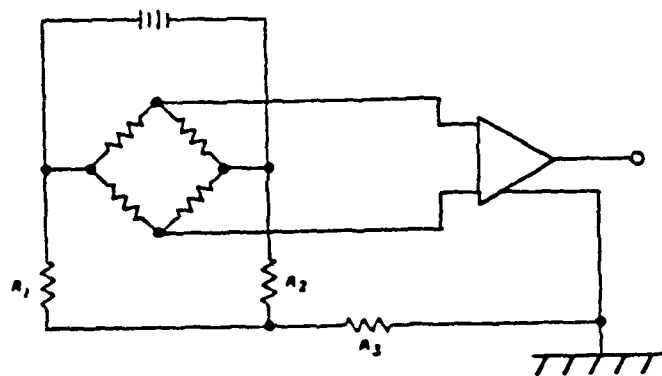
FIGURE 11   WAGNER GROUND - BRIDGE
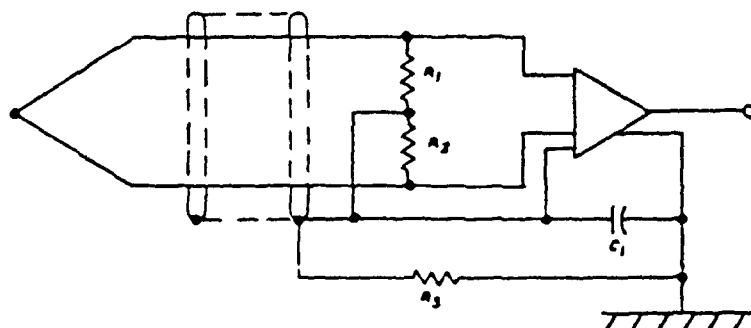
FIGURE 12   WAGNER GROUND - THERMOCOUPLE
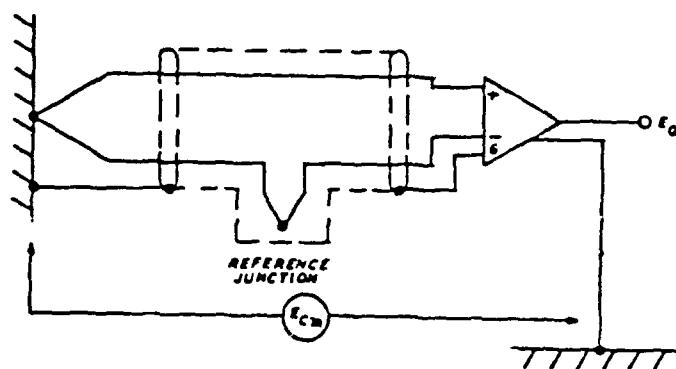
FIGURE 13 BONDED THERMOCOUPLE
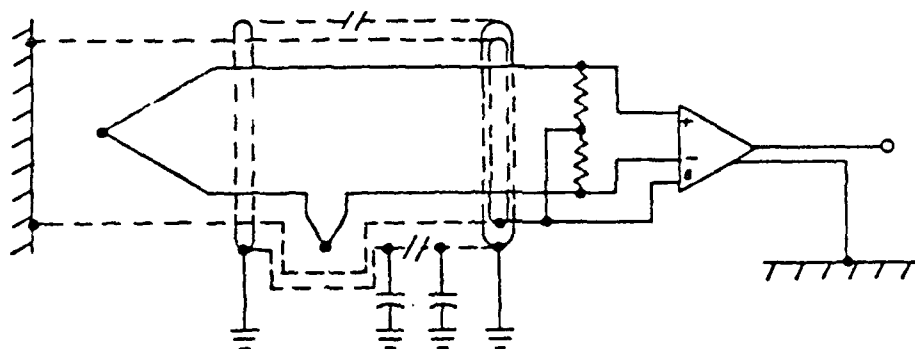
FIGURE 15   FLOATING THERMOCOUPLE - DOUBLE SHIELD

141
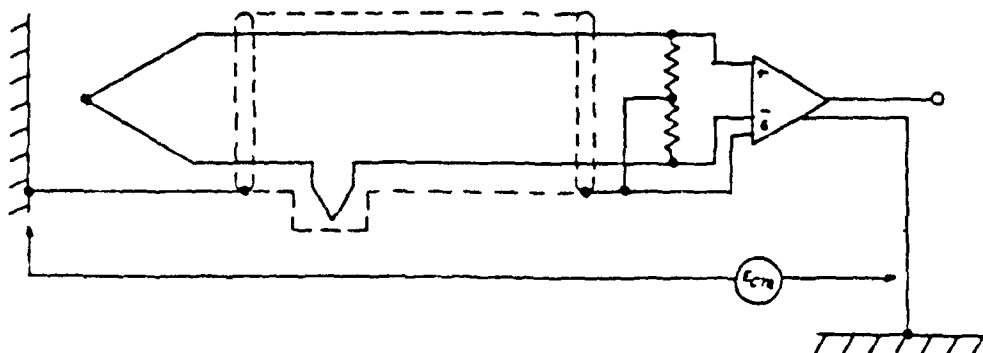
FIGURE 14 FLOATING THERMOCOUPLE - WAGNER GROUND
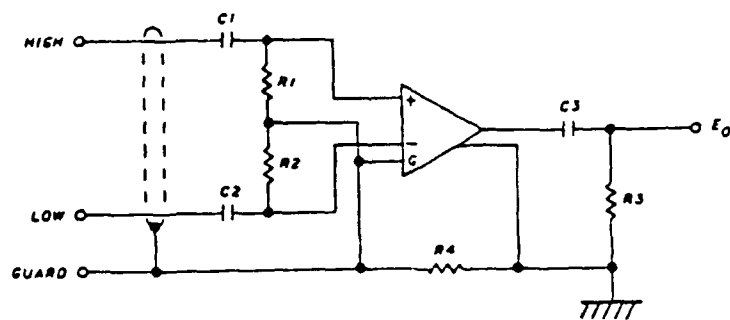
AC COUPLED INSTRUMENTATION AMPLIFIER
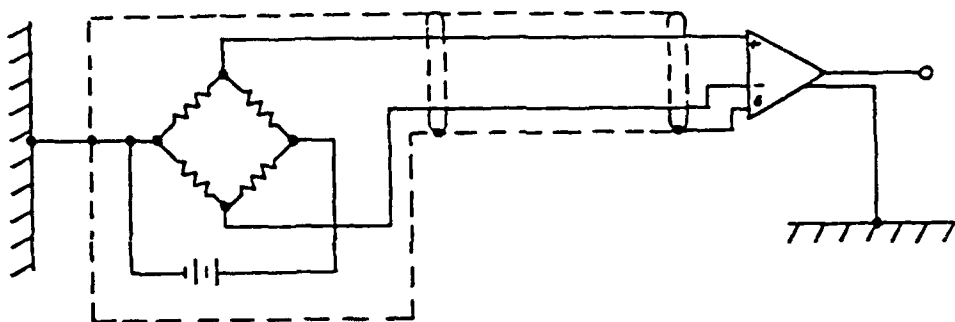
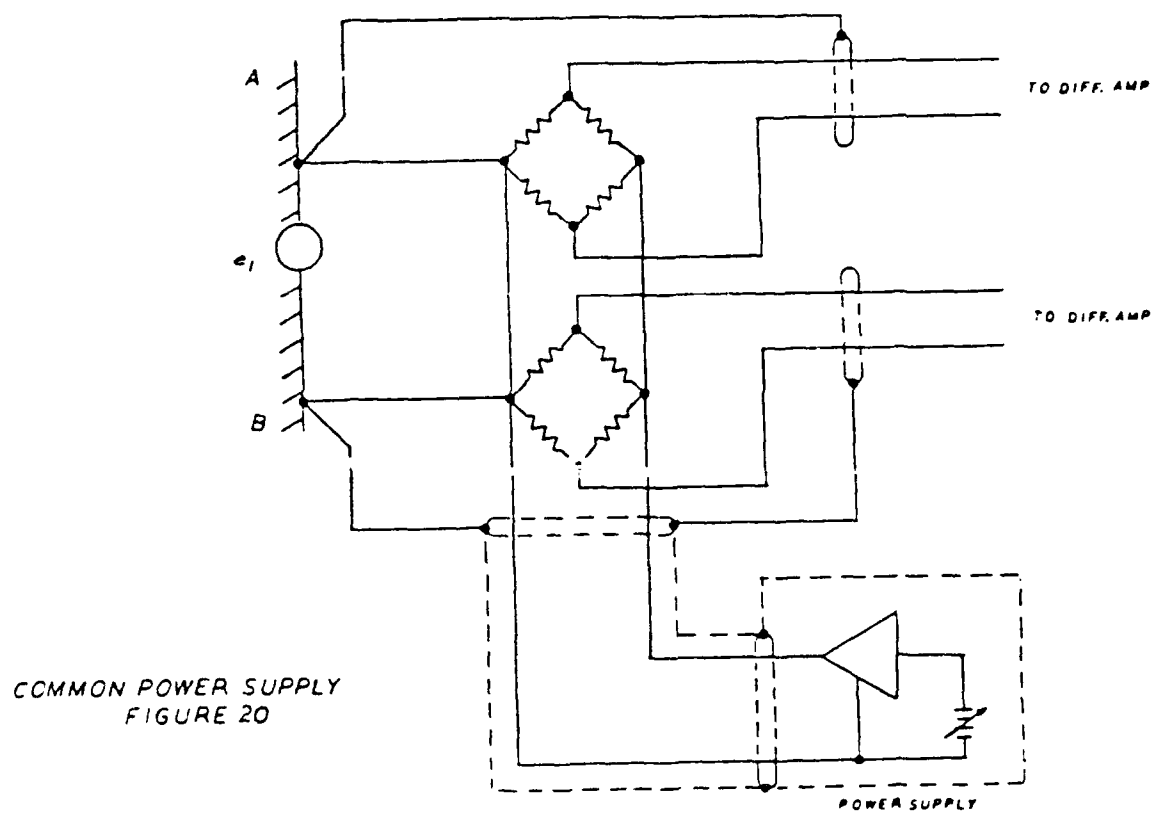FIGURE 17   GROUNDED FULL BRIDGE
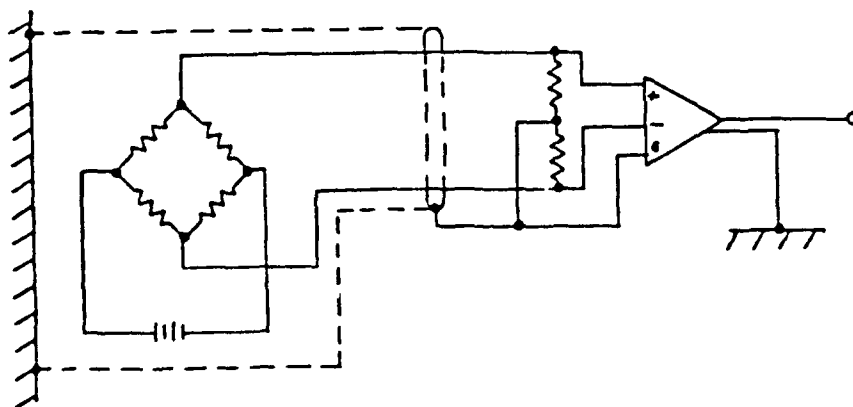
FIGURE 18   FLOATING FULL BRIDGE
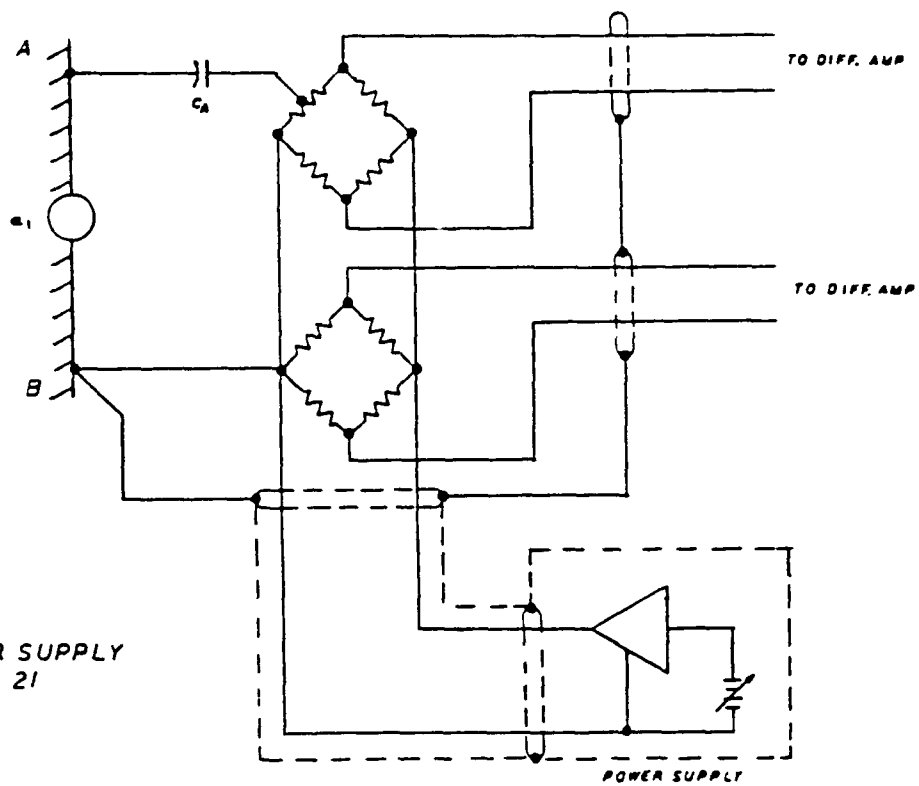
142
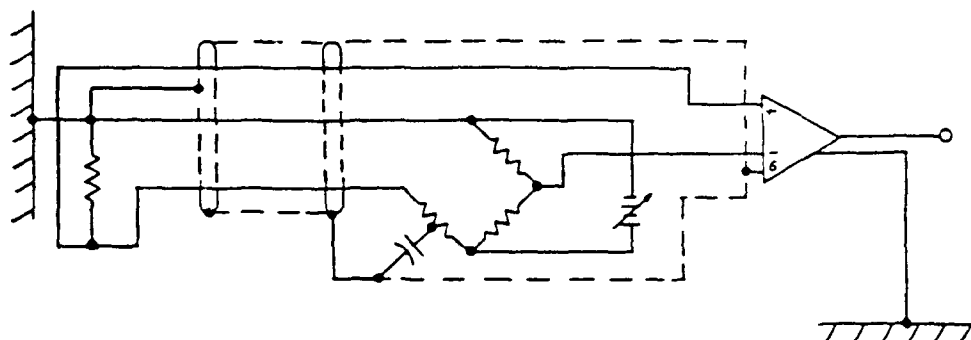
FIGURE 19   SINGLE ACTIVE ARM BRIDGE

COMMON POWER SUPPLY
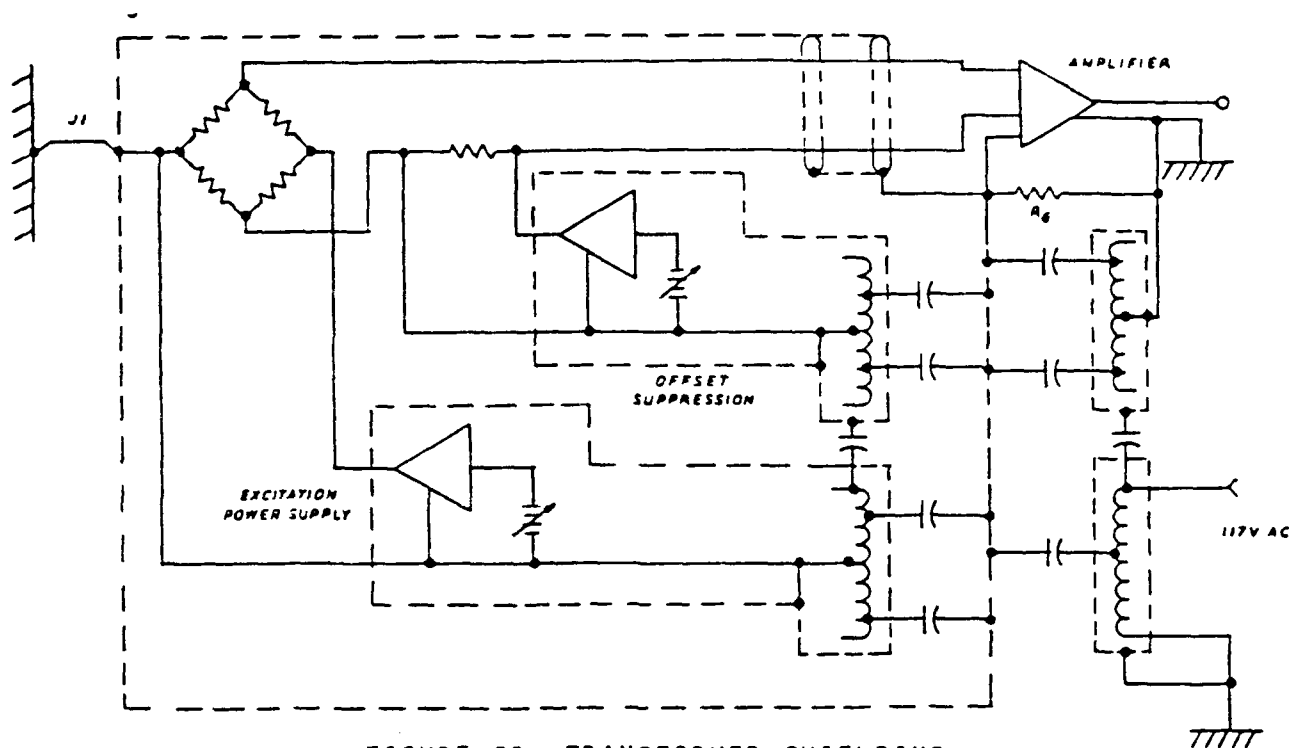FIGURE 20

143

COMMON POWER SUPPLY
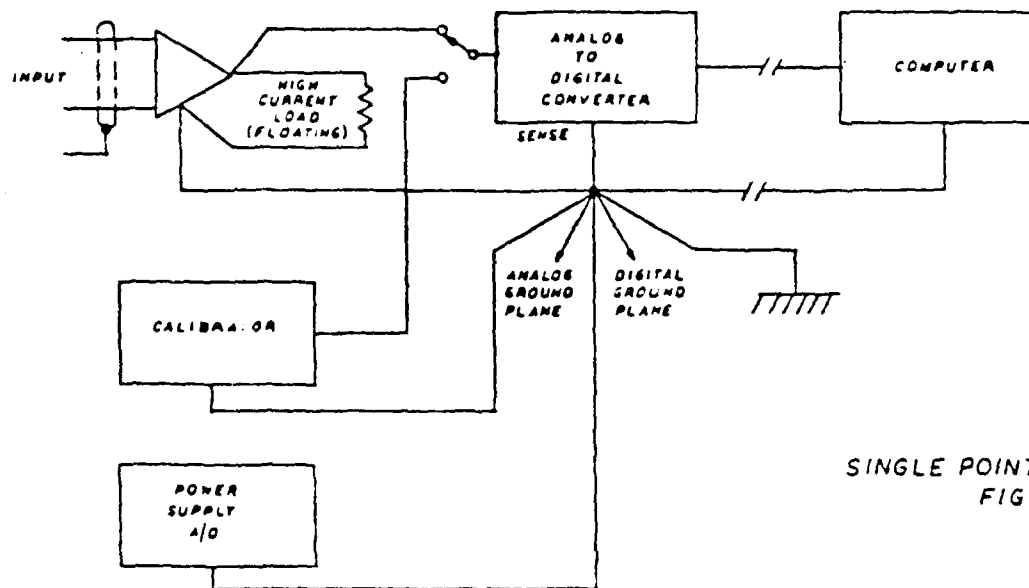FIGURE 21

144

FIGURE 22   TRANSFORMER SHIELDING

350 OHM BRIDGE

PRIMARY POWER 117V @ 60 HZ

CALCULATE LEAKAGE CAPACITANCE

FOR A 1uV ERROR

$$I = \frac{1uV}{350 \text{ OHMS}}$$

$$= 2.8nA$$

$$C = \frac{1}{2\pi 60C} = \frac{117V}{2.8nA}$$
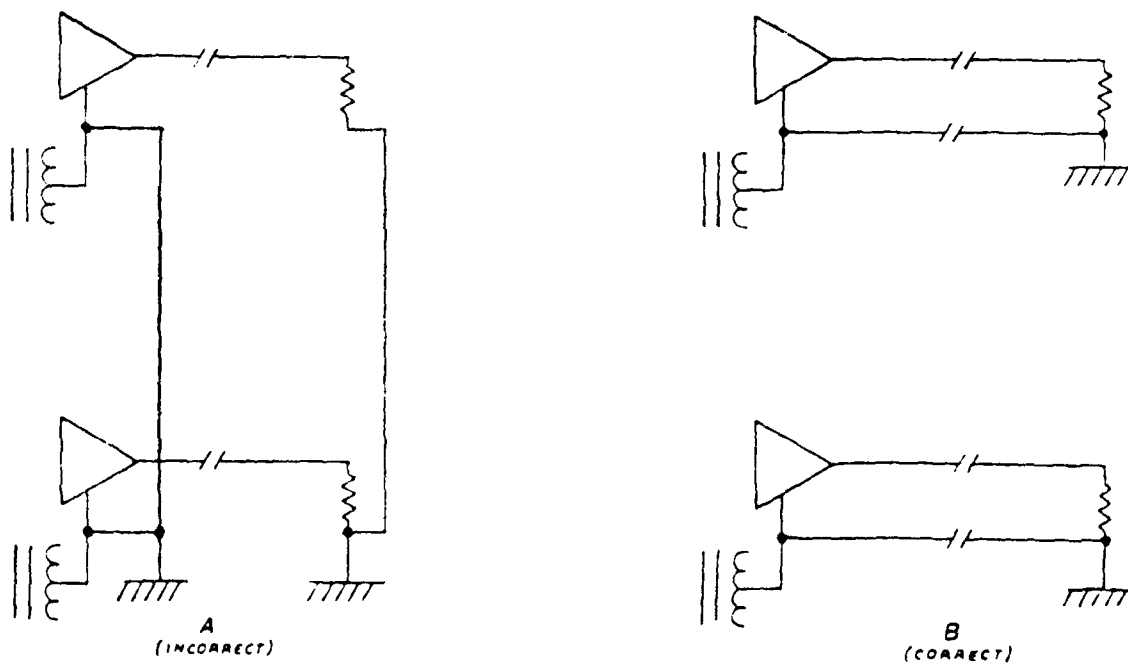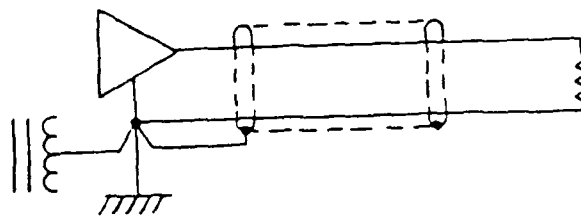
$$= .06pf$$

SINGLE POINT "STAR" GROUND
FIGURE 23

A
(INCORRECT)
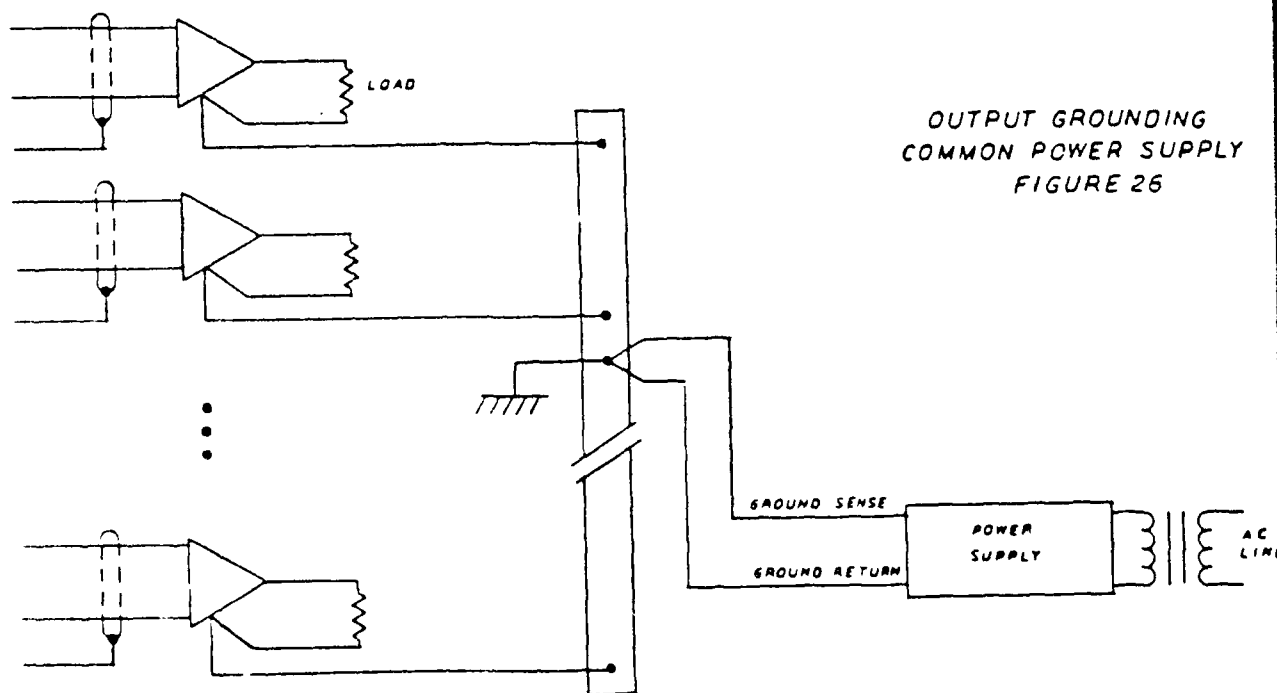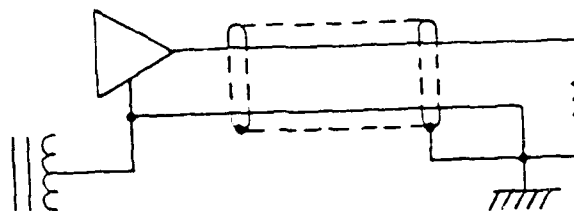
B
(CORRECT)

FIGURE 24   GROUNDING ISOLATED OUTPUTS

147

OR

LOAD

OUTPUT GROUNDING
COMMON POWER SUPPLY
FIGURE 26

GROUND SENSE

GROUND RETURN

POWER
SUPPLY

AC
LINE

FIGURE 27   SINGLE ENDED MULTIPLEXER
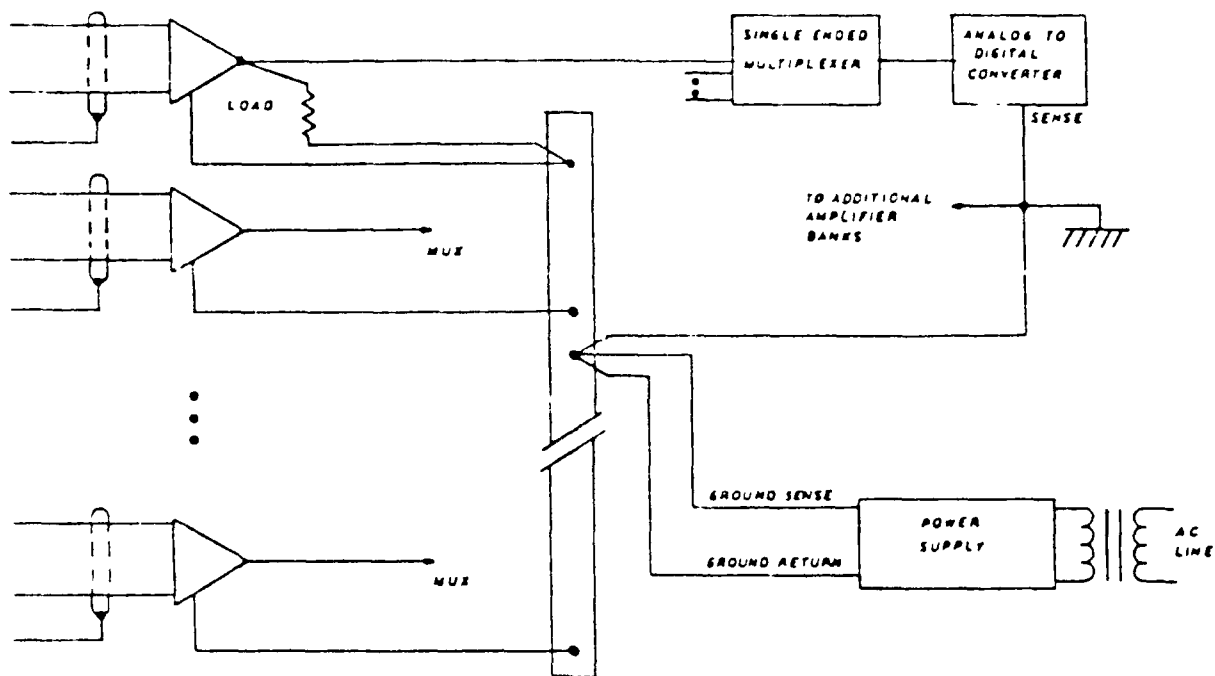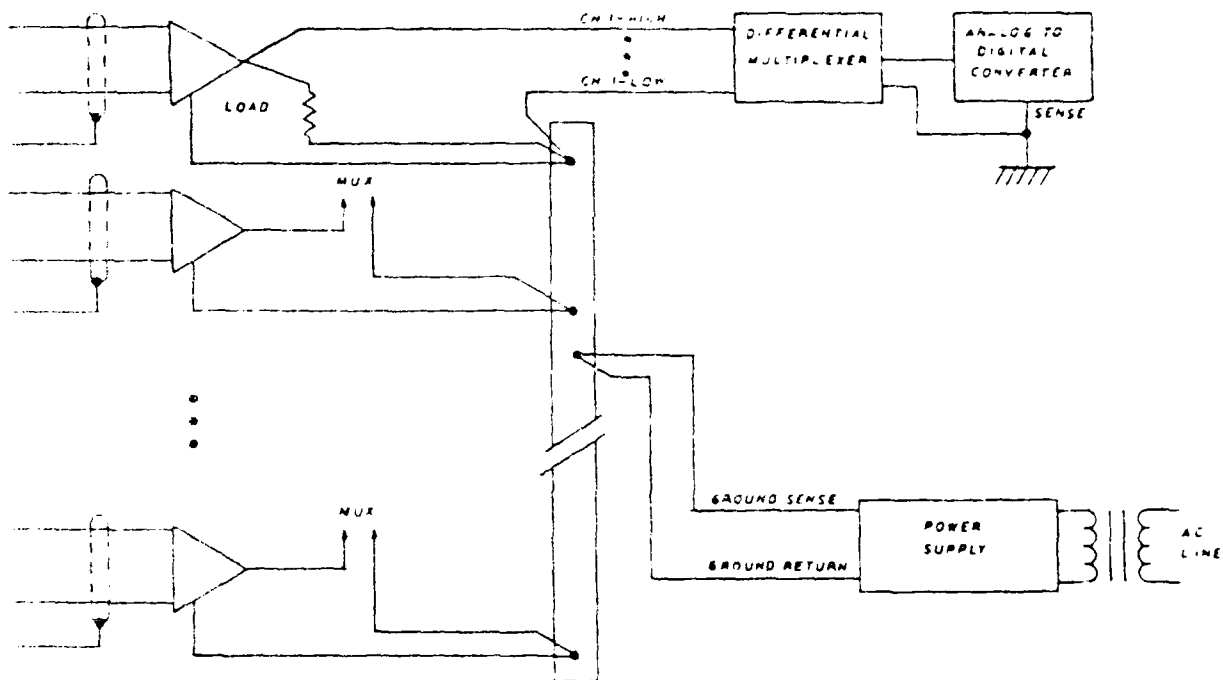
FIGURE 28 DIFFERENTIAL MULTIPLEXER

RULE: 1 SHIELDING MUST BE CONNECTED TO THE ZERO SIGNAL REFERENCE
         FOR ALL CIRCUITRY CONTAINED WITHIN IT.

RULE: 2 INPUT AND OUTPUT WIRING MUST BE CONNECTED IN
         SUCH A MANNER THAT NO NON-SIGNAL CURRENTS ARE CARRIED BY
         THE SIGNAL WIRING.

RULE: 3 IN ANY ISOLATED SYSTEM, USE ONE AND ONLY ONE
         CONNECTION TO GROUND.

DYNAMIC MEASUREMENTS ARE SELDOM ROUTINE

By: J. F. Lally
PCB Piezotronics, Inc.
Depew, NY 14043

Excerpts from tutorial presented at:

15th Transducer Workshop
Cocoa Beach, FL
June 20-22, 1989

3. UNDERSTANDING THE SIMILARITIES OF VOLTAGE MODE INSTRUMENTATION:

QUESTION OFTEN COMES UP ON THE DIFFERENCES IN CHARGE AND VOLTAGE MODE INSTRUMENTS? THE QUESTION USUALLY COMES FROM SOMEONE FAMILIAR WITH CHARGE MODE SYSTEMS. WE FIND IT HELPFUL TO ANSWER IN TERMS OF "SIMILARITIES" SINCE SIGNAL CONDITIONING FUNCTIONS IN BOTH SYSTEMS ARE BASICALLY THE SAME. THE FUNCTIONS MAY, HOWEVER, BE ACCOMPLISHED IN DIFFERENT LOCATIONS IN EACH SYSTEM.

THREE BASIC SIGNAL CONDITIONING FUNCTIONS IN BOTH SYSTEMS ARE:

1.)   IMPEDANCE CONVERSION

2.)   SIGNAL NORMALIZATION

3.)   GAIN ADJUST

ALL THREE FUNCTIONS ARE COMMON TO BOTH SYSTEMS—ONLY THE LOCATION AND METHOD OF ACCOMPLISHING THE FUNCTION MAY VARY.

IMPEDANCE CONVERSION:-THE FIRST FUNCTION

THE PRIMARY FUNCTION OF ANY PIEZO SIGNAL CONDITIONER IS TO CONVERT HIGH IMPEDANCE CHARGE OUTPUT FROM CRYSTAL INTO A USABLE LOW IMPEDANCE VOLTAGE SIGNAL SUITABLE FOR RECORDING PURPOSES.

IN CHARGE SYSTEM THIS IS ACCOMPLISHED REMOTELY BY A HIGH GAIN CAPACITIVE FEEDBACK AMPLIFIER IN THE CHARGE AMPLIFIER. IN THE VOLTAGE MODE SYSTEM IMPEDANCE CONVERSION IS ACCOMPLISHED BY MOSFET OR JFET MICRO-ELECTRONIC AMPLIFIER SEALED INSIDE THE SENSOR.

TECHNICAL AND ECONOMIC SIGNIFICANCE:

THE LOW IMPEDANCE VOLTAGE MODE SYSTEM OFFERS IMPROVED SIGNAL/NOISE CHARACTERISTICS, ESPECIALLY WHEN DRIVING LONG CABLES IN ADVERSE FIELD, FACTORY OR UNDERWATER ENVIRONMENTS. ECONOMIC SIGNIFICANCE INVOLVES USE OF LOWER COST STANDARD COAXIAL CABLE AND SIGNAL CONDITIONERS.

SIGNAL NORMALIZATION (OR STANDARDIZATION)-THE SECOND FUNCTION

CHARGE AMPLIFIERS HAVE A POTENTIOMETER CIRCUIT TO ENTER CHARGE SENSITIVITY.

VOLTAGE MODE SYSTEM

1. NORMALIZATION MAY BE ACCOMPLISHED WITHIN SENSOR, OR

2. IN THE POWER/SIGNAL CONDITIONER

NORMALIZATION INSIDE THE SENSOR-TECHNICAL ADVANTAGES

1. SIMPLIFIES OPERATION

2. MINIMIZES RECORD KEEPING IN MULTI-CHANNEL SYSTEMS

3. FACILITATES INTERCHANGEABILITY WITHOUT MAKING CIRCUIT ADJUSTMENTS

GAIN ADJUSTMENT-THIRD FUNCTION

1. GAIN ADJUSTMENT CIRCUITRY IN CHARGE AMPLIFIER

2. VOLTAGE MODE SYSTEM UTILIZES GAIN AVAILABLE IN READOUT INSTRUMENT OR IN POWER UNIT, IF REQUIRED

TECHNICAL AND ECONOMICAL SIGNIFICANCE

IN A CONTROLLED LABORATORY ENVIRONMENT OR OTHER CONDITIONS SUITABLE FOR OPERATING HIGH IMPEDANCE CIRCUITRY, GAIN ADJUST IN CHARGE AMPLIFIER ALLOWS FULL UTILIZATION OF THE VERY BROAD DYNAMIC RANGE OF PIEZO SENSORS.

SINCE MOST APPLICATIONS INVOLVE LIMITED DYNAMIC RANGE, IN THE VOLTAGE MODE SYSTEM, GAIN, IF NEEDED, MAY BE OBTAINED FROM LOW COST POWER UNITS, EXISTING INSTRUMENTATION AMPLIFIERS, OR IN THE READOUT INSTRUMENT ITSELF.

--------WHICH SYSTEM IS BEST??? -----------

THAT DEPENDS ON THE TECHNICAL CONSIDERATIONS INVOLVED WITH THE APPLICATION. THE TECHNICAL AND ECONOMICAL ADVANTAGES OF OPERATING WITH A LOW IMPEDANCE VOLTAGE SYSTEM ARE READILY APPARENT WHEN:

1.   DRIVING LONG CABLES

2.   OPERATING IN ADVERSE ENVIRONMENTS NOT SUITABLE FOR HIGH IMPEDAN : CIRCUITRY

3.   AND IN CONTINUOUS UNATTENDED MONITORING APPLICATIONS

ON THE OTHER HAND, IN THE LABORATORY WHERE CONDITIONS ARE DIFFERENT, THE CHARGE AMPLIFIER SERVES A USEFUL PURPOSE WHEN VERSATILITY IS REQUIRED FOR USE WITH A WIDE RANGE OF PIEZO SENSORS. IN INTERIOR BALLISTICS APPLICATIONS, THE ELECTROSTATIC CHARGE AMPLIFIER FACILITATES STATIC CALIBRATION, IN SOME PRESSURE AND FORCE APPLICATIONS IT PROVIDES FOR QUASI-STATIC RESPONSE.

SIGNAL CONDITIONING FUNCTIONS IN CHARGE AND VOLTAGE MODE SYSTEMS:

* IMPEDANCE CONVERSION
* NORMALIZATION
* GAIN ADJUST

CHARGE MODE SYSTEM:

NORMALIZATION
10 TURN POT

pC/G HIGH IMPEDANCE OUTPUT

LOW NOISE CABLE

CHARGE ACCELEROMETER

gain

CHARGE AMPLIFIER

GAIN

READOUT

GAIN ADJUST
(REDUNDANT IN CHARGE SYSTEM)

IMPEDANCE CONVERSION

NORMALIZATION
(IN ACCELEROMETER)

mV/g LOW IMPEDANCE OUTPUT

VOLTAGE MODE ACCELEROMETER WITH BUILT-IN AMPL.

ORDINARY COAXIAL OR RIBBON WIRE CABLE

CURRENT SOURCE

GAIN

MODERN FFT ANALYZER OR VIBRATION MONITOR WITH BUILT-IN CURRENT SOURCE FOR I.C.P. ACCELEROMETERS

VOLTAGE MODE SYSTEM:

PCB®
PIEZOTRONICS

4. LONG CABLE CONSIDERATIONS:

HISTORICALLY, DRIVING LONG CABLES HAS BEEN ONE OF THE MOST "GREMLIN" PLAGUED APPLICATIONS. COMMON PROBLEMS HAVE BEEN ASSOCIATED WITH ENVIRONMENTAL CONDITIONS SUCH AS DUST, MOISTURE, LIGHTNING AND RODENTS EATING THE CABLES. OPERATIONAL PROBLEMS INCLUDE GROUND LOOPS, POOR SIGNAL/NOISE AND AMPLITUDE/FREQUENCY CALIBRATION OF LONG LINE SYSTEMS.

THE CAPABILITY OF THE LOW IMPEDANCE VOLTAGE MODE SENSOR TO DRIVE LONG ORDINARY COAXIAL CABLES IN ADVERSE ENVIRONMENTS HAS HELPED NEUTRALIZE OR AT LEAST MINIMIZE THE EFFECTIVENESS OF THE "GREMLINS".

THERE ARE SEVERAL GENERAL GUIDELINES FOR DRIVING LONG CABLES THAT WILL HELP MINIMIZE PROBLEMS AND IMPROVE MEASUREMENT RESULTS.

   SEE ILLUSTRATIONS: GENERAL GUIDELINES FOR LONG CABLE DRIVING

                                       SIGNAL DELAY AMPLITUDE ATTENUATION

                                       LINE RESONANCES

SINCE IT IS RELATIVELY SIMPLY TO TEST YOUR LONG LINE SYSTEM, THE MESSAGE HERE IS "TEST", "DON'T GUESS"!
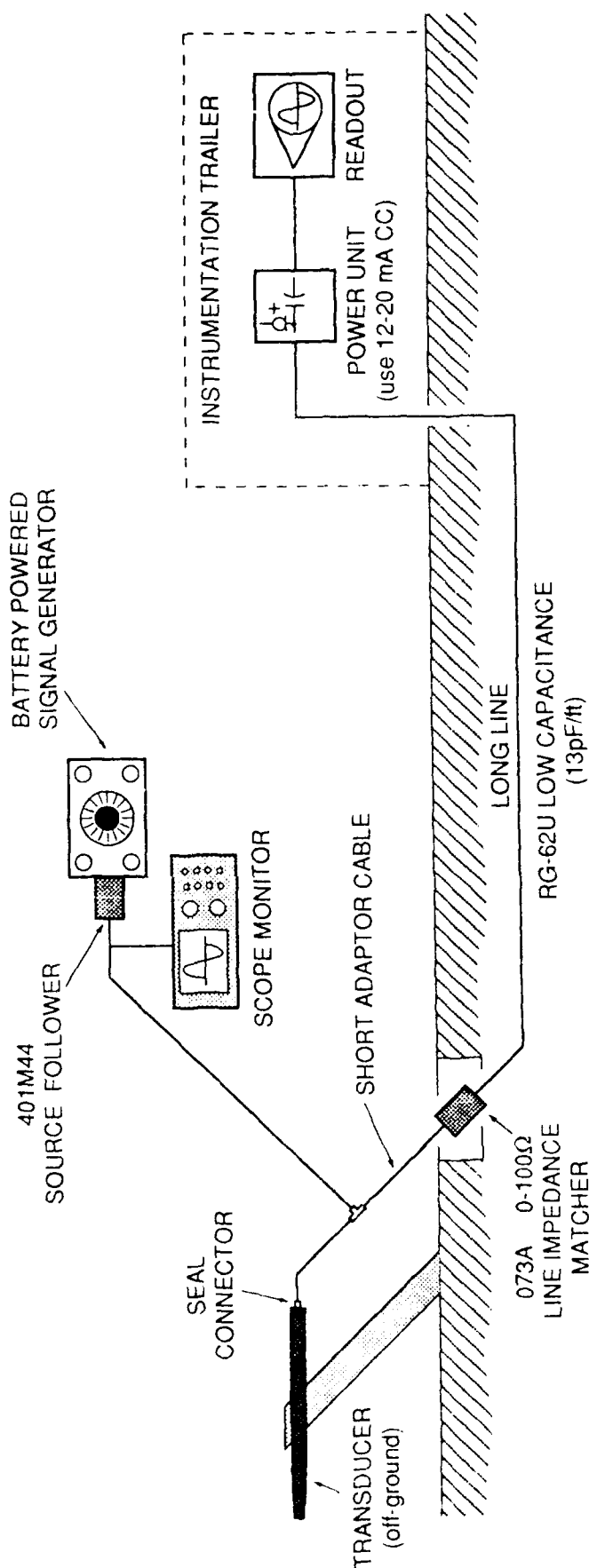
GENERAL GUIDELINES FOR LONG CABLE DRIVING APPLICATIONS & SYSTEM CHECKOUT

1) GROUND ISOLATE SENSOR - SEAL CONNECTIONS.

2) USE LOW CAPACITANCE RG-62U COAXIAL CABLE FOR LONG RUN - CABLE CAPACITANCE ACTS AS LP FILTER (use short adaptor cable at transducer).

3) USE HIGH CONSTANT CURRENT POWER UNIT - [12-20 mA] (locate with readout instrumentation).

4) USE 073A LINE IMPEDANCE MATCHER.

5) TEST FOR FREQUENCY AND AMPLITUDE WITH SIGNAL GENERATOR AND UNITY GAIN SOURCE FOLLOWER. USE SQUARE WAVE TO CHECK FOR LINE RESONANCES - TRIM OUT BY ADJUSTING 073A IMPEDANCE MATCHING RESISTOR.
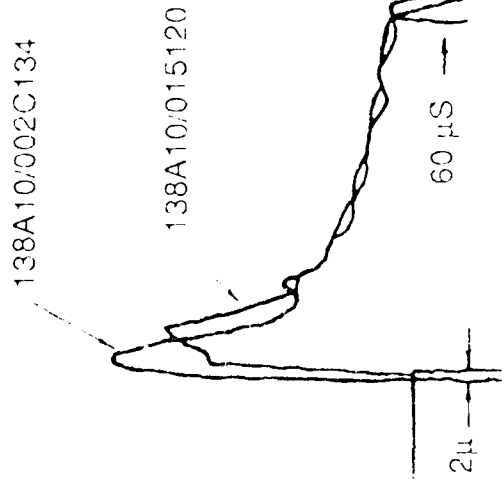
SIGNAL DELAY & AMPLITUDE ATTENUATION
CAUSED BY FILTER EFFECT OF HIGH
CAPACITANCE CABLE.

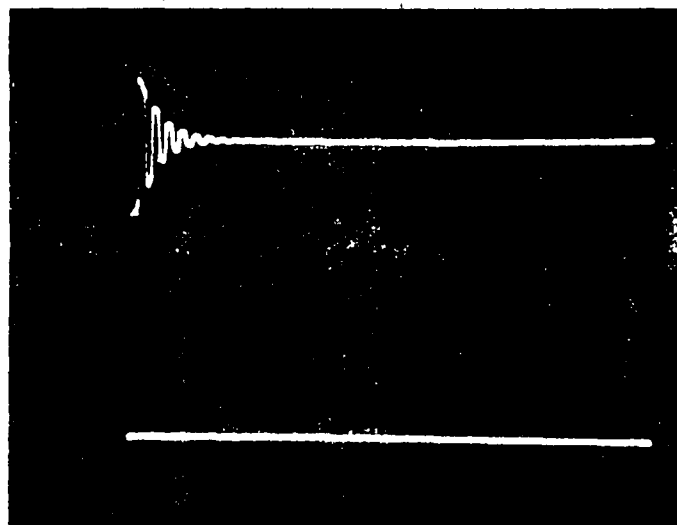LINE RESONANCE (overshoot)   ADJUSTING 073A LINE IMPEDANCE
RESULTING FROM SQUARE   MATCHING RESISTOR TRIMS OUT
WAVE, FAST RESPONSE, TEST   LINE RESONANCE
SIGNAL INPUT

400 ft. RG-62U - No Series Resistor   400 ft. RG-62U - 91Ω Series R (073A)
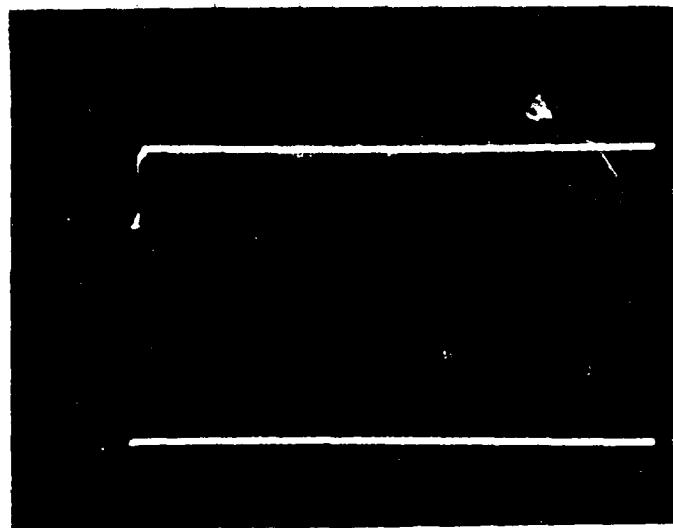
LINE RESONANCE (overshoot) IS CAUSED BY INDUCTANCE IN THE
LONG LINE. THE SERIES RESISTOR ACTS LIKE AN LP FILTER AND CAN
BE ADJUSTED TO TRIM OUT OVERSHOOT.

OPERATING IN LOW IMPEDANCE VOLTAGE MODE PERMITS WIDE SELECTION OF STANDARD LOW COST CABLES AND CONNECTORS.

ORDINARY COAX

RG-58U
RG-62U

BNC   BNC

2-PIN SOLDER CONNECTOR
10-32 THD

RIBBON WIRE

STD IDC
(Insulation Displacement Connector)

RIBBON

ADHESIVE
MOUNTING
PAD

161
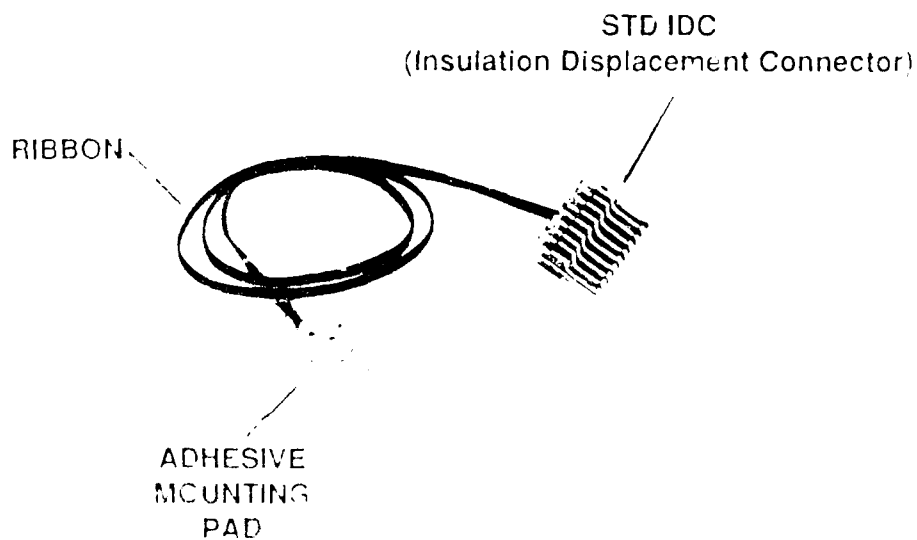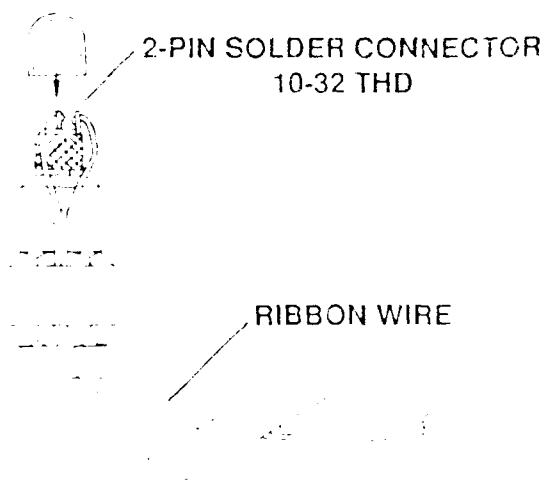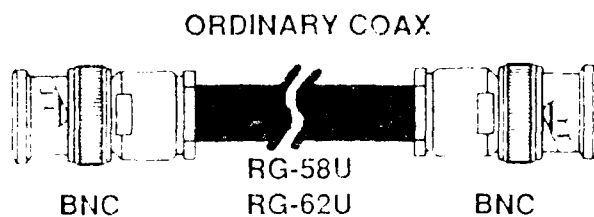
5. RANGING:

QUESTIONS OFTEN COME UP ON RANGING OF PIEZO SENSORS. WHY WOULD A
PRESSURE TRANSDUCER RANGED FOR 100 PSI BE SUGGESTED FOR A ONE PSI
MEASUREMENT? WHY DO SOME TRANSDUCERS LIST A 5 VOLT AND 10 VOLT OUTPUT?
HOW DO I SELECT A TRANSDUCER TO MEASURE $\pm$ 1 PSI AT A STATIC LEVEL OF
1000 PSI?

PIEZO TYPE SENSORS HAVE A VERY WIDE LINEAR DYNAMIC RANGE WHICH CAN BE
AS MUCH AS ONE MILLION TO ONE. IF WE TAKE A LOOK AT THE CONSTRUCTION
OF A TYPICAL QUARTZ PRESSURE SENSOR COMPARED TO A STRAIN TYPE SENSOR,
IT WILL HELP UNDERSTAND HOW THE WIDE LINEAR RANGE IS ACHIEVED.

SEE ILLUSTRATIONS: QUARTZ PIEZO PRESSURE SENSOR

STRAIN GAGE

NOTE THAT THE PRIMARY DIFFERENCE IN THE TWO SENSORS ILLUSTRATED IS THE
THIN DIAPHRAGM ON THE QUARTZ SENSOR IS ALMOST FULLY SUPPORTED BY A
HIGHLY PRELOADED RIGID QUARTZ SENSING ELEMENT. THE PRELOAD IMPARTS
EXCELLENT LINEARITY FOR LOW LEVEL MEASUREMENTS AND THE RIGID QUARTZ
COLUMN SUPPORTS THE DIAPHRAGM TO ESSENTIALLY THE YIELD STRENGTH OF THE
QUARTZ.

QUARTZ PIEZO
PRESSURE SENSOR
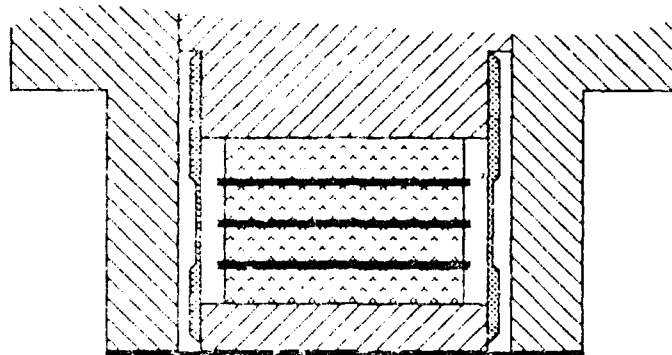
THIN METAL DIAPHRAGM
SUPPORTED BY A RIGID
COLUMN OF QUARTZ

STRAIN GAGE

RESISTIVE
STRAIN
ELEMENT
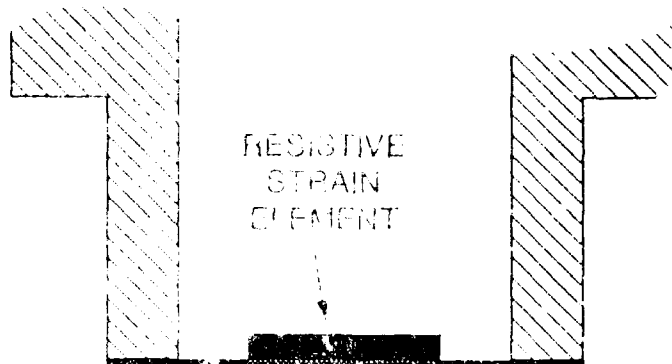
THIN UNSUPPORTED
DIAPHRAGM

AS CAN BE SEEN, THE DIAPHRAGM OF THE STRAIN TYPE SENSOR IS UNSUPPORTED. THE DIAPHRAGM MUST FLEX IN ORDER FOR THE STRAIN SENSITIVE ELEMENT TO CHANGE RESISTANCE. DIAPHRAGM THICKNESS IS, THEREFORE, GAGED TO SUPPORT A LIMITED PRESSURE RANGE.

DYNAMIC RANGE TO 10,000 PSI. AS AN ICP, (INTEGRATED CIRCUIT PIEZO SENSITIVITIES AND RANGES.

SEE ILLUSTRATION: -RANGING

DESCRIBES HOW A TYPICAL WIDE DYNAMIC RANGE CHARGE MODE TRANSDUCER IS RANGED AS AN ICP VOLTAGE MODE DESIGN

THE BIAS, (TURN ON VOLTAGE), OF THE BUILT-IN IC CIRCUIT AND POWER SUPPLY VOLTAGE DETERMINE THE VOLTAGE SWING:

12 V BIAS   18 VOLT POWER = 5-6 VOLT SWING

12 V BIAS   24 VOLT POWER = 10 VOLT SWING

THE CAPABILITY TO MEASURE SMALL DYNAMIC PRESSURES UNDER HIGH STATIC LOAD IS A UNIQUE CAPABILITY OF PIEZO PRESSURE TRANSDUCERS. SELECT A TRANSDUCER WITH HIGHEST SENSITIVITY WITH SUITABLE OVERRANGE CAPABILITY.

RANGING

TYPICAL CHARGE MODE ICP PSi PRESSURE SENSOR

LINEAR DYNAMIC RANGE   0 - 10,000 psi

RANGED AS AN ICP VOLTAGE MODE SENSOR

(Cpen circuit voltage sensitivity 50 mV/psi)

	SENSITIVITY	5V FS RANGE	10V FS RANGE
	50 mV/psi	0 - 100 psi	0 - 200 psi
CAPACITOR AT INPUT OF IC ATTENUATES SIGNAL & INCREASES RANGE	10 mV/psi	0 - 500 psi	0 1000 psi
	5 mV/psi	0 - 1000 psi	0 - 2000 psi
	1 mV/psi	0 - 5000 psi	0 - 10,000 psi
	.5 mV/psi	0 - 10,000 psi	-----

BIAS VOLTAGE OF BUILT-IN IC AND POWER SUPPLY AND

VOLTAGE LEVEL DETERMINES 5 OR 10V RANGE CAPABILITY

12V BIAS   18V POWER   =   5V RANGE

12V BIAS   24V POWER   =   10V RANGE

6. MODELING:

COMPUTER MODELING IN THE FORM OF FINITE ELEMENT ANALYSIS, PERFORMED PRIOR TO EXPERIMENTAL TESTING, PROVIDES INSIGHT INTO THE PERFORMANCE CHARACTERISTICS OF THE TEST STRUCTURE.

IT IS EQUALLY IMPORTANT, WHENEVER POSSIBLE, TO SET UP AND MEASURE PERFORMANCE CHARACTERISTICS OF A BEHAVIOR MODEL OF THE TEST STRUCTURE.

SEE ILLUSTRATION OF COMMON BEHAVIOR MODELS

TYPICAL EXAMPLES
OF BEHAVIOR MODELS

SHOCK TUBE (helium driven)	GUN TUBE 22 CALIBER
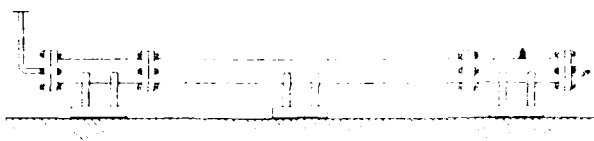
DYNAMIC CALIBRATION AND FREQUENCY RESPONSE TESTING OF TRANSDUCER.
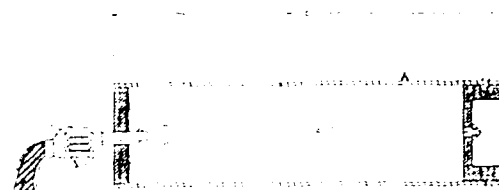
CHECK OUT BLAST TRANSDUCERS.

PLEXIGLAS DROP SHOCK MACHINE
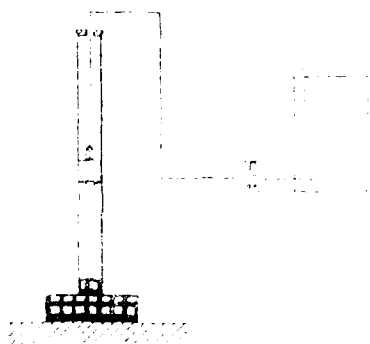
SMALL COMPRESSOR

CHECK OUT ACCELERATION SHOCK SENSORS. CHANGE MATERIAL IN IMPACT BASE TO ALTER g LEVEL AND FREQUENCY
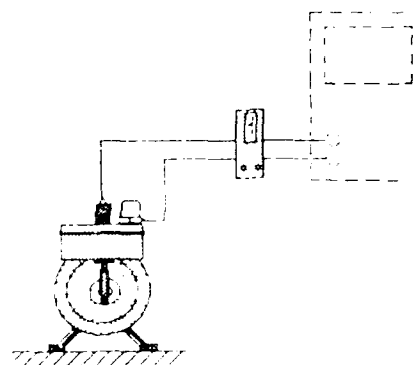
PROVIDES REPEATABLE OSCILLATING PRESSURE SOURCE.

SMALL CALIBER GUN TEST BARREL

OTHER MODEL IDEAS:

SMALL ONE CYL. ENG. — COMBUSTION

MODEL SOLID ROCKET — THRUST

M-80 S — FREE FIELD BLAST

TEST BALLISTIC TRANSDUCERS. PRECISION MOUNTING PORTS.

MEASUREMENT OF THE KNOWN PERFORMANCE CHARACTERISTICS OF A BEHAVIOR MODEL PROVIDES FOR:

• FAMILIARIZATION & CHECKOUT OF INSTRUMENTATION IN A CONTROLLED ENVIRONMENT WITH LITTLE RISK OF DAMAGE TO EQUIPMENT

• SYSTEM CHECKOUT -- YOU KNOW INPUT AND DESIRED RESULTS FROM BEHAVIOR MODEL

• TRAINING OF NEW PERSONNEL IN MEASUREMENT APPLICATION

• TROUBLE SHOOTING -- TESTING OF QUESTIONABLE INSTRUMENTS IN BEHAVIOR MODEL

• BETTER ASSURANCE OF SUCCESSFUL MEASUREMENT (ESPECIALLY IMPORTANT IN COSTLY 1-SHOT TEST)

DISCHARGE TIME CONSTANT

DEFINITION: DISCHARGE TIME CONSTANT (DTC) - TIME REQUIRED FOR A
TRANSDUCER OR MEASURING SYSTEM TO DISCHARGE ITS SIGNAL
TO 37% OF THE ORIGINAL VALUE FROM A STEP CHANGE OF
MEASUREAND. DISCHARGE TIME CONSTANT DIRECTLY RELATES TO
THE LOW FREQUENCY MEASURING CAPABILITY FOR BOTH
TRANSIENT AND SINUSOIDAL EVENTS. (DTC SHOULD NOT BE
CONFUSED WITH RISE TIME WHICH RELATES TO HIGH FREQUENCY
RESPONSE.)

DISCHARGE TIME CONSTANT IS SOMETIMES CONFUSED WITH "RISE TIME". AS
NOTED ABOVE, DTC DEFINES LOW FREQUENCY RESPONSE. A RECENT CALLER WHO
WANTED TO MAKE A FAST RESPONSE SHOCK WAVE MEASUREMENT, LOADED THE SCOPE
INPUT WITH A 50 OHM RESISTOR TO "SHORTEN THE TIME CONSTANT" UNDER THE
ASSUMPTION IT WOULD INCREASE THE RISE TIME.

THIS CONFUSION MAY ARISE FROM THE DEFINITION OF "TIME CONSTANT" TAKEN
FROM THE ELECTRONIC DICTIONARY, M^{C}GRAW-HILL 1978 WHICH READS:

> "TIME CONSTANT IS THE TIME REQUIRED FOR A VOLTAGE OR
> CURRENT IN A CIRCUIT TO RISE TO APPROXIMATELY 63% OF
> ITS STEADY STATE FINAL VALUE -----OR----- FALL TO
> APPROXIMATELY 37% OF ITS INITIAL VALUE.

DISCHARGE TIME CONSTANTS ASSOCIATED WITH ICP INSTRUMENTS INCLUDE:

THE TRANSDUCER DTC WHICH IS LISTED ON THE SPECIFICATION SHEET, AND THE
AC COUPLED POWER UNIT WHICH DECOUPLES THE BIAS VOLTAGE RIDING ON THE
TRANSDUCER SIGNAL LEAD.

WITH CAPACITIVE BIAS DECOUPLING, THE CAPACITOR AND THE INPUT IMPEDANCE OF THE READOUT INSTRUMENT ESTABLISHES A HIGH PASS FILTER WHICH DETERMINES THE LOW FREQUENCY RESPONSE.

POWER UNITS ARE ALSO AVAILABLE WITH ACTIVE OP-AMP BIAS DECOUPLING CIRCUITS WHICH PROVIDE A ZERO BASED LOW IMPEDANCE OUTPUT. THIS TYPE OF POWER UNIT MAINTAINS THE TRANSDUCER DISCHARGE TIME CONSTANT INTO ANY READOUT LOAD IMPEDANCE. IT IS ESPECIALLY USEFUL WHEN COUPLING INTO TAPE RECORDERS WHICH HAVE INPUT IMPEDANCE AS LOW AS 20K.

DISCHARGE TIME CONSTANT AND OTHER TECHNICAL INFORMATION IS DESCRIBED IN MORE DETAIL IN OUR TAN COLORED "GENERAL GUIDE TO ICP INSTRUMENTATION".

APPLICATION ENGINEERING SUGGESTIONS TO HELP SMOOTH OUT
THE MEASUREMENT PROCESS

DIGITAL PEAK METER:

WHEN RECORDING MEASUREMENT DATA WITH A DIGITAL PEAK HOLDING METER, MONITOR THE INPUT WAVE FORM WITH A SCOPE. OTHERWISE YOU COULD BE MONITORING NOISE FROM A LOOSE CONNECTION OR DISTORTED TRACE FROM POOR SENSOR INSTALLATION.

TRANSDUCERS WITH LONG DISCHARGE TIME CONSTANTS:

MAY TAKE LONGER TO TURN ON. MOST PCB UNITS HAVE A COLOR CODED METER THAT MONITORS THE TURN ON (BIAS VOLTAGE) OF THE SENSOR. ALLOW A FEW MINUTES AFTER TURNING POWER UNIT ON TO SEE IF THE METER POINTER SWINGS INTO THE "GREEN" REGION INDICATING PROPER TURN ON.

REPAIR SERVICE:

WHEN RETURNING AN ITEM FOR SERVICE, ATTACH A TAG TO THE ITEM GIVING DETAILS OF THE PROBLEM. ALSO COMMUNICATE WHEN YOU FEEL THE ITEM HAS NOT PROVIDED GOOD SERVICE LIFE-THIS INFORMATION IS VALUABLE WHEN MAKING WARRANTY ADJUSTMENTS. PROVIDE A NAME AND TELEPHONE NUMBER SO YOU CAN BE CALLED IF NEEDED

ORDER SPARE CABLES:

CABLES ARE GENERALLY RECOGNIZED A- THE WEAKEST ELEMENT IN THE MEASUREMENT SYSTEM. IF YOU DON'T MAKE YOUR OWN CABLES OR MAINTAIN A STOCK, ORDER SPARE CABLES. CABLES WILL LAST LONGER IF THEY ARE TAPED OR TIED DOWN TO RELIEVE STRESSES AT THE SENSOR CONNECTOR.

TRANSDUCER INSTALLATION

THE IMPORTANCE OF DETAILED ATTENTION TO SENSOR INSTALLATION CANNOT BE OVEREMPHASIZED. PROBABLY NO OTHER SINGLE FACTOR HAS AS MUCH EFFECT ON THE QUALITY OF YOUR MEASUREMENT DATA. POOR INSTALLATIONS USUALLY OVERSTRESS SENSOR HOUSINGS AND DISTORTED DATA. THE SOLUTION TO A POOR SEAL SURFACE IS NOT MORE TORQUE.

SEE ILLUSTRATION: SEE PRESSURE SENSOR INSTL. & FORCE SENSOR
MOUNTING

MOST MANUFACTURERS PROVIDE DETAILED MACHINING INSTRUCTIONS, SURFACE PREPARATION, AND RECOMMENDED MOUNTING TORQUE FOR THEIR PRODUCTS. IF YOU DIDN'T GET THIS INFORMATION WITH YOUR PRODUCT, REQUEST IT.

PRESSURE SENSOR INSTALLATION

APPLY
RECOMMENDED
TORQUE TO CLAMP
NUT

OFF-CENTER
SIDE WALL
STRAIN

EVENLY
CENTERED

PROPER ALIGNMENT
STRAIN FREE MOUNT

FORCE SENSOR MOUNTING

EDGE
LOADING
(avoid)

CENTRAL
LOADING

TEST
STRUCTURE
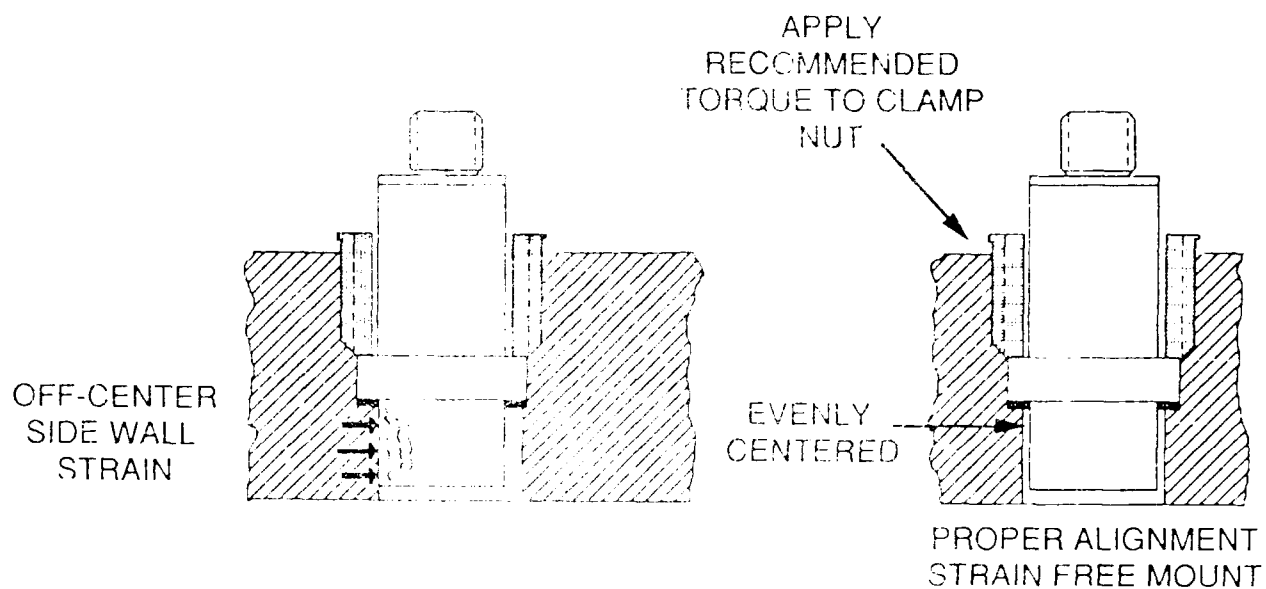
FORCE
SENSOR
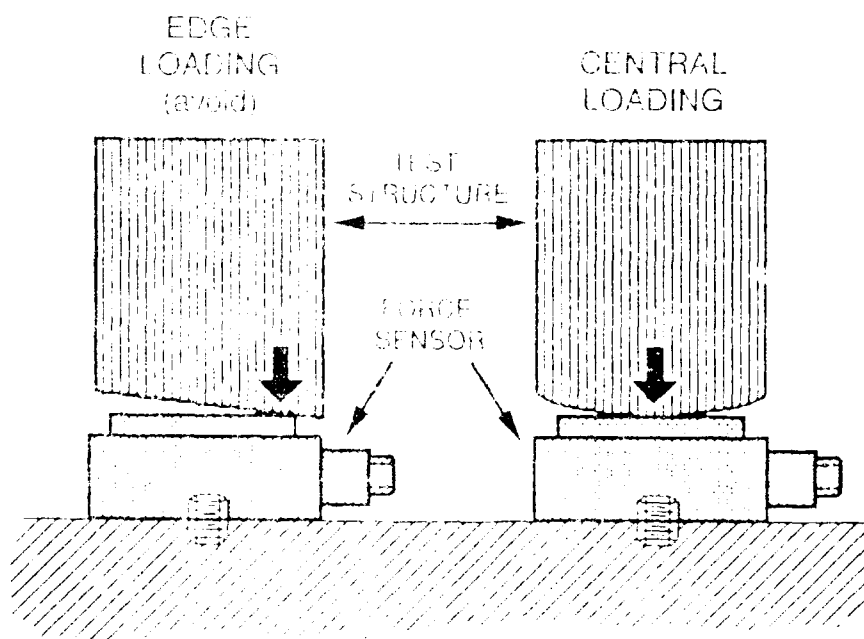
COMMUNICATIONS:

WHEN CALLING IN FOR APPLICATION ASSISTANCE, PROVIDE AS MUCH DETAIL AS YOU CAN. A BRIEF DESCRIPTION OF YOUR APPLICATION, APPROXIMATE RANGE, FREQUENCY RESPONSE UNUSUAL ENVIRONMENTAL CONDITIONS, AND WHETHER IT IS A TEST OR CONTINUOUS MONITORING IS IMPORTANT.

EG: QUESTION: WILL YOUR TRANSDUCER OPERATE AT $1200^{O}F$?

     ANSWER: YES AND NO, IT DEPENDS ON A LOT OF OTHER FACTORS.

BETTER QUESTION: DO YOU HAVE A SENSOR THAT WILL MEASURE LOW PRESSURE EXHAUST PRESSURE PULSATIONS IN A DIESEL ENGINE AT $1200^{O}F$?

     ANSWER: YES, MODEL 112A21 50 mV/PSI ACCELERATION COMPENSATED TRANSDUCER MOUNTED IN THE MODEL 64 WATER COOLED ADAPTOR OPERATES VERY WELL FOR YOUR APPLICATION. THEY ARE DESCRIBED ON PAGES 13 AND 26 IN THE CATALOG. ARE THERE ANY OTHER UNUSUAL ABOUT THIS APPLICATION.

WHEN CALLING ABOUT EQUIPMENT PROBLEMS OR OPERATION.

1.) HAVE MODEL NUMBERS OF SENSORS AND SIGNAL CONDITIONERS.

2.) HAVE CATALOG AND MANUAL IF YOU CAN LOCATE IT AT HAND.

WHAT DOES SHORT-TERM STATIC RESPONSE MEAN?

YOU MAY SEE REFERENCE IN THE LITERATURE TO THE EFFECT THAT A SENSOR MAY HAVE "SHORT-TERM" STATIC RESPONSE AND IS SUITED FOR "QUASI-STATIC" MEASUREMENTS.

THE USE OF SUCH UNDEFINED TERMINOLOGY IS PURPOSELY USED TO ILLICIT CUSTOMER QUESTIONS ON WHAT IS MEANT BY "SHORT-TERM" AND TO OBTAIN MEASUREMENT DETAILS NECESSARY TO DETERMINE IF THE SENSOR IS SUITABLE FOR THE APPLICATION. KEEP IN MIND THAT MANY QUARTZ SENSORS HAVE EXTENDED DISCHARGE TIME CONSTANTS LONG ENOUGH TO PERMIT STATIC CALIBRATION. IN SOME CUSTOMER APPLICATIONS REQUIRING NEAR STATIC RESPONSE, CERTAIN CHARACTERISTICS OF THE QUARTZ SENSOR MAY BE HIGHLY DESIRABLE.

SUCH DESIRABLE CHARACTERISTICS MAY INCLUDE:

     HIGH STIFFNESS

     SMALL SIZE COMBINED WITH HIGH RANGE

     HIGH VOLTAGE OUTPUT

     RUGGEDNESS AND LONG LIFE IMPARTED BY SOLID STATE DESIGN

HOW LONG A QUARTZ TRANSDUCER WILL MEASURE A STATIC EVENT IS DETERMINED BY SEVERAL VARIABLES, INCLUDING:

     DISCHARGE TIME CONSTANT OF THE SENSOR AND

     THERMAL AND OTHER ENVIRONMENTAL CONDITIONS

DURING THE APPLICATION DISCUSSION, THE TIME DURATION OF THE MEASUREMENT EVENT IS DETERMINED RELATIVE TO THE DTC, TEMPERATURE VARIABLES AND OTHER ENVIRONMENTAL CONSIDERATIONS. WITH THIS INFORMATION, THE APPLICATION ENGINEER CAN DETERMINE IF THE SENSOR IS SUITABLE FOR THE CUSTOMERS APPLICATION.

OFTEN, WHAT IS "STATIC" AND WHAT IS "DYNAMIC" IS IN THE EYES OF THE BEHOLDER.

A TECHNICAL REPORT REFERS TO A TEST RUN TIME OF 1.5 TO 6 MILLISEC WHICH IS ENOUGH TO ACHIEVE "STEADY STATIC CONDITIONS".

"ANOTHER CUSTOMER ADVISES HIS PRESSURE APPLICATION IS DYNAMIC--"IT CHANGES TWICE A DAY".

BIAS VOLTAGE

AN OUTPUT OFFSET VOLTAGE, COMMONLY REFERRED TO AS "BIAS" OR "TURN-ON" VOLTAGE, IS A NATURAL CHARACTERISTIC OF FIELD EFFECT TRANSISTORS USED IN ICP SENSORS WHEN POWERED FROM A CONSTANT CURRENT POWER SOURCE.

IN AN ICP SENSOR INCORPORATING A TWO WIRE SYSTEM; THE SIGNAL RIDES ON TOP OF THE DC BIAS VOLTAGE. THIS DC VOLTAGE IS REMOVED IN THE POWER UNIT BY MEANS OF A CAPACITIVE BIAS DECOUPLING CIRCUIT OR AN ACTIVE OP-AMP CIRCUIT.

MONITORING THE DC BIAS VOLTAGE WITH A METER CIRCUIT IN THE POWER UNIT, INDICATES NORMAL OR FAULTY SYSTEM OPERATION. THE COLOR CODED READOUT METER, OR LED, INDICATES NORMAL OR FAULTY OPERATION.

ICP SENSORS ARE AVAILABLE WITH BIAS VOLTAGE IN THE 3 TO 5 VOLT AND 10 TO 12 VOLT RANGE.

BY ORIENTING THE CRYSTALS IN THE SENSOR TO PROVIDE EITHER PLUS OR MINUS OUTPUT POLARITY AND CHOOSING EITHER A LOW OR HIGH BIAS ELECTRONICS, ICP SENSORS CAN BE PROVIDED TO OPERATE FROM VIRTUALLY ANY SUPPLY VOLTAGE.

SEE ILLUSTRATION-TYPICAL 2 WIRE ICP SYSTEM

TYPICAL 2-WIRE ICP SYSTEM

178
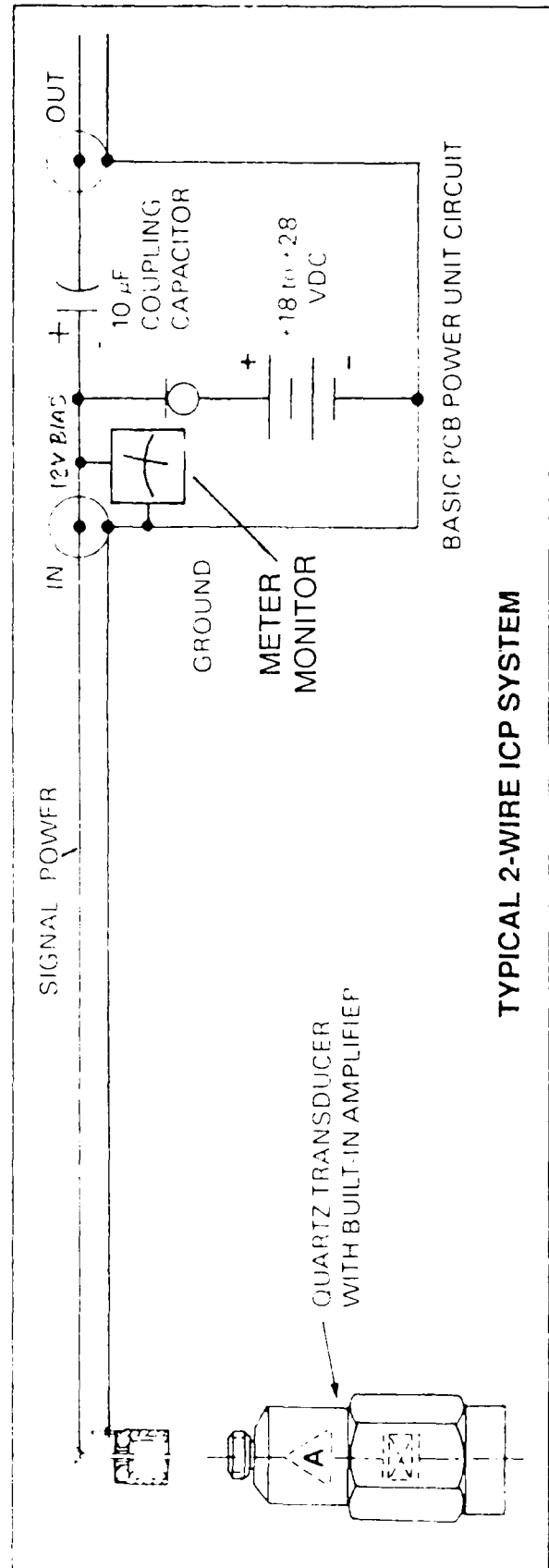
ZERO SHIFT

THERE ARE SEVERAL CAUSES OF ZERO SHIFT, AND APPARENT ZERO SHIFT.
POTENTIAL CAUSES OF ZERO SHIFT AND THE CONDITIONS WHERE IT IS LIKELY TO
OCCUR ARE ILLUSTRATED.

SEE ILLUSTRATION-ZERO SHIFT

ZERO SHIFT
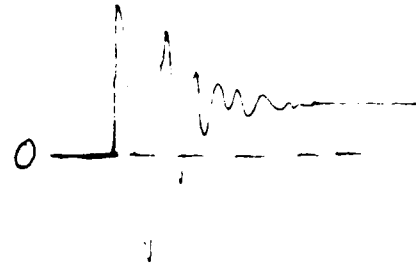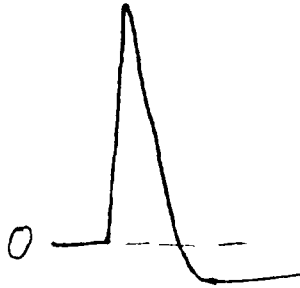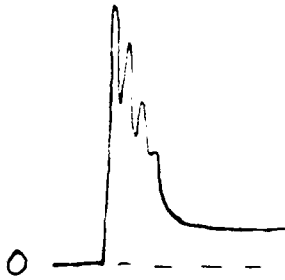
ZERO SHIFT CAUSES:	MEASUREMENT CONDITIONS LIKELY TO PRODUCE ZERO SHIFT:
Sensor design or quality	High frequency metal-to-metal impact
Mounting stress on sensor	Non-precision mounting surface or port overtorquing
Transient thermal effect	Flash temperature associated with shock or blast waves-no thermal ablative
Short discharge time constant	Longer duration half-sine or nuclear simulation events
Uneven loading	Edge or side loading of sensor
Non-symetrical filtering	High frequency, heavily-filtered data
Spurious electrical inputs	EMI, RF or electrically actuated events
Erratic connection: open circuits	High shock environment

RECOGNIZING ERRATIC CONNECTION

SEE ILLUSTRATION-THE MICRODOT CONNECTOR

ON MANY SENSORS USING MICRODOT CONNECTORS, THE GROUND CONNECTION PASSES THROUGH THE FLOATING THREADED CONNECTOR.

IF THE CONNECTOR LOOSENS DURING A MEASUREMENT CAUSING AN INTERMITTENT OPEN CIRCUIT, IT CAN ACT LIKE A SWITCH. IN ICP TRANSDUCERS, THE SIGNAL WILL GO TO THE SUPPLY VOLTAGE AND SHOW FULL SCALE SPIKES AS ILLUSTRATED.

SEE ILLUSTRATION-SOLDER CONNECTOR

THE SOLDER CONNECTOR ADAPTOR, RECOMMENDED ESPECIALLY FOR HIGH SHOCK APPLICATIONS, IS OF ONE PIECE DESIGN, AND MAKES A MORE POSITIVE GROUND CONNECTION.

THE MICRODOT CONNECTOR
AN ELECTRICAL SWITCH?

FLOATING
NUT

CONTACT MUST BE MADE
AT THIS INTERFACE TO
PREVENT OPEN CIRCUIT

SHIELD
GND

SIGNAL/
POWER
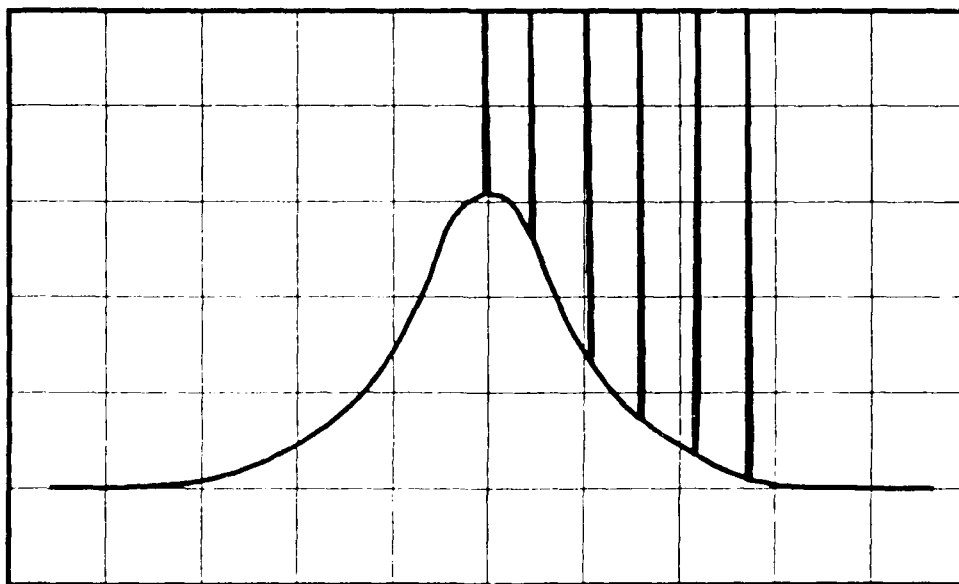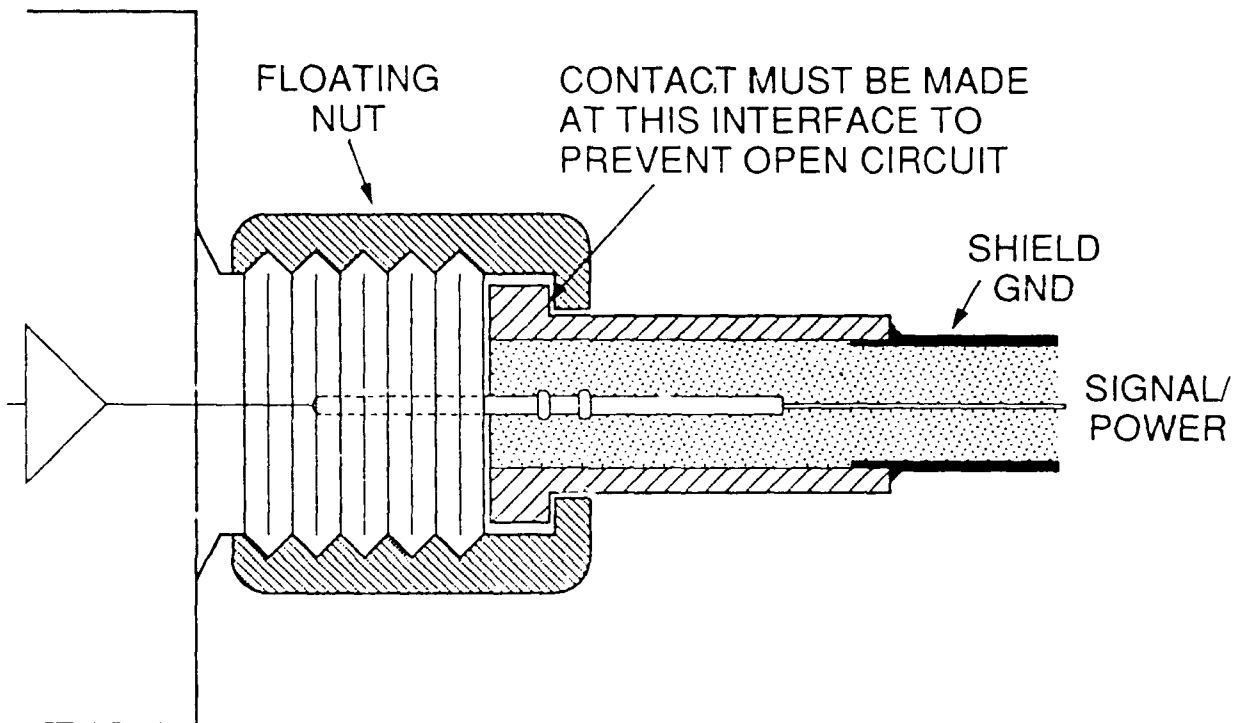
ERRATIC CONNECTION USUALLY PRODUCES
FULL SCALE SPIKES

SIG/PWR

GND

FUSED
GLASS/METAL
FEEDTHRU

GND
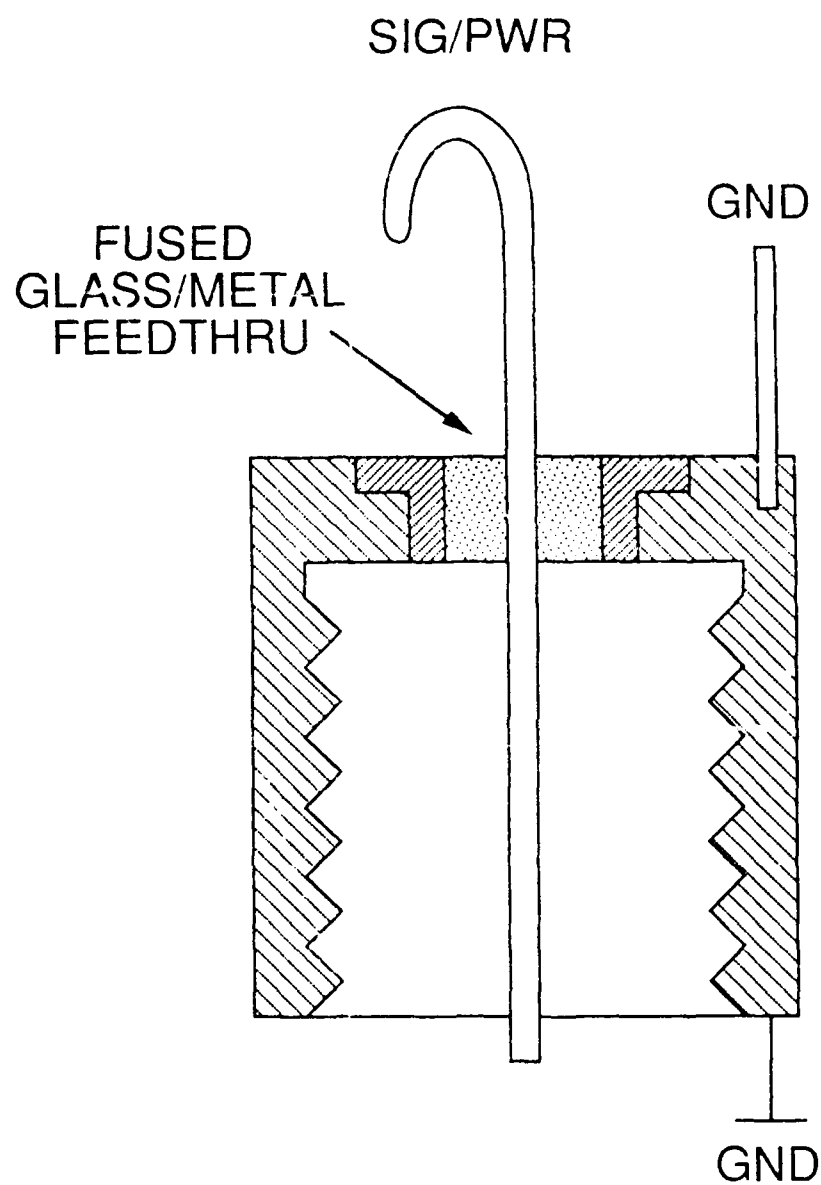
070A09
10-32 SOLDER CONNECTOR

COMPLEX SYSTEMS

SEE ILLUSTRATION-COMPLEX SYSTEM

THIS ILLUSTRATION IS NOT NECESSARILY THE APPLICATION ENGINEERS

PERCEPTION OF YOUR DATA ACQUISITION SYSTEM. HOWEVER, IT IS NOT UNUSUAL

FOR THE APPLICATION ENGINEER TO BE ASKED TO INTERPRET THE OUTPUT DATA

AFTER IT HAD BEEN RATHER EXTENSIVELY CONDITIONED.

AFTER PURSUING POSSIBLE SENSOR INSTRUMENTATION PROBLEMS INCLUDING

GROUND LOOPS, CABLE INTEGRITY, AND OTHER ENVIRONMENTAL CONDITIONS, HE

WILL MOST LIKELY SUGGEST:

     1.   LOOKING AT THE INPUT ON A REAL TIME BASIS TO DETERMINE

     IF THE INPUT IS GOOD OR

SEE ILLUSTRATION-492A SENSOR SIMULATOR

     2.   TO PROVIDE A KNOWN INPUT TEST SIGNAL DISCONNECT THE

     SENSOR AND APPLY A KNOWN TEST SIGNAL FROM THE 492A SENSOR

     SIMULATOR. THE 492A PROVIDES A 100 Hz SQUARE OR SINE WAVE

     INPUT OF KNOWN AMPLITUDE.

ONCE YOU HAVE DETERMINED THAT THE INPUT SIGNAL LOOKS GOOD, THEN IT MAY

BE A JOB FOR A SYSTEMS ANALYST!

SENSOR SIMULATOR

Model 492B
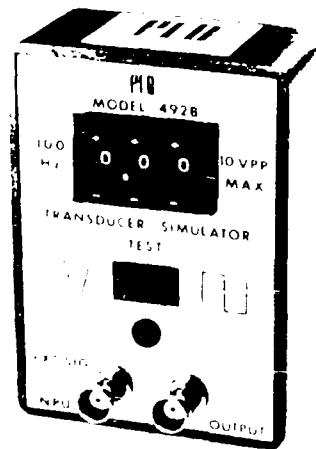
SPECIFICATIONS Model No		492B
Gain (Isolation Amplifier)		unity (1.0)
Oscillator Frequency (sq. or sine wave) Hz		100
Oscillator Voltage (pk. to pk. adjustable) V		0.10
Size (h x w x d)	in	4 x 3 x 1.5
Connectors		BNC
Batteries, two std 9V (not supplied) V		18

CONCLUSION

WHILE DYNAMIC MEASUREMENTS MIGHT STILL BE <u>SELDOM</u> ROUTINE, THEY ARE
BECOMING MORE AND MORE ROUTINE. INCORPORATION OF BUILT-IN
MICROELECTRONICS HAS IMPROVED PERFORMANCE, SIMPLIFIED OPERATION AND
MADE SENSORS MORE TOLERANT OF ADVERSE ENVIRONMENTS. IN ADDITION TO
GREATLY REDUCING THE PER CHANNEL COST.

TODAY, ICP TYPE SENSORS ARE USED EXTENSIVELY AND SUCCESSFULLY FOR
UNATTENDED CONTINUOUS MONITORING OF DYNAMIC PHENOMENA ON MACHINERY AND
STRUCTURES IN TOUGH FACTORY, FIELD, AND UNDERWATER ENVIRONMENTS.

WHEN YOU GET INVOLVED WITH THAT "UNUSUAL APPLICATION", SEEK APPLICATION
ENGINEERING SUPPORT - DON'T USE THE "DART BOARD" APPROACH.

SEE ILLUSTRATION-DART BOARD

Latest Technology
QUARTZ ACCELEROMETERS
with built-in electronics

High Accuracy
rmal and Base Strain San

ation	High Temp.	Low Cost OEM		Rugged Industrial		Triaxial	High Sensitivity	Shear Gener Purpo
UMBER n modes	302A21	307A21	321A	328B02		342A	346A	348A	3
(3) m v/g	15	50 ★	100 ★	100	1000	50 (± 2%)	50 ★	100 (±2%)	5
output ± g	60 (±2.5V)	100	50		5	100	100	50	
g	0.0	0.002	0.001		0.0005	0.002	0.002	0.001	
mid 2 kHz	30	40		18	7.2	25	10	20	
ge ±5% (6) Hz	5-3000	1-4000	1000	0.4-1000 ★	1-2000	1-3000	2-1000	1-2000	1
Hz		0.4-6000 ★				0.5-6000		0.5-4000	
uency µS		10		10		10	10	10	
Time > s		0.5		1.2	1			0.5	
arly zero straight ne									
edance ★ k ohm	1000	100	100	100	100	100		100	
max %		5	5	0.5 ★	5	5	5	5	
g√ in		0.03	0.05	0.01	0.001	0.002 ★	0.002 ★	0.0005 ★	0
Range °F	-100 +400	65 to +250	100 +300	5 +160	0 to +150	00 +250	-100 to +250	-100 to +250	65
cient max %/°F	0.03	0.03		0.05	0.04	0.03	0.03	0.03	
max ±g pk	500	500	500	500	100	500	500	250	
g pk		5000	1000	600				250	
quartz	upright	upright	upright	upright	flexural (ceramic)	so-strain ★	so-strain ★	so-strain ★	she

Instrumentation System Requirements

For Measuring

Time Varying Phenomena

Pat Walter

Sandia National Laboratories

I. Basic Measurement System Considerations for Static and/or Dynamic Measurands

A. System Must Incorporate Evaluated Components

1. Calibrate Components Over Range of Use

2. Test Components in Use Environments

   a. Vibration

   b. Mechanical Shock

   c. Temperature

   d. Electromagnetic Radiation

   e. Humidity

   f. Etc.

2. Accomplish as Close as Possible to System Use and Repeat After Termination of Measurement and During Quiesent Periods if Required

3. Cover all Frequencies and Amplitudes of Interest

4. Reference: RCC Document 118-79, Test Methods for Telemetry Systems and Subsystems, Volume 1, End-To-End Test Methods for Telemetry Systems, Chapter 2, Test Methods for Transducer Based System Calibration, pp I-2-1 to I-2-35, Available: Secretariat, Range Commander's Council, White Sands Missile Range, NM

B. System Calibrations are Required
1. Account for all System Interfaces
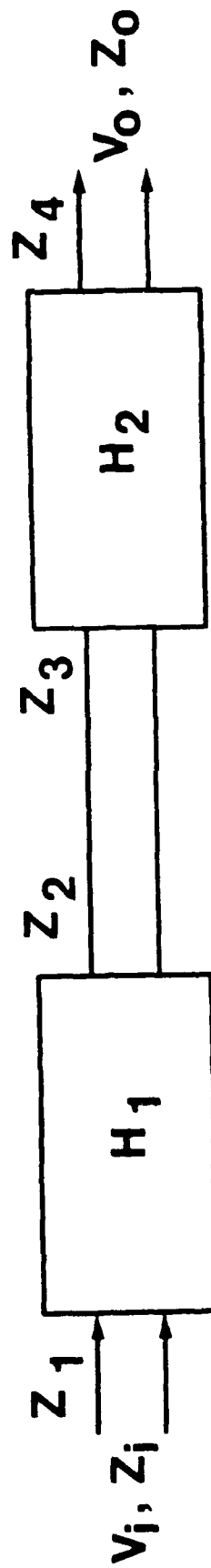
$$v_1 = \frac{v_i z_1}{z_i + z_1}$$

$$v_3 = \frac{v_i z_1 z_3 H_1}{[z_i + z_1][z_2 + z_3]}$$

$$v_o = \frac{v_i z_1 z_3 z_o H_1 H_2}{[z_i + z_1][z_2 + z_3][z_4 + z_o]}$$

Note: $v_o = H_1 H_2 v_i$ if Input Impedances
z_1, z_3, z_o are Large and Output Impedances
z_i, z_2, z_4 are Small

Recall: All H's and Z's are Complex Functions of
Frequency Typically Displayed as Bode Plots

193

C. System Signal/Noise Must be Documented
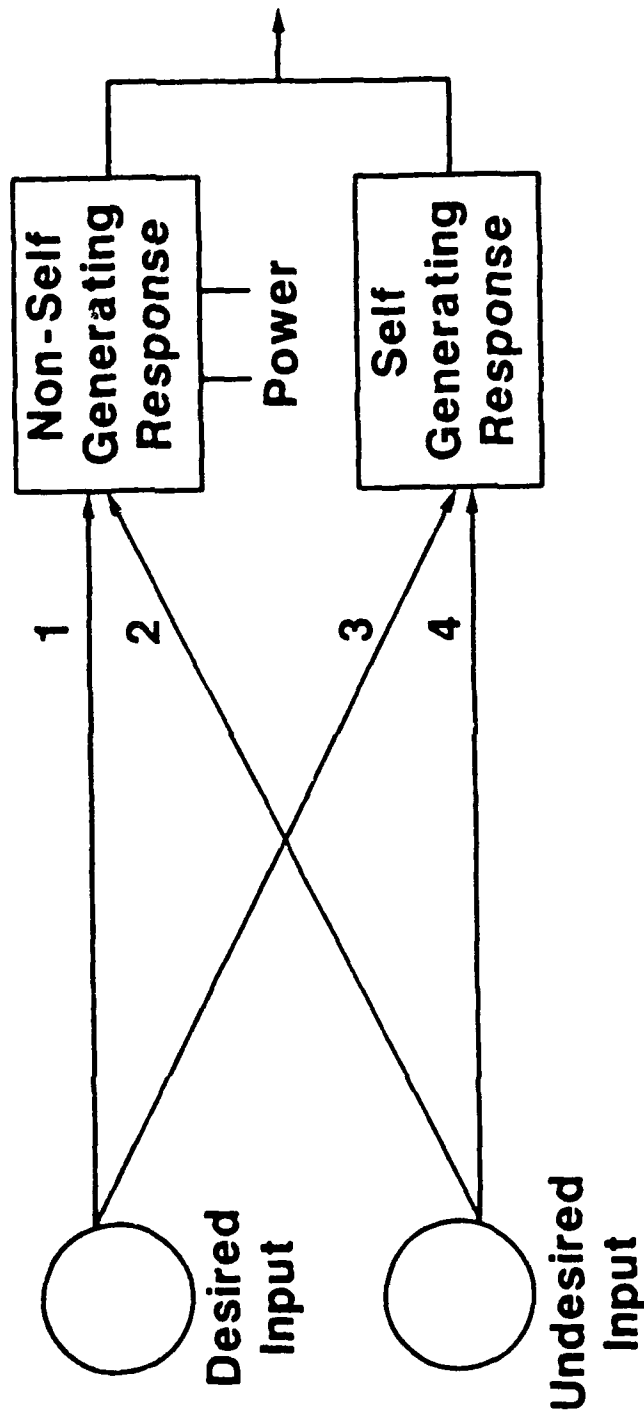
- e.g., Define Signal to be Path 1
  Noise Checks:
  Remove Power Yields Paths 3 & 4
  Removed Desired Input Yields Paths 2 & 4

- If When the Desired Input is Removed There
  is no Path 2 & 4, and When Power is Removed
  There is no Path 3 & 4, Then the Measured
  Output is the Desired Signal Path 1 (i.e., Noise = 0)

II. Measurement System Examples

A. Simple System

Transducer — Cable — Recorder
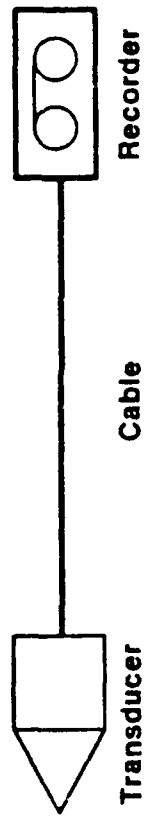
B. Complex System (RF Telemetry)

Transducer — Amplifier — Filter — Encoder — VCO — Transmitter — Flight Antenna

Ground Antenna — Pre-Amp — Multicoupler — Receiver — Diversity Combiner — Discriminator #1 — Decomutator — Discriminator #2 — Recorder
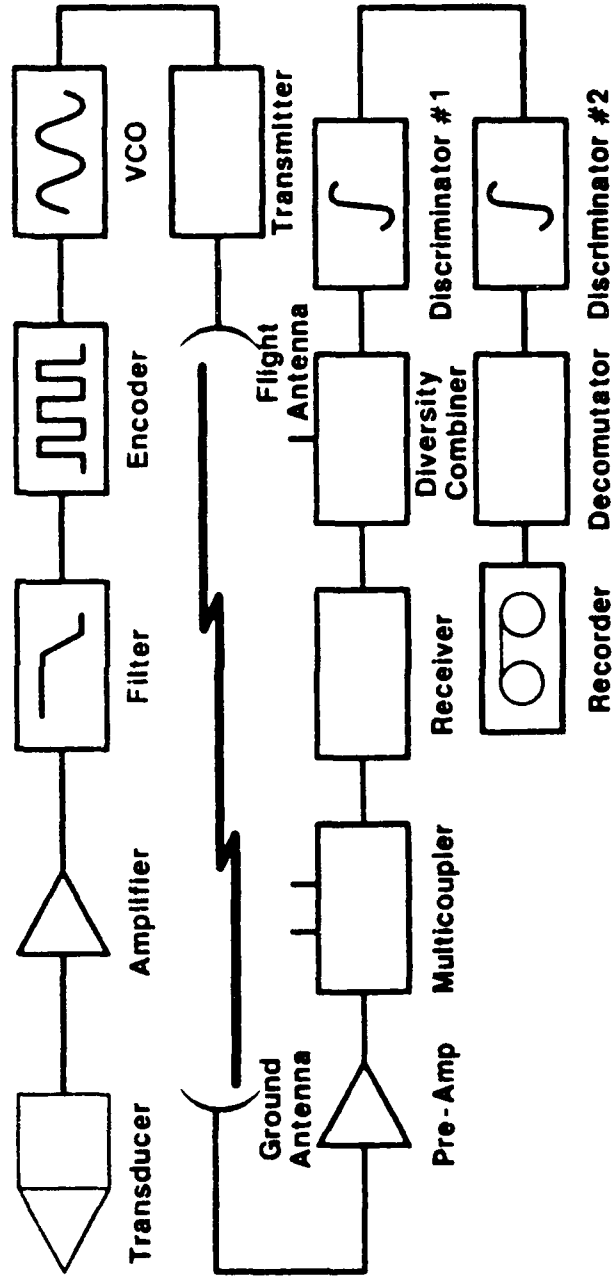
III. Types of Time-Varying Measurands

A. Sinusoid
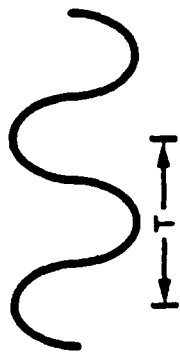
B. Periodic
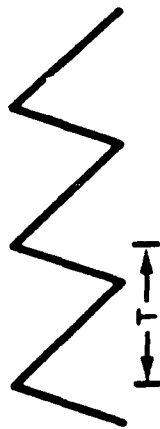
C. Random
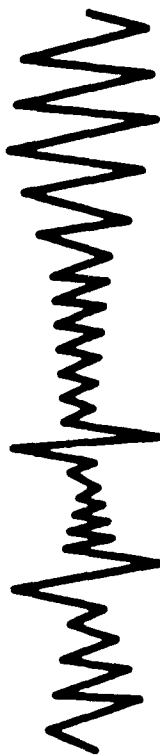
D. Pseudo-Random
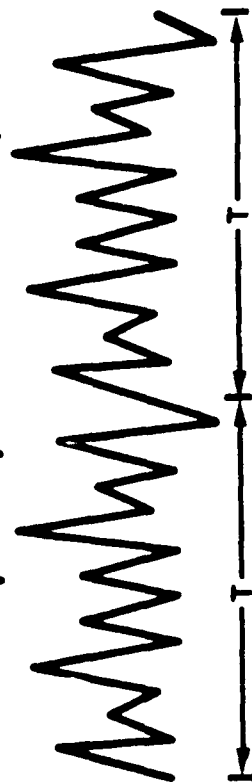
E. Transient
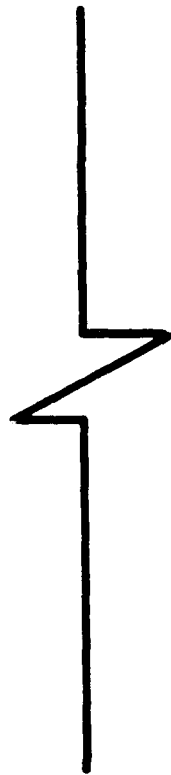
IV. Frequency Domain Representation of Time-Varying Measurands

f(t) ⟷ F(jω)
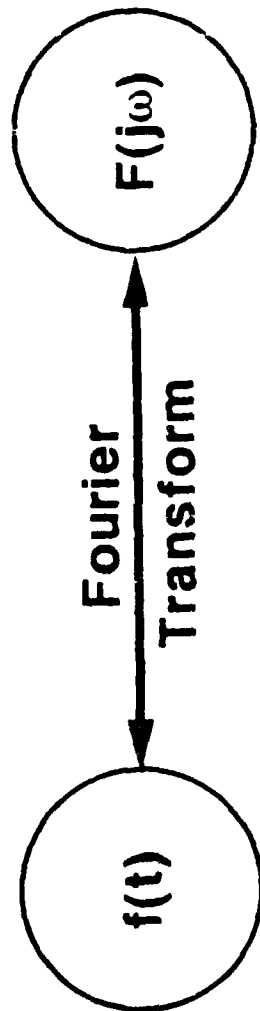
Fourier Transform

A. Deterministic Signal (e.g., Sinusoid, Periodic, Transient) Representation

   1. Fourier Transform

   2. Fourier Series

B. Nondeterministic Signal (Random) Representation

   1. Power Spectrum

   2. Cepstrum

197

V. Ideal Measurement System Requirements of Flat Amplitude Response, Linear Phase Response, and Linear Input-Output Relationship

A. Flat Amplitude Response

Amp

Frequency

B. Linear Phase Response

φ
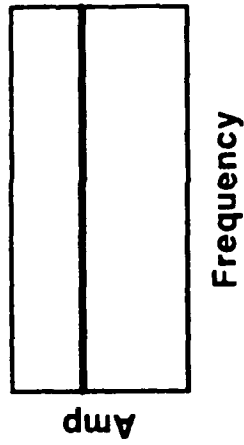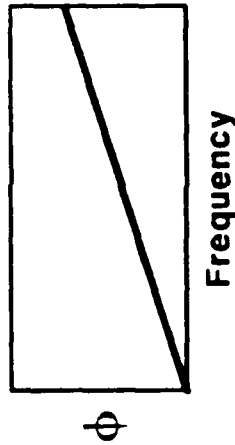
Frequency

C. Linear Input/Output Relationship

Input

Output
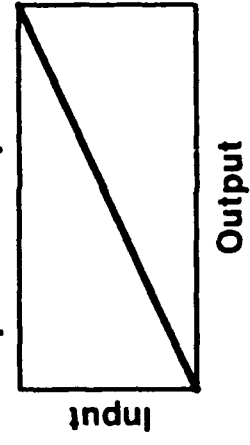
VI. Problems in Deviation in Amplitude Response From Flatness and Phase From Linearity

A. High Pass First Order System

$$RC = \tau$$
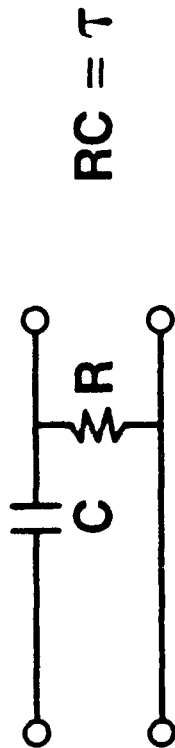
1. Amplitude Frequency Response
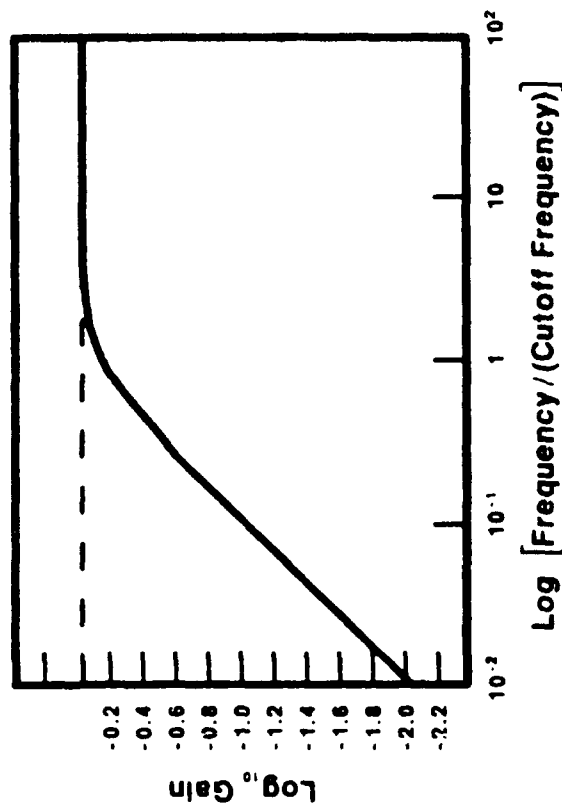
2. Phase Frequency Response
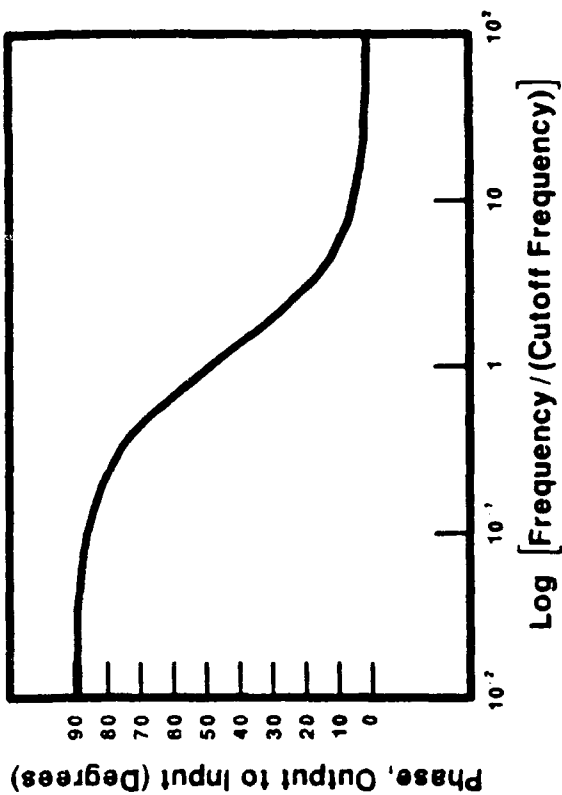
3. Distorted Response to a Half Sine

$t_c/\tau = .2$

Nondimensional Amplitude

Nondimensional Time
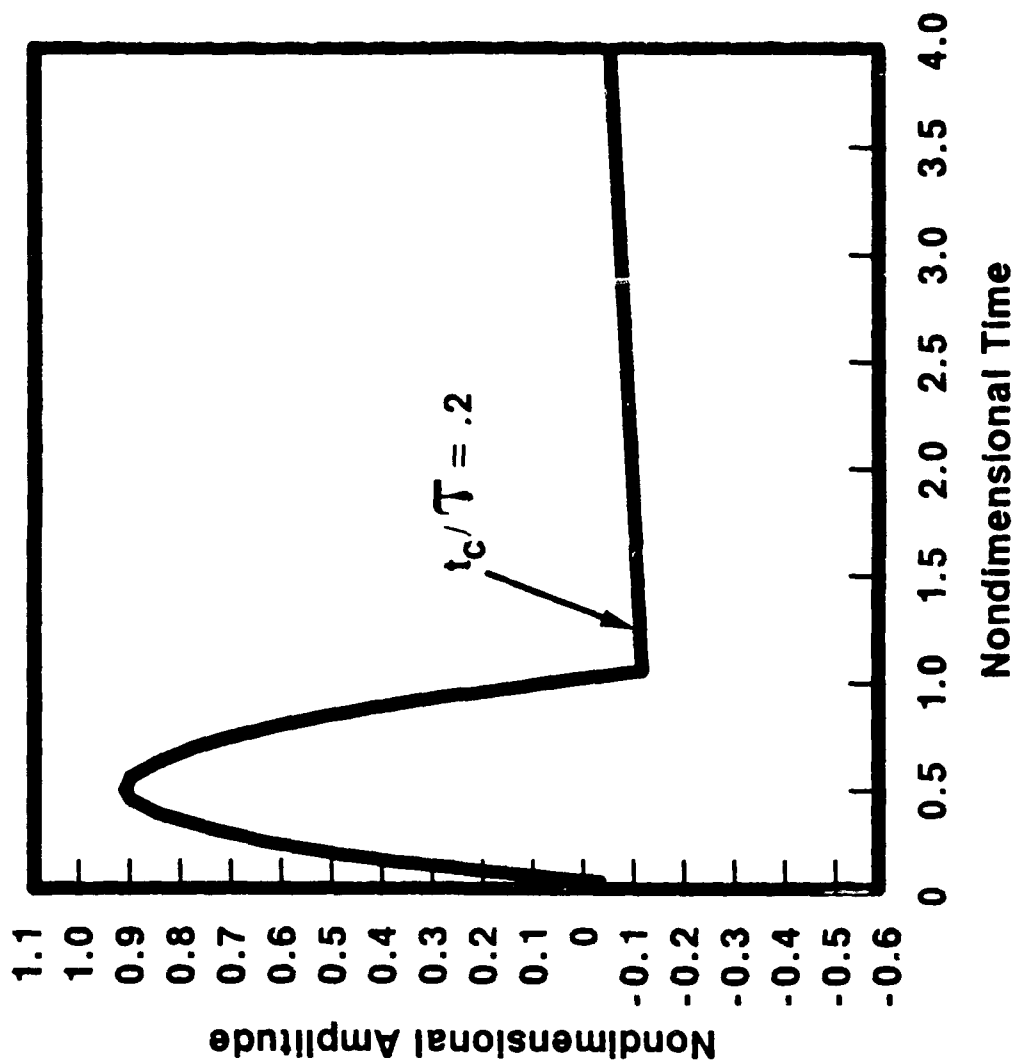
B. Low Pass Second Order System

2. Phase Frequency Response
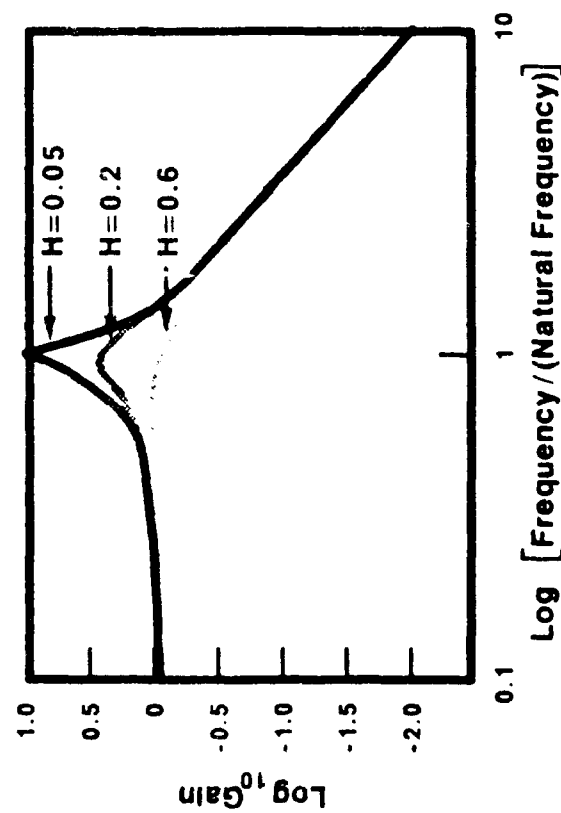
1. Amplitude Frequency Response
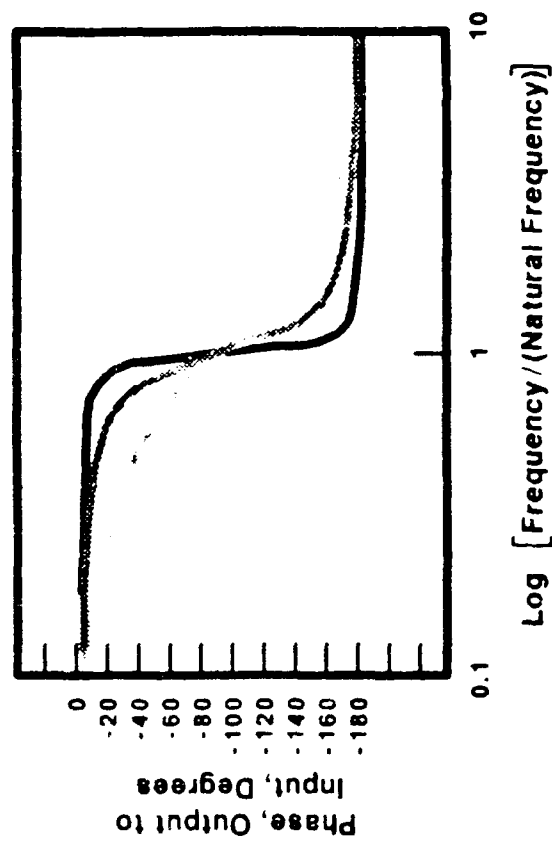
3. Distorted Responses to a Half Sine Pulse (Damping=.05 Critical)
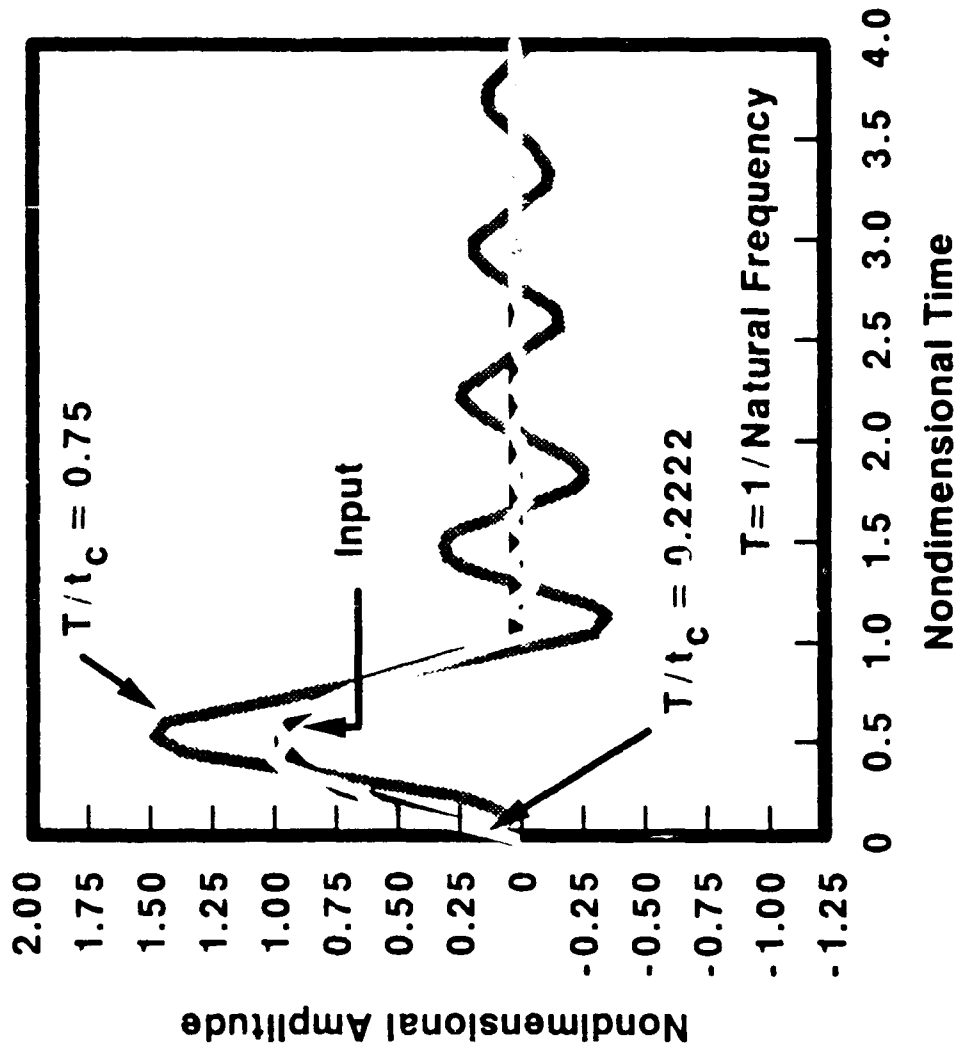
C. Isolate Phase Non-Linearity Effects From Non-Flat Amplitude Response Effects

1. Periodic Input Time Function
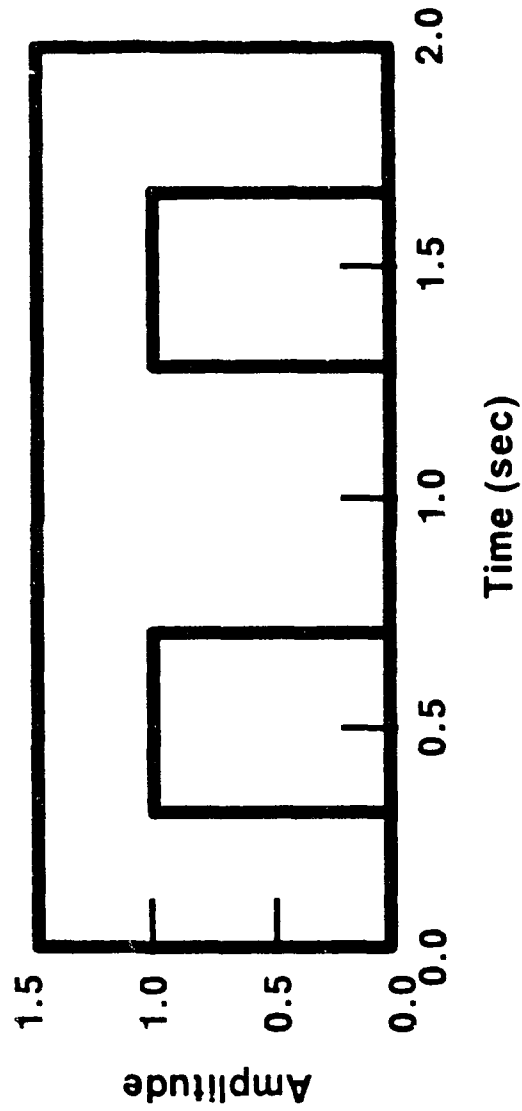
2. Ideal "Boxcar" Lowpass Filter Amplitude Frequency Response
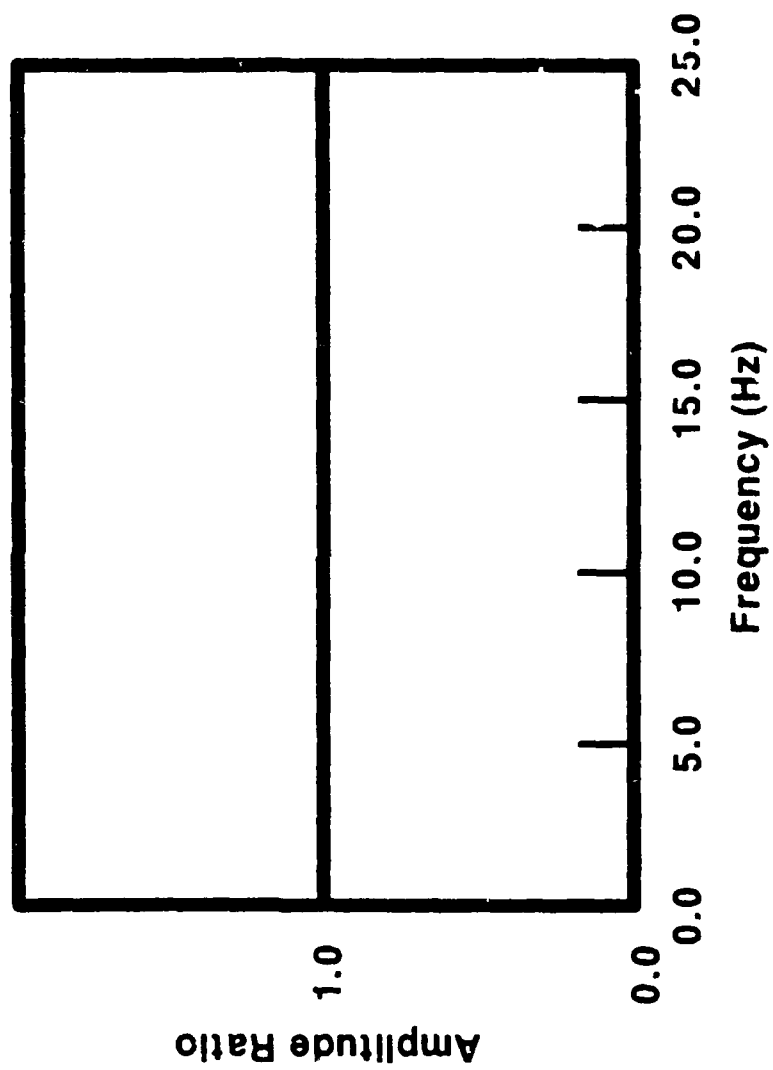
3. Phase Frequency Responses Associated with "Boxcar" Filter

Curve labels: $\phi = \sqrt{2\pi\,\omega}$, $\phi = 0.2\,\omega$, $\phi = \dfrac{\omega^2}{250\,\pi}$, $\phi = \dfrac{\omega^3}{12{,}500\,\pi^2}$

Vertical axis: Phase Lag (radians) — 0.0, 5.0, 10.0, 15.0, 20.0, 25.0, 30.0, 35.0

Horizontal axis: Frequency (Hz) — 0.0, 5.0, 10.0, 15.0, 20.0, 25.0
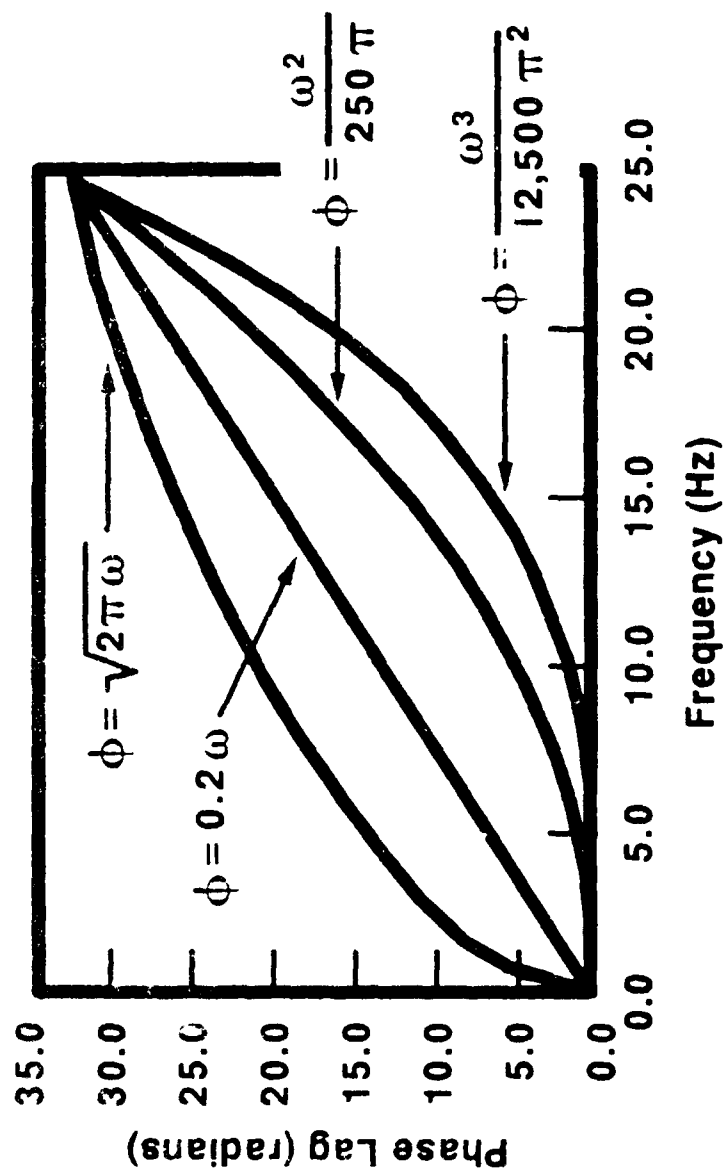
4. One Period of Input Through "Boxcar" Filter With Zero Phase Shift
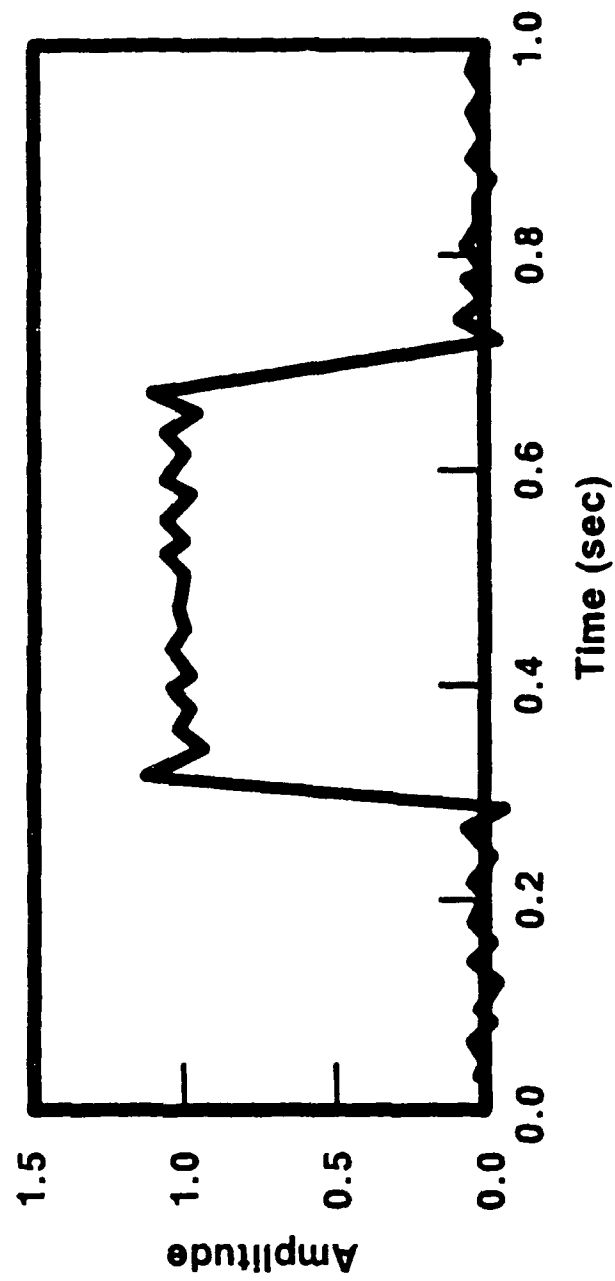
5. One Period of Input Through "Boxcar" Filter With Linear Phase Shift
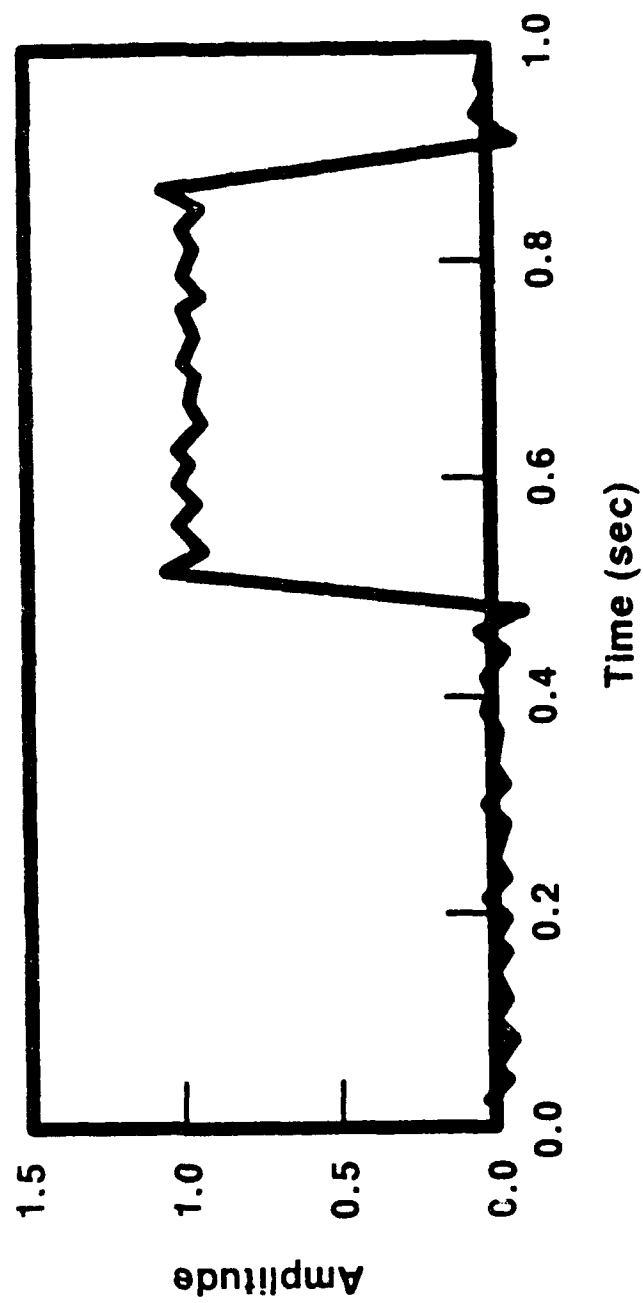
6. One Period of Input Through "Boxcar" Filter With Various Nonlinear Phase Shifts
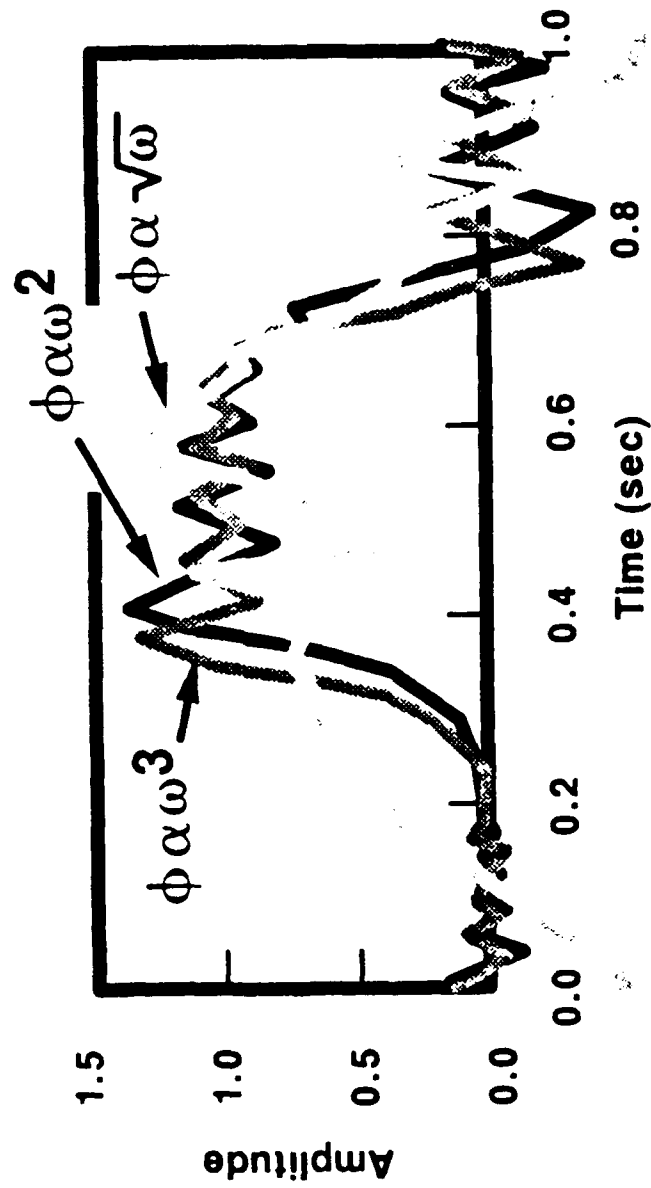
VII. Problems With Nonlinear Input/Output Relations

A. Example of Nonlinear and Linear Process

Nonlinear

$\cos(\omega_1 t)$

$\cos(\omega_2 t)$

X

Nonlinear $\cos(\omega_1 + \omega_2)t$

$\cos(\omega_1 - \omega_2)t$

Bandpass Filter at $(\omega_1 - \omega_2)$

$\cos(\omega_1 - \omega_2)t$

X Nonlinear

$\cos \omega_2 t$

$\cos(\omega_1 t)$

$\cos(\omega_1 - 2\omega_2)t$

Bandpass Filter at (ω_1)

$\cos(\omega_1 t)$
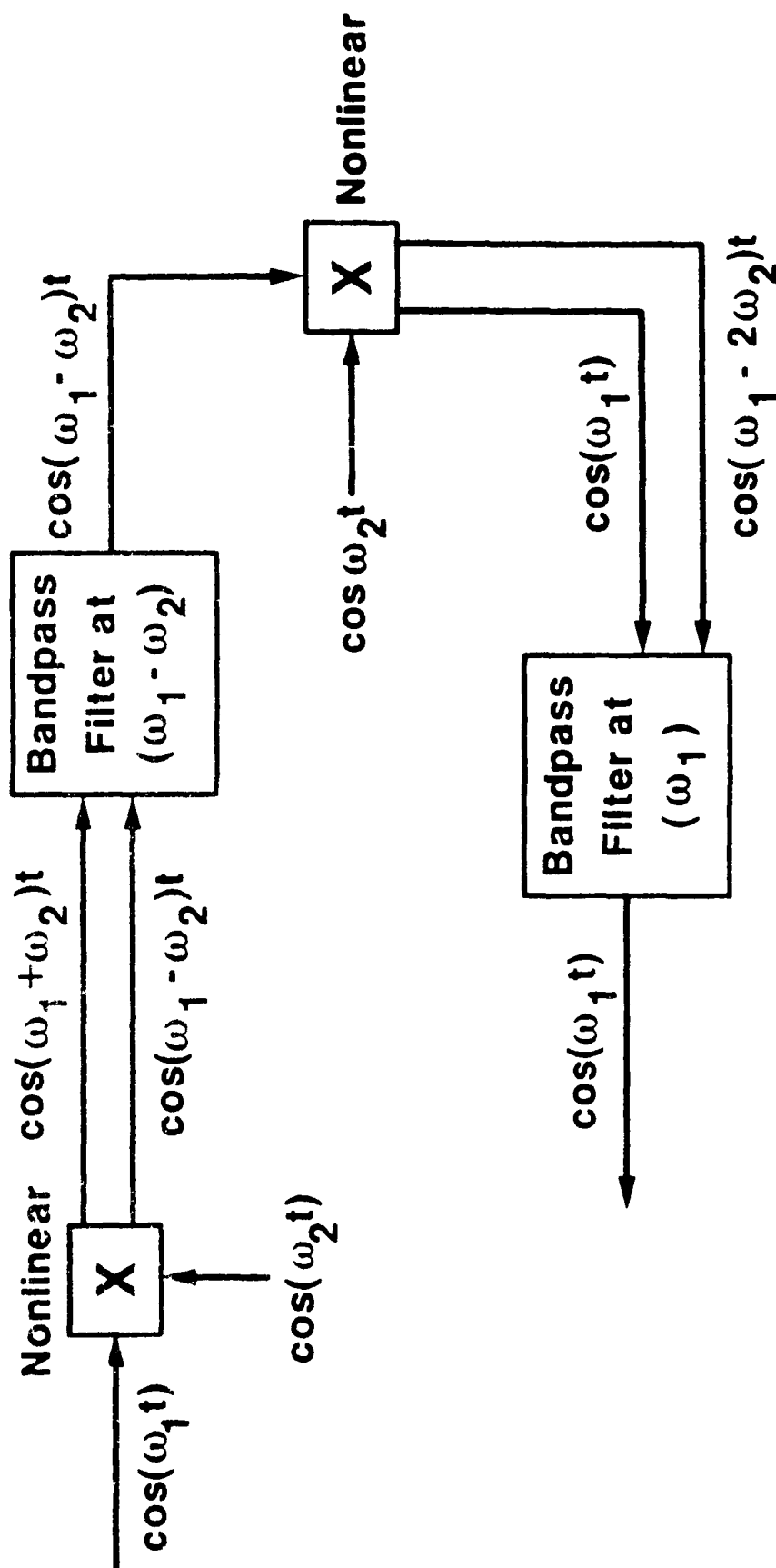
Overall Linear Operation

209

B. Slew Induced Nonlinearities in Operational Amplifier

1. Signal Slope $2\pi Vf$ Exceeds Amplifier's Slew Rate In Filter Configuration

2. Curve A Acquired at 60 Percent of Filter Full Scale Low Frequency Output

3. Curve B Acquired at 20 Percent of Filter Full Scale Low Frequency Output
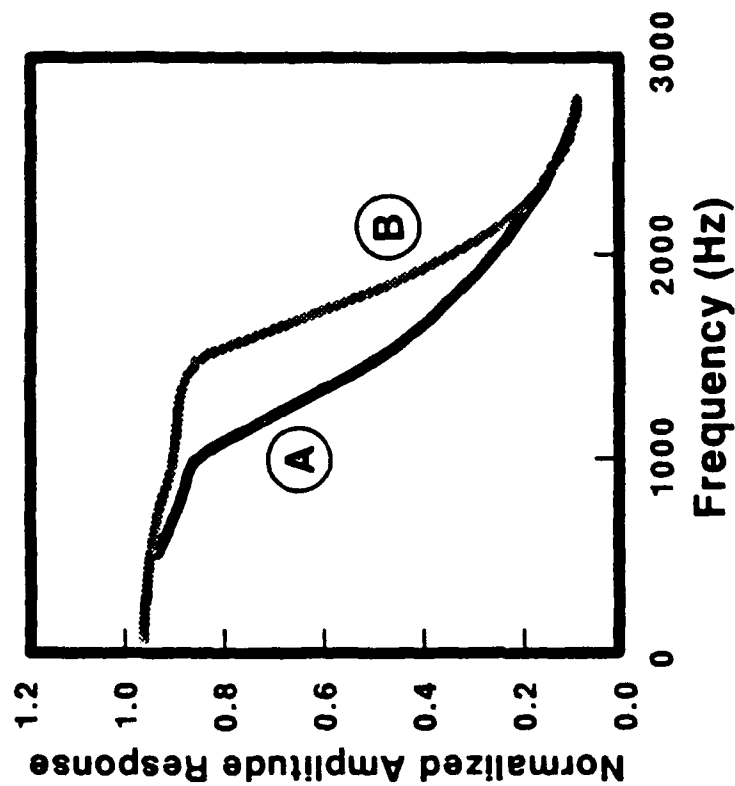
4. 100 Hz and 1600 Hz Linearity Checks
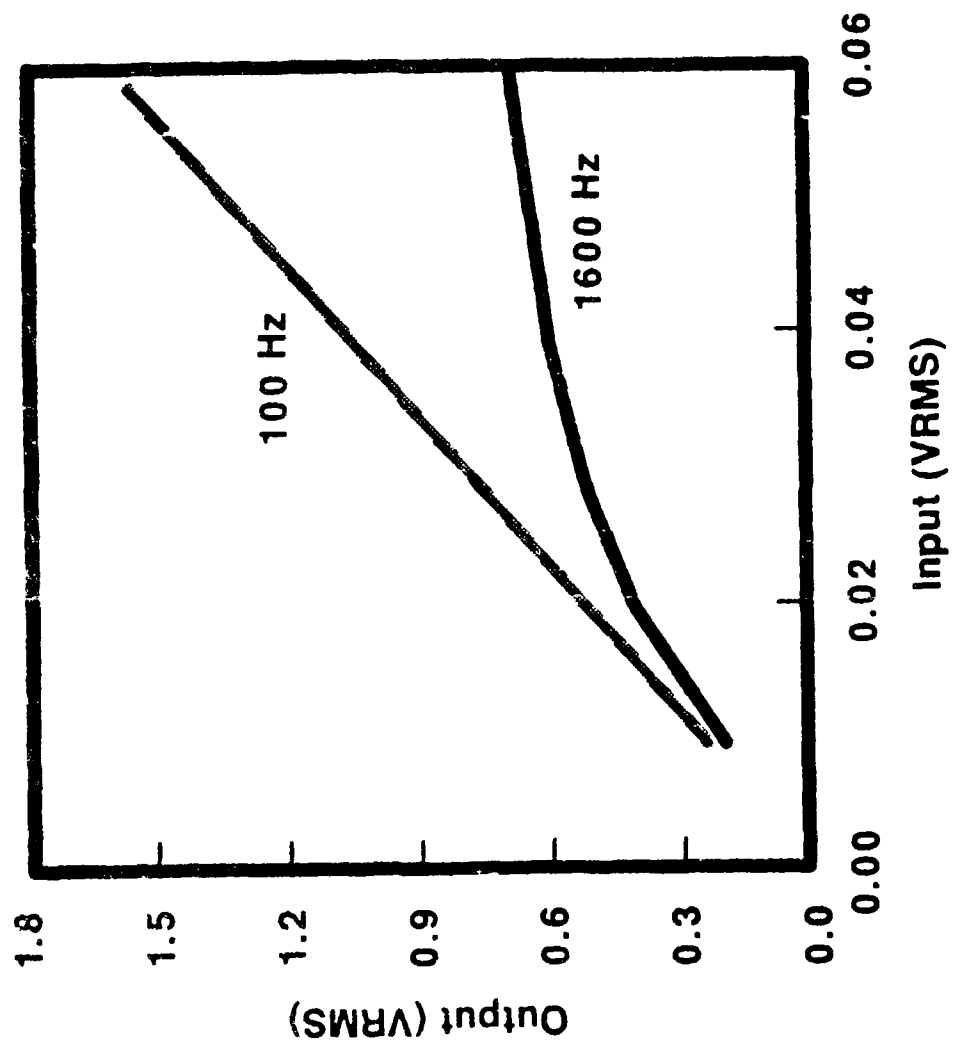
VIII. Conclusions

A. Evaluated Measurement System Components are Required

B. System Signal/Noise Must be Documented

C. Requirements for Measuring Time-Varying Phenomena Include:

   1. Flat Amplitude vs. Frequency Response

   2. Linear Phase vs. Frequency Response

   3. Linear Input/Output Relationship

D. System Calibrations Must Verify Requirements of Conclusion C are Met

212

SESSION 4

DATA ACQUISITION

PROGRAMMABLE TRANSDUCER MICROCHIP DEVELOPMENT

Kenneth E. Appley
Manager-Electrical Engineering
Vibra-Metrics,Inc.
Hamden, CT U.S.A

Richard Talmadge
Senior Electrical Engineer
Flight Dynamics Laboratory
Air Force Wright Aeronautical Laboratories
Air Force Systems Command, USAF

ABSTRACT

Miniature piezoelectric, piezoresistive, and resistive transducers are now used in diverse applications, in large numbers for a single test, in permanent and temporary installations, and in remote and harsh environments. Much processing of the transducer signal is accomplished with unique external equipment. Matching varying applications requires selection of both a transducer and the interface configuration involved with conditioning the sensor data. This paper describes the work in progress of a project to facilitate application of these transducers by developing an integral chip with field selectable functions operated over a common interface.

INTRODUCTION

The purpose of the project is to define, design, fabricate and test signal conditioning and processing electronics in a microchip that will be integral to miniature transducers.

Although these transducers differ in their structure and function, it is the commonality of the application considerations that contribute to the extension of a single chip for use in capacitive and resistive sources.

The specific goals for the chip design are to:

a) provide conditioning and processing of the sensed input signal including impedance matching, filtering, gain selection, integration/differentiation, and calibration,

b) generate output codes that permit remote sensor identification and test signals for evaluation of signal quality,

c) minimize the effects of temperature variations and excessive input signals,

d) use a common interface to external processing equipment, and

e) provide the capability to configure any selectable features in the field (after the chip is installed in the sensor).

Another aspect of the project is the choice of the chip fabrication technology. The classical approach would be to breadboard the functions with discrete components, to fabricate a reduced size single unit, and then to create a unique mask set for the chip manufacture. In recent years the advent of practical semi-custom and hybrid processes has created alternatives to the classical approach.

SENSOR BACKGROUND

Although the subject of this paper is the transducer electronics, some discussion of the basic sensing mechanization and interface considerations will give perspective to the chip design.

Piezoelectric

A piezoelectric transducer transfers vibratory force, shock force, pressure force or direct force to a piezoelectric crystal which responds with a charge developed across two opposite faces. (For purposes of clarity the outputs from these various transducers are referred to as Engineering Units (EU).) The charge with certain bandwidth restrictions is proportional to the applied acceleration, pressure or force.

Resistive

A resistive transducer consists of a wire or conductive path whose resistance changes as it is elongated and a platform for attaching this sensing element to the surface to be measured. The change in resistance is small and is usually converted to a voltage by making the sensing element a leg in a "bridge" circuit.

Piezoresistive

This transducer is similar to the resistive type, except the sensing element is a piezoresistive material.

Interface

The output signal of the basic transducers can be sensed directly, but in some applications the signal levels are low and even with care in transmission the signal is not much greater than the noise. In those cases the distance to the amplification must be short to recover a usable signal. The capacitance and resistance of the cable to the remote amplifier also affect signal quality and limit the use of the sensed data. Special transmission techniques and interface hardware have been developed to compensate for the problems inherent in data acquisition from these transducers.[1]

As with most sensors, the basic elements are limited in their range of output and are sensitive to changes in temperature, humidity and pressure. These characteristics are usually addressed through construction of units designed for a specific application and environment.

FABRICATION TECHNOLOGY

The possible use of alternate technologies needs to be considered at the beginning of the project, since the final implementation is limited by the availability of components or use of defined building blocks and, therefore, the design becomes a function of these factors in addition to the desired performance specifications.

Preliminary investigations into available alternatives to the classical approach to chip fabrication have resulted in the following comparisons.

	Classical	Thin Film	Std Cell
Development Cost (includes proto qty.)	Med+ (1)	Low (1-5)	Med (25)
Time to Production (after design concept)	10-12 mo	5-6 mo	7-9 mo
Production Unit Cost			
Qty. 100	High	Med	Med+
1000	High	Med-	Med
1000+	Low	Med-	Med-
Cost of Revision			
Breadboard	Low	Low	Low
Proto	Med	Low	High
Time for Revision	3-4 mo	1-2 wk	1-2 mo

Although the investigation has not been that rigorous or exhaustive (based only on budgetary vendor and engineering estimates for an assumed circuit complexity), the indication is that a thin film approach has the advantage of the earliest results with the least cost for the anticipated initial quantities. The low cost and faster turnaround of revision is also attractive for a development project. The classical approach has the best chance of reaching the final chip size goal and may be ultimately necessary for the production chips.

DESIGN APPROACH

System Considerations

Before detail design of the microchip can begin some questions must be answered and some trade-offs made concerning the operation of the transducer in a data acquisition system. The areas addressed involve the interface, processing, testing, and ...

Transducer Interface

One of the goals of the project is to develop a practical transducer interface that will be common to many types of sensing elements. (The connection to the sensing element will be unique to the input and made at the time of installation in a transducer).

To be fully functional the microchip will require an interface module that supplies power, provides a path and conditioning for programming data, receives transducer AC and test signals, and drives recording and analysis equipment.

A question that has not been resolved at this point is if there is a need to provide an interface to existing installations (with the loss of any interactive functions and with a modification for added power).

The common output interface is anticipated to be a standard two-wire or coaxial transmission line. A ?-wire interface is being considered to allow larger signal swing, to facilitate circuit isolation and reduce the internal power conditioning requirements.

Processing

Some processing functions are easily defined based on present applications (impedance matching, filtering, gain, integration, differentiation). Others require more analysis as to their need generally and their value as an integral part of the transducer (FST thresholding, A/D conversion, averaging)

Testing

Testing of installed transducers is becoming necessary due to increasing applications in remote or inaccessible locations, and for monitoring accuracy for units operating for longer periods and in harsh environments.

The chip operation can be monitored either by routine signal level checks or by more rigorous frequency analysis and reasonableness checks of the processing. Other testing questions relate to completeness (i.e., applying signals through the sensing element, exercising all ranges and functions), analysis performed remotely or on the chip (i.e., report status only) and the response to a fault condition (i.e., force the output to a fixed level to generate an error status).

Calibration is usually requiring some reference to be applied either remotely or at the transducer. In each case some switching of the normal signal is needed.

Control

One of the most significant contributions the microchip will make to transducer application is that of having field selectable functions. This will greatly reduce the need for various types of transducers, allow definition of the data collection system before the data characteristics are well defined, and permit the use of a single system for a wider range of tests

User questions related to a programmable system involve the complexity of the programming hardware and its use. It is planned that the microchip will be programmed through the transducer common interface using an RS-232 connection to a PC. All chip functions will be bit selections that will be retained in nonvolatile memory on the chip until reprogrammed.

MICROCHIP FUNCTIONS

Figure A is a block diagram of the microchip functions and the major data paths. The "FS" input lines are the control bits indicating programmable selections for that function.

The input signal from the selected sensor is filtered, gain adjusted (including attenuation), and either passed directly, integrated or differentiated, and driven to the transducer common interface. Program data is received and test data is also transmitted over the common interface.

The characteristics of each block are:

a) Capacitive Sensor Input - receives signals from piezoelectric sensing elements having a sensitivity from 1 mv/EU to 1 v/EU and a capacitance range of 50 to 1,000 pf.

(Although present devices have larger ranges this has been done to achieve the largest signal to noise ratio at the source. This will not be necessary with the electronics at the sensing element.)

The input impedance selection occurs at this stage. Selections are from 1 x E7 to 10 x E9 in nine discrete steps (i.e., 1, 2, 5 10 in each range)

Input overload protection (i.e., prefiltering) is applied before the first amplifier. (2)

b) Resistive Sensor Input - receives signals from bridge type strain gages having sensitivity from 1 to 20 mv/EU, and having a resistance in the range of 100 to 1000 ohms. As with the Capacitive Sensor Input, a reduced range is usable with the electronics at the sensing element. A current source strain gage (3) input may also be provided.

c) Input Select - factory connection based on the type of sensor.

d) Filter - a high pass Butterworth filter having a 24 dB per octave cutoff with a selectable 3 dB point at 1, 5 or 10 Hz and low pass filter with a

selectable 3dB point at 0.5, 2, 5, or
10K Hz. The rolloff of the low pass
filter may be selectable to accommodate
a smooth tailoring of compensation for
crystal resonance and therefore, extend-
ing the transducer bandwidth. A bypass
selection of either or both filter
sections is also possible.

e) Gain - selections of x1, x10, x100
increase or decrease in signal ampli-
tude. Automatic gain control could be
applied, but this would require an indi-
cation to the data acquisition equipment
of the magnitude of the new gain factor
and at what point the change occurred.

f) Integrate/Differentiate - one or two
stages of integration or differentiation
of the filtered signal is selectable.

g) Output Select/Drive - an analog
selection between the sensed signal and
the test data. The output is a low impe-
dance cable drive. The selection is made
on command from the Interface Module.

h) Power - generates the voltage levels
needed for chip operation and sensor
bias. Changes in power levels are sensed
to initiate control actions.

i) Test - generates test excitation
signals and evaluates responses, and
generates serial output data. The test
data is selectable by external command
and could include a status code with
summary operating conditions, a pulse
train of variable length and frequency,
and an ID code (an ASCII pulse train
with the model, transducer type, and
location coded).

j) Control - decodes commands and sets
conditions to control operation.
Commanded operations include:
        - input new stored data,
        - transmit ID code,
        - transmit pulse train of "n"
          pulses at "m" frequency,
        - perform test,
        - perform calibrate.

The output will remain in the sensor
signal condition until a command is
received.

FIGURE A. MULTIFUNCTION TRANSDUCER MICROCHIP BLOCK DIAGRAM

SUMMARY

The development of a programmable micro-
chip that can be installed in capacitive
and resistive transducers will eliminate
many of the application decisions now
required to properly instrument environ-
mental testing and data collection.

Applying signal conditioning and pro-
cessing functions at the point of the
sensed signal will improve data quality
while reducing the hardware required for
data acquisition.

Although only the specification and con-
cept phase of the project are complete,
and the detail design and breadboard
fabrication phase is just beginning,
based on experience with related devel-
opments, we feel the project will be
completed successfully. The questions
discussed in this paper will be investi-
gated and resolved in parallel with the
design of the defined chip elements in
the next quarter. Production chips are
planned to be available before the end
of the year.

References:

(1) Noise Immunity - Low Impedance
Systems v. Charge/Voltage Amplifiers;
        Judd, John H.
        Measurements & Control 1980

(2) Pre-Filters In Low Impedance
Accelerometers Eliminate Unwanted High
Frequency Noise;
        Judd, John H.
        AN 115 Vibra-Metrics, Inc. 1980

(3) Non Self-Generating Transducer
Signal Conditioning Techniques;
        Talmadge, Richard
        Flight Dynamics Laboratory
        Air Force Wright Aeronautical
          Laboratories
        Air Force Systems Command, USAF

A COMPUTER PROGRAMMABLE TRANSDUCER MICRO CIRCUIT

Q: **Steve Baker (Oakridge National Laboratories)**: I notice that you have several chips on board right now in the hybrid state and you are finally going to have one chip. Where do you get the power for this chip? Does it come down the line?

A: **Kenneth Appley**: Right, down the line, over the same two wires. This is standard now. That is not new technology. The power is being supplied and the sense signal comes back over the same lines.

Q: **Steve Baker**: Just one or two questions about performance. What's the resolution in terms of bits of your signal? Is it going to be like a 12-bit signal coming out?

A: **Kenneth Appley**: We are still working on that. My first calculation showed that it is probably going to be at least that. Now this is an analog signal coming down the line. There is no A to D converter in it. That is about the resolution that we are going to need. We are not sampling so we don't have all of those problems right now.

Q: **Pat Walter (Sandia National Labs)**: Acceleration signals by definition in nature are typically wild. What logic are you putting into gain changing? What is the criteria to autorange it? The double differentiation is really a tough problem, especially if there is any noise present at all. Any comments on that?

A: **Kenneth Appley**: On the first question, we don't think that accelerometer signals are that wild. We are not trying to assume how this thing would be used or what your environment is. Everything is programmable. We are putting in capabilities to do things and it is up to the user to decide what he wants to do and when. The capability will be there to program gain selections of 1, 10, and 100. So if you find that the things are too high, or that your signals are getting clipped, at that point you can change the gain. It is not an autoranging. Autoranging is a tough thing to do, especially in a test environment. If this device arbitrarily goes out and changes the gain for you, I don't think that you are going to be very happy unless it does two other things: it tells you when it did it, and it tells you by how much it did it. Now those two things are a little more than we want to bite off right now to fit into the data stream. This is not an autoranging device. The whole thing is set up as a programmable device. Some of the programming is done at the factory. Some of the programming is to be done as the device is installed, and then others in on-line programming. The gain change and frequency response, those are things we feel that you would probably want to do installed. In other words, you do not want to take the accelerometer or the transducer out and put it on a programmer. That is why one of the program paths is through the interfaces. It is there all of the time. All you have to do is interrupt the data flow. You do that before or after the test. Now, on your other question about double differentiation, we don't know what we are going to do with that second stage of differentiation. It is talking about disappearing unless somebody here can really see a need for it. The double integration is ob-

viously necessary. The first stage of differentiation is good but, we don't know what the noise environment is going to be and double differentiation surely wouldn't help that.

Q: Steve Kuehn (Sandia National Labs): Exactly what does your cell test scheme encompass? Are you verifying that the crystals are actually working, or are you just putting a signal in after the crystal input or what?

A: Kenneth Appley: Right. There's two techniques th t we have used already for accelerometers. In both techniques, the signal goes through the crystal. We are actually injecting it into the crystal. That means that any acceleration you have during the time of the test is going to foul up that test data a little bit. That is under the user's control. You have got to be careful when you are doing some of these things. If you want to verify that your primary sensor is working, it can't be doing other things at the same time and that is obvious. That is the only thing that you sacrifice, but we are injecting the signal directly through the crystal and then evaluating this on the other side. We have the capability of running this pulse train through the crystal, too. There is some thought that by analysis of a square wave signal coming back you may be able to determine frequency responses, so that is why the square wave is in there: for your selection to set the pulse train and the pulse width. It may be very useful in testing to have to know that you have started with a controlled square wave, and see what happens as it comes through your whole system.

Q: Leroy Bates (NSWSES): Are you designing this for a specific application or as a general purpose?

A: Kenneth Appley: No, it's a general purpose. Like I said we are trying not to make as many judgments on how it's going to be used. It is all programmable. We are making judgments on the extent of the program. Like I showed in the one slide depending on how many iterations we have to do around the trade-off loop, trading off the size as to the functionality, like the second differentiation if it doesn't give us enough function, if it really not that useful and it is taking up a lot of real estate, that is one of the tradeoffs that you would make.

Q: Steve Baker (Oakridge National Labs): You haven't talked any about what happens at the PC end, or how you get the data on and off. Have you worked any on that end of it, and if so, what are you planning on providing?

A: Kenneth Appley: On the PC end? We have looked at the protocol and the data transfer, and I have some thoughts on how I am going to do that. It is not going to be very complex. It is not going to require a big software package. It is a standard RS232 interface to send over some ASCII characters. The device will interpret those ACSII characters and set up the system to do that. There will be a minimum of a two-word transfer the way it looks right now, maybe up to as many as a 10- to 15-word transfer to do different things. Another function that we are going to include is temperature compensation.

The sensitivity of crystals in the accelerometer changes with temperature. There will be a sensor on board to sense the temperature and make adjustments in the output as a result of temperature changes.

Q: **Larry Rambert (Allison Gas Turbines):** Have you given some thought to the time between selecting accelerometers? In other words, if you are in a multiplexing system you have to address each one of these things to give you a signal back. Your simultaneity of data is going to be some what degraded, I would think.

A: **Kenneth Appley:** In the initial stages, we are proposing one interface module for the chip. As far as the multiplexing scheme, it is very easy just to multiplex the modules. But that is a system consideration, and has to be of a concern. I haven't calculated loop-time specifically, the time you trigger it until the time you get a response, but it is going to be in the millisecond range. I know that if you are looking at 500 devices, that could be a long time. But that comes down to the system design. In other words, you could set it up so these were addressed in parallel and intermediate memory is there to handle that, or you can just take time off-line and talk to them all. It is completely under your control when the tests are done and when all of the communications are done.

Editors Note: **Dick Talmadge:** I think that there might be a misconception as to what role the PC plays in this system. The microcircuit in a normal measurement mode is transparent to the operation of the transducer. The PC is used to program the function of the transducer (filter characteristics, integration, differentiation, etc.) and is normally done on the bench. At that time, the transducer will store and maintain the functionality and produce an analog data signal output as before. The calibration and self-identification features of the chip require an interface control in the signal-conditioning system to command the responses which are sent over the two-wire data line as a serial bit stream. The signal conditioning system will have to include the processing system for this data or it could be recorded with the data and post processed.

A REMOTE SENSOR/CABLE IDENTIFIER*

William H. Andrews, Jr. and Steven P. Baker
Development Engineers
Instrumentation and Controls Division
Oak Ridge National Laboratory**
Post Office Box 2008
Oak Ridge, TN 37830-6003

ABSTRACT

Errors in field wiring can result in significant correction costs (if the errors are discovered prior to use), in erroneous or unusable data (if the errors are not discovered in time), or in serious accidents (if the errors corrupt mission-essential data). Detailed field wiring checkout and rework are tedious and expensive, but they are essential steps in the quality assurance process for large, complex instrumentation and control systems.

A recent Oak Ridge National Laboratory (ORNL) development, the remote sensor/cable identifier (RSCI), automates verification of field wiring. In the RSCI system, an identifier module is installed on or integrated into each component (sensor, actuator, cable, distribution panel, etc.) to be verified. Interrogator modules, controlled by a personal computer (PC), are installed at the connections of the field wiring to the inputs of the data acquisition and control system (DACS). Interrogator modules poll the components connected to each channel of the DACS and are able to determine the path taken by each channel's signal to or from the end device for that channel. The system will provide not only the ID code for the cables and patch panels in the path to a particular sensor or actuator, but individual cable conductor IDs as well. One version of the system uses existing signal wires for communications between RSCI modules. Another, more powerful version requires a dedicated conductor in each cable. Both versions can operate with or without instrument power applied, and neither interferes with the normal operation of the DACS. Identifier modules can provide a variety of information including status and calibration data.

Details of this technology, which received a 1987 IR-100 Award, and plans for adapting it to NASA launch pad applications are discussed.

INTRODUCTION

As we become increasingly reliant upon computers and other intelligent devices to control equipment and to automate processes, we also increase our dependance on electronic sensors and actuators and on interconnecting wiring. Fortunately, this trend is accompanied by a sharpened awareness of the issues of quality assurance, safety, and reliability.

A DACS comprises several components: the computer/controller, sensors and actuators, signal conditioning/multiplexing circuits, and signal transmission media. Various segments of the instrumentation, computer, and electronics industries are addressing the quality issues relating to these components. Redundancy, higher levels of embedded intelligence, computer-aided engineering tools, on-line self-testing, and innovative design techniques are being applied to ensure quality and to increase reliability.

However, the problems of configuration control and field wiring integrity seem to have eluded such technically sophisticated approaches. DACS today can include thousands of sensors, actuators, intermediate termination points and many cables consisting of miles of wires. Confidence in system configuration depends on the answers to three basic questions: What sensor or actuator is actually connected to which channel? What is the signal path from each sensor or actuator to its connection at the computer/controller? What is the integrity of that path? These questions are very important. Even though individual DACS components function reliably, the resulting data cannot be trusted unless interconnecting wiring is verifiably correct.

EXISTING TECHNOLOGY

The process control industry has begun to address the area of system configuration and integrity in a somewhat indirect manner. Multi-drop communication links are available that simplify the interconnection of digital components and communications standards (e.g., RS-485 or BitBus) promote interoperability by specifying hardware interfaces, data rates, electrical characteristics, and loading factors. Commercially available special-purpose transceivers assist in implementing many of these standards. All of these developments provide tools for attacking configuration control and wiring integrity problems, but, clearly, they are insufficient alone.

For several years, the industry has recognized the shortcomings of purely analog signal links to field devices. A new class of sensors with embedded intelligence is becoming available from process control equipment manufacturers. Most "smart sensors" still use traditional 4- to 20-mA analog current-loop signaling, but high-frequency digital signals can be superimposed for communication with hand-held programmers. This technique limits the use of smart sensors to low-bandwidth DACS. Because of the proprietary nature and incompatibility of the hardware and protocols in existing systems, smart sensors have yet to gain wide acceptance.

In response to these incompatibility problems, the ISA SP-50 Committee is developing the FieldBus standard. This standard will specify signal transmission media, signal levels, and communication protocols for a multidrop serial digital data link for communication between field instruments. Committee members represent manufacturers, government, and end users. The standard should be issued for comment by the end of this year.

PREVIOUS WORK

During the 1970s, the Instrumentation and Controls Division of ORNL began to realize that an automated system for verifying the configuration of large research experiments could be extremely valuable. As the power of available computers increased, the size and complexity of the experiments and processes that they controlled grew and the number of parameters to be monitored and controlled swelled correspondingly. Systems with several thousand sensors and actuators were not uncommon, and configuration control became a major issue.

In the early 1980s, work began on sensor identifier technology, and, after several approaches had been evaluated, the first demonstration system was built and tested in 1984. This system featured a single-board computer that interrogated passive "dumb" identifier devices via the sensor signal wiring. This system was able to provide the identity code of the end device connected to each channel of a star-wired data acquisition system.

DESCRIPTION OF RSCI SYSTEM

The RSCI system expands the capabilities of previous developments by distributing intelligence to the remote identifier modules and is intended for retrofitting to existing DACSs or for integration into new DACSs.

The RSCI system has three basic components as shown in Fig. 1. A host computer and its resident software provide an operator interface and maintain the overall system data base. Intelligent master modules provide the field wiring interface and intermediate storage for configuration data. Intelligent ID modules attached to (or integrated into) each cable, sensor, actuator, or other component to be identified respond to inquiries from their master modules by providing identification, status, and housekeeping data. The RSCI system operates with active or idle DACSs and does not interfere with normal DACS operation.

On power-up, a master module sends an initialize instruction down a dedicated data line to the first module in the serially connected chain of identifiers. This ID module responds by sending its unique ID code back to the host and placing itself in "transparent" mode so that subsequent commands from the master module are passed through. The next initialize command

ORNL-DWG 89-11356

RSCI Data Line

DACS Signal Line
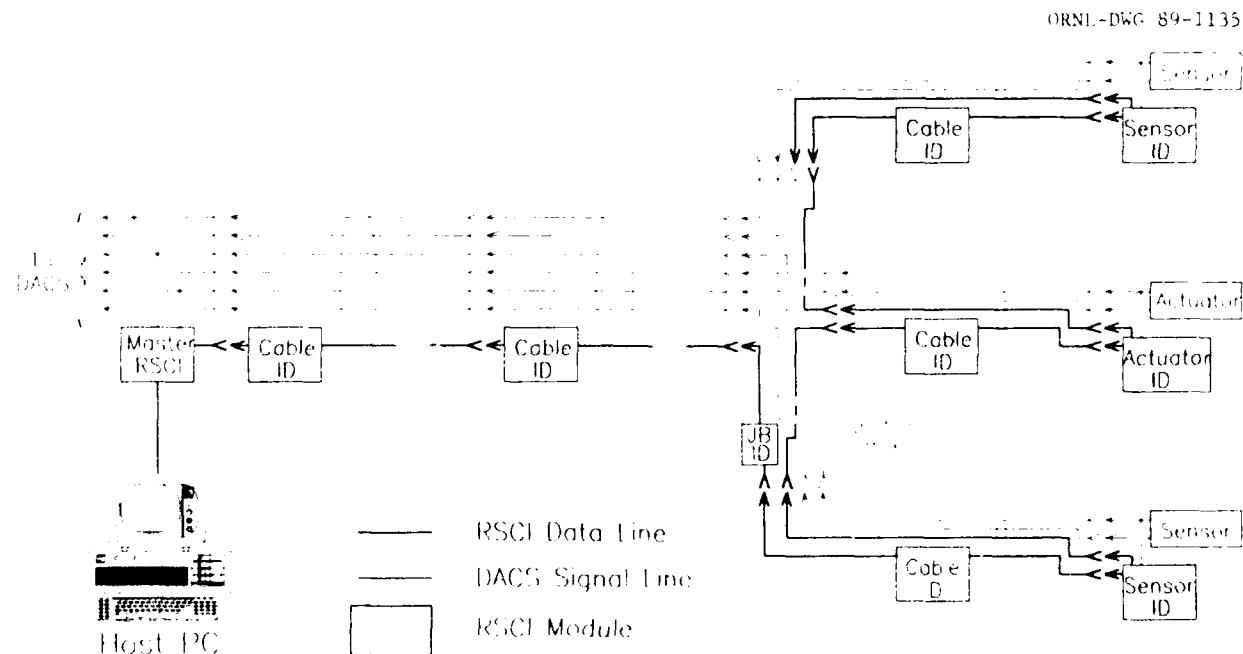
RSCI Module

Host PC

Fig. 1. Connection of RSCI components.

reaches the second ID module in the chain, which responds with its own code and then places itself in transparent mode. This process continues until all modules in the "daisy chain" have identified themselves. Thus the master unit knows not only the ID codes for all modules connected to it, but the order of their connection as well.

The master module assumes that all ID modules have been polled if a predetermined time increment passes with no response to the last initialize instruction. It then sends an initialization complete message with ID number. The ID modules then take themselves out of transparent mode and listen for messages from the master module. If an ID module receives a message addressed to the master module or to another ID module, it simply retransmits the message in the appropriate direction. If an ID module receives a message addressed to itself, it checks its own status or retrieves the required information from memory and responds accordingly.

When the master module has identified all of the ID modules connected to it, it proceeds to determine which end device (sensor or actuator) is connected to each DACS input/output (I/O) channel. To do this, it excites one of the signal wires connected to each channel with a high-frequency pulse train and then interrogates the end-device ID modules (via the RSCI data line) to find which ones can detect the pulses on their signal lines.

Master modules perform configuration updates at regular intervals to detect any changes that may occur. Upon instruction by the host computer, the master modules execute "configuration dumps" or perform other, more specialized tasks such as fetching housekeeping information from an ID module, rechecking the status of a suspect ID module, or performing diagnostic tests.

In this manner, the host computer is able to present system configuration information from the system data base in several useful formats:

1. A graphical presentation of the system configuration, or a more detailed description of a specified subsystem
2. Identification of the end device on any particular DACS I/O channel
3. The path (including cable and junction box IDs) to any given end device
4. A list of all end devices whose data or control signals pass through a given cable.

ID modules can store other useful information such as in-service dates, calibration and data, and descriptive information about the type of component to which the module is attached. The end user will determine what "housekeeping" data to include. If calibration dates are included, for example, the user could instruct the system to poll all end devices and assemble a list of all components that will require recalibration in the following month.

Each module contains a microcontroller, a communications interface, and power-conditioning circuitry. Each ID module has a failover switch to allow messages from other modules to pass through in the event of a local hardware or software failure (Fig. 2a). Master modules and end-device modules have connections to selected DACS signal lines (Fig. 2b). The serial data line is also used to distribute power, thus minimizing the number of cable conductors that must be dedicated to the RSCI system.

In the system under development, each master module can accommodate up to 30 ID modules. Usually, one master module will be required for each trunk cable (a multipair cable carrying signals from several sensors). In smaller systems, the host communicates with the master modules using standard serial
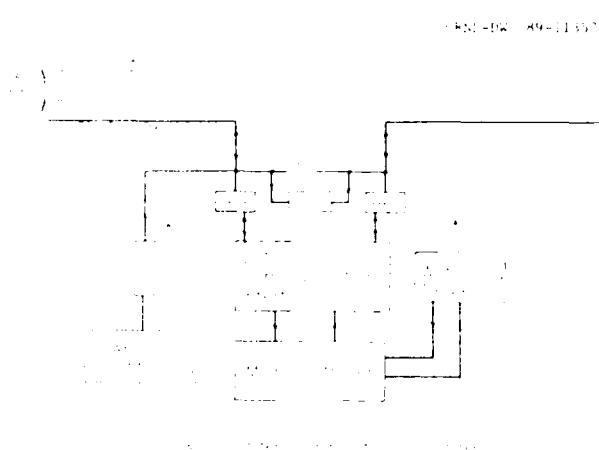
Fig. 2a. RSCI cable ID module.
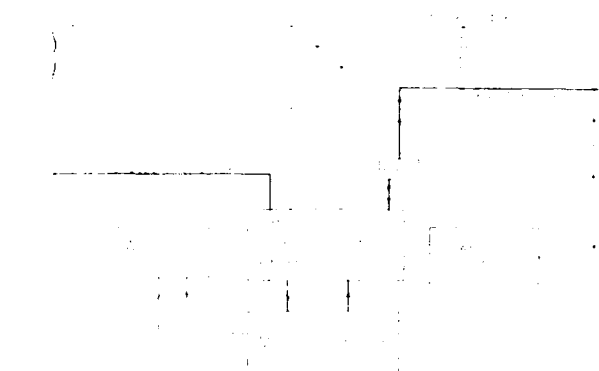
Fig. 2b. RSCI master module.

ports. In large systems, the host is linked to the master modules through data concentrators over a commercially available local-area network (LAN) as shown in Fig. 3.

ID modules are designed around the Motorola 68HC05 high-speed CMOS microcontroller. This chip was selected as the RSCI module CPU for its (1) low power consumption; (2) built-in serial communications interface; (3) large number of digital I/O lines; and (4) availability with internal PROM, EPROM, or EEPROM. Another feature of the chip, the high-speed serial peripheral interface, will be used to add "hot backup" redundancy to future versions of the RSCI modules. EEPROM chips are being used in the early development stages and will be used for applications in which field reconfiguration is desirable.

Modularity and maintainability are being emphasized heavily in software development, which is using state transition techniques. ID module programming is in assembly language for speed and code compactness.

Design goals for the RSCI system include:

1. Module cost: less than the cable or end device to which the module is attached.
2. Size: diameter equal to or less than a trunk cable connector so that cable ID modules can remain attached to the cables when they are pulled.

Fig. 3. Large RSCI system architecture.

3. Speed: ten minutes to determine the configuration of a 6000-component system.

PROJECT SCOPE AND STATUS

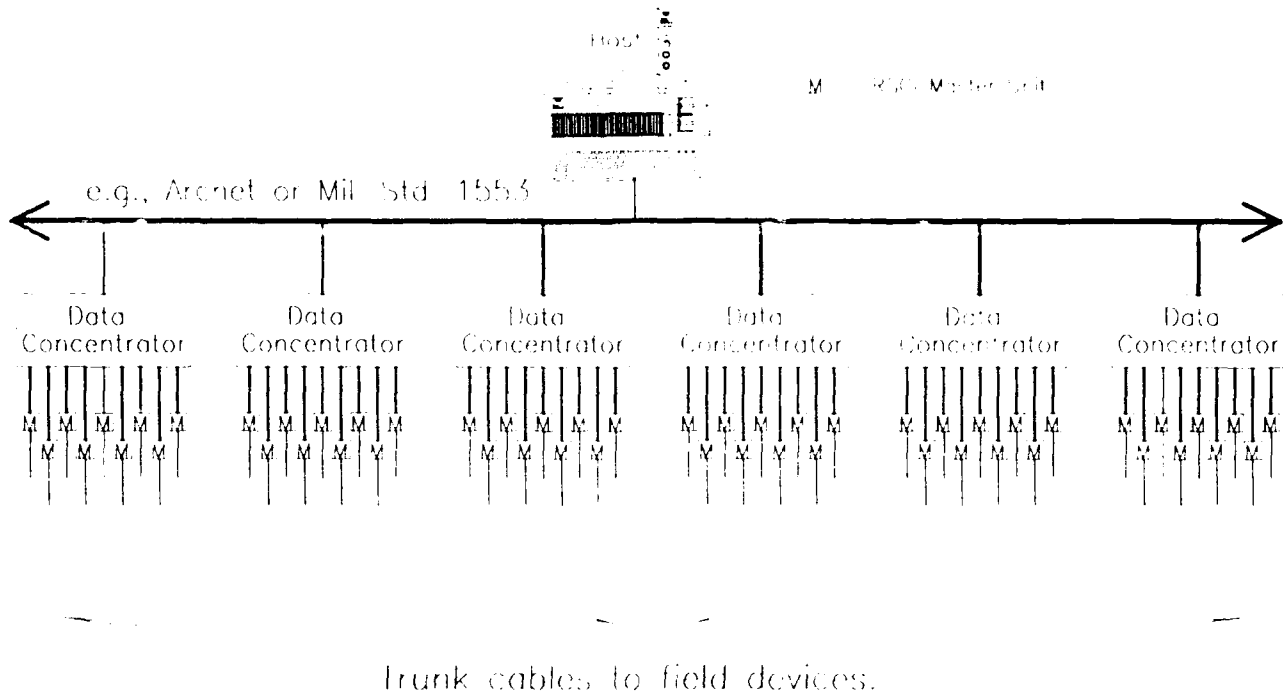The RSCI development effort is being sponsored by the Engineering Directorate of NASA's Kennedy Space Center for potential application to the Advanced Launch System (ALS) Launch Processing System (LPS). This system will be a large, complex, geographically distributed DACS; several thousand components must be included in its configuration control program.

This development effort is divided into three one-year phases. The first phase will deliver a system that determines the cable and sensor configuration of a small DACS, thus demonstrating the validity of the basic software, hardware, and communications protocol designs. The second phase is aimed at exploiting the distributed intelligence of the RSCI modules by adding the capability to process a variety of housekeeping data, to identify every cable conductor in the path to every end device, and to detect and locate wiring faults. Additional phase two efforts will include designing the system data base, developing effective ways to present the configuration data to operators and to other computers, and integrating the data concentrators and the LAN into the overall system.

The final phase will concentrate on miniaturizing RSCI modules and ensuring that they meet KSC environmental requirements. A medium-scale RSCI system with ~100 end-device modules and ~200 cable modules will be delivered in this phase. KSC technical involvement in the project is directed toward using an expert system to process data generated by the RSCI system, thus reducing the effort required to analyze the configurations of large DACSs.

Thus far, several prototype RSCI master and ID modules have been built and the system's ability to determine the physical ordering of interconnected modules has been demonstrated. Efforts are under way to fit the prototypes to a mock DACS for a demonstration of the system's sensor-channel matching capability.

CONCLUSIONS

The RSCI system offers valuable features not now available and not promised by new industry standards currently under development. Its self-documenting autoconfiguration function will greatly reduce the manual labor required in cabling checkout, whether for troubleshooting or for quality-assurance purposes. Records generated by the system are useful for highly reliable archival data storage, for post-incident analysis, or for tracking individual cable or component histories.

This technology has application in many different industries—wherever there is a need to verify the integrity and configuration of a system of electrical devices, active or passive. Potential applications to fossil and nuclear power plants are under evaluation. Integration of certain RSCI features with the emerging FieldBus standard will be examined when it is issued.

A REMOTE SENSOR/CABLE IDENTIFIER

Q: **Ray Reed (Sandia National Labs)**: I think this is really an exciting prospect having a capability like this. I think anyone who has been in the field with a large system and a small staff and has any concept of the need for validating measurements has to appreciate what you are doing. I had one question. A number of years ago when we were in the coal gasification research we fielded large systems with many, many thermocouples and other sensors as well. I would really have loved to have a system like this available because we were having to do manually a number of things that you are trying to automate. One of the things that we did at that time was to note that while most signal systems, most multiplexers deal with cables pair by pair and fixed pairing, that in some instances, particularly with regard to thermocouples and perhaps other sensors as well, you have a number of validation possibilities where you are looking not simply pair by pair but looking at individual lines paired in different ways. For example, you frequently want to measure the isolation of a sensor from ground or from other sensors. I am wondering if your system might be adaptable to multiplexing of the signal lines in various ways?

A: **Steve Baker**: You mean maybe with separate pairs of signals coming into a large system or something? Not necessarily a cabled system; is what you are saying?

Q: **Ray Reed**: Some sensors can be designed to benefit with multiple lines; not simply a single pair but perhaps 3, 4, or 5 lines. Any shielded coax, for example, has three lines and normally you think of the signal pair, but very often you would like, for validation purposes - and that is one of your concerns - to be able to measure quantities not only between the signal pair but between each individual signal line and ground. I just mention that would be another augmentation of this system that would amplify your validation possibilities considerably.

A: **Steve Baker**: What I really didn't show when I said that we would be capacitively coupled to the signal line or sensor is that from a master module we can couple to every line going out to a transducer, be it signal lines, be it power, be it any other control signals. We can put that high frequency pulse train on all of those lines. Because all of those go to the sensor therefore they all go to that sensor ID module. We can look at each line separately and determine the integrity of it and we can communicate all of it back on that one line that is dedicated for us. We can't do things like meg it or tell if the insulation resistance wire to wire is not high. We can verify that indeed there is a continuous route through each one of those signal lines.

Q: **Bill Cardwell (GE, Evendale)**: I think that you partially answered my question in your last statement, but looking at something like this for a test cell environment where we have many cells coupled to a single data room, and not all of the lines in a particular cell may be utilized for a particular engine test, most of our sensors do not have the smart response and consequently wouldn't have any active feedback. Would it be possible to use something like this in a system where not every wire bundle or every wire pair was connected at a par-

ticular time? In other words, could I put it at the end of the cable and just use that as a method of identifying which wire pair was in fact hooked up for a particular test?

A: Steve Baker: Yes, I think you could. Every cable that we have in the system, be it a large cable that would carry multiple signals or be it a small cable that goes out to a single transducer, we would have smarts built into the cable connector so that all of the signals that went out whether they were connected to a sensor or not, would be interrogated. It is really based upon the idea that every wire that you have going out of your system can be interrogated. We can tell you that that wire gets from point A finally through to point Z. We are really not integrating this into the sensor as such, we are integrating it into the cabling, into the transmission media. We do it simply by having a commercial manufacturer or manufacturers produce these things, like 10-pin Amphenol cables, 61 pin, 100 pin, 20 pin or whatever. As long as the assumption is, for example, pin AA, wire AA is dedicated for our use. That is all we have to have. I didn't really describe this, but there will be some programming boxes where technician enters all of this housekeeping information. It is entered into a nonvolatile memory on that little connector. Then he takes that off and goes out into the field and screws it in between the sensor cable and the sensor (and hopefully, it would be waterproof, etc. and it would have the same type of integrity that the cable does) and voila you have your intelligence. If that goes bad, you unscrew it, take it out, and put another one in. We hope that it is going to be somewhat like the last talk, ("A Computer Programmable Transducer Micro Circuit") it would be a universal system that would really have a number of types of modules, the types and numbers of cable connectors that you have.

Q: Marty Willis (Rocketdyne): If I understand correctly, what you're planning to do is to have a module with each sensor and the module is separate from the sensor itself, correct?

A: Steve Baker: Correct.

Q: Marty Willis: I think the concept is really wonderful. I know that we have a lot of problems with cable identification to sensors. What I don't understand is now you've created a problem: where, what, if the module gets separated from the sensor that it goes to, don't you have to have Quality Control now to verify that you put the correct module with the correct sensor? Otherwise, you're doing your checks, and it is transferring information, but you still have a potential where the module is identifying itself, but it is not identifying the correct transducer. I still see human error in quality control there.

A: Steve Baker: That's right. But what we would expect to do is have a security wire connecting them, or you would have heat shrink, or somehow you make it in effect permanently connected to the cable.

Q: Marty Willis: If I know NASA though, no one is going to be happy with just safety wire.

A: **Steve Baker:** Somewhere it needs to be done once. It could be put into the sensor. For example, NASA wants to know what cable is connected to what cable, what the configuration is so somewhere you have to supply this device. You are right the first time out; you would have to verify that.

Q: **Marty Willis:** And then, anytime there is a change I still see the same sort of a problem. You are trying to eliminate a problem where someone goes and swaps out a transducer at the last minute, the calibration information hasn't been placed into the data base, and someone is running out there doing make-and-break tests or rap tests. It would eliminate that but I still think there is a place for giving a false sense of security, that everything is ok but it isn't.

A: **Steve Baker:** Well there is one thing that I am planning to do whenever the transducer comes into the calibration facility for recalibration. A lot of QA testing and records are done at that time so a module reprogrammed in the calibration lab and permanently affixed again to that cable/sensor would be the best that we could do. Somewhere on the line there has to be human intervention and what we are trying to do is once we have done that, and once it is permanently attached you can swap these transducers all over the place in the field. There has to be a point where that is integrated in with that sensor or that actuator or that cable. At that point you have to be especially careful of QA because if it breaks down there it obviously breaks down. What we are expecting is that there will be enough controls in place one time and that you will properly check it and you can permanently affix it so that it becomes a permanent fixture, a permanent part of that cable. If NASA has 3000 cables out here in their supply cabinet and these all have intelligent cable modules attached to them and you assume that when they were attached the QA was done and it was done right. I really don't think that that is a false sense of security.

Q: **Marty Willis:** Well, it doesn't fit; right now you're assuming that when someone hooks up a transducer that quality control was there and they hooked it up right. But I myself have rotated items on an engine, and I thought they were right until someone came back later and said, "Should this be an xy or a yx"? This data doesn't jive. We had photographs and we knew that someone had switched them. We had quality control, too. It's just that it happens. I was just curious about how you were going to deal with that. Also, you have all of the cable ID modules - and maybe it is just to eliminate doing troubleshooting at the time - but if you just had the one module with the sensor and your master module verifies that the sensor is in the location that you said, and if it doesn't come back and say that it is in the proper location then you would assume you have an error in one of your junction connections?

A: **Steve Baker:** Yes, also NASA wanted to be sure that from a QA standpoint that the right cables were connected together, and if there was a failure somewhere in a cable, this system would tell you which cable it was and would allow technicians to immediately change that. What if you had a problem in a termination box, which may very well be where the cables split out to the individual sensors? It will tell you exactly what box it is, and you should know where it is.

Q: Marty Willis: Just to eliminate having to go through and verify each junction until you find the right one?

A: Steve Baker: Yes, it essentially maps the entire system automatically for you.

Q: Dennis Reed (EG&G): Two questions on your mapping procedure. Since its a serial mapping until you reach an open end how does it determine if there is a broken line along the line?

A: Steve Baker: This line broken?

Q: Dennis Reed: Yes, if that is broken somewhere along the line and you are looking for an open end how does it ....?

A: Steve Baker: If that is broken somewhere along the line it stops at that point. That is a potential problem. You need to know that a line is verified correctly and it is broken. Really there is nothing you can do because it is physically broken so your system comes back and says these are the only components in it. Then you know what should be there. Therefore, that immediately tells you that I've got a problem in this cable. You would go check that out.

Q: Dennis Reed: So the first time that you map that you have to physically go through and verify that what the computer says matches what you think you have?

A: Steve Baker: That is what you would always do. You know what you think should be there because of the way the system has been cabled. Then you know what the computer tells you. If it tells you something different then you need to go check at that point.

Q: Dennis Reed: If you are looking at various transducers in a serial method; if you were to have two transducers that were miswired, say they are wired in parallel, could you determine that there are two transducers on that line instead of just one?

A: Steve Baker: The way this system is, and it is probably kind of hard to see, in the cables that go out to the sensor we require two dedicated lines, one going out to the sensor and the other one coming back to the terminal box. Really the way that this system is set up it is impossible to be wired in parallel. Using one dedicated line and using two dedicated lines in the final cable which goes out to the sensor, it is impossible to wire them in parallel. The fact that they are wired in serial allows us to tell you the order that they are in, and therefore the physical mapping; so really they can't be in parallel. If they are we have big problems

Q: Marty Willis (Rocketdyne): Have you started taking a look at environmental use? If these modules are going to be mounted close to the sensors, in quite a few of the cases aren't you going to have them in situations where they will be exposed to extreme cold and perhaps extreme heat, and obviously a lot of vibration? It seems to me if we could build modules like that we would already have smart sensors that

could perform in those environments and we don't. At least not that I know of. Have you started addressing those issues or maybe you don't have environmental problems?

A: **Steve Baker:** We are starting to address those issues. If you think about it, more and more transducers are becoming smart now. The particular microprocessor we are using is available in the mil-grade version. It is high-speed CMOS can withstand -30° to +60° C. Obviously, the way it's made, the circuit board should be able to withstand a fair amount of vibration. It should be able to withstand most environments. It will be sealed as it is part of the cabling system. Everything is sealed because of the salt water environment. From that standpoint it will be able to live in the environments of most sensors.

Comment: **Marty Willis:** I know with the shuttle, in most cases when they start chilling down things for quite a period of time things are going to be pretty cold.

A: **Steve Baker:** It can't withstand 200 C type environment, as no electronics can. But it should be rugged enough that it can withstand most of the environments that sensors would normally be in. There may be a few exceptions.

VOICE ACTIVATED HOT MIC.

Sidney R. Jones, Jr.
Naval Air Test Center
Airborne Instrumentation
Patuxent River, MD 20670

Abstract

In many instrumentation applications, a good clear Intercom System (ICS) is a necessity. This holds true for instrumentation personnel at various ground sites as well as aircrew in multiple seat aircraft. When the ICS is operated in the "Hot Mic" mode, the microphones are constantly keyed or held open. This allows the aircrew to fly their test points without keying the mic every time they want to talk. Thus all of the breathing and other extraneous noise is transmitted over the ICS. By installing a Voice Activated Switch (VOX) which triggers on the crew's voice, the majority of the background noise that is transmitted on the ICS is eliminated, making for a much quiter intercom system.

Introduction

At the Naval Air Test Center (NATC) in Patuxent River, Maryland, a lot of flight testing is done on a variety of planes. Many of these are multiple seat aircraft which are already equipped with a voice activated hot mic (VOX) mode. When a trainer, a two seat version of a particular single seat aircraft, was being tested at NATC, the pilots wanted the clear transmission which they had experienced with previous VOX equipped planes. As a result, the Airborne Instrumentation Department was tasked to build and install an instrumentation level VOX circuit for this aircraft during the time it was undergoing flight test at NATC.

System Operation

The goal was to design a circuit tnat would detect whenever voice was coming through the microphone. When detected, the voice would be passed to the ICS. Any input that was not voice would be rejected. Among the several design approaches considered was to use a Fast Fourier Transform chip to detect an input that was within the voice frequency range. After noting the complexity of this circuit, we opted for a simpler solution. A sound level detect circuit, similar to those found in other VOX installations was chosen. When considering the majority of noise will be iow level background noise, this circuit should perform adequately.

VOX/ICS Interface Diagram
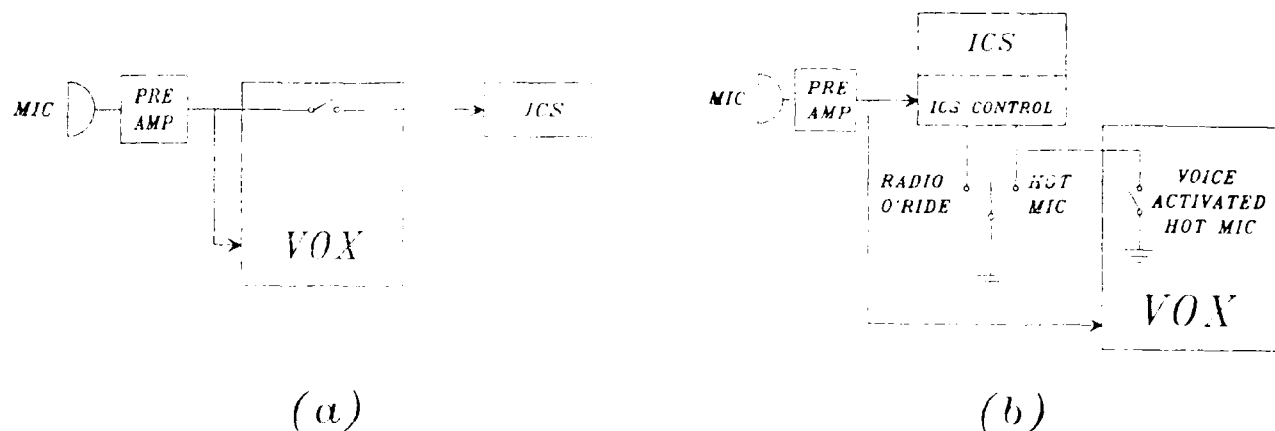

(a)   (b)

FIGURE 1

Once voice is detected on the mic lines, it has to be switched through the ICS system. The first approach was to make and break the mic lines to the ICS with a relay (see figure 1a). Whenever the voice is to be passed, the VOX circuit closes the control switch. The mic is then directly connected to the ICS system. After building this circuit, loading problems were discovered between the microphone pre-amp and the ICS. The VOX circuit was set up so a normal voice level coming into the mic would trigger the relay. When the relay was energized connecting the mic lines to the ICS, the ICS would load the pre-amp so badly the resulting signal level would no longer trigger the VOX circuit. The relay would be disabled, disconnecting the mic from the ICS. The signal level would jump back to its previous level triggering the circuit again. As long as there was a voice input, the relay would "chatter". Another approach was needed.

The ICS system has two control lines--hot mic and radio over ride. In the cockpit, to use either mode a switch is thrown which grounds the appropriate control line. To get voice to activate the hot mic mode for brief periods of time, VOX is used to ground the hot mic control line (see figure 1b).

Interfacing the VOX circuit to the ICS in this way solved the loading problem. Also, this was a much better solution from a safety of flight standpoint. In the worst case scenario of a VOX failure, the control switch would be closed. No communications would be lost since the ICS would see it as normal hot mic mode. However, using the previous method (figure 1a), in the worst case the control switch would be open. The aircrew would no longer be able to talk to the ground or each other.

CIRCUIT DESCRIPTION

The microphone lines are run into an amplifier and filter circuit (see figure 2). The amplifier is adjusted to get maximum gain without saturating the amplifier (see figure 3a). This provides greater sensitivity in the following threshold detect circuit. The filter, with a cutoff frequency of 5 KHz, will attenuate the noise with a frequency greater than that of the voice. As a result, the higher frequency noise gets filtered out before it can trigger the VOX circuit.
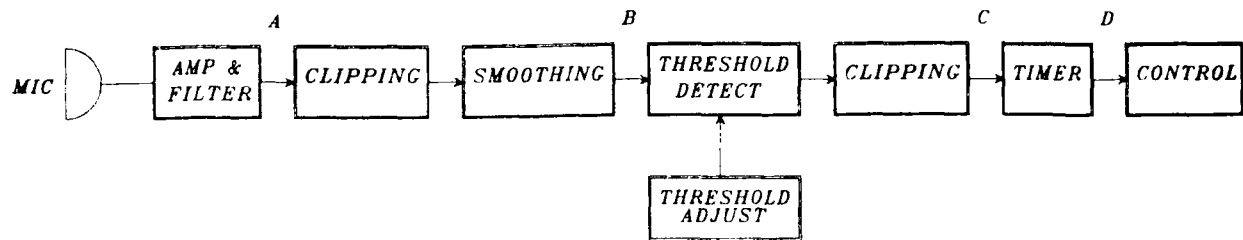
VOX Block Diagram

MIC — AMP & FILTER — **A** — CLIPPING — SMOOTHING — **B** — THRESHOLD DETECT — CLIPPING — **C** — TIMER — **D** — CONTROL

THRESHOLD ADJUST → THRESHOLD DETECT

FIGURE 2

VOX Waveforms

A — AMP & FILTER OUTPUT
+15 / -15

B — THRESHOLD DETECT INPUT
+15 / -15 — Threshold

C — TIMER INPUT
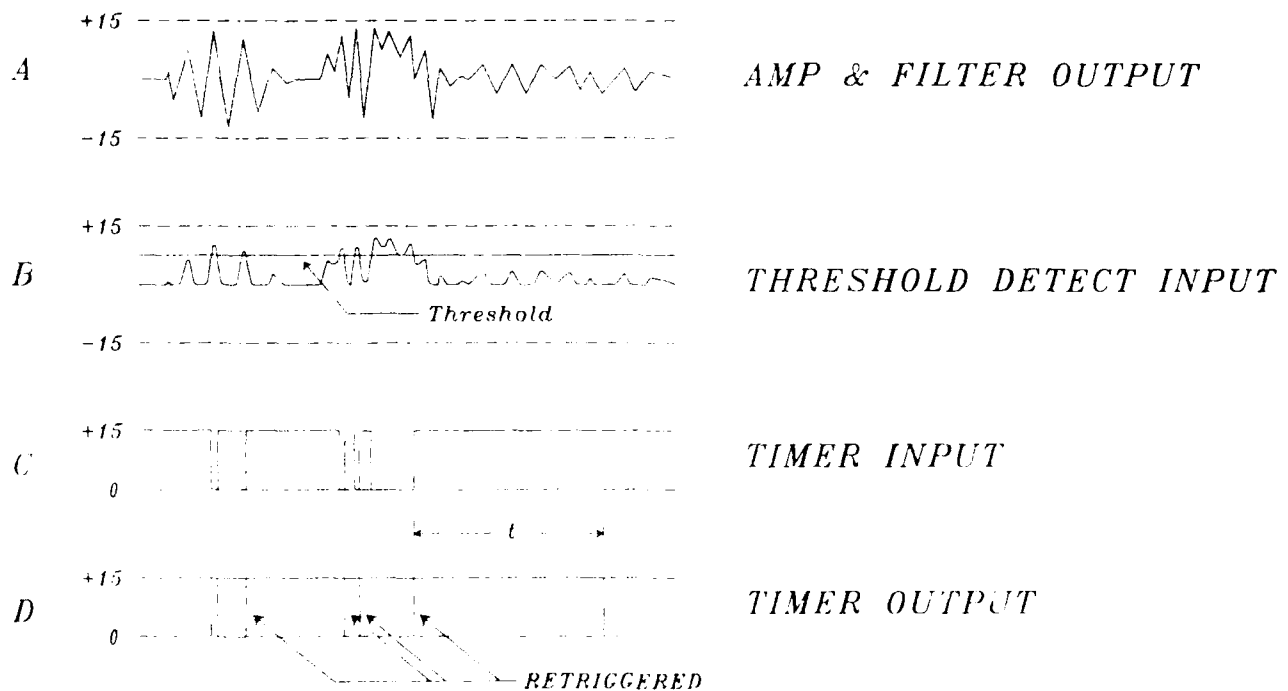+15 / 0 — t

D — TIMER OUTPUT
+15 / 0 — RETRIGGERED

FIGURE 3

284

The voice signal tends to be reasonably symmetrical. Since the detect circuit looks at the amplitude of the signal, the negative portion isn't necessary. The signal is sent through a clipping circuit before being fed into a smoothing circuit. The smoothing circuit rounds the spikes. It keeps the threshold circuitry from triggering on spikes close to the threshold level. We now have a 0 to 15 volt signal input to the threshold detect circuit. The threshold detect circuit uses a comparator to compare the modified voice signal with the threshold adjust voltage (see figure 3b). As long as the signal is below the threshold, the comparator output is kept constant at +15 VDC. Whenever the signal exceeds the threshold, the output drops to -15 VDC. In order to protect the input of the next stage, a clipping circuit is used to limit the signal to a 0 to 15 volt square wave (see figure 3c).

While the timer input is high (no voice detected) , the timer output remains low keeping the control circuit relay disabled. When the timer input swings low (voice detected) , the output rises, energizing the relay which grounds the hot mic control line. As long as the input remains low (voice still present) , the relay is kept energized. When the input swings high again (voice disappears), the timer starts its time out sequence. If the input doesn't drop low again (no voice detected) before a predetermined period "t" has been reached, the relay is disabled allowing nothing to reach the ICS. If the input does drop low before the time out period has been reached (voice reappears) , the timer is reset and doesn't begin its time out sequence again until the input goes high (see figure 3d).

After manufacturing a working circuit card, the board was redesigned with a much greater density and a few enhancements. The idea was to make a generic board that with minimum effort could be configured for individual requirements. Among these enhancements are:

- A dual channel board measuring 2 3/4 inches by 4 inches.
- The ability to use the control relay normally open or normally closed.
- The choice of using a pot instead of a fixed resistor for amplifier gain control.
- The availability of placing resistors on either side of the threshold adjust pot to achieve any desired threshold adjust sensitivity.

OTHER USES

Although the circuit was designed as a VOX control circuit, the more correct name is a voltage activated switch or voltage monitor card. When looking at the circuit in this way, a whole range of possible applications opens up. In any given instrumentation system there are a variety of transducers. The majority of these transducers provide a DC output. Those remaining could be run into signal conditioning to provide a DC output. Any of these transducers could be used as the front end to this circuit. When properly configured this circuit could be an over/under voltage indicator, temperature indicator, RPM indicator, position indicator, etc.

CONCLUSION

Upon completion of the initial phase of the VOX project, the Navy as well as the aircrew liked the design so well, that we are currently trying to find a suitable packaging scheme to incorporate VOX as a fleet wide modification. Airborne Instrumentation is looking into placing VOX units in the test engineer stations within our ground station. This will enable the test engineer to hear the pilot's voice through VOX whether the aircraft has one installed or not. These are only a few of the applications of this simple but versatile circuit.

Dual Channel VOX Circuit
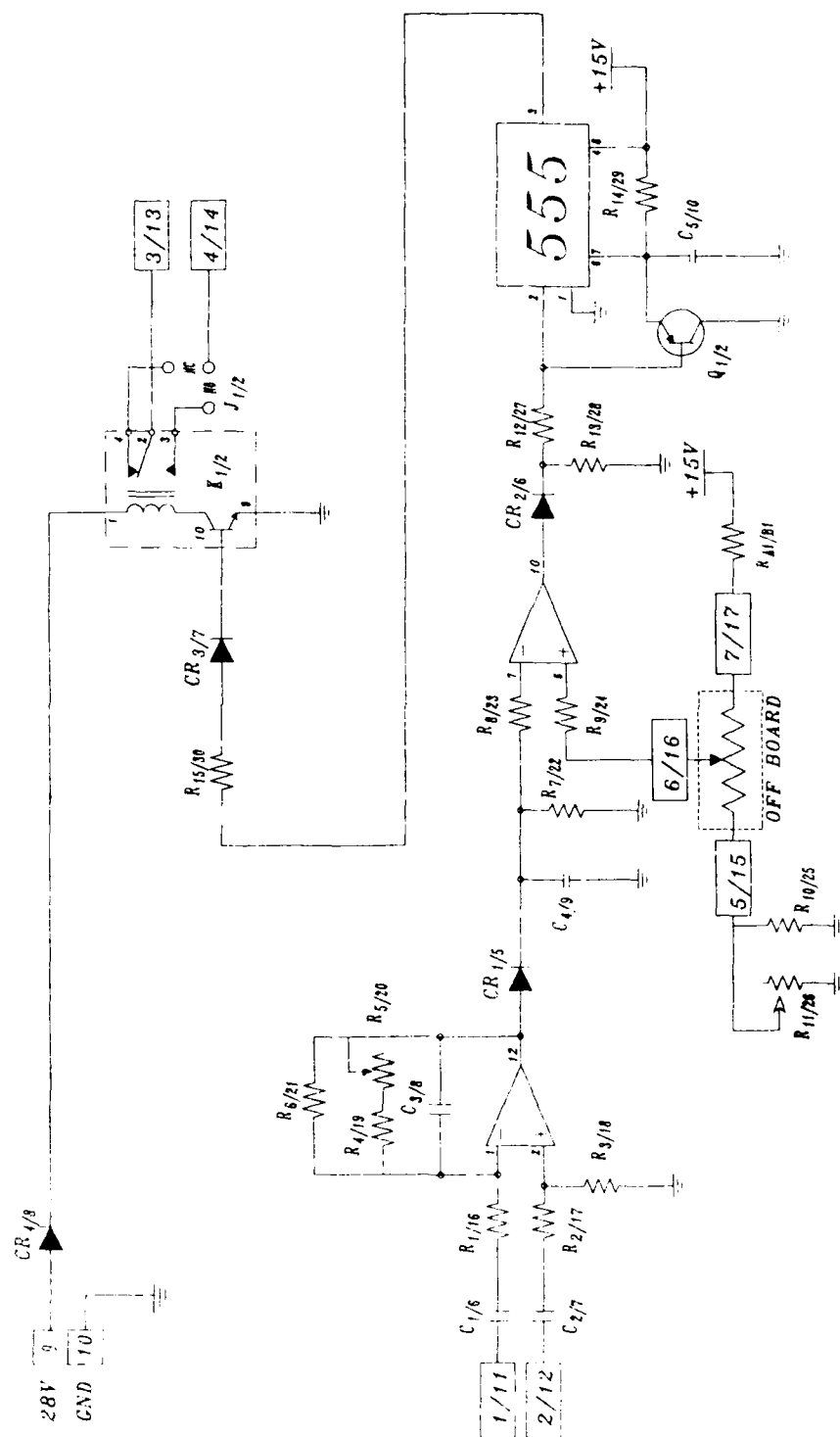
Channel 1/Channel 2

FIGURE 4

VOICE ACTIVATED HOT MIC

Q: **Bill Cardwell (GE, Evendale OH)**: Is there a problem on this being in the aircraft with two microphones, the pilot, and the co-pilot being close to each other and both talking at the same time, or multiple circuit activation into the same voice net?

A: **Sidney Jones**: No, this is no different than the aircraft configuration without hot mic.

Q: **Bill Cardwell**: The ground station has to recognize by voice then which is talking?

A: **Sidney Jones**: Yes.

Improving the Response Time and Accuracy of Transient Thermal Measurements in Live Fire Testing (LFT)"

James G. Faller

Live fire vulnerability testing is mandated by law for all major development combat vehicles of the Army. One of the principal aims of such testing is to gain a realistic crew casualty assessment during round penetration of the vehicle. Thermal injury to skin and eyes stemming primarily from direct contact with hot gases, liquids, and particulates represents a major hazard to the vehicle crew. Recent survivability test programs at Aberdeen Proving Ground (APG) have led to the development of test methods and instrumentation to collect rapid, real time, usable and integrable thermocouple temperature and heat flux sensor data desired by the office of the Surgeon General in making their hazard analysis.

A Very Wide Dynamic Range Data Acquisition System

Jack R. Carrel
Senior Engineer
EG&G Energy Measurements, Inc.
Sandia/DoD Engineering
Las Vegas, NV

Abstract

This article presents the design of a data acquisition system that was developed by EG&G Energy Measurements for Sandia National Laboratories. The acquisition system comprises individual seismometers that measure seismic activity at remote stations located several hundred miles from a central data collection facility and control point. The remote stations operate unattended and receive commands for setup and status check from the control point. (Additionally, the stations' operation can be modified by transmitting software modifications from the control point.) At the remote station the data from the seismometers, ranging from 10 microvolts to 4 volts, is digitized and transmitted over telephone lines to the central collection point. Because of the wide-dynamic input voltage range, the system was designed with 16-bit analog-to-digital converters and an autoranging capability, giving an effective 20-bit range. Errors due to noise were kept to a minimum by careful selection of components and effective packaging design; nonlinearity was reduced by oversampling the input signal and then digitally filtering the sampled data.

INTRODUCTION

This document presents the considerations and processes used in the design of a seismic data acquisition system developed by EG&G Energy Measurements, Inc. for Sandia National Laboratories (SNL). The full data acquisition system is described, and the new design of the remote-station data acquisition equipment is presented. The critical problem areas are identified; these include random noise and systematic errors. The careful consideration of these and other error sources in the selection of system components and configuration minimized or negated their effects. The primary challenge in the development of this system was the very wide range of signal amplitude from the various seismometers. By adjusting the system for each seismometer and then segmenting the remaining signal range, a system could be developed that would perform more than adequately.

BACKGROUND

The seismic data acquisition system collects information from seismic stations that are located several hundred miles from a central data collection and control point. Each station is composed of several seismometers that are attached to signal conditioning equipment. The output of the signal conditioning equipment is digitized and transmitted by modem communications to the central data collection facility, where the data is processed for analysis and archival. From the central data collection facility, an operator can send commands to the remote station. These commands include system readiness tests and configuration settings for each seismometer channel. The configuration settings control the attenuation of the signal prior to the analog-to-digital conversion. These attenuator settings are used to condition the seismometer signal for the maximum usage of the analog-to-digital converter operating range. These attenuations are implemented through the actuation of relays. The relays control the connection of a series of resistors that provide fixed amounts of attenuation to the input signal.

The system is tested for readiness by sending a specified current to the calibration coil of the seismometer. The system monitors the resulting output of the seismometer. The operator can then verify that the system is functioning by watching the signal that is collected at the central collection facility. This test verifies that the seismometer mass is not too close to a boundary and that the data acquisition system is functioning properly.

NEW SYSTEM REQUIREMENTS

The design that is being considered in this document is a redesign of the remote-station data acquisition equipment. The customer at SNL and the EG&G operators designated several requirements for the new design. These requirements are:

- Provide five channels per remote station
- Simplify design and operation; remove relays
- Increase sensitivity
- Increase resolution within each range
- Allow remote software modification
- Use high-level language
- Synchronize all of the stations for relative phase measurements

There are five seismometers at each of the remote stations. Each of the five channels at the remote station has a seismometer attached to it.

The details concerning the seismometers will be presented later.

The existing system had two major problems that affected its reliability. First, the system contained a large number of relays. The problems with these relays caused the operators to ask that the new design eliminate relays or at least reduce the number of them. Second, the existing system used STD bus card edge connectors. As is generally the case with card edge connectors, it was necessary to clean and re-seat the cards periodically.

The required sensitivity of the new system is 1 microvolt. The sensitivity of the existing system was 100 microvolts. As will be shown later, the lowest signals expected from the seismometer approach a sensitivity of less than 1 microvolt.

The customer specifically asked that we increase the resolution of the system. The concern is that very small signals contain information that is of interest. If the small-amplitude frequency components are riding on a larger-amplitude component, the existing system would continue to change ranges to ensure that the larger amplitude signal would not be clipped. The resolution of the existing system was 11 to 12 bits within a range. The new system uses fewer ranges and 16-bit analog-to-digital converters to meet this requirement.

To change the operating software of the existing stations, new PROMs would have to be programmed, and then carried out to the remote station to be installed in the system. Since making these changes at most of the stations would require several hundred miles of travel, a better method of upgrading and modifying the system software was required. In the new system, electrically erasable PROMs are used to store the operating program. This program can be changed by way of the modem link from the central data collection facility.

Finally, in order to make the phase measurements between remote stations more accurate, the new system synchronizes the local sampling clocks to WWVB. This synchronization allows measurements with 0.5 milliseconds of relative accuracy.

INPUT REQUIREMENTS

There are three types of seismometers in the seismic system. These three seismometers are shown in Table 1, along with the minimum and maximum signal levels that will be expected from them. Note that the total range covered by these seismometers ranges from 0.9 microvolts as the minimum signal from the SL-210-220 to 4.1 volts as the maximum from the GS-13. These two represent a range of over 130 dB. To cover this range would require that the system have an analog-to-digital converter of 24 bits including the sign bit, since these are only peak voltage values. As is also shown in the table, the expected input signal level of each seismometer type has a range of only 105 dB. This range can be covered with an analog-to-digital converter of 20 bits including the sign bit. That is a substantial reduction in the required performance of the analog-to-digital converter.

The existing system sampled the input signal at 50 samples per second. In order to minimize the impact on the analysis software, the sample rate remained at 50 samples per second for data that is

supplied in real time to the data collection facility.

THE NEW SYSTEM

The new system is represented by the block diagram in Figure 1. The left side of the figure shows the equipment on the seismometer pad, which is a large concrete platform that the seismometers are set on.

In the new system, all possible sources of noise are removed from the pad area. Experience has shown that the two main sources of noise are 60 Hz electrical noise from AC power cables, and mechanical noise generated by such things as cooling fans. Both of these sources can cause subharmonics to be generated that are within the bandwidth of the seismometers and the instrumentation. To remove these sources, two criteria were selected for the new system. First, the instrumentation rack would be moved as far away from the pad as feasible. This would remove all of the sources of mechanical noise from the pad area. Second, the pad would be kept free of any AC power. All of the equipment in the new system that needed to be either in the area or on the pad would be DC voltage.

Since the instrumentation had to be moved from the pad and since the signals from the seismometers are of such a low level, the new system has preamplifiers on the pad. These preamplifiers amplify the seismometer signal and provide a quiet impedance matching to the seismometer output. The preamplifiers use DC power that is supplied from the Distribution Unit. In addition to supplying DC power to the Preamplifiers, the Distribution Unit also supplies the calibration coil signal to each of the seismometers.

As is shown on the right side of Figure 1, a VME chassis was selected to contain the station instrumentation. VME was chosen because of the positive mating connectors and because of the availability of chassis on the commercial market. The signal from the Preamplifiers enters the Analog Module, where it is digitized and transferred to the Processor module. The Processor Module then sends the digitized signal to the central data collection facility through the modem connected to one of its serial ports.

The VME chassis was modified to include separate power supplies for all of the analog circuitry. This modification was necessary because VME chassis are designed for a digital environment and are supplied with a switching regulated power supply, a type of power supply that is inherently very noisy. Also, because digital systems tend to put noise on the power supply because of the digital switching, the analog system was supplied with quieter linear regulated power supplies. In addition to being quieter than the switching regulator power supply, the separate linear regulated power supplies further isolate the analog portion of the system from the digital system and keep the isolation between the two systems intact. The information passed between the analog and digital portions of the system is through optical couplers.

The Calibration Module provides several functions to the system. It supplies the sampling clock to the Analog Modules in the VME chassis; this sam-

Table 1. Input requirements.

INPUT REQUIREMENTS

Seismometer Type	Min Input Volts Pk	Max Input Volts Pk	Range
Geotech SL-21-/220	9.1E-07	1.6E-01	105 dB
Benioff 1051/1101	4.0E-06	7.0E-01	105 dB
Geotech GS-13	2.5E-05	4.4E00	105 dB

Total Range   9.1E-07 to 4.4E00 is 130 dB

Frequency Response is 0.250 Hz to 10 Hz
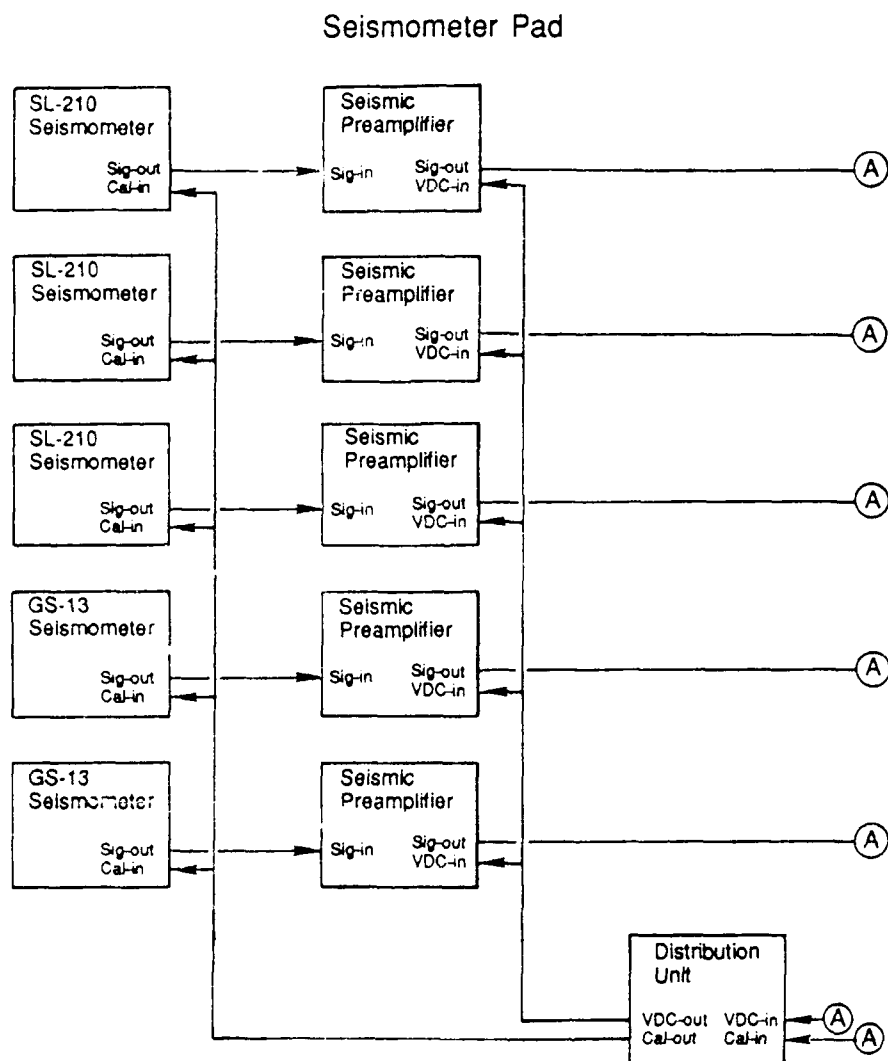
EG&G

SEISMIC STATION BLOCK DIAGRAM

Figure 1.   Seismic station block diagram.

242

SEISMIC STATION BLOCK DIAGRAM (CONCLUDED)
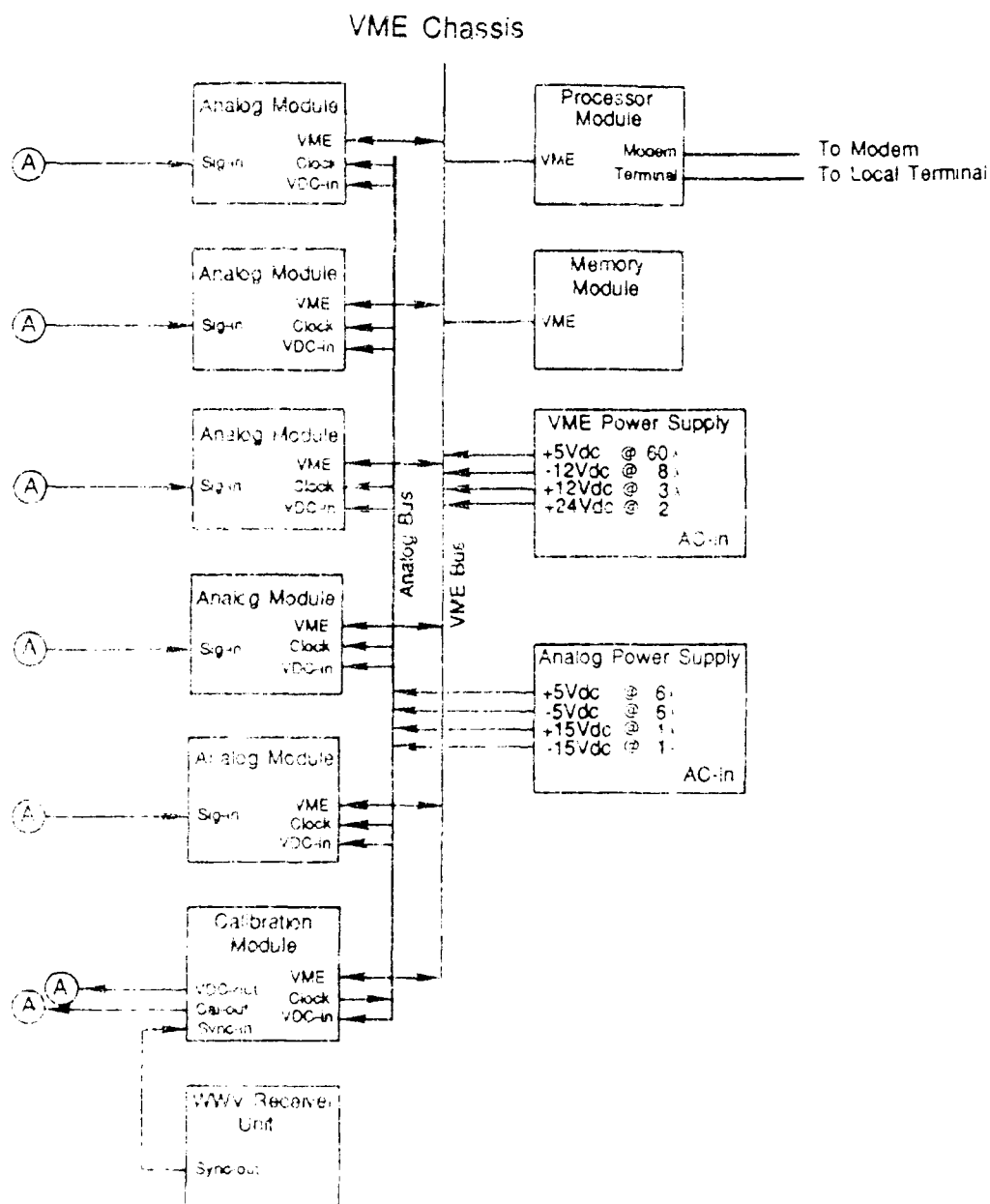
Figure 1. Seismic station block diagram (concluded).

pling clock is synchronized to WWVB. The Calibration Module also generates the calibration signals for the seismometers and provides the DC voltages for the Distribution Unit.

The Memory Module in the VME chassis buffers the data that is transmitted to the Central Data Collection Facility and provides additional memory that can be used by the Processor Module. This memory is CMOS; it has battery backup when power is not applied from the VME bus.

POTENTIAL ERROR SOURCES

The remote-station instrumentation can operate only if the potential sources for errors are considered in the system design. Table 2 lists the major errors that were considered in the design of this system. These errors are generated in the signal, primarily in the analog circuitry.

The gain error and the gain linearity error must be considered in the design of each of the amplifiers in the signal path. Table 3 shows the gain calculations for the resistors in an inverting operational amplifier circuit. These calculations show, of course, that the gain of the amplifier relies more on the ratio of the resistors than on the accuracy of each resistor. Also, the gain stability with temperature depends upon the matching of the temperature coefficients of the two resistors. This means that even if the temperature coefficients of the resistors are not within the 0.0015 percent required by a 16-bit system, the gain error could still be sufficiently small if the ratio of the temperature coefficients of the resistors track within the 0.0015 percent tolerance.

The gain linearity error is the most difficult one to determine and correct. If the temperature coefficients of the gain resistors of the amplifiers do not track, or if their temperature coefficients do not track linearly with each other, nonlinear gain errors will exist in the system. The likelihood of these errors occurring in a large enough magnitude to be a problem is very slight. We have not been able to devise an adequate test to verify the linearity of the system to the full 20-bit accuracy. The problems with this kind of testing involve finding a signal source and a measurement device that will cover the full range of the system. As a result, the best way to test the linearity of the system is to test the various portions of it separately. To do this, we can look at the system as two 16-bit systems. Care must be taken that the integral nonlinearity does not cause a discernible error between the 16 bit ranges.

The DC offset is not of great concern as long as it does not accumulate through the system and cause the lower range of the system to be unusable. The information from the seismometers is studied mostly in the frequency domain. Therefore, as long as the DC offset is low enough to allow the collection of the other frequency components, it is not a problem. The DC-offset drift can be a problem if it is of sufficient frequency that it appears to be seismic information. Because the seismic information is of such low frequency, the DC offset drift with temperature can be a source of error and should be considered throughout the design.

Because of the extremely low levels of some of the signals from the seismometers, noise is an important factor in the design of the instrumentation system. As previously discussed, there are two types of noise in this system: electrical and mechanical. The effects of the mechanical noise are greatly reduced by the removal of the instrumentation rack and its associated cooling fans from the seismometer pad.

The electrical noise has three major sources: component, circuit, and 60-Hz power lines. The component noise is a result of the random thermal motion of electrons and although very small can still add to the overall circuit noise. The circuit noise results from the configuration of components that reinforce or inhibit noise generation and accumulation through the system. (Component noise sources such as flicker noise and shot noise should also be considered, especially with the use of monolithic operational amplifiers.) As is true with most instrumentation systems, the insertion of 60-Hz signals into the measurement signal must be eliminated or at least reduced. Often in an instrumentation system, the problem is not the existence of 60-Hz noise in the environment, but rather the insertion of 60-Hz signals as a result of improper circuit configuration and improper grounding and shielding techniques.

Another possible source of error in the system can be the generation of frequency-dependent deviations in the amplitude response of the system in the frequency band of interest. The most likely cause of this error is the improper alignment of poles from the filters that are used throughout the system. If the poles line up, then the ripple from each filter can accumulate into an error that is substantial enough to affect the performance of the system. The filters of the system need to be designed to ensure that this does not occur. This is the one error discussed here that can also be caused by the digital portion of the system.

DESIGN APPROACH

The approach followed in the design of the remote station instrumentation system was to pay attention to the generation of errors in the analog portion of the system, keep the digital portion from causing errors to feed into the analog signal, and keep the digital signal processing from generating errors through numerical methods. The first of these considerations, the generation of errors in the analog portion of the system, required the greatest amount of attention. The following guidelines were used to achieve the minimum amount of error in the analog signal:

- Minimize components in the signal path
- Use low noise components
- Keep the signal path quiet

The number of components in the signal path was kept to a minimum because all electrical components generate noise that will accumulate in the circuit. Once in the system, the noise will either add or multiply, but in either case it will accumulate throughout the circuit and will influence the measurement signal.

By selecting low-noise components, the accumulation of noise in the system can be kept to a minimum. For instance, the thermal noise in resistors is proportional to the temperature and the resistance value of the resistor. In this design we did
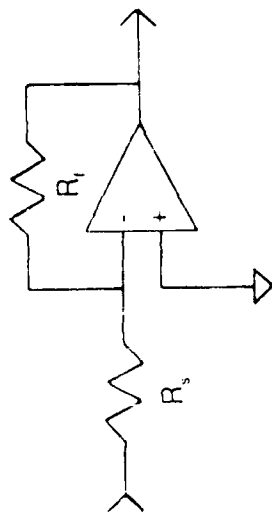
ERROR SOURCES

- Gain Error

- DC Offset/Drift

- Gain Nonlinearity

- Noise
  - Component
  - Circuit
  - 60 Hz

- Filter poles - no alignment

1/2 LSB of 16 Bit ADC is ±150 µV

or 0.0015% full scale, 10 volts

EG&G

Table 3. Gain calculations for resistors in an inverting operational amplifier circuit.

$$\text{Gain} = \frac{R_f}{R_s}$$

With resistor tolerance included:

$$\text{Gain} = \frac{R_f + R_f \cdot t_f}{R_s + R_s \cdot t_s} = \frac{R_f}{R_s} \cdot \frac{1 + t_f}{1 + t_s}$$

For worst case of $t_f = -t_s$:

$$\text{Gain} = \frac{R_f}{R_s} \cdot \frac{1 - t_s}{1 + t_s}$$

If $t_s = 1\%$ then:

$$\text{Gain} = \frac{R_f}{R_s} \cdot 0.98$$

So if $t_f = t_s$ then:

$$\text{Gain} = \frac{R_f}{R_s}$$

EG&G

not concern ourselves with the temperature, but we did attempt to select resistor values that were not greater than absolutely necessary. For the active components in the analog circuit, primarily monolithic operational amplifiers, particular attention was paid to flicker noise and shot noise in each device that was selected.

The operational amplifiers that were selected for the input stage in the preamplifier, the Burr-Brown OPA111, were selected for the low current noise figure [illegible] amperes. Because of the [illegible], we did not want to have [illegible] from the instrumentation coupling to the mass motion and generating erroneous signals. We could not find a second source for this amplifier. The other operational amplifiers in the analog circuit are Burr Brown OPA27 low noise operational amplifiers. Second sources for the OPA27 [illegible] are Linear Technology and Precision Monolithics, I[illegible].

Separate linear regulated low noise power supplies [illegible] for all of the [illegible] of the system to keep the [illegible] ratio as low as feasible.

The [illegible] of [illegible] the system required that we also pay attention to the shielding and guarding of signal lines. This is extremely important for the connection between the Preamplifier and the Analog Module. [illegible] of the remote stations, this line [illegible] long. Because of its length and the low [illegible] transmitted, care had to be taken to avoid generating currents in the shields. Also, the system was configured so that the low level signal lines were kept [illegible] the [illegible]. For [illegible] the [illegible] of the Preamplifier was selected [illegible] amplitude [illegible] of the signal amplitude [illegible] amplified to a magnitude that is above the [illegible] of the ambient and circuit noise for the long transmission line to the Analog Module. [illegible] several of the [illegible] in the system [illegible] in [illegible] level of [illegible], the [illegible] for the long transmission line between the Preamplifier and the Analog Module, [illegible] differential mode [illegible]

[illegible]

[illegible] Once digitized, [illegible] all of the noise that [illegible] the analog [illegible] the noise that was added [illegible] the analog-to-digital converter. The noise that is added to the signal by the analog-to-digital converter is wide band and is aliased into the frequency band up to one-half the sampling frequency. The effects of this noise can be reduced by increasing the sampling frequency. The noise is distributed throughout the Nyquist bandwidth, so oversampling allows *more frequencies* for the noise energy to be distributed and therefore will reduce the level of the noise in the band of interest. Once digitized, the oversampled data is filtered and decimated to a lower bandwidth. This noise could be reduced by simply averaging the data and decimating, but a filter such as a finite [illegible] filter is just as easy to implement and is much more effective in reducing the high-frequency noise level.

Figure 4 shows the filter configuration for the system. Shown is the 40-Hz analog low-pass filter and the 16-bit analog-to-digital converter. As will be shown later, this figure represents just one of the ranges that are used to cover the 20-bit signal range. The analog-to-digital converter oversamples the data at a 16K samples per second, a factor of [illegible] the final 50 sample per second rate. In the Analog Module, a digital low-pass filter with a [illegible] cutoff is implemented. After filtering, the 16K samples per second data is decimated by a factor of 64 to an effective sample rate of 250 samples per second. This 250 samples per second data is transferred from the Analog Module to the Processor Module for final processing and transmission to the Data Collection Facility. The final processing is the combination of the two 16-bit range values into a single 20-bit number, the filtering of this data by another 40-Hz low pass digital filter, and the decimation of the data to an effective sample rate of 50 samples per second.

AMPLIFIER CONFIGURATION

Figure [illegible] shows the amplifier configuration for the remote station instrumentation. The Preamplifier has a different gain for each of the types of seismometer that will be attached to it.

SEISMOMETER	GAIN	MAXIMUM OUTPUT
[illegible]	X 128	20.48 Volts Peak
Benioff [illegible]	X 32	22.40 Volts Peak
[illegible]	X 4	[illegible] Volts Peak

The gains of the rest of the amplifiers in the system are the same for all of the seismometers. The Buffer Amplifier in the Analog Module has a gain of [illegible] in order to reduce the differential signal amplitude to a single ended range. The Range 1 Amplifier has a gain of [illegible] and the Range 2 Amplifier has a gain of [illegible]. The analog-to-digital converter has a full scale input range of plus and minus [illegible] volts. Table [illegible] shows the relationship of the gains of the amplifier stages in the Analog Module and their relationship to the analog-to-digital [illegible].

[illegible]

[illegible] the proper selection of components and configuration, a [illegible] seismic data acquisition [illegible] designed that acquires data with a wide range of input amplitudes. As shown, the gain error [illegible] the differences in the tracking of the temperature coefficients of the resistors, especially since the resistors for a particular amplifier [illegible] in the same [illegible] and therefore have the
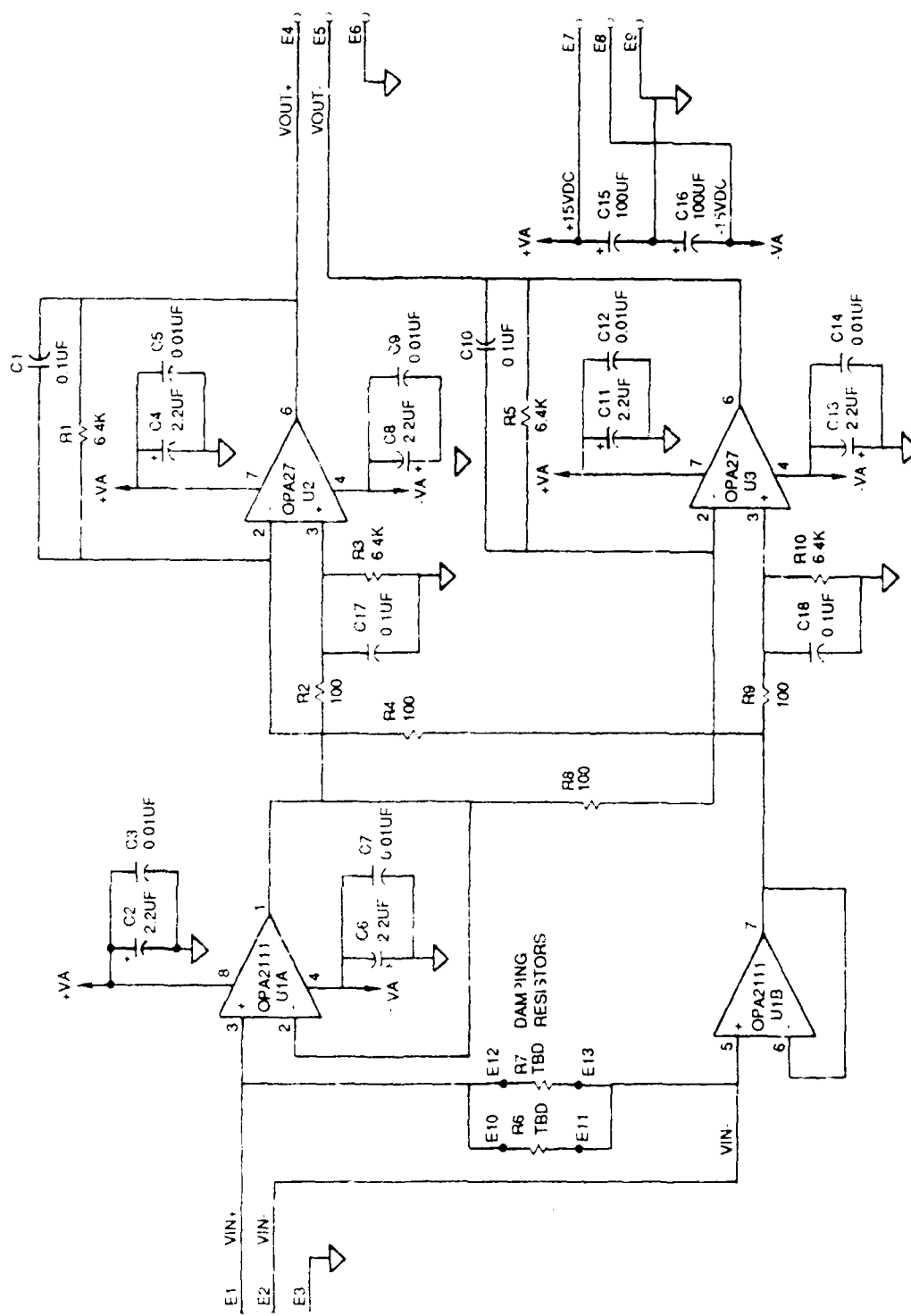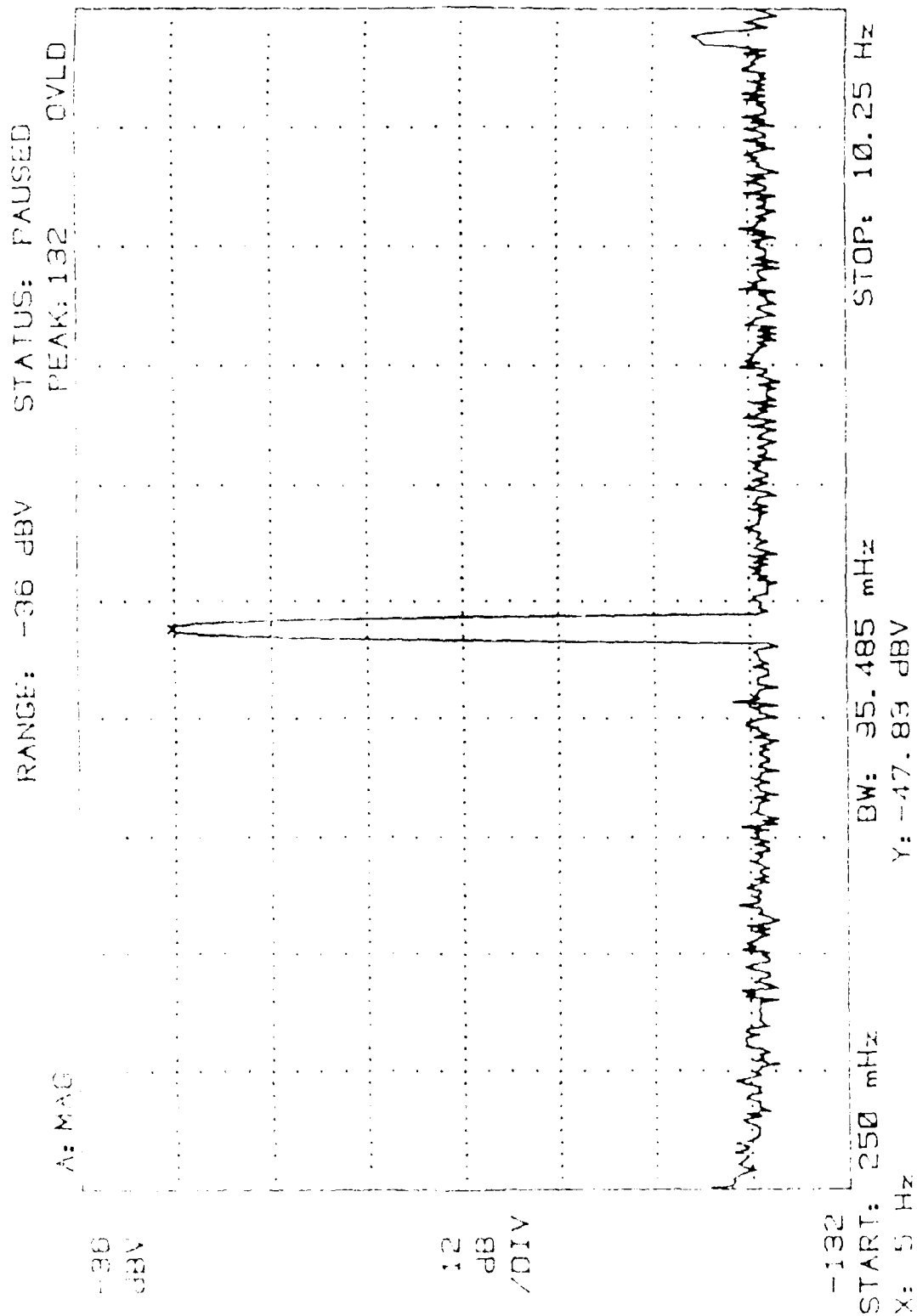
SEISMIC PREAMPLIFIER

Figure 2. Seismic preamplifier.
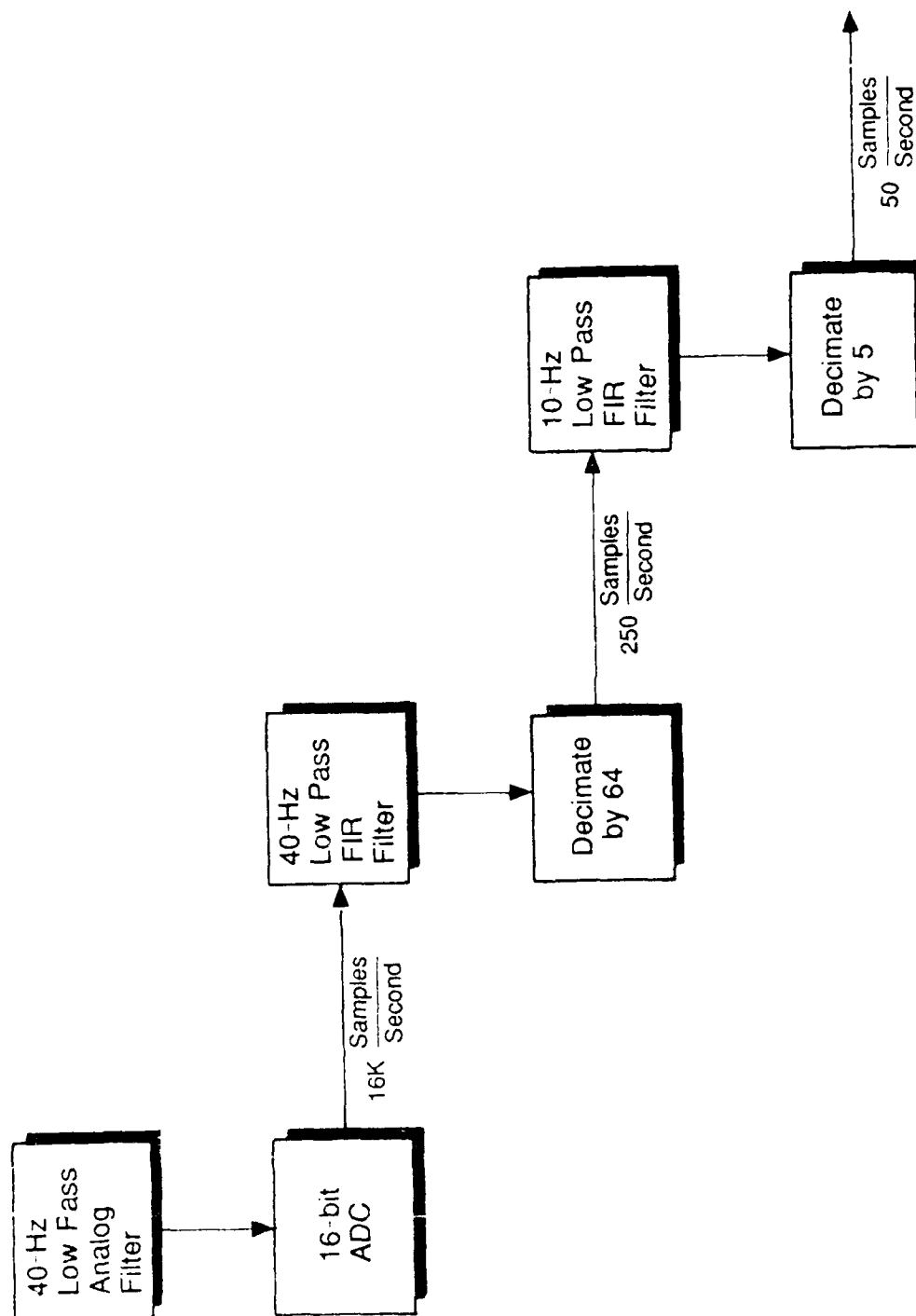
Figure 3. Preamplifier noise performance.

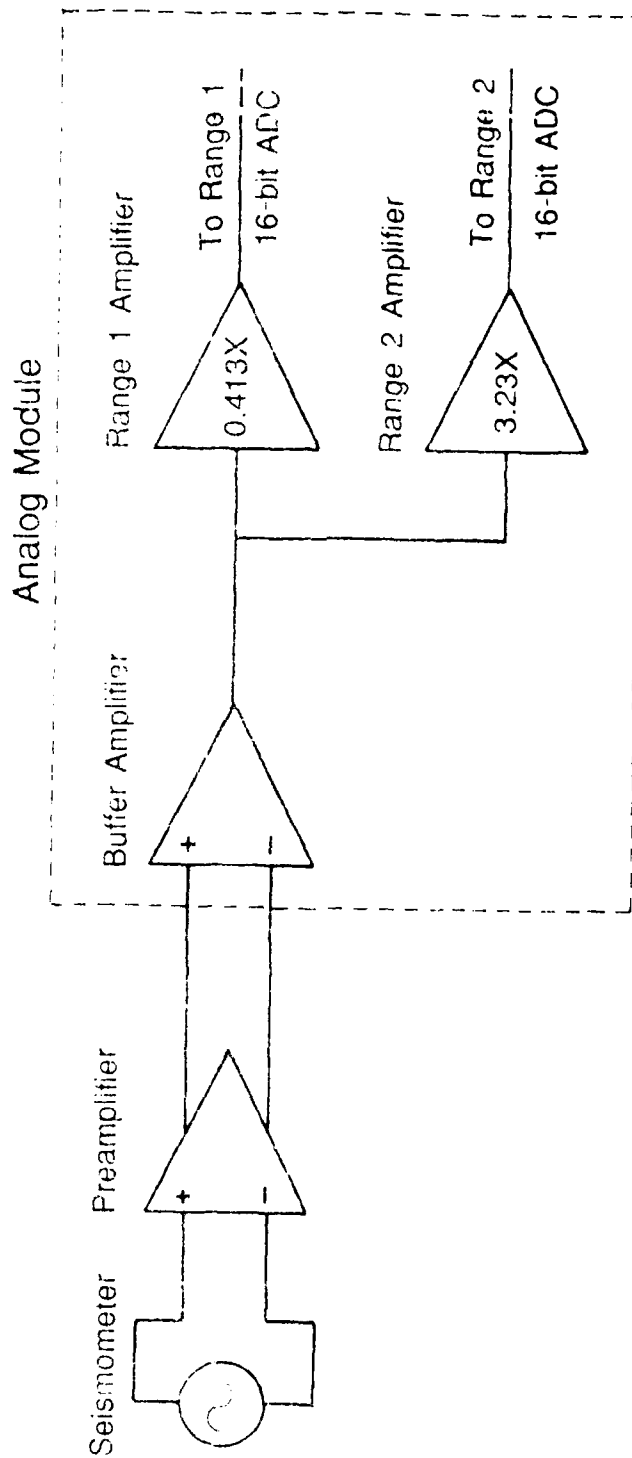Figure 4. Seismic DAS filtering.

SEISMIC AMPLIFIER CONFIGURATION

Figure 5. Seismic amplifier configuration.

Table 4. Analog module ranges.

ANALOG MODULE RANGES

Bits Ref to Buf out	Ref to Buffer Output	Bits Ref to Rng 1	Ref to Rng 1 Output	Bits Ref 2 Rng 2	Ref to Rng 2 Output
18	10.3 V	15	4.25 V	-	-
17	5.12 V	14	2.13 V	-	-
16	2.56 V	13	1.06 V	-	-
15	1.29 V	12	531. mV	15	4.25 V
14	640. mV	11	266. mV	14	2.13 V
13	320. mV	10	133. mV	13	1.06 V
12	160. mV	9	66.4 mV	12	531. mV
11	80.0 mV	8	33.2 mV	11	266. mV
10	40.0 mV	7	16.6 mV	10	133. mV
9	20.0 mV	6	8.30 mV	9	66.4 mV
8	10.0 mV	5	4.15 mV	8	33.2 mV
7	5.00 mV	4	2.08 mV	7	16.6 mV
6	2.50 mV	3	1.04 mV	6	8.30 mV
5	1.25 mV	2	519. µV	5	4.15 mV
4	625 µV	1	259. µV	4	2.08 mV
3	313 µV	0	130. µV	3	1.04 mV
2	156 µV	-	-	2	519. µV
1	78.1 µV	-	-	1	259. µV
0	39.1 µV	-	-	0	130. µV

EG&G

same temperature. The nonlinearity error is still difficult to verify, although it does not appear to be a problem. The DC offset is not a problem because of the stability of the circuit and the monolithic amplifiers that were chosen, the OPA27s. The overall design of the system was simplified by the segmentation of the required 20-bit range for a single digitizer into two overlapping 16-bit ranges. Finally, digital processing techniques such as over-sampling and filtering were used to reduce the effects of unwanted signals.

REFERENCES

1. Franco, Sergio, Design with Operational Amplifiers and Analog Integrated Circuits, McGraw-Hill, 1988.

2. Roden, Martin S., Analog and Digital Communication Systems, Prentice-Hall, 1985.

3. Engineering Staff of Analog Devices, Analog-Digital Conversion Handbook, Prentice-Hall, 1986.

4. Morrison, Ralph. Grounding and Shielding Techniques in Instrumentation, John Wiley and Sons, 1967.

5. Rabiner, Lawrence R. and Gold, Bernard. Theory and Applications of Digital Signal Processing, Prentice-Hall, 1975.

6. Data Book, Crystal Semiconductor Corp., 1988.

7. Data Book, Burr-Brown, 1988.

8. Data Book, Linear Technology, 1988.

A VERY WIDE DYNAMIC RANGE DATA ACQUISITION SYSTEM

Q: **Steve Baker (Oakridge National Laboratory):**   I noticed you used essentially a successive-approximation A/D converter from Crystal, one that gave you a high sampling rate?

A: **Jack Carrel:**   Yes, but I don't think that it is successive approximation.

Q: **Steve Baker:**   The basic question that I had is that the other approach you could take would be to use the slower dual or triple slope integrating A/D converter and I wondered what your thought process was, why you chose this over that?

A: **Jack Carrel:**   Even those converters are going to have the wideband component noise, and given the level, I thought it was more important to have a high sample rate, and then in the digital domain remove that thermal noise, called Johnson noise, from the system.   I would not have that as an option in some of those others.   There is an 18-bit converter that is made by Analog Devices but it only has about a 10 Hz bandwidth and so I don't have a lot of room to play with doing my digital filtering.

In Search of More Output --
Two Strain Gage Bridge Circuits Revisited

by

Roger Noyes
John Kalnowski
EG&G, Inc.

This paper is unavailable for publication in these proceedings. The author may be contacted for information or the procedure to obtain copies of the paper. Mr. Noyes work phone number is 702-295-2532.